Vol. 58 DECEMBER, 1954 No. 12

THE JOURNAL OF PHYSICAL CHEMISTRY

(Registered in U. S. Patent Office)

The Journal of Physical Chemistry is being published monthly in 1954
Notes and Communications to the Editor will be considered for
publication in THIS JOURNAL

THE JOURNAL OF PHYSICAL CHEMISTRY

(Registered in U. S. Patent Office)

Published monthly by the American Chemical Society at 20th and Northampton Sts., Easton, Pa.

Entered as second-class matter at the Post Office at Easton, Pennsylvania.

The *Journal of Physical Chemistry* is devoted to the publication of selected symposia in the broad field of physical chemistry and to other contributed papers.

Manuscripts originating in the British Isles, Europe and Africa should be sent to F. C. Tompkins, The Faraday Society, 6 Gray's Inn Square, London W. C. 1, England.

Manuscripts originating elsewhere should be sent to W. Albert Noyes, Jr., Department of Chemistry, University of Rochester, Rochester 3, N. Y.

Correspondence regarding accepted copy, proofs and reprints should be directed to Assistant Editor, Allen D. Bliss, Department of Chemistry, Simmons College, 300 The Fenway, Boston 15, Mass.

Business Office: American Chemical Society, 1155 Sixteenth St., N. W., Washington 6, D. C.

Advertising Office: Reinhold Publishing Corporation, 430 Park Avenue, New York 22, N. Y.

Articles must be submitted in duplicate, typed and double spaced. They should have at the beginning a brief Abstract, in no case exceeding 300 words. Original drawings should accompany the manuscript. Lettering at the sides of graphs (black on white or blue) may be pencilled in, and will be typeset. Figures and tables should be held to a minimum consistent with adequate presentation of information. Photographs will not be printed on glossy paper except by special arrangement. All footnotes and references to the literature should be numbered consecutively and placed in the manuscript at the proper places. Initials of authors referred to in citations should be given. Nomenclature should conform to that used in *Chemical Abstracts*, mathematical characters marked for italic, Greek letters carefully made or annotated, and subscripts and superscripts clearly shown. Articles should be written as briefly as possible consistent with clarity and should avoid historical background unnecessary for specialists.

Symposium papers should be sent in all cases to Secretaries of Divisions sponsoring the symposium, who will be responsible for their transmittal to the Editor. The Secretary of the Division by agreement with the Editor will specify a time after which symposium papers cannot be accepted. The Editor reserves the right to refuse to publish symposium articles, for valid scientific reasons. Each symposium paper may not exceed four printed pages (about sixteen double spaced typewritten pages) in length except by prior arrangement with the Editor.

Remittances and orders for subscriptions and for single copies, notices of changes of address and new professional connections, and claims for missing numbers should be sent to the American Chemical Society, 1155 Sixteenth St., N. W., Washington 6, D. C. Changes of address for the *Journal of Physical Chemistry* must be received on or before the 30th of the preceding month.

Claims for missing numbers will not be allowed (1) if received more than sixty days from date of issue (because of delivery hazards, no claims can be honored from subscribers in Central Europe, Asia, or Pacific Islands other than Hawaii), (2) if loss was due to failure of notice of change of address to be received before the date specified in the preceding paragraph, or (3) if the reason for the claim is "missing from files."

Subscription Rates: to members of the American Chemical Society, $8.00 for 1 year, $15.00 for 2 years, $22.00 for 3 years; to non-members, $10.00 for 1 year, $18.00 for 2 years, $26.00 for 3 years. Postage free to countries in the Pan American Union; Canada, $0.40; all other countries, $1.20. Single copies, current volume, $1.25; foreign postage, $0.15; Canadian postage $0.05. Back issue rates (starting with Vol. 56): non-member, $1.50 per issue, foreign postage $0.15, Canadian postage $0.05; $12.50 per volume, foreign postage $1.20, Canadian postage $0.40; special rates for A.C.S. members supplied on request.

The American Chemical Society and the Editors of the *Journal of Physical Chemistry* assume no responsibility for the statements and opinions advanced by contributors to This Journal.

The American Chemical Society also publishes *Journal of the American Chemical Society*, *Chemical Abstracts*, *Industrial and Engineering Chemistry*, *Chemical and Engineering News*, *Analytical Chemistry*, and *Journal of Agricultural and Food Chemistry*. Rates on request.

THE JOURNAL OF PHYSICAL CHEMISTRY

VOL. LVIII

1954

EASTON, PA.
MACK PRINTING COMPANY
1954

THE JOURNAL OF
PHYSICAL CHEMISTRY

(Registered in U. S. Patent Office) (Copyright, 1954, by the American Chemical Society)

VOLUME 58 DECEMBER 15, 1954 NUMBER 12

DIMERIZATION OF THE CHLOROACETIC ACIDS IN SOLUTION

BY C. P. BROWN AND A. R. MATHIESON

Department of Chemistry, The University, Nottingham, England

Received March 5, 1954

In the pure form and in relatively concentrated solution in many solvents, carboxylic acids exist largely as hydrogen-bonded dimers. In solvents which are themselves hydrogen bonded, however, the monomer-dimer equilibrium of the acids may be affected by hydrogen bonding between the solvent and monomeric acid molecules. Solvents might be conveniently divided into three types from this point of view, (i) non-hydrogen-bonding solvents, (ii) solvents forming hydrogen bonds preferentially with other molecules, *e.g.*, ether, and (iii) solvents which form a hydrogen-bonded structure, *e.g.*, CH_3OH.

Moelwyn-Hughes and his co-workers[1,2] have used the partition of acetic and propionic acids between water and organic solvents to study association in the organic phase, but there exists a large quantity of partition data relating to the chloroacetic acids which has never been interpreted in this way.

The equilibria involved in the partitions are (i) ionization in the aqueous phase, (ii) distribution of acid molecules between the two phases, and (iii) dimerization in the organic phase, *i.e.*

$$H^+ + RCO_2^- \text{ (aq.)} \rightleftarrows RCO_2H \text{ (aq.)}$$

$$RCO_2H \text{ (aq.)} \rightleftarrows RCO_2H \text{ (org.)}$$

$$(RCO_2H)_2 \text{ (org.)} \rightleftarrows 2RCO_2H \text{ (org.)}$$

The first two equilibria may be combined into the single stoichiometric equilibrium

$$\text{total acid (aq.)} \rightleftarrows RCO_2H \text{ (org.)}$$

which it is appropriate to use when activity coefficients for the aqueous phase are to be employed. Two equilibrium constants may be defined

$$K_1 = \frac{[RCO_2H \text{ (org.)}]}{[\text{total acid (aq.)}]} \quad (1)$$

$$K_2 = \frac{[RCO_2H \text{ (org.)}]^2}{[(RCO_2H)_2 \text{ (org.)}]} \quad (2)$$

the square brackets denoting activities. If c, f are concentration (in moles/l.) and activity coefficient in the aqueous phase, and c' is the concentration in the organic phase, then

$$\frac{c'}{cf} = K_1 + \frac{2K_1^2cf}{K_2} \quad (3)$$

assuming the monomeric and dimeric species in the organic phase to behave as ideal solutes. This equation resembles the relationship employed by Moelwyn-Hughes, *et al.*,[2] except that f replaces $(1 - \alpha)$, where α is the degree of dissociation. Equation 3 allows values of K_1 and K_2 to be determined from partition data if f is known. Some water is carried into the organic phase by the acids; trichloroacetic acid in water-saturated benzene and other solvents exists as $CCl_3CO_2H \cdot H_2O$ and $(CCl_3CO_2H)_2 \cdot 2H_2O$.[3,4] Values of K_2 determined in this way refer to hydrated forms of the acid molecules in the organic phases.

The activity coefficients of acetic and mono-, di- and trichloroacetic acids in aqueous solution have been estimated from existing data and are shown in Fig. 1. The equations

$$j = 1 - \theta/c\lambda(1 + \alpha) \quad (4)$$

$$\log f = -0.4343j - 0.8686 \int_0^c \frac{j}{\sqrt{c}} d\sqrt{c} + 4.5 \times 10^{-4} \int_0^\theta (1 - j)d\theta \quad (5)$$

where θ is the depression of the freezing point and λ the molar depression for water, were used in conjunction with the freezing points,[5] densities.[6,7] and conductances[8-10] quoted in the literature, and

(1) M. E. A. Moelwyn-Hughes, *J. Chem. Soc.*, 850 (1940).

(2) M. Davies, P. Jones, D. Patnaik and E. A. Moelwyn-Hughes, *ibid.*, 1249 (1951).

(3) R. P. Bell, *et al.*, *Z. physik. Chem.*, **A150**, 20 (1930); *J. Chem. Soc.*, 1969 (1934); 1432 (1953).

(4) C. P. Brown and A. R. Mathieson, unpublished results.

(5) Landolt-Börnstein, "Physikalisch-Chemischen Tabellen," Springer, Berlin, 1923.

(6) A. C. Oudermans, *Z. Chem.*, 150 (1866).

(7) L. Mameli, *Gazzetta*, **41**, 294 (1911).

(8) D. A. MacInnes and T. Shedlovsky, *J. Am. Chem. Soc.*, **54**, 1429 (1932).

(9) H. S. Harned and J. E. Hawkins, *ibid.*, **50**, 85 (1928).

(10) B. Saxton and T. W. Langer, *ibid.*, **55**, 3638 (1933).

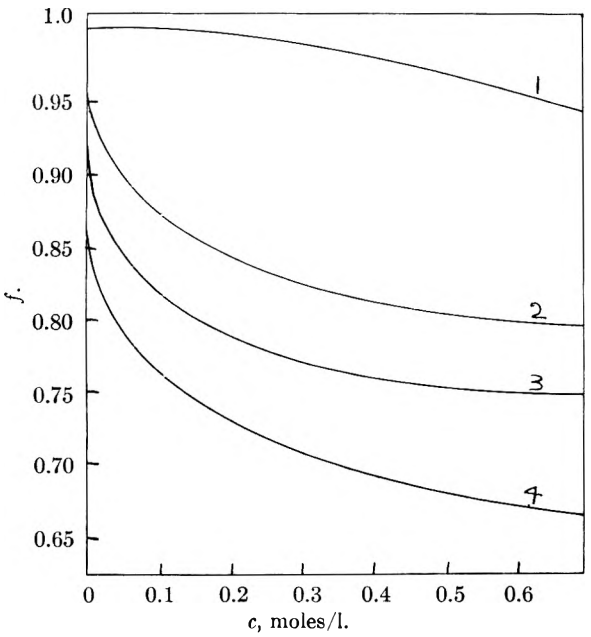

Fig. 1.—Approximate activity coefficients of the acids in water at 25°: 1, CH_3CO_2H; 2, CH_2ClCO_2H; 3, $CHCl_2CO_2H$; 4, CCl_3CO_2H.

the plots of $j/c^{1/2}$ against $c^{1/2}$ were extrapolated to infinite dilution using the equations of the interionic attraction theory, a value of 4 Å. for the mean distance of closest approach of the ions being used, following MacInnes and Shedlovsky.[8] For dichloroacetic acid the equation of Harned and Hawkins[9] was used

$$\log \gamma = -0.357\sqrt{2}\,\mu/(1 + 0.8\sqrt{2\mu})$$

where μ is ionic strength and γ activity coefficient on the basis of moles/1000 g. solvent) and the γ's converted to f's using the density data. This gave good agreement with the single measurement of γ by Harned and Hawkins at a concentration of 0.202 mole/1000 g. solvent (calcd. γ 0.778; expt., γ 0.775). The activity coefficients are probably accurate to 1–2% which is ample for the present purpose.

Measurements of the partition of acetic and the chloroacetic acids between water and organic solvents,[11] chiefly those of de Kolossowsky and Kulikov,[12] have been used to test the validity of eq. 3 and to calculate values of K_1 and K_2. Equation 3 is well obeyed by all four acids in most of the solvents examined where equilibration has been made against aqueous solutions less than 1.0 mole/l. This is illustrated for trichloroacetic acid in six solvents in Fig. 2. Values of K_1 and K_2 (K_2 in g. mole/l.) for all four acids at 25° are shown in Table I. A small number of systems do not obey eq. 3 and these are indicated by a cross in the table. Trichloroacetic acid in the alcohols only obeys the equation up to concentrations of 0.1M in the aqueous phase.

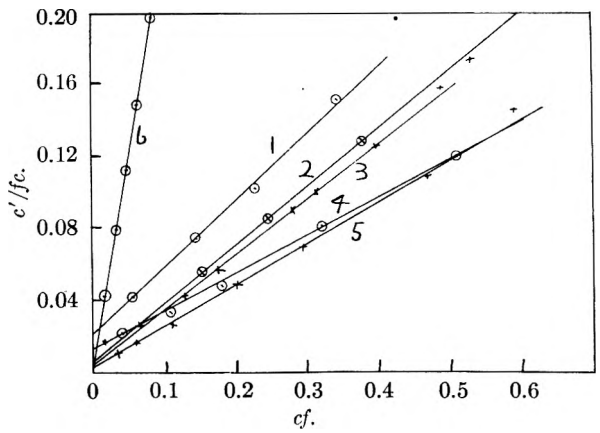

Fig. 2.—Tests of eq. 3 for trichloroacetic acid. Organic phases: 1, $CHCl_3$; 2, CH_3I; 3, nitrobenzene, ordinate × 10^{-1}; 4, toluene; 5, *o*-nitrotoluene, ordinate × 10^{-1}; 6, $(C_2H_5)_2O$, ordinate × 10^{-1}.

The value of K_2 for acetic acid in benzene may be compared with previously quoted figures. Pohl, Hobbs and Gross[13] found $K_2 = 0.0027$ at 30° for dry benzene by dielectric polarization measurements, which is equivalent to 0.0021 at 25° using the dependence of K_2 on temperature observed by Moelwyn-Hughes, *et al.*[2] Moelwyn-Hughes, how-

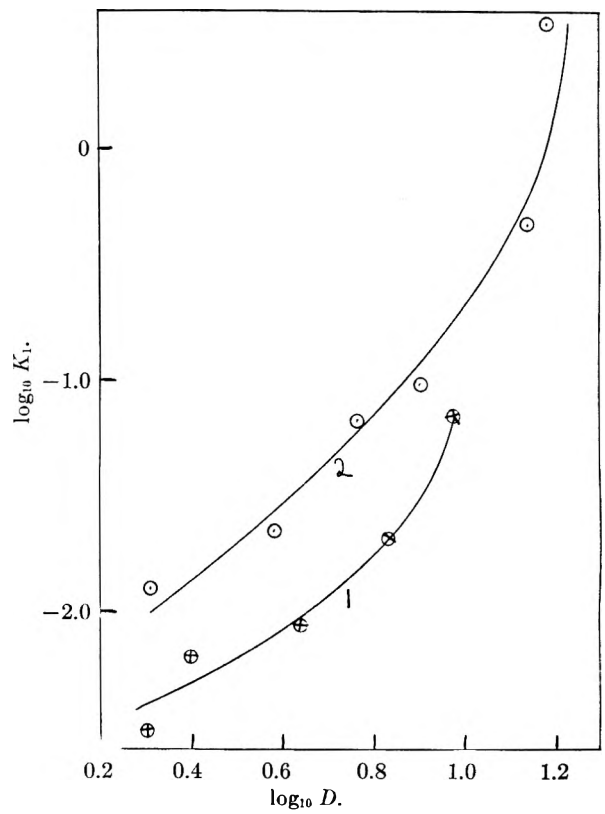

Fig. 3.—Effect of the dielectric constant of the organic solvent on K_1: 1, CH_2ClCO_2H; 2, CCl_3CO_2H.

(11) S. A. Bektourov, *Zhur. Obs. Khimii*, **9**, 419, 1717 (1939); F. S. Brown and C. R. Bury, *J. Chem. Soc.*, 2430 (1923); H. M. Dawson and F. E. Grant, *ibid.*, 512 (1902); W. Herz and H. Fischer, *Ber.*, **37**, 4747 (1904); **38**, 1143 (1905); W. Herz and M. Lewy, *Z. Elektrochem.*, **11**, 818 (1905); N. Lofman, *Z. anorg. Chem.*, **107**, 241 (1919); A. W. Smith and J. C. Elgin, THIS JOURNAL, **39**, 1149 (1935); E. Schreiner *Z. anorg. Chem.*, **122**, 203 (1922); H. W. Smith, THIS JOURNAL, **25**, 160 (1921).

(12) N. A. de Kolossowsky, *Bull. soc. chim.*, [4] **9**, 632 (1911); *Bull. soc. chim. Belg.*, **25**, 183, 235 (1911); N. A. de Kolossowsky, and F. S. Kulikov, *Z. physik. Chem.*, **A169**, 459 (1934); *Zhur. Obs., Khimii*, [4] **66**, 915, (1934); [5] **66**, 60, 1037 (1935).

(13) H. A. Pohl, M. E. Hobbs and P. M. Gross, *J. Chem. Phys.*, **9**, 408 (1941).

TABLE I

Organic solvent	CH_3CO_2H K_1	K_2	CH_2ClCO_2H K_1	K_2	$CHCl_2CO_2H$ K_1	K_2	CCl_3CO_2H K_1	K_2
Diethyl ether	0.46	2.8	1.05	0.022	0.48	0.32	...	...
Diisopropyl ether	.17	1.5	...	...	...	...	...	...
Chloroform	.020	0.089	0.009	.0008	...	...	0.023	0.0012
Benzene	.0060	0.0020	...	...	...	...	...	...
Toluene	...	...	.0075	.002	.017	.0037	.014	.0018
Cumene	...	...	...	...	...	...	.21	.19
Nitrobenzene	X	X	14	.56	.19	.019	.06	.0012
o-Nitrotoluene	X	X	...	...	.19	.042	.020	.0002
Ethyl bromide	...	...	.072	.29	...	...	.12	.014
Methyl iodide	...	...	.024	.061	...	...	.07	.015
n-Amyl alcohol	...	...	X	X	...	...	4.6	.13
Isoamyl alcohol	...	...	X	X	...	...	X	X
Benzyl alcohol	...	...	X	X	...	...	1.6	.036

ever, finds 0.00768[2] and 0.0060[1] at 25° using the partition method. For acetic acid in diethyl ether, Smyth, Rogers and Lindsley[14] find $K_2 = 2.8$, also in good agreement with the value in the table.

The distribution of the monomer favors the aqueous phase except in two cases, and for many solvents the dielectric constant ϵ seems to be decisive in fixing the value of K_1. Figure 3 shows log K_1 plotted against log ϵ for CH_2ClCO_2H and CCl_3CO_2H. Ethers show much higher values of K_1 than this relationship predicts, and this may be due to ability to form hydrogen bonds with the acids. Nitrobenzene and *o*-nitrotoluene show much lower values.

A small value of K_2 indicates that the acid exists largely as the dimer, and this is true generally in non-hydrogen bonding solvents of small ϵ. Ability of the solvent to form hydrogen bonds, and high dielectric constant, encourage the dissociation of the dimers. In a given solvent the more highly chlorinated acids are more highly associated. This is in agreement with the conclusion of Moelwyn-Hughes, *et al.*,[2] that the bonding in the dimers is largely electrostatic in nature.

(14) C. P. Smyth, H. E. Rogers and G. H. Lindsley, *J. Am. Chem. Soc.*, **52**, 1829 (1930).

THE INFRARED SPECTRA OF AMMONIA CHEMISORBED ON CRACKING CATALYSTS[1]

BY J. E. MAPES AND R. P. EISCHENS

The Beacon Laboratories of The Texas Company, Beacon, N. Y.

Received May 1, 1954

The infrared spectrum of chemisorbed ammonia was studied to determine whether the acidity of cracking catalysts results from protons supplied by the catalyst surface or whether it results from the ability of surface atoms to share an electron-pair from the ammonia, as in Lewis type acids. Characteristic absorption bands for both NH_3 and NH_4^+ appear in the spectrum of ammonia chemisorbed on a cracking catalyst which was preheated at 500°. The presence of chemisorbed NH_3 indicates that most of the acid centers are of the Lewis type where the unshared electron-pair of the nitrogen atom fills the electron-pair vacancy of the catalyst, without greatly altering the NH_3 configuration. The presence of adsorbed NH_4^+ is not proof of protonic acid centers, since the added proton may have come from water on Lewis acid centers.

Introduction

Extensive work reported in the literature shows that the activity of cracking catalysts results from the presence of acid centers on the catalyst surface. However, there is disagreement over whether these acid centers fall under the Brönsted or the Lewis definition of an acid. In the work reported here the infrared spectra of chemisorbed ammonia were studied to determine the type of catalyst acid.

Figure 1 shows the two basically different catalyst acid structures that have been proposed in the literature. Structure I, given by Thomas,[2] shows the cracking catalyst as a Brönsted acid. An aluminum ion, which has replaced a silicon ion, is bonded to four oxygens. Since aluminum has a valence of +3, an added proton is required to balance the charge. This proton is considered to be available to take part in reactions, hence the structure is a Brönsted acid.

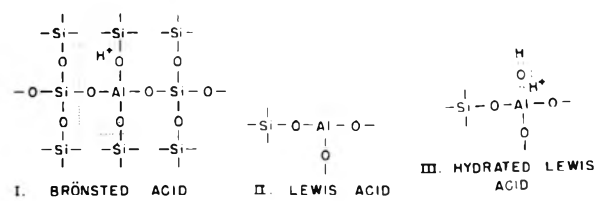

Fig. 1.—Suggested cracking catalyst acid structures from the literature.

Structure II, proposed by Milliken, Mills and Oblad,[3] shows the catalyst as a Lewis acid. Here

(1) Presented before the Catalysis Club of Philadelphia, March, 1953, and before the Petroleum Division of the American Chemical Society, September, 1953.

(2) C. L. Thomas, *Ind. Eng. Chem.*, **41**, 2564 (1949).

(3) T. H. Milliken, Jr., G. H. Mills and A. G. Oblad, *Faraday Soc. Discs.*, No. 8, 279 (1950).

the aluminum ion is bonded to three oxygens, leaving an electron-pair vacancy in its valence shell. This vacancy can be filled by sharing an electron-pair from a base, hence the structure is a Lewis acid.

Structure III, proposed by Tamele and Hansford,[4,5] shows the product formed when water reacts with structure II. The electron-pair vacancy of aluminum is filled by the sharing of one of the free electron-pairs of the oxygen in H_2O, making one of the protons of the water readily ionizable. Proponents of structure III agree with those of structure II regarding the underlying Lewis-acid catalyst structure, but they also agree with the proponents of structure I regarding the presence of ionizable protons on the catalyst surface.

The Brönsted and Lewis definitions are not adequate to describe solid acids where there is the question of underlying structure as well as that of whether there are protons or electron-pair vacancies on the catalyst surface Therefore, structure III will be referred to as a *hydrated Lewis acid* to distinguish it from structures I and II, with the understanding that it reacts as a Brönsted acid in situations which depend on the availability of protons.

In reacting with a Brönsted acid ammonia gains the available proton to form ammonium ion, converting the NH_3 configuration to NH_4^+. In reacting with a Lewis acid the nitrogen in ammonia shares its free electron-pair to fill the vacancy of the acid, thus maintaining the NH_3 structure. Infrared offers a means of distinguishing the two reactions. If NH_3 is indicated by the spectrum of chemisorbed ammonia the presence of Lewis acid centers is shown. If NH_4^+ is observed, the presence of protons on the catalyst surface is shown, but additional work is required to distinguish between structures I and III on the basis of the presence or absence of water.

Studies have been reported in the literature on the infrared absorption spectra of various finely-ground silicious materials in dry form[6-9] and on the spectra of adsorbed molecules.[10-13]

Experimental Apparatus and Procedure

An infrared spectrometer equivalent to the Perkin-Elmer Model 12C was used to obtain the infrared absorption spectra in this work. No change from routine operation of the instrument was required.

In order to heat the catalyst under vacuum, chemisorb ammonia and obtain the infrared spectrum without exposing the sample to moisture a special sample cell was required. Two cylindrical, polished CaF_2 discs were fitted into each end of a section of Pyrex tubing which formed the cell wall. A section of smaller tubing was fused to the inside as a spacer. The catalyst film was deposited on one of the CaF_2 windows by evaporation of an alcohol slurry. The cell was assembled, with the CaF_2 discs loosely in place, and held by Pyrex supports in a large Pyrex tube in a furnace, where it was heated and evacuated. Ammonia was then chemisorbed on the catalyst, and both CaF_2 windows were pushed in place and sealed with Apiezon W. During the sealing operation a continuous stream of nitrogen, dried through two large liquid nitrogen traps, was passed through the tube. The sample cell was then placed in the spectrometer and the spectrum was recorded at room temperature.

The catalyst was a fresh American Cyanamid MS-B silica-alumina cracking catalyst, having 10% alumina. The mean particle diameter[14] was 0.2 μ, obtained by grinding the catalyst in a mechanical mortar and pestle and separating by water sedimentation using the technique of Hunt, *et al.*,[8] as modified by Contos.[15]

As used here, chemisorbed ammonia is defined as that which remains adsorbed after pumping by means of a liquid nitrogen trap for two hours at 175°. The pump-off pressure is of the order of 10^{-4} mm. These conditions were chosen after extensive measurements in conventional adsorption apparatus, in order to ensure a minimum of physically adsorbed ammonia. Pure silica, which could not chemisorb ammonia but which would physically adsorb about the same amount as the silica–alumina catalyst, does not retain any ammonia after pumping at 175°. Under the specified conditions the finely ground catalyst chemisorbs 0.5 meq./g. The thickness of the catalyst film is about 1.5 mg./cm.^{2}. The ammonia used was dried by distillation from sodium before release into the furnace tube.

Results and Discussion

The infrared spectrum of the air-dried catalyst film, before heating in preparation for chemisorption, is shown in spectrum A of Fig. 2. Percentage absorption of radiation by the sample is plotted against wave length. The large amount of liquid water retained by the catalyst from the water sedimentation step is shown by the very strong band at 3.0 μ and the strong band at 6.2 μ. It is interesting to note that the band at 6.9 μ which is characteristic of NH_4^+ is found with the unheated sample. This band is due to a residue of NH_4^+ ions retained by the catalyst during its preparation. The bands in the 5.0–5.5 μ region are due to the catalyst which also has a strong absorption (not shown) starting at 8 μ.[8,9]

Spectrum B of Fig. 2 shows the catalyst after heating at 500° under vacuum for 24 hours. In this blank run NaCl windows were used. NaCl is not satisfactory at this temperature because evaporation of the salt roughens the polished surfaces, causing scattering of the radiation at shorter wave lengths. The OH and H_2O bands at 2.8 and 6.2 μ in (B) are reduced to very small absorbance values. The 3.0 μ band of associated OH is completely removed. The cell had a slow leak in this run and a small part of the observed water may have been picked up through this leak after heating. The NH_4^+ band at 6.9 μ has practically disappeared. Chemisorption measurements show that chemisorbed ammonia would be removed under the conditions of this run.

Spectrum C of Fig. 2 shows a catalyst on which ammonia was chemisorbed after the sample had been heated at 500° under vacuum for 20 hours. It is primarily from this spectrum, and additional confirmatory runs, that the conclusions of this work are drawn. Bands attributed to the chemisorbed am-

(4) M. W. Tamele, *Faraday Soc. Discs.*, No. 8, 270 (1950).

(5) R. C. Hansford, "Advances in Catalysis," Vol. IV, Academic Press, Inc., New York N. Y., 1952, p. 1.

(6) J. M. Hunt, Prelim. Rept. No. 8, API Project 49, Section III, 1950.

(7) W. D. Keller and E. E. Pickett, *ibid.*, Section IV.

(8) J. M. Hunt, M. P. Wisherd and L. C. Bonham, *Anal. Chem.*, **22**, 1478 (1950).

(9) P. J. Launer, *Am. Mineralogist*, **37**, 764 (1952).

(10) L. N. Kurbatov and G. C. Nueimin, *Doklady Akad. Nauk S. S. S. R.*, **68**, 341 (1949).

(11) N. G. Yaroslavskii and A. N. Terenin, *ibid.*, **66**, 885 (1949).

(12) N. G. Yaroslavskii and A. V. Karayakin, *ibid.*, **85**, 1103 (1952).

(13) G. C. Pimentel, C. W. Garland and G. Jura, *J. Am. Chem. Soc.*, **75**, 803 (1953).

(14) Determined from electron micrographs by H. M. Allred of these laboratories.

(15) G. A. Contos, Columbia University, private communication.

monia are found at 3.0, 3.3, 6.1 and 6.9 μ. The 6.1 μ band is superimposed on the position of the 6.2 μ water band which may have been present prior to the addition of ammonia. Since there was no increase in the 2.8 μ OH band over that in (B) all of the increase at 6.1 μ is attributed to chemisorbed ammonia.

The strongest bands characteristic of the N–H stretching and N–H bending vibrations of the NH_3 structure are observed at 3.00 and 6.14 μ in ammonia gas[16] and at 2.96 and 6.08 μ in solid ammonia.[17] The corresponding bands for the NH_4^+ structure, which vary considerably in wave length depending on the compound, are observed in the regions 3.0–3.5 and 6.8–7.2 μ.[18–20] The NH_4^+ bands are most commonly found at about 3.2 and 7.0 μ. Comparison of the bands of chemisorbed ammonia with those reported in the literature for conventional compounds indicates that the bands at 3.3 and 6.9 μ in the chemisorption spectra represent ammonia which is in the form of NH_4^+ ions. The strong band at 3.0 μ and the superimposed band at 6.1 μ represent ammonia which is bonded to the catalyst in such a way that its structure is similar to the pyramidal structure of gaseous ammonia.

The 6.9 μ band in (A) gives a rough measure of the absorption at this position when the catalyst is saturated with water and all of the ammonia is in the NH_4^+ form. Since the 6.9 μ band in (C) is much smaller, it appears that most of the chemisorbed ammonia is in the NH_3 form in the dry catalyst. This conclusion is also supported by the fact that the 3.0 μ band in (C) is larger than the 3.3 micron band. The spectral evidence that most of the chemisorbed ammonia is in the NH_3 form shows that most of the catalyst acid is of the Lewis type illustrated by structure II in Fig. 1. The weaker NH_4^+ band shows the presence of protons on the catalyst surface but does not show whether they originate as Brönsted acid (structure I in Fig. 1) or hydrated Lewis acid (structure III). To assume the protons are from Brönsted acid centers requires the coexistence of the two basically different catalyst structures having the four-coördinated and three-coördinated aluminum. On the other hand, both the water and Lewis acid centers, which are needed to form hydrated Lewis acid, are observed in samples under these conditions.

It is impossible to determine if any water is present from (C) since the 2.8 μ OH band may represent only single OH groups on the surface Si atoms. The 6.2 μ band characteristic of H_2O but not single OH groups is obscured by the ammonia band. The amount of water shown in (B) and other infrared spectra of the dried catalyst may be more than that which is present at 500°, since all deficiencies in technique tend to increase the amount of water on the catalyst. A thoroughly dried catalyst picks up moisture extremely rapidly. Exposure of a dried sample for 40–50 seconds in air caused a sixfold increase in the strength of the 2.8 μ OH band.

(16) G. Herzberg, "Infrared and Raman Spectra of Polyatomic Molecules," D. Van Nostrand Co., Inc., New York, N. Y., 1945, p. 295.
(17) F. P. Reding and D. F. Hornig, *J. Chem. Phys.*, **19**, 594 (1951).
(18) L. F. H. Bovey, *Opt. Soc. Am.*, **41**, 836 (1951).
(19) D. Williams, *J. Am. Chem. Soc.*, **64**, 857 (1942).
(20) F. A. Miller and C. H. Wilkins, *Anal. Chem.*, **24**, 1253 (1952).

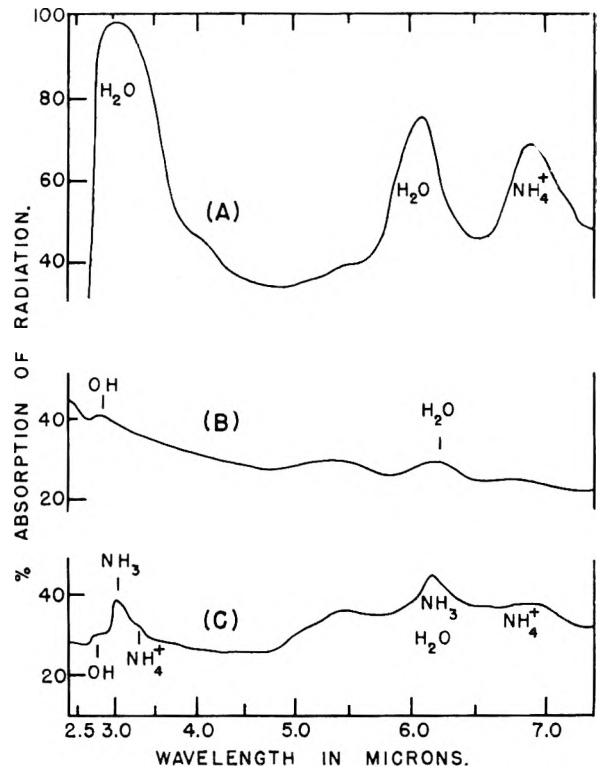

Fig. 2.—Infrared spectra of unheated catalyst (A); catalyst dried at 500° under vacuum (B); and dried catalyst with chemisorbed ammonia (C).

Although it is surprising to find that the catalyst dried at 500° shows evidence of water in addition to surface OH's and it is reasonable to attribute its presence to deficiencies in the sealing technique, there is no proof that the technique is faulty. The water indicated by the 6.2 micron band in (B), may be occluded within the body of the catalyst so that it could not be removed without drastic rearrangement of the catalyst structure.

Partial rehydration of the catalyst containing chemisorbed ammonia provides confirmatory evidence for the interpretation of these spectra. Rehydration would be expected to produce an increase in the 6.9 μ band due to the formation of hydrated Lewis acid sites and a corresponding decrease in the 3.0 and 6.1 μ NH_3 bands. The increase in the 6.9 μ band is observed. This is strong evidence that NH_4^+ ions were formed at the expense of chemisorbed NH_3 molecules. However, it is difficult to observe a corresponding decrease in the NH_3 bands at 3.0 and 6.1 μ because both of these bands are superimposed on bands which increase with increased hydration.

The band at 2.8 μ is characteristic of OH groups under conditions where only a small degree of association is possible. This holds for OH groups occurring singly as in dilute solutions of alcohols,[21] and for the OH groups of dilute solutions of water in CCl_4.[22] With increasing association the band shifts to a maximum at 3.0 μ, as in concentrated alcohol solutions or liquid water. Figure 3 shows the

(21) F. A. Smith and E. C. Creitz, *J. Research Natl. Bur. Standards*, **46**, No. 2 (1951).
(22) L. Kellner, "Report on Progress in Physics," Vol. XV, The Physical Society, London, 1952, p. 3.

unmistakable difference between the appearance of the OH band of a partially hydrated catalyst and the OH band with chemisorbed ammonia superimposed. When the catalyst is dried and then rehydrated in successive steps, the OH bands of increasing strength in the spectrum at the left of Fig. 3 are obtained. If at a certain level of OH content ammonia is chemisorbed on the catalyst, the relatively sharp band of adsorbed NH_3 is superimposed on the OH band to give the spectrum shown on the right.

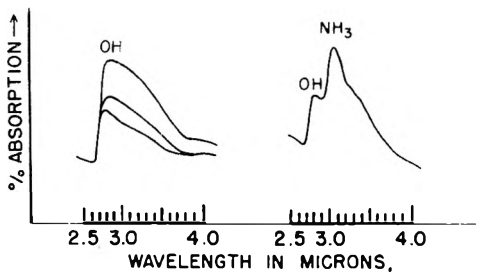

Fig. 3.—Catalyst spectra showing comparison of ammonia and hydroxyl bands.

The O–H bending peak for water shifts from 6.10 to 6.23 with decreasing hydration (compare spectra A and B in Fig. 2). This shift is in the direction expected from a decrease in the hydrogen bonding effect on a bending vibration. Drying the catalyst shifts the peak of the Si–O stretching band from 9.26 to 9.15 μ. This shift to shorter wave lengths may be due in part, or entirely, to the higher stretching frequency for the Si–O–Si structure compared to Si–OH. It could also be due to the typical hydrogen bonding effect on stretching vibrations caused by hydrogen bonding between adjacent Si–OH groups or between these groups and adsorbed H_2O.

Experiments with an improved infrared sample cell are planned to measure the amounts of water and OH groups on the catalyst under controlled conditions and to determine the origin of protons on the catalyst. This will remove the uncertainty from the interpretation of the NH_4^+ bands. Despite this uncertainty the infrared method has successfully shown by the results of these experiments that most of the catalyst acid is of the Lewis type.

We wish to thank Dr. L. C. Roess for his suggestion that we undertake a study of the infrared spectra of molecules adsorbed on solids, and Dr. S. A. Francis for his help in interpreting the infrared spectra.

THE INTERACTION OF ORGANO-PHOSPHORUS COMPOUNDS WITH SOLVENTS AND CELLULOSE ACETATE

BY A. L. GEDDES

Communication No. 1651 from the Kodak Research Laboratories, Eastman Kodak Company, Rochester, N. Y.

Received May 8, 1954

The infrared spectra of several organo-phosphorus compounds in various solvents and in cellulose acetate are reported, and band-frequency assignments in the region 2 to 15 μ are discussed. Information on molecular interaction is obtained from the band-frequency shifts which result from changes in environment of the molecules. The results are interpreted as evidence for (1) hydrogen-bonding between hydroxyl and phosphoryl groups and (2) dipolar interaction between phenyl and carbonyl groups. The infrared method offers a means of approach to a better understanding of the process of plasticization.

Introduction

Molecular interaction forces have an important function in the process of plasticization.[1,2] These forces are, in effect, responsible for the existence of solvent and non-solvent plasticizer types and for variations in the state of dispersion. A study of the mechanism of plasticization of plastics, such as cellulose acetate, emphasizes certain aspects of plasticizer performance, such as compatibility, permanence and efficiency.[3] These properties are all interrelated inasmuch as they are all affected by interaction of the component molecules.

A theoretical treatment of the subject of molecular interaction in high-polymer solutions was developed independently by Huggins[4] and Flory[5] in 1942. As a result, an interaction constant (μ) was introduced which is a measure of solvent power or of interaction forces between solvent and solute molecules. Interaction constants of dilute polymer solutions can be determined experimentally.[6–9] However, in concentrated plastic systems, the experimental difficulties encountered are formidable and the application of μ values of dilute solutions to concentrated solutions involves an uncertainty because of the concentration-dependence of μ.[7]

Several experimental methods have been employed for the study of interaction forces in solutions and in plastic systems.[10–14] These provide valuable information, even though it is not sufficient for the evaluation of interaction constants. In this connection, the application of infrared spectrometry as a method of approach is particularly attractive because of its simplicity. Molecular in-

(1) D. Faulkner, *Brit. Plastics*, **23**, 183 (1950).
(2) W. E. Gloor and C. B. Gilbert, *Ind. Eng. Chem.*, **33**, 597 (1941).
(3) R. F. Boyer, *J. Appl. Phys.*, **20**, 540 (1949).
(4) M. L. Huggins, *Ann. N. Y. Acad. Sci*, **43**, 1 (1942).
(5) P. J. Flory, *J. Chem. Phys.*, **10**, 51 (1942).
(6) G. Gee and L. R. Treloar, *Trans. Faraday Soc.*, **38**, 147 (1942).
(7) M. L. Huggins, *Ann. N. Y. Acad. Sci.*, **44**, 431 (1943).
(8) R. H. Blakey and R. M. Badger, *J. Am. Chem. Soc.*, **72**, 3129 (1950).
(9) P. Doty and H. S. Zahle, *J. Polymer Sci.*, **1**, 90 (1946).
(10) A. K. Doolittle, *Ind. Eng. Chem.*, **38**, 535 (1946).
(11) M. L. Huggins, *J. Appl. Phys.*, **14**, 246 (1943).
(12) G. M. Kosolapoff and J. F. McCollough, *J. Am. Chem. Soc.*, **73**, 5392 (1951).
(13) F. Wurstlin, *Kolloid Z.*, **105**, 9 (1943).
(14) R. F. Boyer and R. S. Spencer, *J. Polymer Sci.*, **2**, 157 (1947).

teraction forces cause changes in frequency and intensity of infrared absorption bands. This communication describes the results obtained in a study of a series of organo-phosphorus compounds dispersed in cellulose acetate and in various solvents.

Experimental

The following five organo-phosphorus compounds were chosen for the investigation.

Triphenyl phosphate	$(C_6H_5—O)_3P=O$
Tributyl phosphate	$(C_4H_9—O)_3P=O$
Triphenyl phosphite	$(C_6H_5—O)_3P$
Triphenyl phosphine oxide	$(C_6H_5)_3P=O$
Triphenyl phosphine	$(C_6H_5)_3P$

Systematic changes in different parts of the basic molecular structure facilitate the valuation of interaction effects of different functional groups. All of the chemicals were Eastman Kodak Co. grade except the sample of triphenylphosphine oxide, which was obtained from Dr. C. F. H. Allen, of the Organic Chemistry Department, Research Laboratories, Eastman Kodak Company.

The cellulose esters were obtained from the Cellulose Acetate Development Division, of the Eastman Kodak Company. The two samples used for most of the work were dope-acetylated acetates containing 23.5 and 43.5% acetyl. Since the acetyl content of these samples is close to the theoretical values of 21.1 and 44.8% for the mono- and triacetates, respectively, the samples will be referred to as cellulose monoacetate and cellulose triacetate A. Some observations were also made on a sample of fibrously acetylated Schering cellulose triacetate B (44.3% acetyl). Attempts to study interaction effects with dextrose, sucrose and dextrose pentaacetate were unsuccessful because of incompatibility of the plasticizers. The compatibility of triphenyl phosphate with sucrose octaacetate was found sufficient for measurements to be made.

Infrared absorption measurements were made in the spectral range from 2 to 15 μ (microns) with a Perkin-Elmer Model 12C Spectrophotometer equipped with a rock salt prism. Reproducibility was found to be of the order of 0.01 μ in the longer wave length region.

The liquid samples were run in calibrated rock salt absorption cells. The cellulose ester and sucrose octaacetate samples were prepared in the form of solid films by coating from solution on rock salt or silver chloride plates. Excess solvent was effectively removed from the films by air-drying at 90°. Spurious absorption bands arising from interference effects were not found to be troublesome. In most cases, the spectra of the medium both with and without plasticizer were run on the same chart to facilitate the accurate location of the plasticizer bands in regions where overlapping of the bands occurs.

Results

The spectra of the plasticizers in carbon disulfide solution and the spectra of cellulose monoacetate and triacetate are shown schematically in Fig. 1. The vertical lines indicate the peak positions and relative intensities of the bands.

It was observed that some of the bands of the plasticizers are not appreciably affected by changes in the environment of the molecules, but others do exhibit considerable changes in frequency. The peak positions of the bands that undergo displacement are shown in Figs. 2 to 7. Triphenyl phosphate was studied in seven different types of solvents as well as sucrose octaacetate and cellulose acetate. Since the primary interest was in the interaction effects of hydroxyl groups and acetyl groups, however, the selection of solvents for the other compounds was limited to alcohols and esters, and the non-polar solvent carbon disulfide for reference purposes. Solvents were selected having absorption characteristics such as to minimize the interference of band overlapping. The absorption of cellulose acetate is relatively low in the long wave length region and, in most cases, does not seriously interfere with the identification of any of the main plasticizer bands in the plasticized samples.

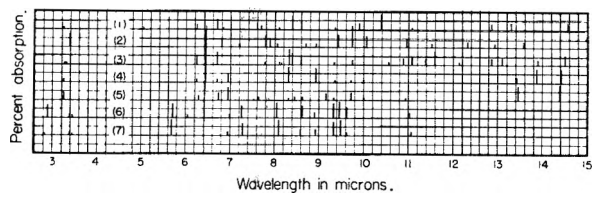

Fig. 1.—Spectra of plasticizers in carbon disulfide solution: 1, triphenyl phosphate; 2, tributyl phosphate; 3, triphenyl phosphite; 4, triphenylphosphine oxide; 5, triphenylphosphine; 6, spectrum of cellulose monoacetate film; 7, spectrum of cellulose triacetate film.

Discussion

Band Assignments.—Vibrational assignments of the absorption bands of the plasticizers are desirable for the interpretation of the spectral data. These have been made empirically on the basis of a survey of a large number of spectra of phosphorus compounds discussed in the literature[15-18] and recorded in the files of the Eastman Kodak Company. Assignments can thus be given with considerable confidence but some changes may be in order when further pertinent information is available.

Referring to Fig. 1, we find the C–H stretching bands in the 3.4 μ region. The characteristic bands near 6.3 and 6.7 μ appear in the spectra of all of the compounds containing a phenyl ring. The bands in the 6.8 to 7.3 μ region arise mainly from C–H deformation vibrations. The covalent P=O bonds give rise to absorption in the 8 μ region, and a shift in the frequency of this band by hydrogen-bonding aids in its identification. This band sometimes appears as a doublet. In triphenylphosphate, tributyl phosphate and triphenylphosphine oxide, it appears at 7.6, 7.8 and 8.3 μ, respectively. The position of this band is dependent upon the electronegativity of the other groups attached to the phosphorus atom; the lower the electronegativity, the longer will be the wave length of the band.

Our knowledge of C–O–C and Si–O–C band assignments in the 8 to 10 μ region is helpful in the identification of bands arising from the P–O–C linkage. Richards and Thompson[19] have reported that the Si–O stretching band is usually found between 9.0 and 9.5 μ. The analysis indicates that in triphenyl phosphate the three bands at 8.40, 8.60 and 9.72 μ are associated with the C–O groups. Triphenyl phosphite has the same three bands plus an additional one at 8.31 μ. Replacement of the phenyl groups with alkyl groups displaces the C–O bands to longer wave lengths, the degree of displacement depending upon the size of the substitu-

(15) M. Halmann and S. Pinchas, *J. Chem. Soc.* (*London*), 626 (1953).

(16) L. J. Bellamy and L. Beecher, *ibid.*, 728 (1953).

(17) L. W. Daasch and D. C. Smith, *Anal. Chem.*, **23**, 853 (1951).

(18) C. I. Meyrick and H. W. Thompson, *J. Chem. Soc.* (*London*), 225 (1950).

(19) R. E. Richards and H. W. Thompson, *ibid.*, 124 (1949).

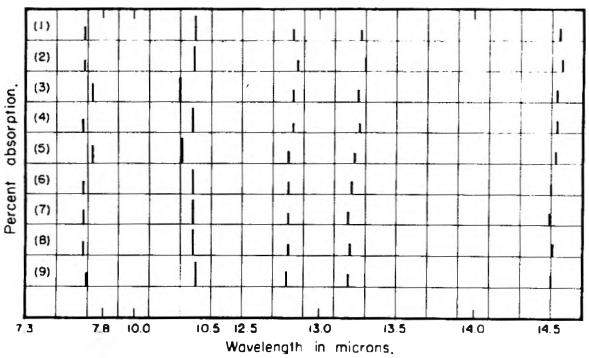

Fig. 2.—Band positions of triphenyl phosphate in various media: 1, (liquid state); 2, carbon disulfide; 3, *n*-amyl alcohol; 4, *n*-butyl ether; 5, isobutyric acid; 6, methyl isobutyl ketone; 7, propionaldehyde; 8, *sec*-butyl acetate; 9, sucrose octaacetate.

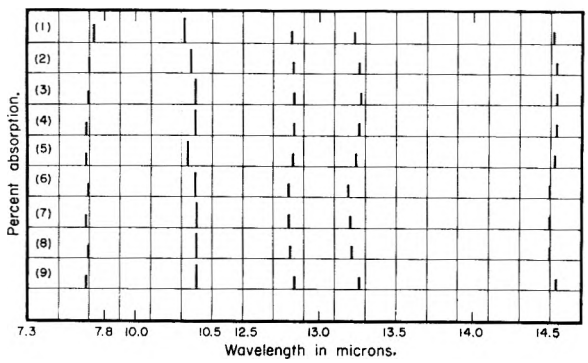

Fig. 3.—Band positions of triphenyl phosphate in cellulose esters: 1, 5% in monoacetate coated from acetone–water; 2, 20% in monoacetate coated from acetone–water; 3, 80% in monoacetate coated from acetone–water; 4, 20% in monoacetate coated from formic acid; 5, 20% in monoacetate coated from trifluoroacetic acid; 6, 20% in triacetate A coated from methylene chloride–methyl alcohol; 7, 20% in triacetate B coated from methylene chloride–methyl alcohol; 8, 30% in triacetate A coated from formic acid; 9, 30% in triacetate A coated from trifluoroacetic acid.

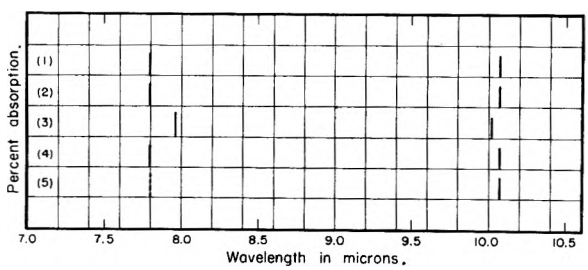

Fig. 4.—Band positions of tributyl phosphate in various media: 1, (liquid state); 2, carbon disulfide; 3, isoamyl alcohol; 4, *sec*-butyl acetate; 5, cellulose triacetate film.

ent group. In tributyl phosphate, these bands appear at 9.43 and 9.72 μ.

In triphenyl phosphate and tributyl phosphate, the P–O bands are found at 10.40 and 10.07 μ, respectively. The observation that H-bonding of the P=O groups is accompanied by a shift of the P–O bands to higher frequency, as expected, aids in their identification. In triphenyl phosphite, the band is located at 11.6 μ. In this case, the absence of the phosphoryl oxygen increases the electronegativity of the phosphorus atom and causes the P–O shift to the longer wave length region.

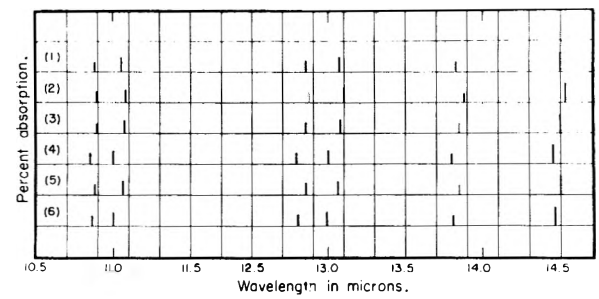

Fig. 5.—Band positions of triphenyl phosphite in various media: 1, (liquid state); 2, carbon disulfide; 3, isoamyl alcohol; 4, isopropyl acetate; 5, cellulose monoacetate film; 6, cellulose triacetate film.

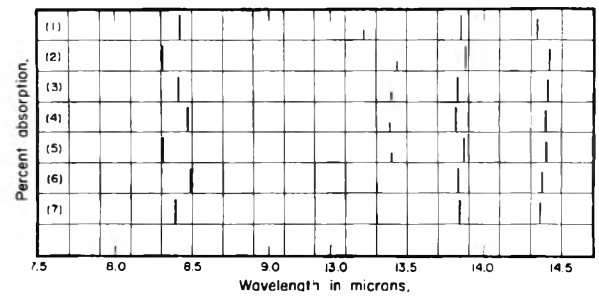

Fig. 6.—Band positions of triphenylphosphine oxide in various media: 1, (solid state); 2, carbon disulfide; 3, *sec*-butyl alcohol; 4, isobutyric acid; 5, isobutyl acetate; 6, cellulose monoacetate film; 7, cellulose triacetate film.

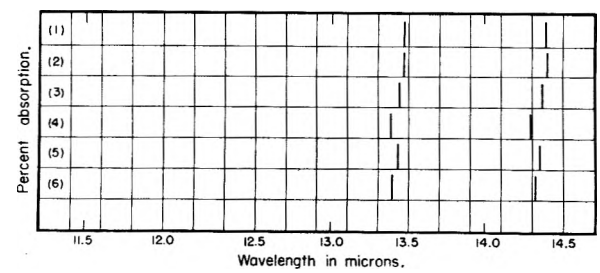

Fig. 7.—Band positions of triphenylphosphine in various media: 1, (solid state); 2, carbon disulfide; 3, isopropyl alcohol; 4, methyl acetate; 5, cellulose monoacetate film; 6, cellulose triacetate film.

The P–C bonds in the phosphine compounds, associated with aromatic groups, give rise to a weak band at 10.0 μ and a strong band at longer wave lengths. In general, C–C vibrations absorb in the 9 μ region and Si–C vibrations near 12.5 μ, so the strong P–C bands would be expected to be found in the region above 12.5 μ. In triphenylphosphine oxide, this band appears at 13.9 μ. Since it is not in evidence in the spectrum of triphenylphosphine, it is probably shifted to the region above 15 μ because of the higher electronegativity of the phosphorus atom.

The two characteristic phenyl bands are readily identifiable near 14.5 μ and in the 13.0 to 13.5 μ region. Phenyl groups also exhibit weak bands in the 8.5 to 9.5 μ region, so some of the weak bands in these spectra may arise from this source. In the case of tributyl phosphate, the two bands near 12.5 and 13.6 μ are associated with the butyl group.

Interaction Effects.—Although the vibrational frequencies of functional groups in molecules are remarkably constant under different conditions of environment, it is well known that infrared spectra

are modified by the influence of electronic force fields in the vicinity of the oscillating molecules. The effect is evident, for example, in the band frequency and intensity changes which occur when a compound is changed from the gaseous to the liquid or the solid state. The frequency shifts may be to either higher or lower values, depending upon the disposition of the forces involved.[20] Molecular interaction results from the electrostatic attractive forces between sets of oscillating dipoles. Strong interaction, such as H-bonding, may cause band shifts not only of the functional groups involved but in other regions as well, owing to the over-all change in charge distribution in the molecule. The magnitude of the band displacement is a measure of the strength of the interaction forces involved.

Band shifts in the spectra of **triphenyl phosphate** are shown in Figs. 2 and 3. In carbon disulfide solution, the effects of interaction forces are minimized. Hydrogen-bonding[12] in alcoholic or acid solution is evident by a shift of the P=O band near 7.7 μ to longer wave lengths and a corresponding shift of the P–O band near 10.4 μ to shorter wave lengths. The shift of the P–O stretching band to higher frequency is to be expected if H-bonding of the P=O group increases the electron-accepting power of the phosphorus atom. Hydrogen-bonding is evident at low concentrations in cellulose monoacetate, but the effect rapidly diminishes as the concentration is increased. This may be due to the inability of the O–H and P=O groups to become arranged in close proximity. However, in view of the fact that no interaction is indicated in the long wave length region, and the spectrum becomes almost identical with that of the liquid phase, the indications are that most of the plasticizer is dispersed as a non-solvent type in cellulose monoacetate.

Dipolar interaction between triphenyl phosphate and the various solvents is indicated by a shift of bands in the long wave length region, especially of the phenyl bands, to higher frequencies (Fig. 2). It is interesting to note that the interaction is greater in solvents containing carbonyl groups than in alcohols or ethers. Apparently the magnitude of the band shift is dependent upon the electron-donating power of the oxygen. Interaction between carbonyl groups and phenyl groups is not unreasonable in view of the polarizability of the latter. In cellulose triacetate, this interaction is fairly strong, which may account for the high compatibility of the plasticizer, even though strong H-bonding centers, such as OH groups provide, are not present to an appreciable extent.

It is of interest to mention some observations made on the effect of the coating solvent on the interaction of triphenyl phosphate with cellulose acetate (Fig. 3). A film of monoacetate containing 20% plasticizer and coated from formic acid, displays less H-bonding than a similar sample from acetone–water solution. This may be due partially to further esterification by the formic acid and partially to the enhanced crystallinity in the coating from formic acid. Owing to the more compact structure of the crystalline regions, the concentration of plasticizer in the amorphous regions is increased. Coatings of the monoacetate from the trifluoroacetic acid exhibit slightly more phenyl group interaction and a shift of the P–O band to higher frequency, but very little change in the P=O band. This irregularity is believed to be due to further esterification of the monoacetate. In the case of cellulose triacetate, the phenyl group interaction is progressively decreased as the coating solvent is changed from methylene chloride to formic acid to trifluoroacetic acid. It is probable that this effect is due to enhanced crystallinity of the triacetate. The spectra of triphenyl phosphate in triacetates A and B are the same if both esters are coated from the same solvent.

Tributyl phosphate is a relatively inactive plasticizer. The spectra in Fig. 4 indicate strong H-bonding in alcohol solution between O–H and P=O groups, by the P=O and P–O band shifts, but no other spectral changes are in evidence. This inactivity accounts for the low compatibility in cellulose acetate. In the monoacetate, the compatibility was found to be so low that absorption measurements were not feasible, and in the triacetate the limit was of the order of only 10%. The incompatibility may be explained by the low polarizability and low electron-accepting power of the alkyl radical, which does not favor interaction with oxygen donor atoms of the cellulose acetate. It might be expected that H-bonding of the P=O groups with OH groups of the monoacetate would appreciably enhance the compatibility. The observation that it does not provides further evidence that phenyl group interaction plays an important rôle in plasticizer performance, since triphenyl phosphate has good compatibility.

In the spectra of **triphenyl phosphite** (Fig. 5), the P–O band at 11.6 μ is not shifted under the different conditions of environment of the molecule, because active P=O hydrogen-bonding centers are not present in this compound. However, in the 10 to 15 μ region a number of bands are shifted to higher frequency by molecular interaction. These include the prominent phenyl bands near 13.1 and 14.5 μ. As in the case of triphenyl phosphate, the strongest interaction is between phenyl groups and carbonyl groups, and the results are consistent with the observation that the interaction is greater with cellulose triacetate than with cellulose monoacetate.

The spectral characteristics of **triphenyl phosphine oxide** (Fig. 6) are of particular interest because of the high polarity of the molecule. Strong H-bonding of the P=O groups takes place in all media containing O–H groups; even in cellulose monoacetate which shows very little H-bonding with triphenyl or tributyl phosphate. The reasons proposed for this are that the phosphine oxide molecules are more compact and can more easily penetrate the polymer structure and that the phosphoryl oxygen is more negative and has greater H-bonding strength when the ester oxygen atoms are absent. The shift of the P=O band is accompanied by a shift of the P–C band near 13.9 μ to higher frequency. This shift is to be expected for the same reason that the observed P–O band shift occurs in triphenyl phosphate. This observation also helps to

(20) M. Davies, *J. Chem. Phys.*, **16**, 267 (1948).

verify the assignment of the P–C frequency. It is interesting to note that the spectrum of the solid phase indicates intermolecular bonding between the P=O and the phenyl groups. As explained in the previous cases, interaction between the phenyl groups and the donor oxygen atoms is evident in the 13.4 and 14.4 μ regions, especially in the case of the cellulose esters. Similar phenyl band shifts are also apparent in the spectra of **triphenylphosphine** (Fig. 7).

In general, the evidence obtained of molecular interaction effects in the systems studied is self-consistent. The prominent effects observed appear to be associated with (1) hydrogen bonding between hydroxyl and phosphoryl groups and (2) dipolar interaction between phenyl groups and carbonyl groups. Interaction forces of this nature play an important rôle in the mechanism of plasticization.

CONDUCTANCES OF SALTS IN 1:2 ETHYLENEDIAMINE–METHANOL SOLUTIONS IN THE TEMPERATURE RANGE −20 TO 20°[1]

BY LYLE R. DAWSON AND WILLIAM M. KEELY

Contribution from the Department of Chemistry, University of Kentucky, Lexington, Ky.

Received May 10, 1954

Conductances of silver nitrate, strontium bromide, potassium, silver and strontium iodides, and magnesium, strontium and barium chlorides in the temperature interval −20 to 20° have been measured. The uni-univalent salts are somewhat associated, with silver iodide having the lowest dissociation constant. All unsymmetrical salts studied behave as incompletely dissociated uni-univalent electrolytes. The alkaline earth chlorides exhibit increased association as the atomic number of the metal decreases, paralleling their behavior in pure methanol. As the temperature is lowered, the Walden product decreases and the dissociation constant becomes greater.

In an earlier paper,[2] evidence was presented which indicated that the alkaline earth halides behave like comparatively strong bi-univalent electrolytes at low concentrations in methanol. Reported herein are data relative to the conductance of some of these salts, also silver nitrate, silver iodide and potassium iodide, in a mixed solvent consisting of a 1:2 mole ratio of ethylenediamine to methanol. The mixed solvent provided a medium for studying the influence of dielectric constant, viscosity and the nature of the solvent on the properties of the solution.

Hartley and associates[3] have reported rather extensive investigations on the conductance behavior of the alkali halides and the alkaline earth thiocyanates in methanol. Recently data for sodium and potassium chlorides in anhydrous methanol have been reported by Butler, Schiff and Gordon.[4] Isbin and Kobe[5] and Bromley and Luder[6] have studied solutions of electrolytes in ethylenediamine.

Experimental

The purification of the salts and of methanol, the apparatus employed, and the experimental procedures have been described previously.[2]

Eastman Kodak Co. ethylenediamine was stored over sodium hydroxide for several days, then kept over sodium for one day and finally distilled over fresh sodium. All-glass connections were used throughout. The specific conductance of the ethylenediamine used in this investigation ranged from 7.5×10^{-7} to 9.0×10^{-7} ohm^{-1} cm.$^{-1}$ at 20°. Physical properties of ethylenediamine at 20° are as follows: density = 0.895; viscosity = 0.0185 poise (referred to methanol as 0.00593 at 20°); dielectric constant = 15.1.

The mixed solvent was prepared by combining weighed quantities of the components; solutions were prepared on a weight basis also. All transfers were made in a dry atmosphere. The maximum value of the specific conductance of the mixed solvent was 1.0×10^{-6} ohm^{-1} cm.$^{-1}$.

TABLE I

PROPERTIES OF THE MIXED SOLVENT 1:2 ETHYLENEDIAMINE–METHANOL

Temp., °C.	−20	0	20
Density, g./ml.	0.9211	0.9025	0.8829
Viscosity, poise	0.0837	0.0324	0.0167
Dielectric constant	35.7	31.1	27.2

TABLE II

RESULTS DERIVED FROM CONDUCTANCE DATA ON SOLUTIONS OF SALTS IN 1:2 ETHYLENEDIAMINE–METHANOL

Salt	Temp., °C.	Λ_0	$\Lambda_{0\eta}$	Dissociation constant × 10^3	$a \times 10^8$
KI	20	96.5	1.60	1.47	1.83
$AgNO_3$	20	84.1	1.41	1.95	1.91
	0	41.3	1.34	1.58	1.69
AgI	20	63.9	1.07	1.09	1.75
	0	31.7	1.03	1.48	1.67
$MgCl_2$	20	85.2	1.42	0.98	1.73
	0	42.7	1.38	1.45	1.67
	−20	15.2	1.27	2.36	1.65
$SrCl_2$	20	86.6	1.44	1.42	1.82
	0	43.7	1.42	1.63	1.70
	−20	16.0	1.34	2.45	1.66
$SrBr_2$	20	96.0	1.54	1.66	1.87
	0	47.6	1.54	2.83	1.83
SrI_2	20	94.0	1.57	1.62	1.86
	0	51.1	1.66	2.35	1.83
$BaCl_2$	20	94.2	1.57	1.47	1.83
	0	53.2	1.72	1.44	1.67
	−20	18.5	1.55	1.94	1.59

(1) This work was supported in part by a research contract with the U. S. Army Signal Corps, Fort Monmouth, New Jersey.

(2) L. R. Dawson and W. M. Keely, *J. Am. Chem. Soc.*, **73**, 3783 (1951).

(3) (a) A. Unmack, E. Bullock, D. A. Murray-Rust and H. Hartley, *Proc. Roy. Soc.* (*London*), **A132**, 351 (1925); (b) J. E. Frazer and H. Hartley, *ibid.*, **A109**, 351 (1925); (c) A. Unmack, D. M. Murray-Rust and H. Hartley, *ibid.*, **A127**, 228 (1928); (d) T. H. Mead, O. L. Hughes and H. Hartley, *J. Chem. Soc.*, 1207 (1933).

(4) J. P. Butler, H. I. Schiff and A. R. Gordon, *J. Chem. Phys.*, **19**, 752 (1951).

(5) H. Isbin and K. A. Kobe, *J. Am. Chem. Soc.*, **67**, 464 (1945).

(6) W. H. Bromley and W. F. Luder, *ibid.*, **66**, 107 (1944).

Results

The conductance of the solution was corrected by subtracting the conductance of the pure solvent, and the data represent averages of confirmatory determinations made on separate solutions prepared independently. Blank runs on pure solvent carried through all of the transfers involved in a typical series of determinations showed that the resistance did not change more than 0.15%.

Summaries of pertinent data are presented in Tables I and II.

Discussion

The conductance curves resulting from plotting the equivalent conductance, Λ, as a function of the square root of the concentration, C, in moles per liter, all display slopes greater than would correspond to the limiting Onsager equation for strong electrolytes in this solvent mixture (Figs. 1–6). Therefore, it may be assumed that some degree of ion association is present in all of these systems. Accordingly, the Shedlovsky[7] extrapolation method was used to determine the limiting equivalent conductance, Λ_0, and to calculate the dissociation constant, K, in each case. From the K-values, the effective electrostatic radii a were calculated by the method of Fuoss and Kraus.[8] Since the molar conductance of strontium iodide in 1:2 ethylenediamine–methanol is approximately equal to that of potassium iodide, and considerably less than

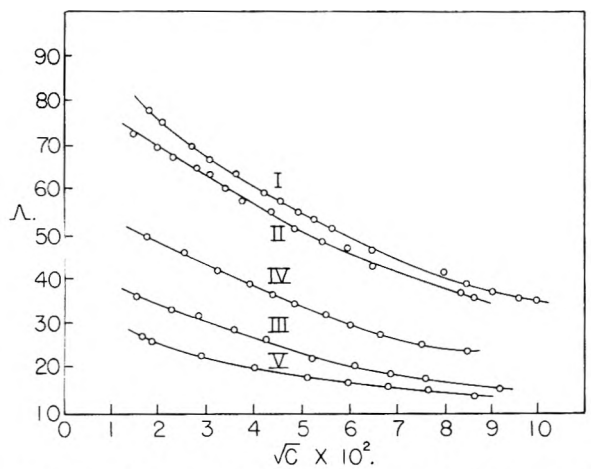

Fig. 1.—Solutions of KI, $AgNO_3$ and AgI in one mole of ethylenediamine–two moles of methanol: I, KI at 20°; II, $AgNO_3$ at 20°; III, $AgNO_3$ at 0°; IV, AgI at 20°; V, AgI at 0°.

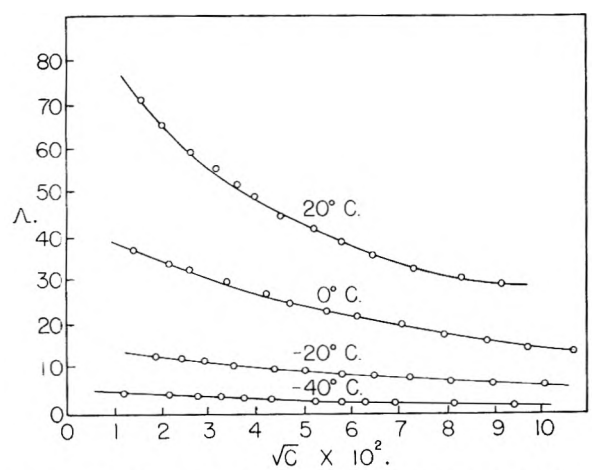

Fig. 2.—Solutions of $MgCl_2$ in one mole of ethylenediamine–two moles of methanol.

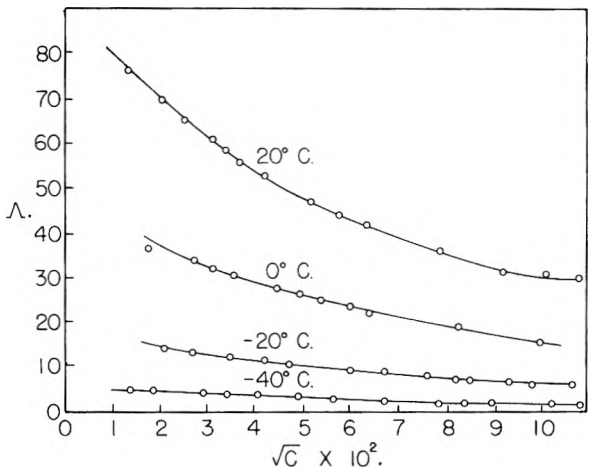

Fig. 3.—Solutions of $SrCl_2$ in one mole ethylenediamine–two moles methanol.

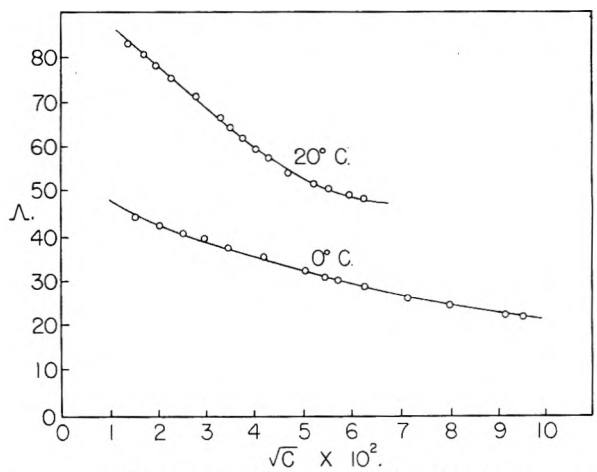

Fig. 4.—Solutions of $SrBr_2$ in one mole ethylenediamine–two moles methanol.

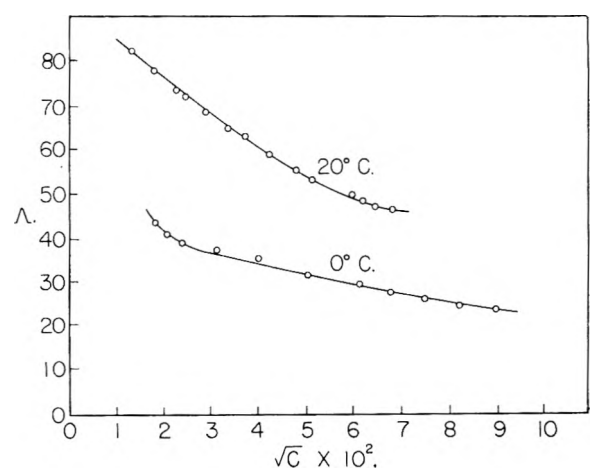

Fig. 5.—Solutions of SrI_2 in one mole ethylenediamine–two moles methanol.

(7) T. Shedlovsky, *J. Franklin Inst.*, **225**, 739 (1938).

(8) R. M. Fuoss and C. A. Kraus, *J. Am. Chem. Soc.*, **55**, 1019 (1933).

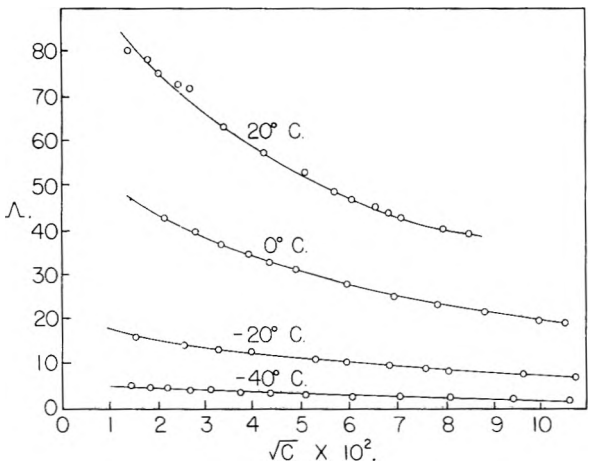

Fig. 6.—Solutions of $BaCl_2$ in one mole ethylenediamine–two moles methanol.

half its value in pure methanol, it seems evident that the strontium salt dissociates in the solvent mixture essentially as a uni-univalent electrolyte, $SrI_2 \leftrightarrows SrI^+ + I^-$. Similar considerations apply to the halides of the other alkaline earths; hence, molar conductance of these salts is shown as equivalent conductance in the Kohlrausch plots (Figs. 2–6).

Inasmuch as the dissociation constants, or reciprocal association constants as they may be designated, derived from conductance data include terms in activity and migration velocity higher than $C^{1/2}$, they should not be considered as describing a very definite physical condition. Probably these values serve as measures of the number of relatively "free" ions in the solutions. Increased dissociation as the temperature is lowered is observed in all cases except for silver nitrate. This behavior may be attributed to a larger dielectric constant at the lower temperatures. The negative effect shown by silver nitrate is difficult to explain; however, it is well known that solutions of nitrates frequently behave in an anomalous manner.

The parameter, a, having the nature of a distance related to the effective diameters of the electrostatic units, has been calculated for each system by the method of Fuoss and Kraus.[8] The values may seem to be unexpectedly low; however, it should be noted that they are of the same order of magnitude as the a-values calculated for these salts in acetonitrile and benzonitrile.[8] In general, smaller "distances of closest approach" for ions appear in solvents having larger electric moments. Acidic and basic solvent constituents, such as methanol and ethylenediamine, may interact to form complex units, thus effectively increasing the dipole moments of many of the units constituting the solvent medium.

Evidence of the "close approach" effect, in addition to electrostatic forces, appears in the case of silver iodide which is associated to a greater extent than the corresponding nitrate. The unexpected behavior of strontium iodide may be attributed to the same effect.

The data in Table II reveal that for a given anion the degree of association increases with decreasing atomic number of the alkaline earth metal. Corresponding behavior of the alkaline earth halides in methanol has been observed, but the reverse is shown by the chlorides of the alkali metals in hydroxylic solvents. In non-hydroxylic solvents, halides of the alkali metals display increased association as the atomic number of the cation decreases. Considering the systems described herein, it seems plausible that single-stage dissociation of the alkaline earth halides leaves progressively larger solvated positive ions as the atomic number of the metal increases. The increase in size of the cation, MX^+, more than counterbalances the decrease in its solvation resulting in lessened force between the positive and negative units of the solute, hence more dissociation occurs. This is somewhat parallel to the situation with the alkali chlorides in non-hydroxylic solvents where only the cation is solvated.

Except for strontium iodide and barium chloride, which show some irregularities, the Walden product connecting the limiting equivalent conductance of the solute and the viscosity of the solvent, decreases as the temperature is lowered. A larger decrease in mobility of the ions than would result from the increased viscosity of the solvent is evidence of greater effective size of the solvodynamic units. Decreased thermal agitation, as the temperature is lowered, would permit more molecules of solvent to be associated with the ions.

PHASE EQUILIBRIA IN THE SYSTEM $CaO-TiO_2$[1,2]

BY R. C. DEVRIES, R. ROY AND E. F. OSBORN

Contribution No. 53-64, College of Mineral Industries, The Pennsylvania State University, State College, Pa.

Received May 12, 1954

A phase equilibrium diagram has been determined for the system $CaO-TiO_2$. Two compounds exist: $CaO \cdot TiO_2$ and $3CaO \cdot 2TiO_2$, the former corresponding to the mineral perovskite. $CaO \cdot TiO_2$ melts congruently and forms a eutectic with TiO_2 at 1460° at 83 wt. % TiO_2. $3CaO \cdot 2TiO_2$ melts incongruently at 1750° to give a liquid containing 42 wt. % of TiO_2 in equilibrium with $CaTiO_3$. The eutectic between $Ca_3Ti_2O_7$ and CaO is at 1695° and 39 wt. % TiO_2.

Introduction and Previous Investigation

A recent study of phase equilibria in the system $CaO-TiO_2-SiO_2$ in this Laboratory[3] emphasized the need for the establishment of a consistent phase diagram for the binary system $CaO-TiO_2$. Phase equilibria in this system have been studied by several investigators, but an unequivocal representation of the phase relationships is not available. Three partially complete phase diagrams of the system have been published. The diagrams of van Wartenberg, *et al.*,[4] Umezu and Kakiuchi,[5] and Fukusima[6] are shown in Fig. 1. The work of the first was done by observing the melting of cones and only the liquidus curve was presented. This study suggested the existence of the compounds $3CaO \cdot TiO_2$ and $2CaO \cdot TiO_2$ in addition to the 1:1 mole ratio compound. Umezu and Kakiuchi[5] studied the system under reducing conditions in a graphite furnace and used both thermal analysis and melting techniques. Fukusima's study of a portion of the system ($CaTiO_3-TiO_2$) was based on quenching studies only. The form of the portion of the diagram from $CaTiO_3$ to TiO_2 is in general agreement although temperatures given for the eutectic range from 1400 to 1437°. It is plain from the figure that the main source of confusion in the system is in the region from CaO to $CaTiO_3$. This situation is further complicated by the solid state reactions reported by Tanaka,[7] Parga-Pondel and Bergt,[8] Ershov[9] and Fisk.[10] A summary of these workers' conclusions is shown in Table I. The obvious disagreement in regard to the composition, number and stability of the compounds in this system needs clarification. The present investigation may serve to clarify some of the discrepancies. In this regard considerable care has been taken to ensure the reproducibility of the data by using several different techniques with emphasis on the attempt to extend the advantages of the quenching method to as high temperatures as possible in this system.

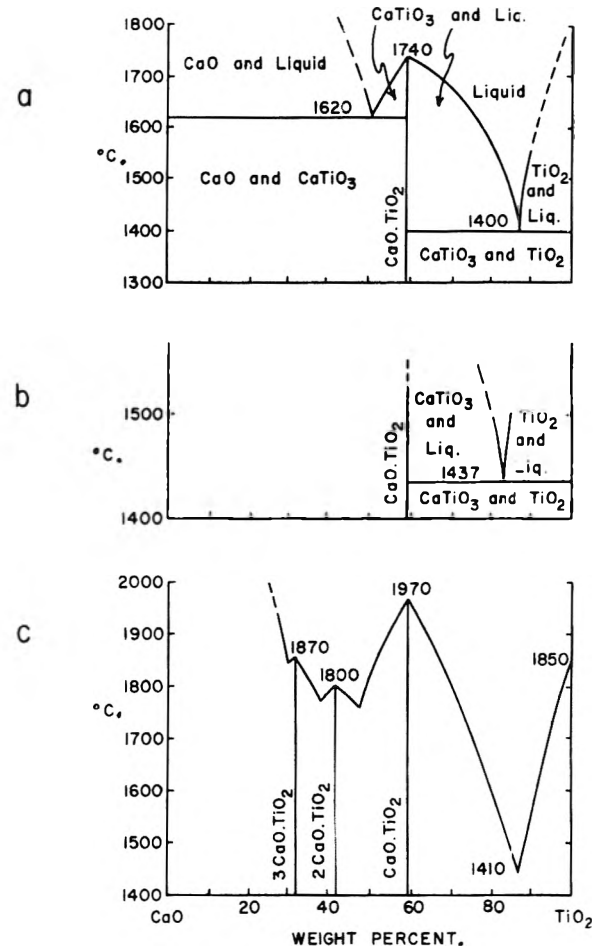

Fig. 1.—Previous versions of the system $CaO-TiO_2$: a, Umezu and Kakiuchi[5]; b, Fukusima[6]; converted from the original version in terms of $CaTiO_3$ and TiO_2 by the present authors; c, v. Wartenberg, *et al.*[4]

Experimental Procedure

The mixtures to be studied were made from reagent grade chemicals which were thoroughly mixed and then sintered in platinum crucibles at 1300° for at least 48 hours with intermediate crushing and mixing at 12-hour intervals.

Quenching, thermal analysis and pellet-melting methods were used. Quenching runs on the sintered mixtures were made using conventional quenching techniques in a platinum-wound tube type furnace for temperatures up to 1600°.[11]

(1) Paper presented at the Annual Meeting of the American Ceramic Society, April 28, 1953.

(2) This paper is based on a part of a dissertation entitled, "Phase Equilibria in the System $CaO-TiO_2-SiO_2$" submitted by R. C. DeVries in partial fulfillment of the requirements for the degree of Doctor of Philosophy at The Pennsylvania State University, August, 1953.

(3) R. C. DeVries, R. Roy, and E. F. Osborn, *J. Am. Cer. Soc.*, in press.

(4) H. van Wartenberg, H. J. Reusch and E. Saran, *Z. anorg. Chem.*, **230**, 257 (1937).

(5) S. Umezu and F. Kakiuchi, *Nippon Kogyo Kwaisi*, **46**, 866 (1930).

(6) M. Fukusima, *Kinzoku no Kenkyu, Tokyo*, **11**, 590 (1934).

(7) Y. Tanaka, *J. Chem. Soc. Japan*, **61**, 345 (1940).

(8) I. Parga-Pondel and K. Bergt, *Anal. soc. espan. fis. quim.*, **31**, 623 (1933); *Cer. Abs.*, **13** [5] 131 (1934).

(9) L. D. Ershov, *Gosudarst. Vsesoyuz. Inst. Proektirovaniyu Predpriyatii i Nauchno-Issledovatel Rabote; Tsement., Prom. Giprotsement Trudy*, **1**, 5 (1940).

(10) H. C. Fisk, *J. Am. Cer. Soc.*, **34**, 9 (1951).

(11) This technique was originally described by Shepherd, Rankin and Wright[12] and has been redescribed in many papers from the Geophysical Laboratory of The Carnegie Institution of Washington and this laboratory.

(12) E. S. Shepherd, G. A. Rankin and F. E. Wright, *Am. J. Sci.*, **28**, 293 (1909).

Table I

Summary of Previous Studies in the System $CaO–TiO_2$

Investigator	Compounds (mole ratio) ($CaO:TiO_2$)	Remarks
van Wartenberg, *et al.*,[4]	1:1, 3:1, 2:1	Phase diagram, liquidus curve only; m.p. $CaTiO_3$, 1970°
Umezu and Kakiuchi [5]	1:1	Phase diagram; m.p. $CaTiO_3$, 1740°
Fukusima[6]	1:1	Phase diagram; ($CaTiO_3$–TiO_2)
Tanaka[7]	1:1	Solid solution of CaO in $CaTiO_3$
Parga-Pondel and Bergt[8]	1:1, 3:1	$CaTiO_3$ stable up to 1300°, $3CaO·TiO_2$ forms at 1400°
Ershov[9]	1:1, 3:2	
Fisk[10]	1:1, 3:2	

A strip furnace of the type described by Roberts and Morey[13] was used for quenching experiments up to 1860° (by using 60Pt40Rh strips). An oxy-hydrogen flame was used for melting pressed pellets of the mixtures. Temperatures were measured by means of calibrated 90Pt10Rh thermocouples in the tube furnaces and by an optical pyrometer on the strip furnace and pellet runs. The reproducibility of temperatures recorded with methods using thermocouples is 3°; for the optical pyrometer measurements, about ±10°. The accuracy of both types of measurements as referred to absolute temperature scales has been discussed in another paper.[14]

To determine the first appearance of liquid (solidus) by both the strip furnace and tube furnace quenching methods a sample is heated to successively higher temperatures until evidence of liquid formation can be detected by binocular microscope observation after quenching. The final disappearance of crystals (liquidus) as determined on the strip furnace is based on the interpretation of a characteristic appearance, namely, complete flow of the sample with no visible mounds of unmelted material remaining. This condition cannot be determined as precisely as the solidus since a "mush" of crystals and liquid may exhibit the same characteristics.

The temperature of the first appearance of liquid as determined from heating pellets in the oxy-hydrogen flame was not as reproducible as on the strip furnace because of the inherent inaccuracies of the method. The temperature interpreted as the liquidus (sudden very rapid flow) was remarkably reproducible (±15°) and consistent for a series of mixtures, considering the nature of this technique. Here, too, a few crystals may be present in the liquid in which case the liquidus temperatures would be low.

Due to the difficulties frequently encountered in differential thermal analysis (*e.g.*, stray A.C. e.m.f. due probably to thermionic emission or conduction) at high temperatures, only thermal analysis runs were made. The calibrated Pt10Rh thermocouple was surrounded by the mixture in a 1-ml. platinum crucible. A motor-driven variac was used for heating the same type of tube furnaces used for quenching. By this method runs as high as 1720° have been made. Heating rates of 8–9° per minute were most satisfactory. The temperatures of the heat effects (taken as the initial break of the curve) are reproducible to ±5°, and they agreed well with the temperatures found by the quenching method. There was no evidence for appreciable supercooling in the melts.

The phases were identified both optically and by X-ray methods. The high indices of refraction of the crystalline phases forming in this system and the non-quenchability of the liquids (to a glass) seriously limit the use of the former method for detecting and identifying primary phases. The physical aspects of the formation of liquid can be observed optically, and therefore the first appearance of liquid can be determined by binocular observation alone. Solid immersion media (2.2–2.5) were used to enable examination of some of the quenched runs by means of transmitted light.

A GE XRD-3 diffractometer was used for all the spacing measurements and for most of the identification. In favorable cases measurements are reproducible to ±0.01 2θ on this instrument with the methods used. Copper radiation filtered through nickel was used. Calibration was made against the quartz peaks at 50.186 and 26.664° (2θ).

(13) H. S. Roberts and G. S. Morey, *Rev. Sci. Instr.*, **1**, 576 (1930).

(14) R. C. DeVries, R. Roy and E. F. Osborn, *Trans. Brit. Cer. Soc.*, Sept. (1954).

Results of Investigation

The results of quenching runs, thermal analyses and pellet-melting are presented in Table II. The proposed phase diagram is shown in Fig. 2.

Table II

Summary of Runs on Mixtures in the System $CaO–TiO_2$

Composition (wt. %) CaO	TiO_2	Time, hr.	Temp., °C.	Phases present[c]
85.0	15.0	0.05	1710[a]	Liq, xl
		0.05	1680[a]	Xl
		0.25	1605	CaO, $Ca_3Ti_2O_7$
		48.0	1300	CaO, $Ca_3Ti_2O_7$
67.8	32.2		1860 ± 4[b,4]	Liq
		0.05	1860[a]	Liq
		0.05	1835[a]	Liq, CaO
		0.05	1700[a]	Liq, xl
		0.05	1675[a]	Xl
			1670[b]	First app. of liq.
		1.0	1600	$Ca_3Ti_2O_7$, CaO
		0.6	1501	$Ca_3Ti_2O_7$, CaO
		48.0	1300	$Ca_3Ti_2O_7$, CaO
63.0	37.0		1800[b,3]	Liq
		0.05	1795[a]	Liq
			1725[b,4]	First app. of liq.
		0.05	1715[a]	Liq, xl
			1698	Heat effect—thermal analysis
		0.05	1690[a]	Xl
		48.0	1300	$Ca_3Ti_2O_7$, CaO
58.4	41.6	0.05	1805[a]	Liq
		0.05	1770[a]	Liq, xl
		0.05	1760[a]	Liq, $Ca_3Ti_2O_7$
			1748[b,3]	Liq
		0.05	1700[a]	Liq, xl
		0.05	1680[a]	Xl
			1678 ± 9[b,3]	First app. of liq.
		1.0	1600	$Ca_3Ti_2O_7$, CaO
		2.0	1500	$Ca_3Ti_2O_7$, CaO
		48.0	1300	$Ca_3Ti_2O_7$, CaO
55.0	45.0	0.05	1865[a]	Liq
			1753 ± 8[b,3]	First app. of liq.
		0.05	1720[a]	Liq, $Ca_3Ti_2O_7$
		0.05	1695[a]	Liq, xl
		0.05	1675[a]	Xl
		48.0	1400	$Ca_3Ti_2O_7$, CaO
51.29	48.71		1878 ± 15[b,3]	Liq
		0.05	1765[a]	Liq, xl
		0.05	1745[a]	Xl
		0.05	1720[a]	Xl
		0.5	1600	$Ca_3Ti_2O_7$
		72.0	1539	$Ca_3Ti_2O_7$
		48.0	1300	$Ca_3Ti_2O_7$

TABLE II (*Continued*)

Composition (wt. %) CaO	TiO_2	Time, hr.	Temp., °C.	Phases present[c]
48.65	51.35		1932 ± 15[b,3]	Liq
		0.05	1800[a]	Liq, xl
		0.05	1775[a]	Liq, xl
		0.05	1750[a]	Xl
		0.05	1725[a]	Xl
		0.05	1695[a]	Xl
		0.05	1650[a]	Xl
		0.25	1605	$Ca_3Ti_2O_7$, $CaTiO_3$
		140.0	1546	$Ca_3Ti_2O_7$, $CaTiO_3$
46.0	54.0		1950 ± 10[b,3]	Liq
		0.05	1800[a]	Liq, xl
		0.05	1765[a]	Liq, xl
		0.05	1735[a]	Xl
		0.05	1685[a]	Xl
		12.0	1594	$Ca_3Ti_2O_7$, $CaTiO_3$
		72.0	1539	$Ca_3Ti_2O_7$, $CaTiO_3$
		72.0	1300	$Ca_3Ti_2O_7$, $CaTiO_3$
43.6	56.4		1980[b,2]	Liq (very little liq. up to this temp.)
		0.05	1790[a]	Liq, xl
		0.05	1770[a]	Liq, xl
		0.05	1735	Xl
		0.05	1700	Xl
		0.05	1650	Xl
		0.25	1605	$CaTiO_3$, $Ca_3Ti_2O_7$
		140.0	1546	$CaTiO_3$, $Ca_3Ti_2O_7$
41.2	58.8		1954 ± 18[b,4]	Liq
		72.0	1539	$CaTiO_3$
30.0	70.0		1853 ± 25[b,2]	Liq
			1460[2]	Heat effect (thermal analysis)
20.0	80.0	0.05	1645[a]	Liq
		0.05	1595[a]	Liq, xl
		1.5	1501	Liq, TiO_2, $CaTiO_3$ (?)
			1469	Heat effect (thermal analysis)
		1.0	1468	Liq, xl
		1.5	1456	Xl
15.0	85.0	0.05	1595[a]	Liq
		0.05	1545[a]	Liq, xl
		1.0	1524	Liq, TiO_2
		0.5	1465	Liq, xl
			1462	Heat effect (thermal analysis)
		4.0	1457	Xl
10.0	90.0	0.05	1690[a]	Liq
		0.05	1645[a]	Liq, xl
		0.25	1464	Liq, xl
		0.5	1458	Xl
			1456	Heat effect (thermal analysis)

[a] Strip furnace runs. [b] Pellet melts; superscript number = number of determinations; temperature and σ are result of statistical treatment of these determinations. All other runs made in Pt-wound quench furnaces. [c] Phases present at temperature indicated; at room temperature "liq" = liquid crystallized during quenching as observed under the microscope; xl = crystals.

$CaTiO_3$–TiO_2.—The eutectic temperature between perovskite ($CaTiO_3$) and rutile (TiO_2) was found to be 1460 ± 5° by both thermal analysis and quenching techniques. Since the liquids forming in this system are extremely fluid, their first appearance is very easy to detect by noting the wetting of the platinum envelope. The quenching method does not allow for positive identification of the primary phases since all mixtures quenched from above the temperature of the eutectic contain the two crystalline phases, perovskite and rutile, at room temperature. The composition of the eutectic agrees within the limits of experimental error with Fukusima's value of 17% CaO.

The melting point of perovskite, 1970°, is that given by van Wartenberg, *et al.*[4] The average temperature (four determinations) determined in the present investigation for this point was 1954 ± 18°. Quenching molten pellets resulted in a product that had low, often wavey birefringence, a refractive index of about 2.35, and often displayed alternating isotropic and anisotropic bands. This last feature may be the result of a rapid inversion not inhibited by quenching.

$CaTiO_3$–CaO.—The portion of the diagram from $CaTiO_3$ to CaO received the main emphasis of the study and was investigated above 1300°. Our interpretation of the data is in agreement with Ershov[9] and Fisk,[10] namely, that the 3:2 mole ratio composition was found to be the only other binary compound besides perovskite ($CaTiO_3$) existing in the system. All mixtures higher in CaO than the 3:2 mole ratio, contain only $3CaO{\cdot}2TiO_2$ and CaO. The 3:2 composition melts incongruently to $CaTiO_3$ and liquid (about 42% TiO_2) at 1750 ± 10°. The eutectic between $3CaO{\cdot}2TiO_2$ and CaO has the composition, 39% TiO_2, and the temperature, 1695 ± 5°.

From Table III the similarity of the powder diffraction patterns of $CaO{\cdot}TiO_2$ and $3CaO{\cdot}2TiO_2$ will be easily seen. It should be noted that the latter compound has reflections overlapping those of each perovskite line. The question to be decided is whether the composition $3CaO{\cdot}2TiO_2$ does in fact represent a unique compound or whether it is the limit of solid solution of excess CaO in $CaTiO_3$. (A third possibility which may be nearest the truth is a combination of the above two, resulting in the existence of both unique compounds and some solid solution in each.) The latest analysis of the mineral perovskite structure by Murdoch[15] gives a pseudocubic unit cell with a_0 = 15.26 Å. Examples are well known of solid solution of various ions in compounds with the perovskite structure resulting in the increase or decrease of the extent of "distortion" from the ideal cubic arrangement. The problem at hand was therefore to distinguish between the case where new diffraction lines due to a new compound appear when compositions are varied from 50 to 60 mole per cent. CaO, and that in which the perovskite pattern (with the superstructure and distortion already present) is altered continuously by the entry of excess Ca^{2+} ions. Increasing the complication is the very likely fact that perovskite itself may have a high temperature form (which admits more or less Ca^{2+} than the low form) and the fact that the extent of solid solution may increase appreciably with temperature. If this were the case,

(15) J. Murdoch, *Am. Min.*, **36**, 573 (1951).

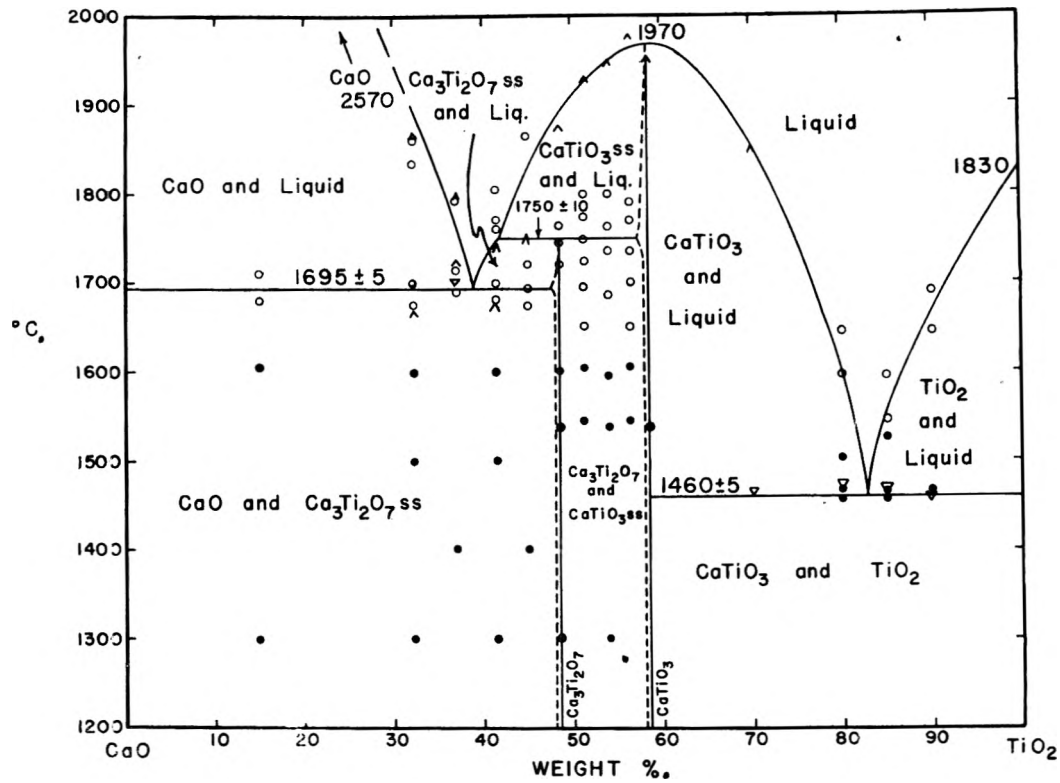

Fig. 2.—Proposed phase diagram for the system CaO–TiO_2: solid dots, conventional quenching runs; open circles, strip furnace runs; ∧ (at apex), pellet melting runs; ∇ (at lower apex), thermal analysis runs; ss, solid solution.

(and as has been shown by DeVries and Roy[16] for other systems involving $CaTiO_3$, high-temperature forms may remain "quenched in") the problem takes on major proportions.

Table III

Interplanar Spacings for Compounds in the System CaO–TiO_2

$3CaO·2TiO_2$		$CaO·TiO_2$	
d	I/I_0	d	I/I_0
9.77	41	3.83	12
4.887	65	3.43	3
3.762	12	2.708	100
2.730	100	2.417	2b[a]
2.710	76	2.362	2b
2.481	6	2.304	8
2.254	7	2.219	9
2.080	18	2.201	7b
1.9509	65	2.122	5b
1.9141	53	2.049	3b
1.8860	20	1.9141	64
1.5826	26	1.8579	6
1.5679	20	1.7142	5
1.3912	6	1.6922	2
1.3662	12	1.6779	6
1.3423	6	1.5655	23
1.2303	5	1.5583	26
1.2119	5	1.3524	17
		1.2094	7b
		1.1013	2b

[a] b = broad.

The experimental work done in addition to identification powder patterns was as follows: powder X-ray diffraction patterns were run at a rate of $1/5°$ 2θ per min. on a series of samples of the two "compounds" prepared under various conditions especially as quenched from different temperatures. Mechanical mixtures were also made of these two compounds and their patterns run. The same slowly scanned patterns were then also obtained for the significant runs made on compositions between 50 and 60 mole per cent. TiO_2. Some idea of the type of data obtained is conveyed through Fig. 3. Our interpretation of all the data leads to the conclusion that a definite compound with the composition $3CaO·2TiO_2$ exists, but that both this phase and $CaO·TiO_2$ may admit some excess CaO into their structures. The determination of the extent of this solid solution with any degree of reliability in these structures and especially as a function of temperature was considered to be a minor consideration not justifying the great deal of work necessary. A reflection near 4.9 Å. in the powder pattern of $3CaO·2TiO_2$ appears at first to be convincing evidence of the uniqueness of this composition. However, 4.91 also corresponds to the basal spacing of $Ca(OH)_2$, and Fisk[10] had claimed that $3CaO·2TiO_2$ was "hydraulic." We refluxed the compound with water for a period of 24 hours at 100° and could find no evidence of any change of pattern. Moreover, there is also a weak line at 9.8 Å. of which the 4.9 Å. line is the second order, and it is unlikely that single crystal studies of $Ca(OH)_2$ would have missed such an obvious feature. Furthermore, the other strong reflections of $Ca(OH)_2$ are absent (at least in their proper intensity ratios). Careful study of the spacings also showed that the spacing associated with $3CaO·2TiO_2$ compound was 4.89 as com-

(16) R. C. DeVries and R. Roy, paper presented at the Annual Meeting of the American Ceramic Society, April, 1954.

pared with 4.92 for $Ca(OH)_2$; and it was actually possible to show the existence of both reflections in mixtures containing more CaO than the $3CaO \cdot 2TiO_2$ ratio which had hydrated in the atmosphere. It will also be seen from Fig. 3 that in addition to the fact that compositions between 50 and 60 mole per cent. CaO yield patterns which are essentially superpositions of the $CaTiO_3$ and $3CaO \cdot 2TiO_2$ patterns, there is in some cases a systematic shift in both patterns. It is felt that the inconsistent results obtained were due to inability to retain the high temperature structure by sufficiently rapid quenching in all cases. A definite shift has been noted in several patterns leading to the qualitative representation shown in Fig. 2 in which some solid solution is shown in each compound toward the CaO end with the extent of solid solution decreasing at lower temperatures. No quantitative values can be ascribed to the extent of solid solution but it would appear to be less than 2–3 wt. per cent. in each case. Thus the X-ray diffraction data, though not straightforward, confirm the thermal data regarding the presence of the compound $3CaO \cdot 2TiO_2$.

Optical examination of these end members and mixtures although performed under unfavorable conditions due to their high indices of refraction provided confirmatory evidence for this interpretation. When mounted in solid immersion media of index 2.3, both phases can be detected in the mixtures ($3CaO \cdot 2TiO_2$ as birefringent, subhedral laths less than 2.3; $CaTiO_3$ as isotropic, or nearly isotropic anhedral to rounded grains of index greater than 2.3). This is in agreement with Fisk's[10] data on the refractive indices.

Quench runs of the $3CaO \cdot 2TiO_2$ composition from all temperatures have the same pattern, and microscopic examination fails to show any other phase. All mixtures higher in CaO than the $3CaO \cdot 2TiO_2$ composition contain $3CaO \cdot 2TiO_2$ in the same form as the pure compound as determined by both X-ray and microscopic methods.

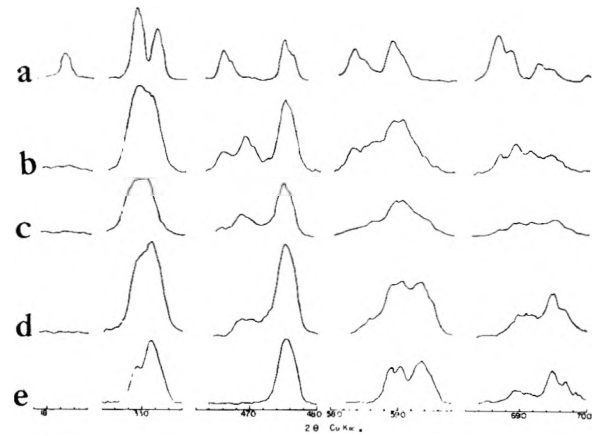

Fig. 3.—X-Ray diffractometer patterns of a series of mixtures from $Ca_3Ti_2O_7$ to $CaTiO_3$ (after melting and quenching) illustrating difficulties in interpretation of these data; composition of mixtures in weight %, CaO/TiO_2: a, 51.29/48.71 ($Ca_3Ti_2O_7$); b, 48.65/51.35; c, 46.00/54.00; d, 43.60/56.40; e, 41.24/58.76 ($CaTiO_3$). Each subdivision, 0.2° 2θ Cu Kα.

This interpretation of the data is seen to agree with most of the more recent work such as that of Ershov[9] and Fisk[10] and explain some aspects of the earlier work. Failure to retain high temperature phases on quenching to room temperature and the similarities between the two binary compounds would appear to explain some of the discrepancies

Acknowledgment.—This work was performed as part of a program sponsored by the U. S. Army Signal Corps, Contract No. DA 36-039 sc5594, to investigate the synthesis and stability of synthetic crystals.

CHEMORHEOLOGY OF SOME SPECIALLY PREPARED SILICONE RUBBERS

BY D. H. JOHNSON, J. R. MCLOUGHLIN AND A. V. TOBOLSKY

Contribution from the Frick Chemical Laboratory, Princeton University, Princeton, N. J.

Received May 12, 1954

Specially prepared silicone rubbers were formulated from octamethylcyclotetrasiloxane, cross-linking agent and catalyst. These rubbers were extremely labile as evidenced by stress relaxation measurements. The lability could be overcome by tying up the acid catalyst with water vapor or pyridine.

Introduction

Ring siloxanes such as octamethylcyclotetrasiloxane $[(CH_3)_2SiO]_4$ may be catalytically transformed into long chains by shaking with a small quantity of sulfuric acid.[1,2]

It was desired to prepare films of lightly cross-linked silicone rubber directly from octamethylcyclotetrasiloxane by incorporation of a cross-linking agent and a catalyst. The catalyst was based on sulfuric acid, but since sulfuric acid is not soluble in the silicones in the desired concentration range, a means was found to incorporate this catalyst without separation into two phases. The cross-linking agent was added to prevent thermoplastic flow.

Once these films were prepared, they were found to be highly labile because the presence of catalyst caused continual interchange of the SiO bonds. These interchanges were manifest by a loss of weight in the samples if they were not kept in closed containers. This undoubtedly was due to the formation of volatile ring siloxanes.

The great lability of the rubber films prepared in this way was also manifest by the extremely rapid

(1) W. Patnode and D. F. Wilcock, *J. Am. Chem. Soc.*, **68**, 358 (1946).

(2) A. V. Tobolsky, F. Leonard and G. P. Roeser, *J. Polymer Sci.*, **3**, 604 (1948).

stress relaxation that could be observed in these samples under certain conditions. This will be described more fully later in this paper.

The rubber films could be stabilized both as regards loss of weight and as regards stress relaxation by addition of suitable stabilizers.

Materials

Octamethylcyclotetrasiloxane.—Cyclic dimethylsiloxanes can be obtained by the hydrolysis of dichlorodimethylsilane and isolated from the resulting mixture of linear and cyclic dimethylsiloxanes by fractional distillation. The total yield of cyclics runs about 50% of the hydrolyzate of which approximately 80% is the tetramer. The linear siloxanes produced by the hydrolysis can be converted to cyclic materials by heating them under vacuum to 350–400° at which temperature range the Si–O bonds undergo thermal rearrangement with the cyclics distilling off. With the use of sodium hydroxide as a catalyst, a 90% yield of low cyclics is obtained of which about 25% is the tetramer. The pyrolysis of these linear siloxanes takes place without observable rupture of carbon–silicon bonds.

The cyclotetrasiloxane for this work was obtained by the above procedure and also by fractional distillation of General Electric "Dri-Film" which contains about 35% of the tetramer. This yield was substantially increased by thermal rearrangement of the residue.

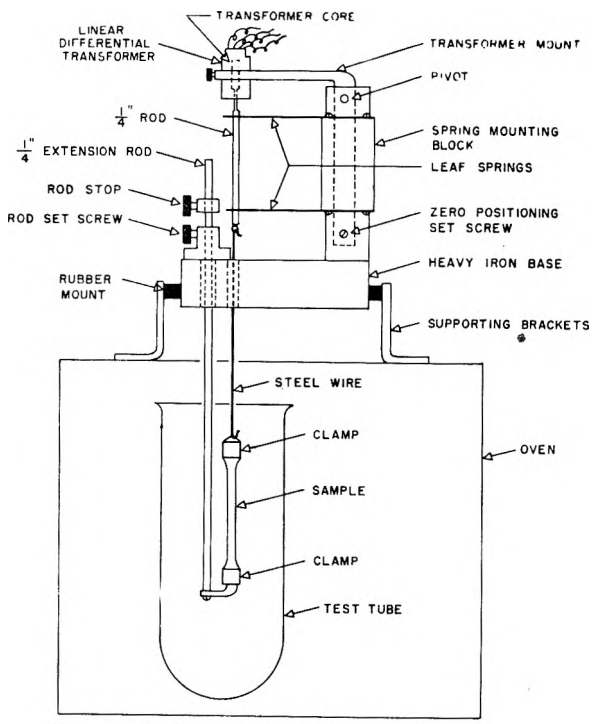

Fig. 1.—Rubbery state stress relaxation unit.

Cross-linking Agent.—A polysiloxane cross-linking agent was prepared by the cohydrolysis of dichlorodimethylsilane and methyltrichlorosilane. A 1:1 mole ratio of the di- and trichlorosilanes was hydrolyzed in a mixture of water, toluene and butanol. The organic layer was separated, washed and rid of solvents by distillation under reduced pressure. The resulting mixture had a number average molecular weight of 1320 by a cryoscopic measurement.

Catalyst.—A mixture of 90 g. of the methyl tetramer and 7.2 ml. of 20% fuming sulfuric acid was vigorously shaken in a separatory funnel. The excess acid was then separated by either long standing followed by decantation or by centrifugation. A clear, viscous liquid results that is very reactive to water, water vapor and basic materials. Immediate polymerization results from contact with any of the above substances.

The catalyst prepared in the manner described was titrated against alcoholic KOH using phenolphthalein as indicator and found to contain 7.0–8.0 $\times 10^{-3}$ mole H_2SO_4 per gram of sample.

Catalysts were also prepared using phosphoric, formic *p*-toluenesulfonic and acetic acids. In these cases, however, it was necessary to reflux the mixture to obtain a convenient rate of reaction.

Preparation of Samples.—It was decided that the most convenient specimen with which one could study and evaluate the polymer properties would be in the form of films. In order to obtain suitable specimens for this purpose, various methods of casting films were explored. Although the adhesion of silicones to metal surfaces is generally poor, difficulty was encountered in removing coherent films from metal surfaces. It was found very convenient to cast the films on mercury surfaces.

Clean mercury was placed in an appropriate diameter crystallizing dish and the polymerization mixture poured on top of the mercury in such an amount as to give a film of the desired thickness. The crystallizing dish was then placed in a desiccator to maintain a controlled humidity and heated to the desired temperature. The relative ease with which films with parallel faces can be prepared by this technique is important for use in measurement of stress relaxation.

Using the method of film preparation just described, films of various compositions were prepared to determine a formulation suitable for the study of the polymer properties. The films were prepared in most cases at 60° since this temperature gives a reasonable balance of rate of cure *versus* loss of the monomer by vaporization. A close control of the humidity during the polymerization was also important for reproducibility of results.

Except where noted, the film formulation used in the succeeding studies was

Octamethylcyclotetrasiloxane	10.0 parts by wt.
Cross linking agent (see Materials section)	0.3 part by wt.
Catalyst (see Materials section)	1.0 part by wt.

The above mixture was polymerized at a controlled low humidity ("Drierite") for 24 hours at 60°.

These films show the very interesting property of practically zero shrinkage.[2]

Stress Relaxation.—Subsequent examination of the physical properties of the silicone rubber films whose preparation has just been described were carried out by the stress relaxation technique.[3] The stress relaxometer used is shown in Fig. 1. A complete description of the use of this apparatus is available elsewhere.[4]

It was found that samples conditioned and tested at high humidity supported stress indefinitely, whereas samples conditioned and tested in vacuum flowed down around the clamps before the relaxation experiment could be started.

In order to make a quantitative study of the effect of relative humidity on the stress relaxation of these rubber films, concentrated solutions of sodium hydroxide were used to control the humidity. The sodium hydroxide solution was poured into the bottom of a large test-tube-like glass container about 12 inches deep and 2 inches in diameter. The glass tube was clamped against a metal plate to seal off the upper end, using a rubber gasket. The rod for extending the sample and a thin wire from the top clamp of the sample to the load-measuring element above, passed through this plate; the wire passing through a capillary sealed into the plate. A rotating shaft equipped with a propeller on its lower end also passed through a bushing in the metal plate and served to keep the air in the container circulating over the sample and the constant humidity solution. The relaxometer shown in Fig. 1 was used to measure and record the stress as a function of time after stretching the sample to a fixed length.

Figure 2 shows stress divided by initial stress for samples kept over dry calcium chloride and over solutions of varying NaOH concentrations which produced the relative humidities shown in the figure. The experiments were all performed at 60°. It is striking that at low relative humidities

(3) A. V. Tobolsky, I. B. Prettyman and J. H. Dillon, *J. Applied Phys.*, **15**, 380 (1944).

(4) J. R. McLoughlin, Ph.D. Thesis, Princeton University, 1951. The experimental work contained in this paper is described more fully in this thesis, including other experiments on the stress relaxation of silicone rubber samples.

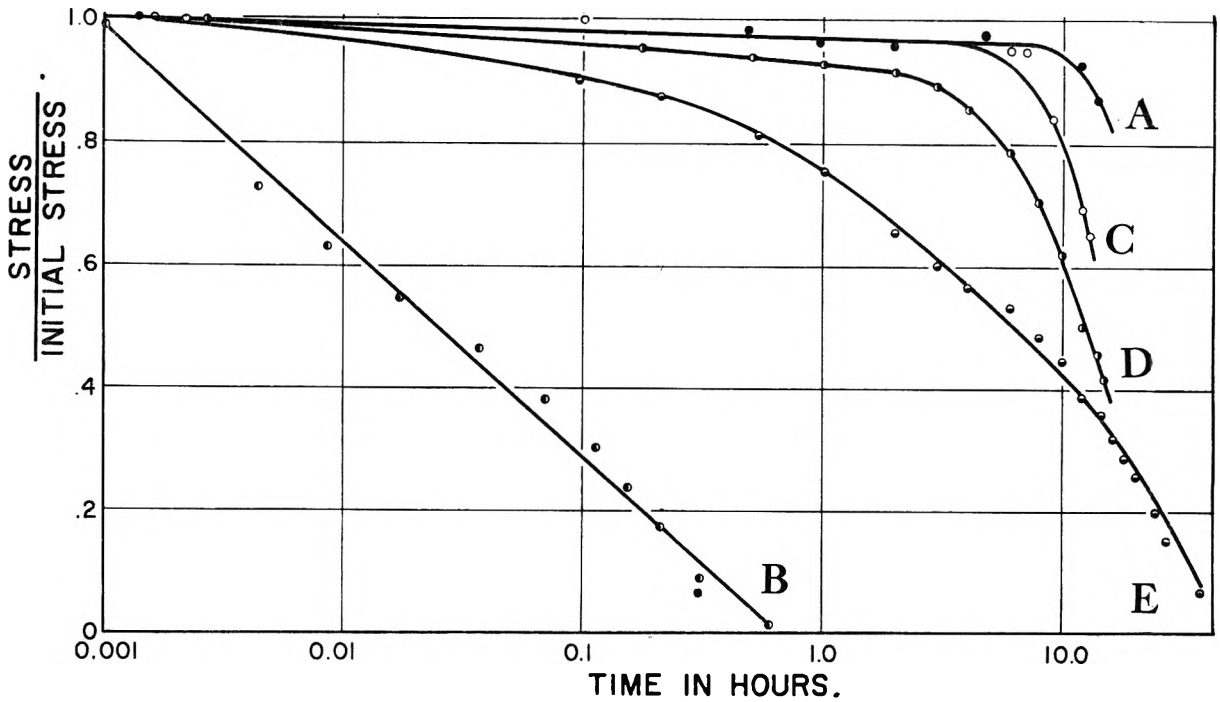

Fig. 2.—Relaxation of stress of specially prepared silicone rubber under various humidities at 21% elongation: (A) ●, satd. $CaCl_2$, 18% R.H.; (B) ◐, dry $CaCl_2$, 1% R.H.; (C) ○, 6.2% R.H., over NaOH; (D) ◑, 3.35% R.H., over NaOH; (E) ◒, 1.47% R.H., over NaOH.

the samples showed a very rapid chemical stress relaxation, whereas at high relative humidities the stress delay was slowed up very considerably.

Evidently free sulfuric acid (or its esters) in the silicone polymers is capable of catalyzing extremely rapid interchanges manifested by the stress relaxation experiment. Water appears capable of tying the activity of the sulfuric acid, although this effect is reversible as can be observed by again lowering the relative humidity.

When pyridine was allowed to soak into the polymer, it exerted a permanently stabilizing effect so that low humidities no longer resulted in high rates of stress relaxation. Obviously the pyridine was acting to neutralize the acid catalyst.

THE HYDRATES OF MAGNESIUM PERCHLORATE

BY L. E. COPELAND AND R. H. BRAGG

Portland Cement Association, Research and Development Division, Chicago 10, Ill.

Received May 19, 1954

Aqueous vapor pressures for the equilibria: $Mg(ClO_4)_2 \cdot 2H_2O + 2H_2O = Mg(ClO_4)_2 \cdot 4H_2O$, $Mg(ClO_4)_2 \cdot 4H_2O + 2H_2O = Mg(ClO_4) \cdot 6H_2O$ have been measured at 23°. The equilibrium pressures are 8.15 ± 0.54 and 20.9 ± 1.1 × 10^{-3} mm., respectively. For the equilibrium $Mg(ClO_4)_2 + 2H_2O = Mg(ClO_4)_2 \cdot 2H_2O$ the vapor pressure is less than 0.56 × 10^{-3} mm. The vapor pressure of the saturated solution is 81 × 10^{-3} mm. No evidence indicating the existence of a trihydrate was found.

Introduction

The published studies of magnesium perchlorate and its hydrates are due mainly to Smith and his colleagues.[1-3] Smith and Willard prepared the anhydrous salt in 1922 and proposed its use as a drying agent.[1] They also prepared the hexahydrate, a compound which had been reported previously,[4] and reported the preparation of the trihydrate by drying the hexahydrate over phosphorus pentoxide *in vacuo* at 20–25°. In this latter study their plot of water retained in moles per mole of magnesium perchlorate *versus* time appeared to approach 3 asymptotically. However, equilibrium had not been reached in 4 months, at which time they discontinued the drying. Apparently, the notion of the existence of a trihydrate arose from the belief of Smith and Willard that the composition of the salt was approaching that of a trihydrate.

A further study of the hydrates of magnesium perchlorate was published by Smith, Rees and Hardy in 1932.[2] They predicted on theoretical grounds that in addition to the known hydrates, the di- and tetrahydrates should exist also. Two kinds of evidence were presented to support their contention: (1) data on the vacuum dehydration of the hexahydrate, and (2) X-ray diffraction patterns.

(1) G. F. Smith and H. H. Willard, *J. Am. Chem. Soc.*, **44**, 2255 (1922).

(2) G. F. Smith, O. W. Rees and V. R. Hardy, *ibid.*, **54**, 3513 (1932).

(3) G. F. Smith, "Dehydration Studies Using Anhydrous Magnesium Perchlorate," The G. Frederick Smith Chemical Co., Columbus, Ohio, 1934.

(4) R. F. Weinland and F. Ensgraber, *Z. anorg. allgem. Chem.*, **84** 372 (1914).

Their data indeed give strong support to their arguments for the existence of the di- and tetrahydrates. However, the dehydration data do not suggest a trihydrate. Moreover, the authors did not report X-ray patterns for the trihydrate, although patterns for the anhydrous salt, and the di-, tetra- and hexahydrates were given.

The only other published work on the number of hydrates of magnesium perchlorate is due to Moles and Roquero.[5] These authors concluded that magnesium perchlorate trihydrate is not a definite compound but comprises mixed crystals.

Brownyard,[6] in a review of the literature on magnesium perchlorate, concluded that the hexahydrate unquestionably exists, and that the dihydrate and tetrahydrate probably exist also. He considered the evidence for the existence of a trihydrate to be inconclusive.

There are no published vapor pressure isotherms for the hydrates of magnesium perchlorate. However, from various studies on the efficiency of magnesium perchlorate as a dehydrating agent it is possible to give 10^{-3} mm. as an upper limit for the pressure of the equilibrium anhydrous salt–dihydrate at room temperature.[7] From certain adsorption studies conducted in this Laboratory Brownyard estimated 6×10^{-3} mm. for the equilibrium dihydrate–tetrahydrate.

The data previously cited pertaining to equilibrium vapor pressures are inadequate when it is necessary to know these pressures with precision. This study was conducted in order to determine the number, composition and vapor pressures of the hydrates of magnesium perchlorate at room temperature. It was necessary to have this information because we have used these hydrates as desiccants in our hydration studies.[8]

Materials.—The magnesium perchlorate used in this experiment is sold commercially under the trade name Anhydrone (anhydrous magnesium perchlorate). The water used for hydrating the magnesium perchlorate was distilled twice in an evacuated system.

Apparatus.—The sample was placed in a platinum gauze bucket suspended from a silica spring in a glass jacket. The jacket was connected, by means of a mercury seal ground joint, to a conventional high-vacuum system with associated mercury-diffusion pump and McLeod gage. A tilting McLeod gage, range 0–5 mm., was added to the system adjacent to the jacket when it was discovered that, owing to condensation in the capillary, the conventional gage could not be used over the full range of pressures encountered. Stopcocks were provided so that the water supply tube or the adsorption tube or both could be isolated from the rest of the system. The laboratory temperature was controlled at $23 \pm 0.5°$.

Sample weights were found by calculation from the observed spring elongations and the measured spring sensitivity. Elongations were measured by sighting at reference marks at the ends of the spring with a cathetometer. The spring sensitivity, obtained by calibration before and after the experiment, was 0.03263 g./cm. Since the sample weight was of the order of 0.4 g. and spring lengths were known accurately to 0.005 cm., the calculated molar ratios should be precise to ± 0.005 mole. We estimate the accuracy of the measured molar ratios to be more nearly ± 0.05 mole, because of small uncertainties in the weight of the anhydrous sample and in the weight of the empty bucket.

The tilting McLeod gage, calibrated with dry air against a conventional McLeod gage, was used for all pressure measurements. Heights of the mercury menisci in the tilting gage were measured with the same cathetometer used to obtain spring elongations. Over the range of change found in this experiment the calculated pressures would be precise to 1.5% for non-condensable gases. However, a consideration of the effects of water vapor adsorption in the gage[9] and semi-quantitative calculations based on the available water vapor adsorption isotherms on glass,[10] indicates that the true pressures may be lower than those reported by about 2% at 8 and 20 μ and 3% at 80 μ.

Experimental Procedure.—About 0.4 g. of sample was taken for each run. When water was to be added to the system, the water in the supply flask was first frozen with Dry Ice and the system pumped out for about $\frac{1}{2}$ hour. This procedure helped to prevent a build-up of permanent gas pressure and gave better control over the amount of water vapor added. Following the evacuation the main stopcock and jacket stopcock were closed, and the stopcock to the water supply flask (warmed to 0°) was opened momentarily. The jacket stopcock was then opened very slowly; when opened rapidly the force of the inrushing gas could easily drive the sample and bucket to the tube bottom resulting in a partial or complete loss of sample. Following the addition of water, daily readings were made until no changes in pressure or spring elongation could be detected. Occasionally, *e.g.*, after a long wait for equilibrium, the residual permanent gas pressure was measured by freezing out the water vapor with ice at −78°. The quantity of permanent gas was found always to be insignificant.

Water could be removed from the sample in several ways: (1) vacuum dehydration with the Hg diffusion pump, (2) vacuum dehydration combined with heating the sample with an infrared lamp or tube furnace, and (3) vacuum dehydration using ice at −78° as a desiccant. Although all of these methods were used at various times, the third method had the advantage that very little of the initial supply of water was lost from the system during a run. It was not the most rapid method, but it gave by far the best control over the amount of water removed. To reduce the water below 2 moles per mole of magnesium perchlorate it was necessary to use the second method. The anhydrous salt was obtained in this way. Gradual heating to 250° over a period of 18 hours with continuous pumping produced constant sample weight. These samples, on rehydration, gave the same vapor pressure–composition relationship that they gave before the heat treatment.

Results and Discussion

The data of aqueous vapor pressure *vs.* water of hydration in moles of water per mole of magnesium perchlorate obtained with two different samples are plotted in Fig. 1. Some of the data are probably not representative of equilibrium. It was noted that an extremely long time was required to reach equilibrium when a change of water content occurred near a transition point. Consequently, values obtained prior to equilibrium would tend to be too high on hydration and too low on dehydration. Figure 2 is an example of this phenomenon. Over a period of 15 days the pressure decreased to one-half that of the initial value while the sample weight changed less than 0.3%. It is obvious from the curve that equilibrium had not been reached. Apparently, changing the water of hydration at low pressures has the effect of producing a fairly stable, amorphous, intermediate product which recrystallizes very slowly.[11] This effect was observed both on hydration and dehydration.

(5) E. Moles and C. Roquero, *Anales. soc. españ. fís. quím.*, **31**, 175 (1933).

(6) T. L. Brownyard, short paper on Series 254, Research Laboratory, Portland Cement Association, 1946 (unpublished).

(7) J. H. Bower, *Bur. Stds., J. Res.*, **12**, 246 (1934).

(8) T. C. Powers and T. L. Brownyard, *Proceedings Am. Concrete Inst.*, **43**, 257 (1947); PCA Bulletin 22.

(9) M. Francis, *Trans. Faraday Soc.*, **31**, 1325 (1935).

(10) S. Brunauer, "The Adsorption of Gases and Vapors," Princeton U. Press, Princeton, N. J., 1943.

(11) G. B. Frost, K. A. Moon and E. H. Tomkins, *Can. J. Chem.*, **29**, 604 (1951).

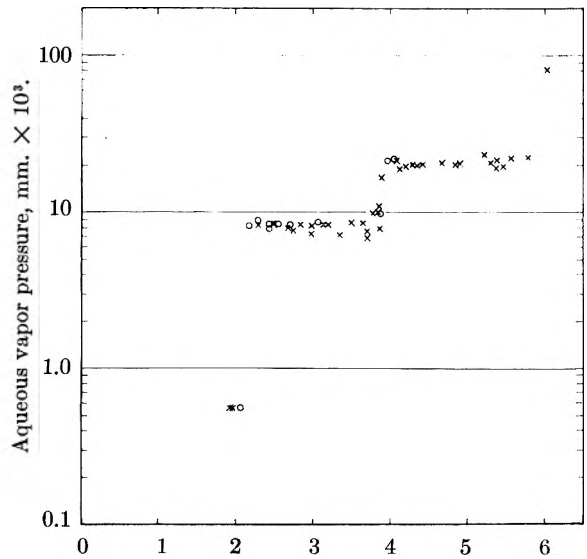

Fig. 1.—Plot of aqueous vapor pressure *versus* water of hydration per mole of magnesium perchlorate at 23°: × = first run; O, second run. The points at 0.56 × 10^{-3} mm. were obtained by drying to constant weight with ice at −78°.

Figure 3 illustrates the role played by the glass walls of the vacuum system. Over a period of 20 days, during which time pressure changes were imperceptible, there was a slow but distinct gain in sample weight. This behavior is best understood by a consideration of the isotherms of both the sample and the glass walls. When the sample is to be hydrated, a small quantity of water vapor at about 20 mm. is introduced into the system, which had previously been evacuated to about 10^{-5} mm. Some of the gas is adsorbed on the system walls, some is captured by the sample as water of hydration, and some remains in the vapor phase. The sample at first forms higher hydrates than are characteristic of the total water content of the system and quasi-equilibrium is reached fairly rapidly. However, the vapor pressure over the glass surface is now less than that required for the quantity of water initially adsorbed. Consequently, molecules of water slowly desorb from the glass and are captured by the sample *with no perceptible change in vapor pressure.* This process continues until the system is in true equilibrium.

The data plotted in Fig. 1 show the nature of the isotherm between 2 and 6 moles of water of hydration. There are well defined plateaus corresponding to equilibrium between water and the di- and tetrahydrate and the tetra- and hexahydrate. The pressures for these regions have means of 8.15 and 20.9 × 10^{-3} mm., respectively. The transitions do not appear to be ideally sharp, and there is some suggestion of a slope in the plateaus. However, tests conducted in the second run showed that both these effects are due to non-equilibrium conditions. There is no suggestion of a break at 3 moles of water.

When the sample was dehydrated over ice at −78°, equilibrium was reached for molar compositions of 1.94, 1.95 and 2.07 moles per mole of magnesium perchlorate at various times. There seems

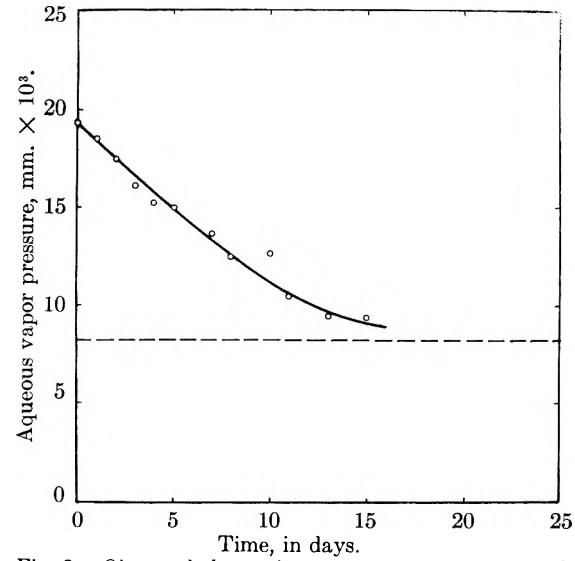

Fig. 2.—Observed change in vapor pressure at 3.68 moles of water per mole of magnesium perchlorate. During this time the sample weight did not change; dashed line is the equilibrium pressure for this composition.

to be little reason to doubt that a transition occurs at 2 moles. Our attempts to obtain points slightly above 2 moles were complicated by the fact that about 0.1 mole (0.003 g.) was the smallest increment which could be made conveniently.

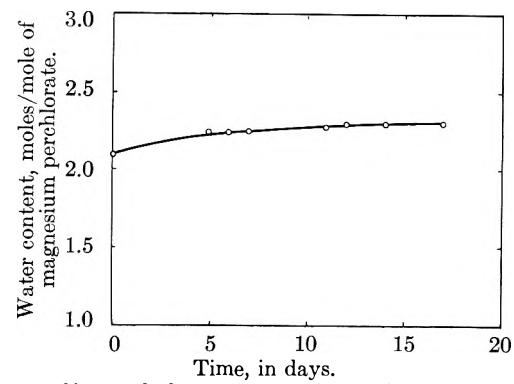

Fig. 3.—Observed change in sample weight at vapor pressure ~ 8.2 × 10^{-3} mm.

We could not obtain equilibrium in the region of 0 to 2 moles, despite attempts extending over several months. Because pressures in this region were of the order of 10^{-5} to 10^{-4} mm., slow leaks or evolution of adsorbed gases could vitiate the pressure determinations. Nevertheless, the plateau must lie below 0.56 × 10^{-3} mm., for in addition to the evidence obtained on dehydration, a sample dried to a composition below 2 moles H_2O was observed to *gain* weight when ice at −78° was used as a water source.

The addition of a quantity of water sufficient to exceed the 6 molar composition resulted in an initial jump in vapor pressure to about 160 × 10^{-3} mm. Over a period of about 6 days the pressure gradually dropped to an equilibrium value of 81 × 10^{-3} mm. This value was also obtained in a preliminary survey of the isotherm and is to be taken as the vapor pressure of the saturated solution. At this point the sample appeared moist, and measurements at higher water contents were not pursued.

TRIAZINES. X. THE INFRARED AND RAMAN SPECTRA OF 1,3,5-TRIAZINE[1,2]

BY JOSEF GOUBEAU, EVA L. JAHN, ALFRED KREUTZBERGER AND CHRISTOPH GRUNDMANN

Laboratory of Inorganic Chemistry, Technische Hochschule Stuttgart, Germany, and The Ohio State University Research Foundation, Columbus, Ohio

Received May 20, 1954

A comparison of the infrared spectrum of the recently discovered trimer of hydrocyanic acid, $C_3H_3N_3$, with those of some 1,3,5-triazine derivatives on the one hand and with the Raman spectrum of $C_3H_3N_3$ on the other hand results in physical evidence besides the chemical proofs that $C_3H_3N_3$ is 1,3,5-triazine, the long sought parent substance of so many 1,3,5-triazine derivatives.

It was recently reported[3] that the compound first prepared by Nef[4] and thereafter called "dimeric hydrocyanic acid," $C_2H_2N_2$, is not a dimer at all but is really a trimer of hydrocyanic acid, $C_3H_3N_3$. As mentioned in this preliminary communication, both chemical and physical methods were used in order to assign to $C_3H_3N_3$ its constitutional formula. While the pure chemical results have appeared elsewhere,[2] some of the physicochemical facts establishing the constitution of $C_3H_3N_3$ are presented here.

The empirical formula $C_3H_3N_3$ allows to construct several constitutional formulas; those with greater probability are listed as

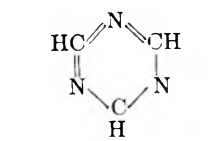

A

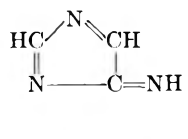

B

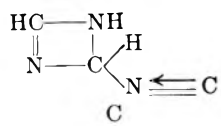

C

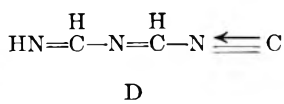

D

At the outset all those ring structures like type B containing an odd number of atoms in the ring can be excluded, since $C_3H_3N_3$ on hydrolysis yields HCOOH and NH_3 quantitatively,[5] thus making impossible the presence of C–C or N–N bondings. To distinguish between A, C and D the infrared and Raman spectra were measured.

In analogy to 2,4,6-triethyl-1,3,5-triazine[6] the infrared spectrum of $C_3H_3N_3$ was determined at first in a carbon disulfide solution (Fig. 1, I) and then compared with those of 2,4,6-trimethyl-1,3,5-triazine (Fig. 1, II), 2,4,6-triethyl-1,3,5-triazine (Fig. 1, III) and cyanuric chloride (Fig. 1, IV). However, that comparison was unsatisfactory insofar as carbon disulfide itself has a broad absorption band between 1400–1600 cm.$^{-1}$, covering in that range all bands of the dissolved substances. Therefore the infrared spectra of these four compounds were then taken in carbon tetrachloride solutions which showed that each of the four spectra contained two very strong, fairly well separated bands just in that region where the aforementioned carbon disulfide band covers everything. These two bands are very characteristic for all four substances and are obviously due to the triazine ring system. Thus, the infrared spectra of the carbon disulfide and carbon tetrachloride solutions supplement each other in yielding extensive and informative infrared spectral data of these compounds (Fig. 2, I–IV). From the similarity of these four spectra the conclusion can be drawn that of all the possible constitutions structure A possesses the greatest probability.

For comparison with the Raman spectrum of $C_3H_3N_3$ the data are compiled in Table I. These data indicate spectra with a relatively small number of lines, this in turn pointing to a highly symmetrical molecule structure as is represented by type A only. Since in both the Raman and the infrared spectra no lines of a triple bond, being expected in the range of 2000–2200 cm.$^{-1}$, were observed, structures like C and D could now be definitely excluded because their terminal isonitrile groupings ought to exhibit a frequency at 2100 cm.$^{-1}$. Thus both chemical and spectroscopical results point at formula A only, wherefore a discussion of the spectroscopical data related to structure A follows.

TABLE I

Raman	Infrared	Class
536 (0)	...	E″
594 (0)	...	E′
676 (2)	673 m.s.	E′
	735 s.	A_2''
921 (½)		E″
991 (4)		A_1'
	1070 v.w.	
1133 (4)		A_1'
	1170 m.	A_2''
1404 (0?)	1410 v.s.	E′
1560 (1)	1560 v.s.	E′
	1775 v.w.	
	1850 v.w.	
	1950 v.w.	
(3025)	3025 v.w.	E′
(3046)		A_1'

The triazine molecule possesses the symmetry D_{3h}; the symmetrical properties (Table II) lead to 10 Raman active vibrations, 3 of which are polarized and 7 depolarized, and furthermore to 7 infrared vibrations, 5 of which are identical with the particular Raman vibrations.

(1) This article is partially based on work performed under Project 116-B of The Ohio State University Research Foundation, sponsored by the Mathieson Chemical Corporation, Baltimore, Md.

(2) Preceding communication: C. Grundmann and A. Kreutzberger, *J. Am. Chem. Soc.*, **76**, 5646 (1954).

(3) C. Grundmann and A. Kreutzberger, *ibid.*, **76**, 632 (1954).

(4) J. U. Nef, *Ann.*, **287**, 377 (1895).

(5) L. E. Hinkel, E. E. Ayling and J. H. Beynon, *J. Chem. Soc.*, 676 (1935).

(6) T. L. Cairns, A. W. Larchar and B. C. McKusick, *J. Am. Chem. Soc.*, **74**, 5633 (1952).

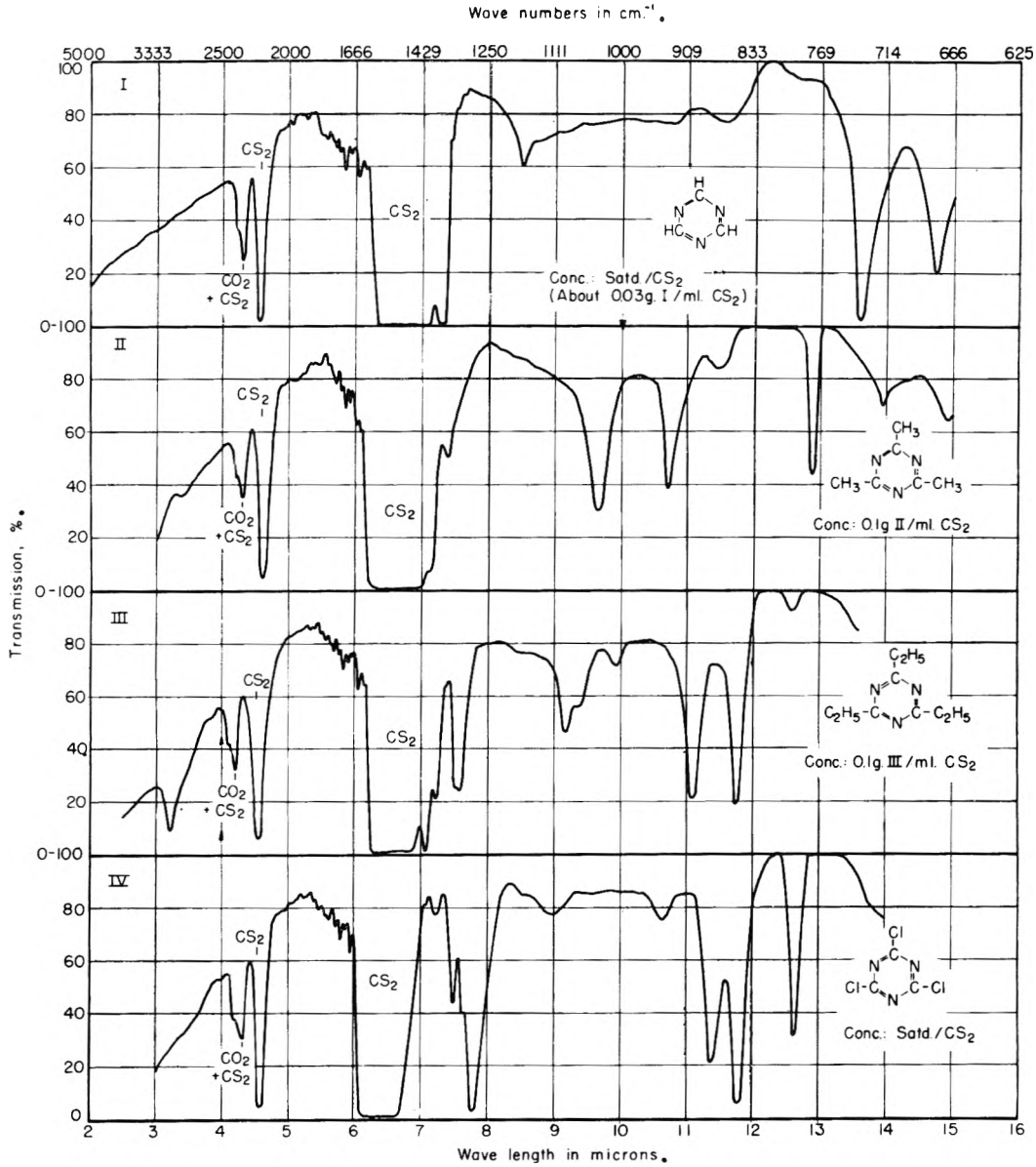

Fig. 1.—Infrared absorption spectra of 1,3,5-triazine (I), 2,4,6-trimethyl-1,3,5-triazine (II), 2,4,6-triethyl-1,3,5-triazine (III) and cyanuric chloride (IV), as determined in carbon disulfide solutions in a cell 0.005 in. thick.

TABLE II

p = polarized, f = forbidden, dp = depolarized, ia = inactive, a = active.

Class	Band type Raman	Band type Infrared	Number of vibrations
A_1'	p	ia	3
A_2'	f	ia	2
A_1''	f	ia	0
A_2''	f	a	2
E'	dp	a	5
E''	dp	ia	2

In the Raman spectrum 8 lines have been observed in the range up to 1560 cm.$^{-1}$. The 2 high CH vibrations could not be found with certainty, since they are likely to collide with the lines of the Hg spectrum. With this considered, the 10 Raman lines required for this type of molecule are indeed present.

From the number of infrared bands no conclusions can be drawn, because infrared frequencies lower than 600 cm.$^{-1}$ have not been measured and in the region above 1600 cm.$^{-1}$ several over- and combination vibrations occur.

In trying to assign the Raman lines observed to the particular vibrations, it must be said that any experimentally unobjectionable proof for the 3 lines of class A_1' is impossible yet, because of lack of polarization measurements. Solely from the intensity it may be inferred that the 2 strong Raman lines 991 (4) and 1133 (4) belong to the aforementioned symmetry class, since no infrared bands of these frequencies have been observed. The third missing vibration of this class must be a CH-valence vibration in the region of 3000 to 3050 cm.$^{-1}$, but it could not be found by the Raman effect in spite of several attempts. Presumably it is masked by a shifted Hg line of 3040 cm.$^{-1}$.

The 2 required vibrations of the class A_2'' which

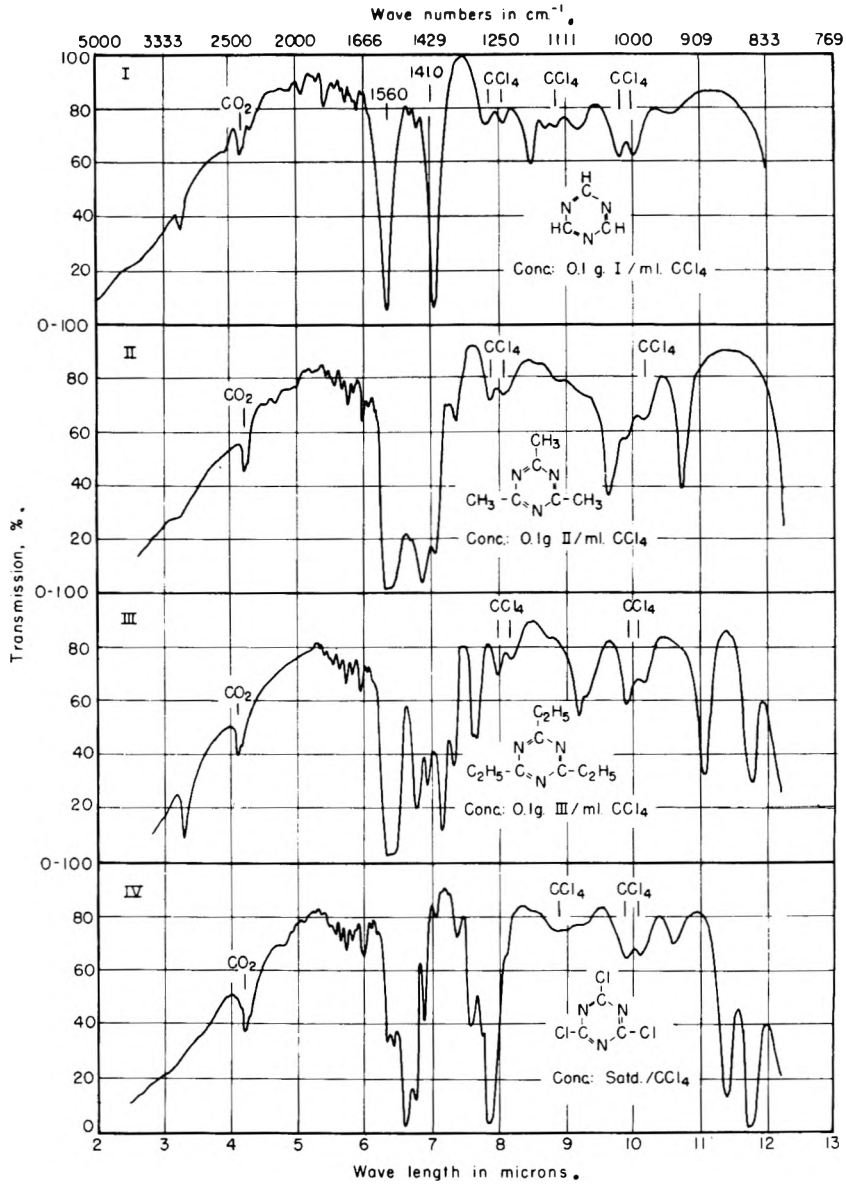

Fig. 2.—Infrared absorption spectra of 1,3,5-triazine (I), 2,4,6-trimethyl-1,3,5-triazine (II), 2,4,6-triethyl-1,3,5-triazine (III) and cyanuric chloride (IV), as determined in carbon tetrachloride solutions in a cell 0.005 in. thick.

are active in the infrared only are 735 and 1170 cm.$^{-1}$.

The frequencies 675, 1407 and 1560 cm.$^{-1}$ can be identified with certainty with 3 of the 5 infrared and Raman active vibrations of the class E′; the remaining 2 vibrations of this class can be assigned one CH-valence vibration and one of the 2 lower Raman lines; the analogy to benzene suggests line 594 cm.$^{-1}$.

For the 2 vibrations of class E″ that are Raman active only, the lines of 536 and 921 cm.$^{-1}$ are left over. Thus all Raman lines and all strong infrared bands have been identified with the expected vibrations of structure A, without difficulty. The very weak infrared bands still remaining can be explained as harmonic and compound vibrations: 1070 = 2.536; 1775 = 594 + 1170; 1850 = 2.921; 1950 = 536 + 1407.

The excellent conformity of the observed spectra with those to be expected of a benzene-like ring structure can be regarded as an extensive evidence for the triazine structure. The similarity of the triazine spectrum with the benzene spectrum, which

TABLE III

( ) = Observable in the infrared only. [ ] = Unobservable frequencies.

D_{6h}: C_6H_6[7]		D_{3h}: Triazine	
A_{1g}	992, 3063	A_1'	991, 1133, [3046]
B_{1u}	[≃1009], [≃3060]		
E_g^+	606, 1176, 1595, 3047	E′	594, 676, 1410, 1560, 3025
E_u^-	(1485), (1037), (3080)		
E_u^+	[406], [690]	E″	536, 921
E_g^-	850		
A_{2u}	(671)	A_2''	735, 1170
B_{2g}	[500], [780]		

(7) K. Kohlrausch, *Monatsh.*, **76**, 215 (1946).

becomes particularly clear in the following comparison of these two spectra (Table III), not only concerns the ring structure but also the binding forces prevailing in the ring system.

Experimental

The infrared data were obtained with a model 12C Perkin–Elmer spectrometer. The prism used was NaCl. The cell windows, too, consisted of NaCl with a $^1/_{10}$ mm. path length.

The 1,3,5-triazine[2] was purified by distillation over sodium metal, followed by slow sublimation at 35° bath temperature, these operations being carried out under exclusion of air moisture.

For the Raman measurements the solvent (CCl_4 or C_6H_6, respectively) was distilled onto the sublimed sample of triazine until a solution saturated at room temperature was obtained. Then this solution was filtered through a frit into the Raman tube. The measurements were carried out in a customary apparatus, for 1.5, 4.5 and 8 hours in CCl_4 solution and for 6 hours in C_6H_6 solution, using Hg 4358 Å. as the activating light source. Activation with Hg 4047 Å. led to decomposition of the substance.

Acknowledgment.—Two of the authors (C. G. and A. K.) are indebted to the Mathieson Chemical Corporation for their generous support of this work. Furthermore we wish to thank Mr. J. A. Curtis, Mathieson Chemical Corporation, Research Department, Niagara Falls, N. Y., for assistance in the infrared measurements.

BOUNDARY SPREADING IN SEDIMENTATION VELOCITY EXPERIMENTS. III. EFFECTS OF DIFFUSION ON THE MEASUREMENT OF HETEROGENEITY WHEN CONCENTRATION DEPENDENCE IS ABSENT

BY ROBERT L. BALDWIN

Contribution from the Department of Biochemistry, University of Oxford, and the Department of Chemistry, University of Wisconsin, Madison, Wisconsin

Received May 20, 1954

The method of Baldwin and Williams for finding $g(s)$, a substance's distribution of sedimentation coefficient, is based on extrapolation to infinite time. In this article the reliability of the extrapolation procedure is studied with the aid of the analytic expression for $g^*(S)$ (the quantity used in extrapolation) that results when $g(s)$ is taken to be Gaussian. Secondly, a method is presented for obtaining the moments of the boundary gradient curve directly from the continuity equation, without having to solve the differential equation for the shape of the boundary, and it is shown that moments obtained in this way confirm Faxen's solution of the differential equation. Finally, higher order terms are derived for the relation between p (the standard deviation of $g(s)$) and the standard deviation, σ, of the boundary gradient curve.

Introduction

The first article[1] of this series considered how the width of a sedimenting boundary could be related to the average diffusion coefficient (D) and the heterogeneity in sedimentation coefficient (s) of the sedimenting substance, for the case in which s and D do not depend on concentration (c). It was found that the contributions to the boundary width from diffusion and from heterogeneity in s depend on different powers of the time, so that it is possible to obtain the distribution of sedimentation coefficient, $g(s)$, by extrapolation to infinite time, in the same way that mobility distributions can be obtained.[2] Gosting[3] made a thorough theoretical study of the extrapolation to infinite time and found the correct function of time to use in order to obtain a linear extrapolation as infinite time is approached.

The problem of obtaining $g(s)$ under these conditions (*i.e.*, no dependence of s and D on c) thus becomes one of reaching this range of time where Gosting's limiting law holds. However, there is a basic limitation on the time for which an ultracentrifugal experiment may be continued: the experiment must stop before the boundary reaches the bottom of the cell. The definition of s ($s = (dx/dt)/\omega^2 x$) may be rearranged to show that the final value of $s\omega^2 t$ is limited[4] by cell and rotor design; consequently the length of an experiment can be increased only by lowering the speed of rotation and this decreases the resolution that can be obtained.

This situation poses two important problems in finding $g(s)$ by extrapolation to infinite time. First, how can one recognize for a given system whether or not the heterogeneity in s is sufficiently resolved that Gosting's limiting law will hold in the range of time accessible to experiment? Second, if one is outside this range, what other method could be used to find $g(s)$? The second problem, although very interesting, is also very difficult and will not be considered here. In order to study the first problem, an analytic expression for the quantity used in extrapolation ($g^*(S)$, the "apparent distribution" of s) has been obtained for the case that $g(s)$ is Gaussian. With this expression, the extrapolation to infinite time can be carried out with calculated values of $g^*(S)$[5] and comparison of the extrapolated with the true values of $g(s)$ made to show by how much the experiment departs from limiting law conditions. The success of the extrapolation is related to the resolution of the various sedimenting species obtained by the end of the experiment. The degree of resolution is characterized here by the ratio of the contributions to σ^2 (the second moment about

(1) J. W. Williams, R. L. Baldwin, W. M. Saunders and P. G. Squire, *J. Am. Chem. Soc.*, **74**, 1542 (1952).

(2) R. L. Baldwin, P. M. Laughton and R. A. Alberty, THIS JOURNAL, **55**, 111 (1951).

(3) L. J. Gosting, *J. Am. Chem. Soc.*, **74**, 1548 (1952).

(4) If t_f is the time elapsed at the end of the experiment, $s\omega^2 t_f = \ln (x_f/x_0) < 0.2$, where x_0 and x_f are the initial and final positions of the boundary.

(5) This method was used[2] to check on the reliability of mobility distributions obtained by extrapolation to infinite time.

the mean of the concentration gradient curve) from diffusion and from heterogeneity in s. Although the resulting conclusions are strictly valid only for the case of a Gaussian $g(s)$, they are quite useful in assessing the extrapolations used to find $g(s)$ for the systems which so far have been reported.[6-10]

Theory

Representation of $g^*(S)$ when $g(s)$ is Gaussian.—The definition[1] of $g^*(S)$ is

$$g^*(S) = \frac{\partial C/C_0}{\partial x}\,\omega^2 t(x^3/x_0^2) \qquad (1)$$

where x is distance from the center of rotation, x_0 marks the position of the meniscus, ω is angular speed of rotation, t is time and $(\partial C/C_0)/(\partial x)$ is the gradient of the total concentration at x, divided by the initial total concentration. The symbol S has been used in $g^*(S)$ to indicate that S is a variable derived from x by the relation

$$x = x_0 e^{S\omega^2 t} \qquad (1a)$$

and, unlike s, is not a property of a solute species.[11] In order to find $(\partial C/C_0)/(\partial x)$, the boundary-spreading equation[3] must be integrated.

$$\frac{\partial C/C_0}{\partial x} = \int_0^\infty \left(\frac{\partial c/c_0}{\partial x}\right)_s g(s)\,ds \qquad (2)$$

where $(\partial c/c_0)/\partial x_s$ is the concentration gradient produced by species of sedimentation coefficient s, divided by this species' initial concentration. In this case, $g(s)$ is given by the Gaussian function

$$g(s) = e^{-(s-\bar{s})^2/2p^2}/p(2\pi)^{1/2} \qquad (3)$$

where

$$\bar{s} = \int_0^\infty s\,g(s)\,ds \qquad (3a)$$

Faxen's[12] solution of the differential equation for the ultracentrifuge[13] may be used to give $(\partial c/c_0)/(\partial x)_s$[14]

$$\left(\frac{\partial c/c_0}{\partial x}\right)_s = \frac{e^{-3s\omega^2 t}}{x_0\sqrt{2\pi a}}\,e^{-z^2/2a}\{(1 - (3/8)a - (15/128)a^2 + \ldots) + z(1/2 - (9/16)a + \ldots) + z^2(3/8 - (45/64)a + \ldots) + z^3(5/16 + \ldots) + z^4(35/128 + \ldots) + \ldots\} \qquad (4)$$

where

$$a = \frac{D}{s\omega^2 x_0^2}(1 - e^{-2s\omega^2 t}) \qquad (4a)$$

$$z = (x_0 e^{s\omega^2 t} - x)/x_0 e^{s\omega^2 t} \qquad (4b)$$

This series converges rapidly in the range of time accessible to experiment, since a will not exceed about 4×10^{-4}. The conditions under which this solution of the differential equation holds are that s and D be constant and that the concentration at the meniscus be zero for all times later than $t = 0$.[15]

After substituting (3) and (4) into (2), the resulting equations can be replaced by a series of known integrals of the form $K_1 \int_{-\infty}^{+\infty} y^n e^{-y^2 - K_2}\,dy$, where $y = K_3(s - \bar{s})$, by expanding the necessary functions of s as Taylor's series about $(s - \bar{s})$. The final expression for $g^*(S)$, in which terms contributing less than 0.2% to $g^*(S)$ have been dropped, is

$$g^*(S) = \left(\frac{e^{-(S-\bar{s})^2/2p^{*2}}}{p^*2\sqrt{\pi}}\right)\left[\frac{3}{2}e^{2b} - \frac{1}{2}e^{3b} + \ldots\right] \qquad (5)$$

where

$$b = (\omega^2 t)(S - \bar{s})/\left(1 + p^2\frac{\omega^4 x x_0 t}{2D}\right) \qquad (5a)$$

$$p^{*2} = p^2 + 2D/\omega^4 x x_0 t \qquad (5b)$$

In carrying out the extrapolation to infinite time with calculated values of $g^*(S)$, it is not necessary to consider what happens to the analytic expression for $g^*(S)$ in the range of time beyond that accessible to experiment (*i.e.*, $s\omega^2 t > 0.2$). The factors which determine the extrapolated value of $g(s)$, for a given s, are the values of $g^*(S)$ for $s\omega^2 t < 0.2$, the way in which these values change with time, and the manner of carrying out the extrapolation. The actual value of $g(s)$ is given by the distribution function—in this case the Gaussian function—used in obtaining the analytic expression for $g^*(S)$. Thus it is allowable to drop terms from the expression (5) for $g^*(S)$ which are negligible during an experiment even though these terms might become large in the range of time corresponding to $s\omega^2 t >> 1$.

A Method for Finding Moments and its Use in the Confirmation of Faxen's Series.—It is possible to confirm Faxen's solution of the differential equation by an unusual approach which is given here because Faxen's equation is used repeatedly in this article and because the approach gives promise of being widely applicable in the problems of sedimentation, diffusion and electrophoresis. This approach makes use of a method for finding moments of the boundary gradient curve of $(\partial c/\partial x)$ *vs.* x, when the equation describing this curve is not known. The case considered by Faxen is that of sedimentation and diffusion of a single solute from a completely sharp initial boundary in a sector cell and changing field, where s and D are constants, the concentration at x_0 is zero for $t > 0$, and the area (Kx) and field strength $(\omega^2 x)$ are proportional to the distance from the center of rotation.

In this case, the n'th moment of the boundary gradient curve is defined by

$$\mu_n = \frac{\int_{x_0}^\infty x^n \frac{\partial c}{\partial x}\,dx}{\int_{x_0}^\infty \frac{\partial c}{\partial x}\,dx} = \frac{\int_0^{c_t} x^n\,dc}{c_t} \qquad (6)$$

(6) L. E. Miller and F. A. Hamm, THIS JOURNAL, **57**, 110 (1953).
(7) J. R. Cann, *J. Am. Chem. Soc.*, **75**, 4213 (1953).
(8) R. L. Baldwin, *Brit. J. Exp. Path.*, **34**, 217 (1953).
(9) A. G. Ogston and E. F. Woods, *Trans. Faraday Soc.*, **50**, 635 (1954).
(10) (a) J. W. Williams, W. M. Saunders and J. Circirelli, THIS JOURNAL, **58**, 774 (1954); (b) J. W. Williams and W. M. Saunders, *ibid.*, **58**, 854 (1954).
(11) Thus S is used in $g^*(S)$ because this is a quantity which is defined (for a given time and experiment) by a position in the cell. On the other hand, s is used in $g(s)$ because, for a given system, this is a property of the solute species with sedimentation coefficient s.
(12) H. Faxen, *Arkiv Mat. Astron. Fysik*, **21B**, No. 3 (1929).
(13) O. Lamm, *ibid*, **21B**, No. 2 (1929).
(14) This equation was obtained by rearranging equation 32 of the article by Gosting,[3] who repeated Faxen's solution and carried additional terms of the series.
(15) If this series were expanded instead about the maximum of the concentration gradient curve, the magnitude of the terms in brackets would be reduced; consequently the choice of $x_0 e^{s\omega^2 t}$ as an origin suggests a greater skewness of this curve than in fact exists. The position in the boundary corresponding to $x_0 e^{s\omega^2 t}$ is the square root of the second moment of the concentration gradient curve[15a] and this position does not coincide with the center of a Gaussian curve.
(15a) R. J. Goldberg, THIS JOURNAL, **57**, 194 (1953).

where c_t, the concentration in the homogeneous solution beyond the boundary, is given by[16]

$$c_t = c_0 e^{-2s\omega^2 t}$$

The n'th moment is a function only of time, in a given experiment, while the concentration is a function of the two variables x and t. In differentiating (6), the equation of Leibnitz[17] for the differentiation of a definite integral is used; x is treated as a function of c and t, since, within the boundary region, any given set of values of c and t uniquely determines x.

$$\frac{d\mu}{dt}n = \frac{1}{c_t}\left\{n\int_0^{c_t} x^{n-1}\left(\frac{\partial x}{\partial t}\right)_c dc + x_w{}^n \frac{dc_t}{dt}\right\} - \mu_n\left(\frac{1}{c_t}\right)\frac{dc_t}{dt} \quad (7)$$

where[13]

$$\frac{dc_t}{dt} = -2c_t s\omega^2 \quad (7a)$$

and x_w denotes the value of x at which c becomes equal to c_t. The partial derivative $(\partial x/\partial t)_c$ has the physical significance of being the rate of movement of a plane at constant concentration.

The continuity equation for a sector cell

$$\frac{\partial c}{\partial t} = -\frac{1}{Kx}\frac{\partial(KxJ)}{\partial x} \quad (8)$$

may be used to transform this into a more tractable form since

$$\left(\frac{\partial x}{\partial t}\right)_c = -\left(\frac{\partial c}{\partial t}\right)_x \Big/ \left(\frac{\partial c}{\partial x}\right)_t \quad (9)$$

The flow per unit area, J, is given by[13]

$$J = -D\frac{\partial c}{\partial x} + cs\omega^2 x \quad (10)$$

for a species of zero net charge. Substituting (8), (9) and (10) into (7), and rearranging with the aid of integration by parts gives

$$\frac{d\mu}{dt}n = ns\omega^2\mu_n + (n)(n-2)D\mu_{n-2} \quad (11)$$

for integral values of n.

This recursion formula may be integrated in a straightforward manner for $n = 0$ and $n = 2$ and then, in successive steps, the positive even moments may be found.

$$\mu_0 = 1 \quad (12a)$$

$$\mu_2/x_0{}^2e^{2s\omega^2 t} = 1 \quad (12b)$$

$$\mu_4/x_0{}^4e^{4s\omega^2 t} = 1 + 4a \quad (12c)$$

$$\mu_6/x_0{}^6e^{6s\omega^2 t} = 1 + 12a + 24a^2 \quad (12d)$$

where a is the quantity defined in equation 4a. In general

$$\mu_{2n}/x_0{}^{2n}e^{2ns\omega^2 t} = \sum_{m=1}^{n}\frac{n!}{m!(n-m)!}(2a)^{n-m}\frac{(n-1)!}{(m-1)!} \quad (12e)$$

The first five even moments are sufficient to confirm the coefficients of Faxen's solution which have been given in equation 4. First $\partial c/\partial x$ is represented by a series of the form

$$\frac{\partial c}{\partial x} = \frac{c_t}{(x_0e^{s\omega^2 t})(2\pi a)^{1/2}}e^{-z^2/2a}\{\alpha + \beta z + \gamma z^2 + \delta z^3 + \epsilon z^4 + \ldots\} \quad (13)$$

where the coefficients

$$\alpha = A + A'a + A''a^2 + A'''a^3 + \ldots \quad (13a)$$

$$\beta = B + B'a + B''a^2 + \ldots \quad (13b)$$

$$\gamma = C + C'a + C''a^2 + \ldots \quad (13c)$$

$$\ldots$$

are to be determined. Next the moments defined by (6) are found in terms of the coefficients of (13). For example

$$\mu_0 = \frac{1}{c_t}\int_{x_0}^{x_w}\frac{\partial c}{\partial x}dx = \frac{1}{(2\pi a)^{1/2}}\int_{-\infty}^{+\infty}e^{-z^2/2a}\{\alpha + \beta z + \gamma z^2 + \delta z^3 + \epsilon z^4 + \ldots\}dz = \alpha + \gamma a + \epsilon(3a^2) + \ldots \quad (14)$$

(The limits of the cell are taken to be infinitely far from the boundary; this corresponds to the assumption used in deriving (4) and (11) that the concentration at x_0 is zero for $t > 0$ and that $c_t = c_0e^{-2s\omega^2 t}$.) By comparing (14) with (12a) one sees that

$$A = 1 \quad (15a)$$

$$A' + C = 0 \quad (15b)$$

$$A'' + C' + 3E = 0 \quad (15c)$$

and so forth.

The significant characteristic of this method for finding moments is that equation 7 splits into a series of integrals, each of which may be evaluated separately. This is a result of the way in which $(\partial x/\partial t)_c$ is derived from the flow equation and of the additivity of flows from separate processes such as sedimentation and diffusion (*cf.* equations 9 and 10). In order to illustrate the usefulness of this method for other problems, consider the case of concentration-dependent diffusion in a rectangular cell. The approach shown in equations 7–10 yields, for this case

$$\frac{d\mu_n}{dt} = \frac{(n)(n-1)}{(c_2-c_1)}\int_{c_1}^{c_2}x^{n-2}\,D\,dc \quad (16)$$

This equation contains two important relations found by Gralén[18]: the first moment is stationary and the second moment is $2D_It$, where D_I is the integral diffusion coefficient. It is interesting to note that equation 16 is derived without use of Boltzmann's assumption that c is a function of the single variable $xt^{-1/2}$.

The Second Moment About the Mean of the Entire Boundary Gradient Curve When Several Components Are Present.—An earlier derivation[1] of the expression for σ^2 was based on several approximations, which could be checked only by numerical examples. It is possible now, with the knowledge that[15a]

$$\frac{1}{c_{i,t}}\int_{x_0}^{x_w}x^2\frac{\partial c_i}{\partial x}dx = x_w{}^2e^{2s_i\omega^2 t} \quad \text{(see also 12b)}$$

and hence that

$$\int_{x_0}^{x_w}x^2\frac{\partial c_i}{\partial x}dx = x_0{}^2c_{0i} \quad (17)$$

to derive this expression in a simple and general manner.

(16) T. Svedberg and H. Rinde, *J. Am. Chem. Soc.*, **46**, 2677 (1924).

(17) *Cf.* I. S. and E. S. Sokolnikoff, "Higher Mathematics for Engineers and Physicists," McGraw-Hill Book Co., Inc., New York, N. Y., 1941, p. 167.

(18) N. Gralén, Dissertation, Uppsala, 1944.

The second moment about the mean is defined by

$$\sigma^2 = \int_{x_0}^{x_w} x^2 \frac{\partial C}{\partial x}\,dx \Big/ \int_{x_0}^{x_w} \frac{\partial C}{\partial x}\,dx - \left\{ \int_{x_0}^{x_w} x \frac{\partial C}{\partial x}\,dx \Big/ \int_{x_0}^{x_w} \frac{\partial C}{\partial x}\,dx \right\}^2 \quad (18)$$

Since $(\partial C)/(\partial x)$, the total concentration gradient at x is $\sum_i (\partial c_i/\partial x)$, these integrals may be replaced in the following way.

$$\int_{x_0}^{x_w} x^2 \frac{\partial C}{\partial x}\,dx = \sum_i \int_{x_0}^{x_w} x^2 \frac{\partial c_i}{\partial x}dx = x_0^2 C_0 \quad (19a)$$

$$\int_{x_0}^{x_w} x \frac{\partial C}{\partial x}\,dx = \sum_i \int_{x_0}^{x_w} x \frac{\partial c_i}{\partial x}\,dx \quad (19b)$$

$$\int_{x_0}^{x_w} \frac{\partial C}{\partial x}\,dx = \sum_i c_{0i} e^{-2s_i\omega^2 t} \quad (19c)$$

where $C_0 = \Sigma c_{0i}$. The same assumptions that were made previously (s_i and D_i are constants, $c_i = 0$ at x_0) are applied so that, according to (18) and (12b)

$$\int_{x_0}^{x_w} x \frac{\partial c_i}{\partial x}\,dx = c_{0i}\, e^{-2s_i\omega^2 t}\{x_0^2 e^{2s_i\omega^2 t} - \sigma_i^2\}^{1/2} \quad (20)$$

$$= x_0 c_{0i} e^{-s_i\omega^2 t}\left\{1 - \frac{\sigma_i^2}{2x_0^2} e^{-2s_i\omega^2 t} - \ldots\right\} \quad (20a)$$

Equations 18 and 4 may be used to give σ_i^2

$$\sigma_i^2 = x_0^2 e^{2s_i\omega^2 t}\left(a_i + \frac{1}{2}a_i^2 + \ldots\right) \quad (21)$$

Then expanding $e^{-ns_i\omega^2 t}$ as a Taylor's series about $e^{-n\bar{s}\omega^2 t}$ gives

$$\Sigma c_{0i} e^{-ns_i\omega^2 t} = C_0 e^{-n\bar{s}\omega^2 t}\{1 + (np\omega^2 t)^2/2 - (nq\omega^2 t)^3/6 + (nr\omega^2 t)^4/24 - \ldots\} \quad (22)$$

where p^2, q^3 and r^4 are the second, third and fourth moments about the mean of the distribution of sedimentation coefficient.

After making the necessary substitutions, equation 18 becomes

$$\sigma^2 = (p\omega^2\bar{x}t)^2\left\{1 - (q^3/p^2)(\omega^2 t) + (\omega^2 t)^2\left[\frac{7}{12}\frac{r^4}{p^2} - \frac{5}{4}p^2\right] + \ldots\right\} + 2\bar{D}t\{1 + \bar{s}\omega^2 t + 2\omega^2 t(\bar{s} - \bar{s}') + (\omega^2 t)^2\left[\frac{9}{2}\bar{s}^2 + \frac{13}{6}\bar{s}'^2 - 6\bar{s}\bar{s}' + \frac{13}{6}p'^2 - \frac{5}{2}p^2\right] + \ldots\right) \quad (23)$$

where

$$\bar{x} = \int_{x_0}^{x_w} x \frac{\partial C}{\partial x}\,dx \Big/ \int_{x_0}^{x_w} \frac{\partial C}{\partial x}\,dx \quad (23a)$$

$$\bar{s}' = \sum_i s_i c_{0i} D_i \Big/ \sum_i c_{0i} D_i \quad (23b)$$

$$p'^2 = \sum_i (s_i - \bar{s}')^2 c_{0i} D_i \Big/ \sum_i c_{0i} D_i \quad (23c)$$

It should be noted that $\bar{s}$, p, $\bar{D}$, etc., all refer to the original solution and not to the homogeneous solution beyond the boundary after it has been diluted by sedimentation. The expression derived previously[1,19] for σ^2 is

$$\sigma^2 = (p\omega^2\bar{x}t)^2\{1 + \ldots\} + 2\bar{D}t\{1 + \bar{s}\omega^2 t + \ldots\} \quad (24)$$

This same approach may be applied to the analogous problem in electrophoresis, to obtain an alternative derivation for the relation[2] between σ^2, $\bar{D}$ and the standard deviation of the mobility distribution.

In estimating the magnitude of the higher terms of (23), it is possible to assign reasonable sample values to p, q and r by considering the properties of familiar distributions. For example, q is zero for any symmetrical distribution and $3p^4 = r^4$ for the Gaussian distribution. Calculation for various cases shows that the higher order terms of (23) (*i.e.*, those not included in equation 24) will rarely be equal to 2% of σ^2.

Discussion

The Extrapolation of $g^*(S)$ to Infinite Time.—Figure 1 shows the change in $g^*(S)$ with time when $g(s)$ is Gaussian, for the case that $p = 1 \times 10^{-13}$ sec. and $D = 5 \times 10^{-7}$ cm.^{2} sec.$^{-1}$. The effects of diffusion are very considerable near the beginning of the experiment ($t = 1 \times 10^3$ sec.) and still quite important at the end ($t = 5 \times 10^3$ sec.). Figure 2 shows, incomparison with the true distribution, the extrapolated one obtained by placing a straight line through two values of $g^*(S)$ plotted against $1/t$, at $t = 2 \times 10^3$ and 5×10^3 sec. The extrapolated values of $g(s)$ are low at the center of the curve, where the error in extrapolation is most serious, and high at the sides. Consequently the error in the area is small and deviations from unity[6] of $\int_0^\infty g(s)ds$ are likely to reflect difficulties with baselines. (The error in the extrapolated values, which is caused by curvature of the plot of $g^*(S)$ *vs.* $1/t$, could be reduced by choosing the two times to be 4×10^3 and 5×10^3 sec. instead; however, such a procedure would unduly magnify the effects of the uncertainty in experimental data on the slope of the extrapolation.)

TABLE I

CALCULATIONS FOR THE CASE WHEN $g(s)$ IS GAUSSIAN: THE RATIO OF THE EXTRAPOLATED TO TRUE VALUES OF $g(s)$ AS A FUNCTION OF R

R[a]	$g^*(\bar{s})/g(\bar{s})$ $t/t_f = 0.2$[b]	t/t_f[b]	Extrap.[c]
100	0.974	0.995	1.000
10	.808	.954	0.996
5	.696	.913	.981
3	.601	.866	.956
2	.523	.817	.922
1	.398	.707	.828

[a] R is the ratio, at the end of the experiment, of the contributions to σ^2 from heterogeneity in s and from diffusion. (σ^2 is the second moment about the mean of the concentration gradient curve and $R = p^2\omega^4 x x_0 t_f/2D$). [b] These values are included to show by how much $g^*(\bar{s})$ changes with time during the experiment. They are calculated from $g^*(\bar{s})/g(\bar{s}) = (1 + 2D/p^2\omega^4 x x_0 t)^{-1/2}$ (see equation 5). For the purpose of calculating the change of x with time, in this equation, x_0 was taken to be 5.8 cm., $\bar{s}$ to be 4×10^{-13} sec., ω^2 to be 3.9×10^{-7} sec.$^{-2}$ and t_f to be 5×10^3 sec. [c] The values of $g^*(\bar{s})$ were extrapolated to infinite time by placing a straight line through values of $g^*(\bar{s})$ plotted against $1/t$ for the two times $t/t_f = 0.4$ and $t/t_f = 1$. (By $g^*(\bar{s})$ is meant $g^*(S = \bar{s})$.)

The ratio, at the end of the experiment, of the boundary width produced by heterogeneity to that by diffusion is a convenient parameter with which to characterize the extrapolation. This ratio (R)

(19) See equations 1 and 2 of reference 1; the term in p^2 of equations 3 and 4 of this reference should be multiplied by $e^{3\omega^2 t}$.

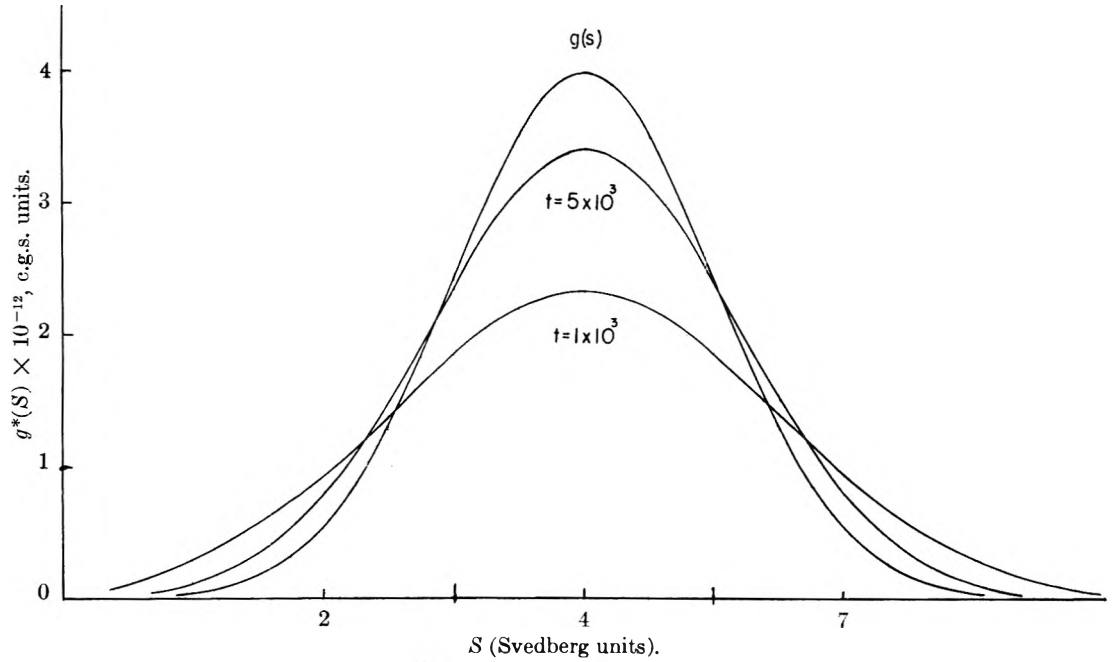

Fig. 1.—An illustration of how $g^*(S)$ changes with time when $g(s)$ is Gaussian. In this example, the standard deviation of the distribution of s, p, $= 1 \times 10^{-13}$ sec., $D = 5 \times 10^{-7}$ cm.^{2} sec.$^{-1}$ and $\omega^2 = 3.9 \times 10^7$ sec.$^{-2}$

is given with sufficient accuracy for this purpose by $p^2\omega^4\bar{x}x_0t_f/2D$ (*cf.* equation 24), where t_f is the time at the end of the experiment. In Table I, the ratio of the extrapolated to the true value of $g(s)_{max.}$ (where the error in extrapolation is most serious) is given as a function of R. Table I should be a useful guide to the feasibility of obtaining $g(s)$ by extrapolation in the case of any symmetrical distribution with only one maximum.

In Table II the value of R has been calculated for the various determinations of $g(s)$ reported in the literature[6-10]; p was estimated from the maximum height of the distribution by the formula for a Gaussian curve and, since t_f has not usually been reported, it was assumed in all cases that $s\omega^2t_f = 0.15$. Also given is the error in the extrapolated value of $g(s)_{max.}$ that would be expected were the distribution Gaussian and the extrapolation to infinite time carried out after the manner of Table I.

TABLE II

RESOLVING POWER OF THE EXTRAPOLATION TO INFINITE TIME, AS ESTIMATED FOR VARIOUS DETERMINATIONS OF $g(s)$

Material	R^a	$\frac{g^*(\bar{s})\ \text{extrap.}^b}{g(\bar{s})\ \text{true}}$	D ($\times 10^7$)	p ($\times 10^{-13}$)	$\bar{s}$ ($\times 10^{-13}$)
γ_1-Globulin[1]	1.9	0.92	4.3	0.7	7.0
Polyvinylpyrrolidone[6] (No. II)	1.8	.91	4.1	.3	1.4
Shiga toxin[8]	2.2	.93	5.7	.8	4.8
Dextran[10]	9.4	.99	(3.3)	.9	3.0
γ-Globulin[7]	0.4		3.8	.3	6.6

[a] In calculating R ($R = p^2\omega^4\bar{x}x_0t_f/2D$), ω^2 was taken to be 3.9×10^7 sec.$^{-2}$ in all cases except that of the Shiga toxin, where $\omega^2 = 3.2 \times 10^7$ sec^{-2}. [b] If $g(s)$ were Gaussian and the extrapolation to infinite time carried out after the manner of Table I, this would be the ratio of the extrapolated to the true value of $g(s)_{max.}$ expected from the corresponding value of R.

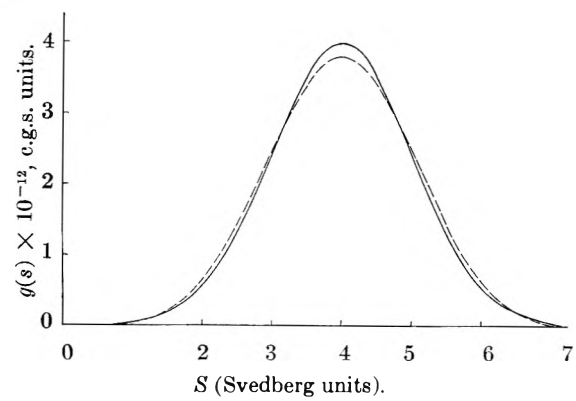

Fig. 2.—Comparison of $g(s)$ (solid line) with the extrapolated values of $g(s)$ (dashed line) when the constants in the expression for $g^*(S)$ (equation 5) are those given in Fig. 1 and the range of time used for extrapolation is 2×10^3 to 5×10^3 sec. ($R = 2.8$).

When there is more than one maximum in $g^*(S)$, the ratio of boundary spreading from heterogeneity to that from diffusion is not a good parameter with which to characterize the extrapolation to infinite time. It would be possible to have a mixture of two components, each homogeneous, where the value of p for the system would be large because of the difference in s of the two components; a high value of R in this case would not mean a good extrapolation to infinite time. Consequently, other ways of checking on the extrapolation are needed.

It is probably safe to infer from Table I that if, at one of the maxima, the value of $g^*(S)$ at $t/t_f = 0.2$ is less than 2/3 its final value (*i.e.*, at $t/t_f = 1$), then the extrapolation to infinite time will not give a good representation of $g(s)$ because too much of the boundary spread has been caused by diffusion. A comparable test is whether or not the same value of $g(s)_{max.}$ is obtained from the extrapolation of

$g^*(S)$ *vs.* $1/t$ as from the extrapolation of $[g^*(S)]^{-2}$ *vs.* $1/t$. In the limiting law range, both procedures give the same intercept,[20] whereas, outside this range, the error in the value of $g(s)_{max.}$ obtained is less when $[g^*(S)]^{-2}$ is extrapolated *vs.* $1/t$. (Equation 5 shows that, for a Gaussian $g(s)$, the plot of $[g^*(S)]^{-2}$ *vs.* $1/xt$ gives the correct value of $g(s)_{max.}$, regardless of the resolving power.)

This article reveals two reasons for focussing interest on the calculation of p from measurements of σ^2. First, since direct calculation rather than extrapolation is used, p can be obtained from values of σ^2 when the degree of resolution is too low for $g(s)$ itself to be obtained from the extrapolation to infinite time. Secondly, comparison of the values of p found from σ^2 and from $g(s)$ would be a valuable general check on the method. Before this can be done, the effects of the dependence of s on c must be taken into account. This is accomplished in finding $g(s)$ by extrapolating[10a,10b] $g(S)$ to infinite dilution (where $g(S)$ is the curve obtained by extrapolation of $g^*(S)$ to infinite time, without correction for the dependence of s on c) or by applying a theoretical correction[21] to $g(S)$. However, extrapolation to infinite dilution of "apparent" values of p (*i.e.*, values calculated from σ^2 without correction for the dependence of s on c) is not feasible, because such "apparent" values would change with time within an experiment. Work is in progress on the explicit correction of σ^2 for the dependence of s on c; thus far only the case of a single solute has been solved rigorously.[22]

Acknowledgments.—A portion of this material was taken from a thesis presented in June 1953 for the degree of Doctor of Philosophy at the University of Oxford. This work was done with the guidance of Dr. A. G. Ogston, to whom I am indebted for helpful advice and encouragement. More recently, the detailed suggestions of Dr. L. J. Gosting have brought about several improvements in the development of the problem. Thanks are also due to Dr. J. W. Williams for his continued and beneficial interest in this research. Finally, the author is indebted to the du Pont Co. for financial support during the academic year 1953–1954.

(20) The difference in the extrapolated value of $g(s)_{max.}$ when $g^*(S)$ is plotted against $1/t$ rather than against σ_1/x^2t (the variable suggested by Gosting[2]) is less than 0.5% for the cases listed in Table I; this is less than the present experimental uncertainty of measuring $g^*(S)$.

(21) R. L. Baldwin, *J. Am. Chem. Soc.*, **76**, 402 (1954). The theory is derived for the case that diffusion is negligible; in order to apply it when diffusion is not negligible, the assumption is required that $g(S)$, the curve found by extrapolation to infinite time, is identical with the curve that would be found if diffusion were negligible.

(22) R. L. Baldwin, *Biochem. J.*, to be published.

VISCOSITY OF THE SODIUM–POTASSIUM SYSTEM

BY C. T. EWING, J. A. GRAND AND R. R. MILLER

Physical and Inorganic Branch, Chemistry Division, Naval Research Laboratory, Washington 25, D. C.

Received May 24, 1954

Viscosity coefficients in the low temperature range from 60° (or the m.p.) to 200° for sodium, potassium and several alloys have recently been published. A nickel viscometer of the Ostwald type has been used to substantiate these measurements and to extend results to 700°. For each metal and alloy, the extended coefficients also exhibited normal temperature variation which is adequately expressed by an equation set forth by Andrade. The coefficients at higher temperatures were intended for engineering application and no attempt was made to duplicate the precision of the results measured in glass. A composite curve of isotherms representing both sets of measurements can be drawn from which the viscosity-temperature curve for any alloy in the sodium–potassium system can be derived.

Introduction

Fluid and thermal properties of liquid metals should become increasingly important as further applications for their use as heat transfer agents become apparent. These properties are also important in basic theoretical studies because of the simplicity and ideality of their atomic structures.

Viscosity coefficients to 200° for sodium, potassium and their alloys were measured by the present authors[1] in a modified Ostwald viscometer of glass. A larger capillary type viscometer of nickel has been used to extend these measurements to 700°. In overlapping temperature ranges, the two independent sets of measurements show good agreement. Viscosity coefficients for the pure metals and their alloys were found to vary with temperature in a continuous family of curves. Composition isotherms, therefore, show no apparent discontinuities at any temperature.

Coefficients for the liquid metals that appear in the literature were covered by references in the previous article. The most reliable work was apparently that of Chiong[2] who used an oscillating sphere method to measure coefficients for the pure metals to 350°. The Naval Research Laboratory results presented for sodium show excellent agreement with Chiong's work having a maximum disagreement of less than 2% at 350°. On the contrary, the values for potassium, though coinciding with those by Chiong at 70°, diverge at higher temperatures and differ by as much as 14% at 350°.

Experimental

Of the applicable viscosity methods, the capillary flow type was most readily adaptable to the conditions of measurement. The chemical activity of the alkali metals with moisture, oxygen, and container materials dictated the design of a nickel, closed-type viscometer. A description of this viscometer and the factors involved in its operation as a relative measuring tool by calibration with water will be described.

Apparatus and Equipment.—The viscometer consisted essentially of two cylindrical 3-liter tanks which were connected by a long capillary. The rate of liquid flow through the capillary was obtained from observed weight change in

(1) C. T. Ewing, J. A. Grand and R. R. Miller, *J. Am. Chem. Soc.*, **73**, 1168 (1951).

(2) Y. S. Chiong, *Proc. Roy. Soc.* (*London*), **A157**, 264 (1936).

the lower tank. For this purpose the tank was positioned directly on the platform of a sensitive dial scale which was arranged to read weight change of the container continuously. To obtain maximum sensitivity for the scales, the movement of the dial pointer was magnified by a calibrated optical-beam system.

To permit introduction of the liquid sample and subsequent operation of the viscometer as a closed system under a controlled atmosphere, the two tanks were interconnected by a system of tubes which had suitable flexibility for weighing travel. A controlled pressurization of either container with covering gas was permitted by the tubing system connected to the top of each tank. Helium was used as covering for the alkali metals and was purified by passage through copper at 450° and then through activated charcoal at the normal b.p. of nitrogen. Another tube, interconnecting the bottom of each tank, was required to speed the return of the fluid to the upper container. This return line was equipped with a 200-mesh strainer and a cold trap seal to prevent downward flow along this route during capillary flow experiments. The liquid was introduced initially from a closed reservoir attached to the return line. Each alkali metal was introduced through a nickel screen pack (200 mesh).

The design of the viscometer permitted close temperature control for the complete liquid path. The temperature sensitive portion of the viscometer, the upper tank and the capillary, were enclosed in an electric furnace controllable to ±0.2°. Insulated windings were also provided for temperature control of the lower tank and the exposed section of capillary connecting the two tanks. Liquid temperatures were determined independently of the control system using calibrated chromel–alumel thermocouples with a precision potentiometer.

Effective Head.—A static head for either water or metal at any temperature and at any position of the liquid relative to the upper and lower tanks was readily determined experimentally by noting the applied pressures on the lower tank that were just necessary to start the liquid flow upward or downward in the capillary. In practice an average static head or an effective head for a given temperature was determined between the positions of the liquid equivalent to those head limits used in the flow experiments. An alternate method, which was used to obtain or to check the effective heads for the liquid metals, was to calculate the value directly from the experimental water head. Since equivalent sample volumes of liquid metal and calibration fluid were always introduced, the effective head for each metal was readily calculable from the measured water head and the density of the metal sample by applying a small correction for any change in head limits with volume expansion.

Calibration and Kinetic Energy.—Calibration of the viscometer with water required some variation of the usual method. With the liquid metals it became necessary to maintain flow rates approaching the turbulent region which resulted in an appreciable kinetic energy factor. The expansion of the nickel capillary over the wide temperature range also had to be incorporated in the calibration procedure. The Poiseuille equation for relative measurements which includes kinetic energy and dimension factors may be reduced to the practical form: $\eta = A\gamma^3 pt - (Bd/t\gamma)$, in which η is the absolute viscosity, p is the mean effective pressure, d is the density, t is the time rate of flow in sec./ml., A and B are viscometer constants, and γ is the ratio of a length of nickel at the temperature of measurement to the length at room temperature.

Water viscosity determinations were made for a wide range of flow conditions by varying both temperature and applied head. A capillary (520 cm. in length and averaging 0.238 cm. inside diameter) was used for all measurements on sodium and three alloys. This capillary was disassembled once during the course of measurements for cleaning purposes; however, a correlation of water data taken before and after the cleaning operation determined that the viscometer was not altered. This simplified the calibration procedure, allowing a single calibration for all four metals.

A convenient graphical method for determining the constants of the viscometer is to plot $\eta(t\gamma/d)$ as ordinate and $pt^2\gamma^4/d$ as abscissa from the straight-line form of the equation presented. Viscosity coefficients for water were obtained from NBS,[3] and densities from the "Int. Critical Tables." A plot of the water calibration data with the capillary described above was linear in the major range of flow conditions for the liquid metals (Reynold's numbers 500 to 2500). Only two measurements for sodium at 140° and two measurements for the 66.9 wt. % potassium alloy below 85° have Reynold's numbers below 500.

The calibration just described was for the capillary used with sodium and three alloys. A smaller capillary (0.159 cm. diameter) of the same length was substituted for the potassium experiments. This capillary also was calibrated with water in a manner identical to that just described.

Results and Discussions

In this section are presented viscosity results for metallic sodium, potassium and three alloys. The experimental results are recorded in Tables I–V. Density values for the metals were obtained from data of this Laboratory and the Mine Safety Appliances Company, Pittsburgh, Pa.[4] The accuracy of the density figures to 700° is better than

TABLE I

VISCOSITY OF SODIUM

Temp., °C.	Density, g./ml.	Viscosity, centipoises	Temp., °C.	Density, g./ml.	Viscosity, centipoises
143	0.917	0.565	371	0.861	0.308
145	.916	.549	447	.842	.268
196	.904	.459	447	.842	.271
198	.903	.453	506	.828	.243
245	.892	.406	506	.828	.238
250	.891	.388	571	.812	.216
292	.881	.354	572	.812	.213
368	.862	.306	686[a]	.783	.183

[a] Based on extrapolation of water calibration.

TABLE II

VISCOSITY OF ALLOY (28.3 WT. % POTASSIUM)

Temp., °C.	Density, g./ml.	Viscosity, centipoises	Temp., °C.	Density, g./ml.	Viscosity, centipoises
144	0.890	0.471	438	0.820	0.235
171	.884	.433	447	.818	.231
176	.883	.421	510	.803	.210
241	.867	.359	516	.801	.207
252	.865	.347	566	.789	.195
325	.847	.301	570	.788	.191
332	.846	.300	637[a]	.772	.174
395	.830	.258	702[a]	.756	.160
395	.830	.255	708[a]	.755	.160

[a] Based on extrapolation of water calibration.

TABLE III

VISCOSITY OF ALLOY (43.3 WT. % POTASSIUM)

Temp., °C.	Density, g./ml.	Viscosity, centipoises	Temp., °C.	Density, g./ml.	Viscosity, centipoises
95	0.888	0.549	392	0.815	0.249
95	.888	.551	464	.799	.217
143	.876	.449	458	.798	.217
146	.876	.447	509	.787	.201
191	.864	.386	517	.785	.200
192	.864	.388	585[a]	.768	.180
250	.850	.333	588[a]	.767	.180
256	.848	.331	651[a]	.752	.166
320	.833	.292	681[a]	.745	.160
327	.831	.291	689[a]	.743	.158
388	.816	.248			

[a] Based on extrapolation of water calibration.

(3) James F. Swindells, *J. Colloid Sci.*, **2**, 177 (1947).

(4) Naval Research Laboratory Report, No. C-3287 (1948).

TABLE IV

VISCOSITY OF ALLOY (66.9 Wt. % POTASSIUM)

Temp., °C.	Density, g./ml.	Viscosity, centipoises	Temp., °C.	Density, g./ml.	Viscosity, centipoises
74.4	0.867	0.604	395	0.791	0.230
76.6	.867	.607	397	.790	.231
142	.851	.432	438	.780	.200
146	.850	.409	460	.775	.202
188	.840	.361	461	.775	.212
195	.838	.356	467	.774	.206
203	.836	.339	479	.770	.187
211	.835	.337	490[a]	.768	.192
221	.832	.319	511[a]	.763	.190
232	.830	.354	560[a]	.751	.182
268	.821	.303	612[a]	.739	.169
275	.819	.296	629[a]	.735	.165
321	.808	.261	669[a]	.725	.154
331	.806	.268	689[a]	.720	.150

[a] Based on extrapolation of water calibration.

TABLE V

VISCOSITY OF POTASSIUM

Temp., °C.	Density, g./ml.	Viscosity, centipoises	Temp., °C.	Density, g./ml.	Viscosity, centipoises
197	0.796	0.312	273	0.778	0.244
197	.796	.309	350	.759	.210
272	.778	.244	350	.759	.216

1%. The composition figure presented for each alloy represents the average of analyses before and after the viscosity determinations. A slight composition change in the two high potassium alloys (0.2 to 0.5%) was attributed to some loss of potassium-rich vapors at the higher temperatures. Within the limits of the experimental method of analysis, the pure metals analyzed to 100.0% purity.

The results at the end of each table identified by an *a* represent those results for which the Reynold's number is higher than that at the limit of the water calibration data. The limit of the water calibration is a Reynold's number of 2500 whereas the result at 689° for the high potassium alloy represents maximum flow conditions for the liquid metals—a Reynold's number of 3500. However, it is felt that streamline flow, for the long capillary under the conditions of measurement, will persist through this flow region and that the Poiseuille calibration will be valid for the full range. The uniformity of the viscosity data for the metals over the full range attests to this conclusion. The measurements for potassium were terminated at 400° due to the development of a leak and subsequent plugging of the capillary.

The temperature variation of viscosity for each of the five metals can be adequately expressed by the equation of Andrade[5]: $\eta v^{1/3} = Ae^{C/vT}$, in which η is the absolute viscosity, v is specific volume, and T is the absolute temperature. Using the method of least squares, the constants for this equation were determined for each metal sample. In each case the equation was derived from the combined nickel and glass data. As the alloy compositions used for the two sets of measurements differed, low temperature results were obtained from the glass measurements by interpolation. A summary of the empirical constants for the Andrade equation, and a comparison for the pure metals with similar constants from NRL data in glass and from data by Chiong, are presented in Table VI. The constants for sodium in all three cases show close agreement. The discrepancies, which have been mentioned, for potassium between the NRL data and Chiong's data are of course evident in the constants.

TABLE VI

EMPIRICAL CONSTANTS FOR ANDRADE FORMULAS

Compn., wt. % potassium	Constants NRL Data: Low temperature work, C	Low temperature work, $A \times 10^{+3}$	Combined high temperature work, C	Combined high temperature work, $A \times 10^{+3}$	Constants Chiong data, C	Chiong data, $A \times 10^{+3}$
0.0	756.9	1.089	739.8	1.142	716.5	1.183
28.3			743.3	1.046		
43.3			722.2	1.052		
66.9			694.0	1.059		
100.0	742.8	0.9114	716.0	0.9673	600.0	1.293

Combining the low and high temperature viscosity results, a composite set of viscosity–composition isotherms can be readily drawn for the full temperature range, from which viscosity–temperature relationships for any composition can be interpolated. Below 200° the isotherms will represent the higher accuracy results in glass, while above 200° they represent the measured results in nickel. Coefficients estimated in this manner should have an error of ±2% below 200° and above 200° a graded error from ±2% to ±10% at the highest temperature. The 10% error would represent a maximum figure taking into account uncertainties in the extension of the water calibration for the higher temperature results.

Acknowledgment.—The authors wish to acknowledge the assistance of Dale D. Williams, H. P. Richey and R. E. Ruskin of this Laboratory.

(5) E. N. daC. Andrade, *Phil. Mag.*, **17**, 698 (1934).

DISCONTINUITIES IN ADSORPTION ISOTHERMS

BY M. L. CORRIN AND C. P. RUTKOWSKI

General Electric Research Laboratory, Schenectady, N. Y.

Received May 26, 1954

Adsorption isotherms of krypton on calcium halophosphate under certain conditions exhibit discontinuities; under other conditions, the isotherms are smooth. The smooth isotherm is probably the equilibrium isotherm. The very marked effect of the time allowed for adsorption of the first increment on the later points is indicated.

The existence of discontinuities in adsorption isotherms, which are equivalent to first-order phase transitions in the adsorbed film, has been a matter of controversy. Such transitions have been reported by Harkins, Jura and their co-workers,[1] and by Ross and Boyd[2]; work on similar but not identical systems by Smith,[3] Young, Beebe and Bienes,[4] and Corrin[5] has failed to confirm the earlier findings. These later workers point out that it was quite possible equilibrium was not attained in those experiments in which discontinuities were observed. Recently Ross and his co-workers[6] have reported the existence of first-order transitions and supersaturation effects on sodium chloride, potassium chloride and asbestos.

We have observed an apparent first-order phase transition for the adsorption of krypton on a calcium halophosphate at 77.3°K. The general experimental setup was that of a surface area system; stopcocks were employed and a thermistor gage served as the pressure measuring device. The sample was contained in a cylindrical glass container 12 mm. in diameter and was degassed 16 hours at 350°. Gage readings are plotted against time in Fig. 1; the readings are sensitive to ±0.05 μa. or, in the pressure region of interest, ±0.3 micron. It should be noted from these plots that apparently equilibrium has been attained in two hours; *i.e.*, with the sensitive pressure measuring system employed, the pressure is apparently then constant with time. The two hour points are plotted in Fig. 2 (open circles) as an isotherm; one marked first-order transition occurs and there are indications that at least two more discontinuities exist.

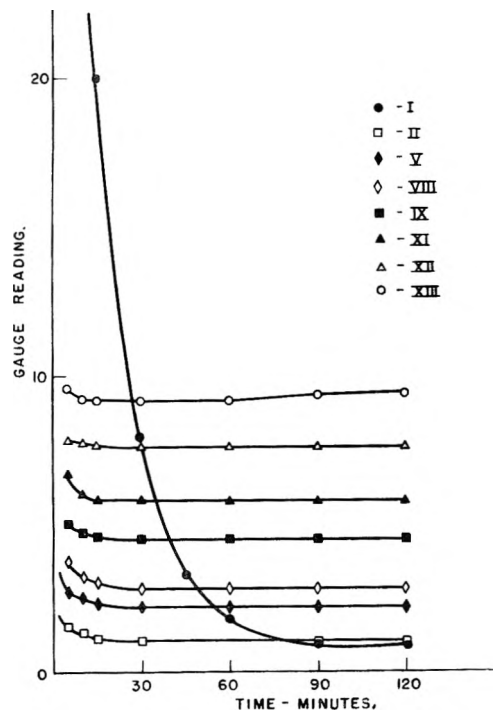

Fig. 1.—Rates of adsorption in cylindrical bulb system. (Only 1 point, V, shown in transition region.)

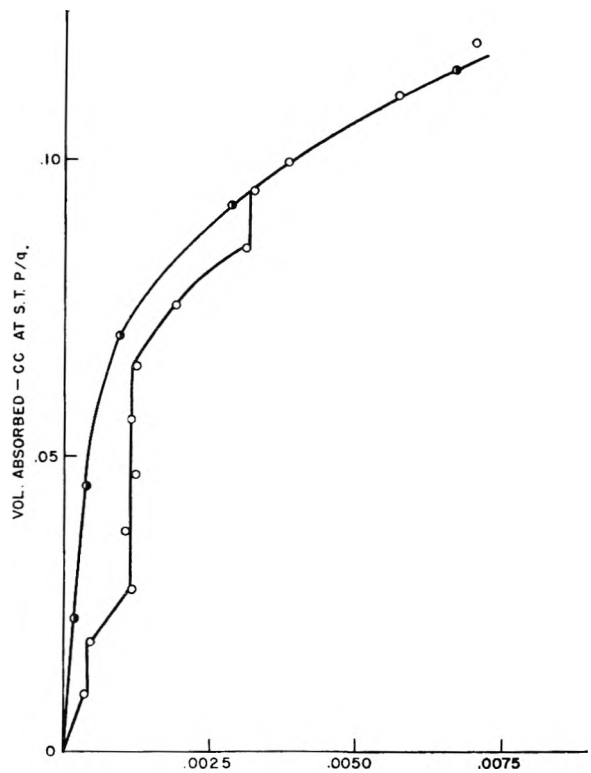

Fig. 2.—Isotherms obtained: open circles, 2-hour points in cylindrical bulb; closed circles in tray system; 16-hour equilibration time for initial point.

A similar sample was then placed in the tray system described by Jura and Criddle.[7] The apparent rates of adsorption appeared less than with the cylindrical bulb and the pressure was still decreasing markedly at the end of two hours.

(1) G. Jura, W. D. Harkins and E. H. Loeser, *J. Chem. Phys.*, **14**, 344 (1946); G. Jura, E. H. Loeser, P. R. Basford and W. D. Harkins, *ibid.*, **14**, 117 (1946).

(2) S. Ross and G. E. Boyd, MDDC Report 864 (1947).

(3) L. N. Smith, *J. Am. Chem. Soc.*, **74**, 3477 (1952).

(4) D. A. Young, R. A. Beebe and H. Bienes, *Trans. Faraday Soc.*, **49**, 1086 (1953).

(5) M. L. Corrin, THIS JOURNAL, in press.

(6) H. Clark and S. Ross, *J. Am. Chem. Soc.*, **75**, 6081 (1953); S. Ross and W. Winkler, paper presented American Chem. Soc. Meeting, Kansas City, Mo., 1954.

(7) G. Jura and D. Criddle, THIS JOURNAL, **55**, 163 (1951).

The sample was then degassed and the first increment of gas allowed to remain in contact with the solid for 16 hours. With succeeding increments the rate of adsorption was quite high and apparently equilibrium attained in five minutes. The isotherm thus obtained is plotted as partially filled circles in Fig. 2. It should be noted that this isotherm is smooth and coincides with the discontinuous isotherm at pressures exceeding 7.5 microns.

We thus have looked at three systems: (1) Two-hour points with a cylindrical sample container. Apparent equilibrium was attained; the isotherm was discontinuous. (2) Two-hour points with a tray sample container. Apparent equilibrium was not attained and adsorption rates were slow as compared to (1). (3) Apparent equilibrium points with a tray sample container; the initial point was measured after 16 hours. The isotherm was continuous. Isotherms (1) and (3) coincide at higher pressures; at equal pressures the amount adsorbed by isotherm (3) is equal to or greater than the amount adsorbed by isotherm (1).

It would appear that the continuous isotherm (3) rather than the discontinuous isotherm (1) represents the equilibrium state. It is not possible, however, to rule out the possibility that (3) represents a "supersaturation" phenomenon and that the discontinuous isotherm has significance. The marked dependence of the rates of adsorption on the time allowed for attainment of equilibrium of the first point is evident; no explanation can be offered at the present time. These findings suggest that any measurements yielding discontinuous isotherms be carefully checked.

KINETICS OF DEAMINATION OF OXIDIZED N,N-DISUBSTITUTED *p*-PHENYLENEDIAMINES

BY L. K. J. TONG

Communication No. 1649 from the Kodak Research Laboratories, Research Laboratories, Eastman Kodak Company, Rochester, N. Y.

Received May 29, 1954

An experimental technique is described for following the reactions of the deamination of oxidized N,N-disubstituted *p*-phenylenediamines. Over a *p*H range of 7 to 12, the deamination of the substituted amino group fits the second-order rate equation involving the product of the concentrations of hydroxide ion and quinonediimine. The deamination of the unsubstituted amino group fits the first-order rate equation in buffered solutions, and the rate constants are insensitive to the change in *p*H. The variations in reactivity due to substitution can be largely accounted for by inductive effects.

Introduction

Many of the processes of color photography employ a substituted *p*-phenylenediamine type of developing agent to obtain a reduced silver image from the exposed silver halide emulsion. In the reduction of silver halide, the diamine is oxidized to the diimine, which then undergoes a coupling reaction with a suitable agent, called a coupler, to form an appropriate dye.[1] In any study of the mechanism of the dye-forming reactions, a knowledge of the stability and reactivity of the diimines is a prerequisite. This paper describes the development of suitable techniques for studying in solution the kinetics of the reactions involved, the application of these techniques to the specific problem of the rate of deamination of the diimines, and the interpretation of the results obtained.

It has been known for a long time that both substituted and unsubstituted quinonediimines undergo deamination reactions in acid solutions.[2,3] In alkaline solutions, N-substituted quinonediimine has been shown by Cameron[4] to be highly unstable, but the reactions involved were not specified. We shall show in a later section that the main reaction involved at high *p*H is the deamination of the substituted imino group.

Experimental

Materials.—For convenience, the developing agents will be referred to in this article by roman numerals as given in Table I. These N,N-disubstituted phenylenediamines belong to a class of color-developing agents commonly used. The samples were as prepared for earlier experiments[5] and have been stored under refrigeration. Compound IX was

TABLE I

STRUCTURE OF DEVELOPING AGENTS

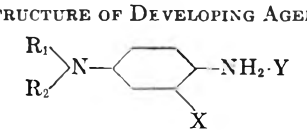

No.	R_1	R_2	X	Y (salt)
I	H	H	H	2HCl
II	CH_3	CH_3	H	HCl
III	C_2H_5	C_2H_5	H	HCl
IV	C_2H_5	C_2H_5	CH_3	HCl
V	C_2H_5	$CH_3SO_2NHC_2H_4$—	H	2HCl
VI	C_2H_5	$CH_3SO_2NHC_2H_4$—	CH_3	H_2SO_4
VII	C_2H_5	$CH_3SO_2NC_2H_4$— (with CH_3)	CH_3	$^1/_2H_2SO_4$
VIII	HO—	—$NH_2 \cdot {}^1/_2(COOH)_2$		
IX	HO—	—$NH_2 \cdot HCl$ (CH_3)		

(1) C. E. K. Mees, "The Theory of the Photographic Process," rev. ed., The Macmillan Co., New York, N. Y., 1954, p. 586. R. M. Evans, W. T. Hanson, Jr., and W. L. Brewer, "Principles of Color Photography," John Wiley and Sons, Inc., New York, N. Y., 1953, p. 257; P. W. Vittum and A. Weissberger, *J. Phot. Science*, in press (1954).

(2) R. Willstätter and E. Mayer, *Ber.*, **37**, 1499, 1501 (1904); R. Willstätter and J. Piccard, *ibid.*, **41**, 1473 (1908).

(3) L. F. Fieser, *J. Am. Chem. Soc.*, **52**, 4915 (1930).

(4) A. E. Cameron, THIS JOURNAL, **42**, 1217 (1938).

(5) R. L. Bent, *et al.*, *J. Am. Chem. Soc.*, **73**, 3100 (1951).

recrystallized from 95% alcohol before use. Fresh solutions of the developing agent were made for each experiment by addition of water to a weighed sample.

Phosphates used for buffers were C.P. K_2HPO_4 and KH_2PO_4. The solutions were made up to an approximate *p*H by addition of concentrated NaOH to 0.2 *M* phosphate. The final *p*H of each reaction mixture was determined directly with a glass electrode. α-Naphthol was Eastman White Label grade. Butyl acetate was Eastman Special grade. $K_3Fe(CN)_6$ was C.P. grade.

Procedure.—Preliminary experiments on the reaction of the diimines with α-naphthol to form cyan dyes established several facts which served as a basis for the development of suitable apparatus and techniques. (1) In aqueous solutions, the rates of deamination of the diimines are quite rapid at high *p*H. (2) The deamination reactions are "stopped" or reduced to a negligible rate when the *p*H is lowered to 6. (3) At *p*H 6, each diimine and one of the products of its deamination couple quantitatively with α-naphthol, giving dyes which are blue and red, respectively. A mixture of these two dyes can be analyzed quantitatively by extracting with butyl acetate and obtaining spectrophotometric curves.

On the basis of this information, a standard procedure was adopted to follow the kinetics of the reactions. First, the developing agent was oxidized with potassium ferricyanide by mixing the solutions of the two reagents. The deamination reaction was then initiated by the addition of alkaline buffer, and, after a predetermined reaction interval, it was stopped by the addition of acid buffer to bring the final *p*H to *ca.* 6–7. More ferricyanide was then added in those experiments where it was not initially added in excess (ferricyanide/developing agent—4/1 mole ratio). Finally, α-naphthol was added, and after 20–30 minutes' standing, the dyes were extracted with butyl acetate and their concentrations determined spectrophotometrically.

At low *p*H values, the deamination reactions are slow, therefore the mixing of solutions was carried out in flasks using hypodermic syringes. At higher *p*H's, however, the fast reactions were followed by the steady-state flow method, using the jet-mixing machine designed by Dr. W. R. Ruby, of these Laboratories. The details of construction of this machine will be published elsewhere. Essentially, the machine has three consecutive mixing chambers separated by spacers of variable path lengths. In the first chamber (A), solutions 1 and 2, below, are mixed, and in the second and third chambers (B,C), solutions 3 and 4, respectively, are added to the main stream. Solution 5 was placed in the receiver. The operating velocities were kept sufficiently high for turbulent flow.

Unless otherwise specified, in all experiments on rates, the concentrations, volumes, and mixing sequences used are those according to Table II. All reaction rates were measured at 25 ± 0.1°.

TABLE II

REAGENTS AND ORDER OF MIXING

	Solution	Concentration	Volume, cc. Machine	Volume, cc. Syringe
1	Developing agent	0.75×10^{-3} *M*	7.33	10.0
2	$K_3Fe(CN)_6$	4.8×10^{-3}	7.33	10.0
3	Alkaline buffer	0.2 *M* Phosphate	14.66	20.0
4	Acid buffer	0.25 *M* KH_2PO_4	29.32	10.0
5	α-Naphthol	2.0×10^{-3} *M*	5.0	5.0

After 20–30 minutes' coupling, the dyes were extracted with 50.0 cc. of *n*-butyl acetate.

Spectrophotometric curves for each dye extract were obtained between 400–700 mμ on a General Electric Recording Spectrophotometer. Under the conditions in the standard procedure, the formation of "blue" dyes is very fast, usually reaching completion in less than one minute. The formation of "red" dyes is somewhat slower, requiring approximately 10 minutes. To provide a safety margin, the normal procedure allows 20 minutes reaction time before the dyes are extracted. In preliminary experiments it was noted that, when α-naphthol was added at higher *p*H, or when a larger excess of oxidant was used, colored products were produced from oxidation of α-naphthol. Fortunately, they disappeared after a few hours of standing in the extract before analysis.

Calculations.—Concentrations of Reactants and Products.—The unreacted oxidized developing agents couple with α-naphthol to produce "blue" dyes of the indoaniline type, while one of the products of decomposition couples with α-naphthol to produce "red" dyes of the indophenol type. The identification of the "red" dye (see later section) established the decomposition reaction to be principally that of deamination with the removal of the substituted imino groups. The concentrations of the two dyes were calculated from the density measurements in butyl acetate at two wave lengths, usually at the λ_{max}'s. The sum of their concentrations could also be calculated from the isosbestic point for the pair.

Molar absorbancies were calculated from measurements with dyes produced from known quantities of the diamine in the presence of excess ferricyanide and α-naphthol. Under these conditions, side reactions are negligible, and the yields were assumed to be quantitative. In cases where isolated and purified dyes were available (compounds II to IV), the absorbancies obtained from them agree with those obtained by the above method, within the limits of experimental error throughout the visible range.

The concentration of the oxidized diamine (A) and that of the deamination product (B) in the aqueous phase are related to the concentrations of the "blue" and "red" dyes, (C) and (D), in butyl acetate by the equations

$$(A) = \frac{V_{BuAc}}{V_{aqueous}} \times (C) \qquad (1)$$

$$(B) = \frac{V_{BuAc}}{V_{aqueous}} \times (D) \qquad (2)$$

where V_{BuAc} and $V_{aqueous}$ are the volumes of the butyl acetate phase and of the aqueous phase, respectively.

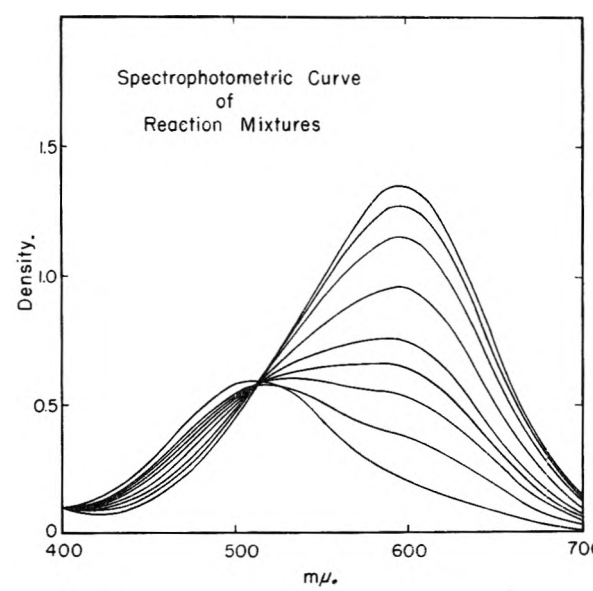

Fig. 1.—Spectrophotometric curves of reaction mixtures.

Treatment of Kinetic Data.—In anticipation of the supporting evidence to be given later, let us assume that the following conditions hold.

In the presence of excess $K_3Fe(CN)_6$, the diamine is quantitatively oxidized to quinonediimine.

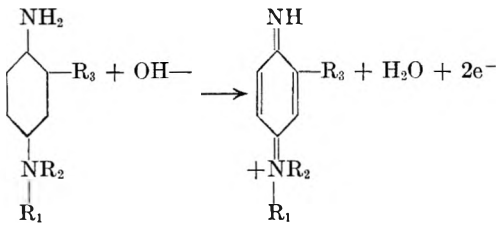

The quinonediimine then reacts according to the scheme

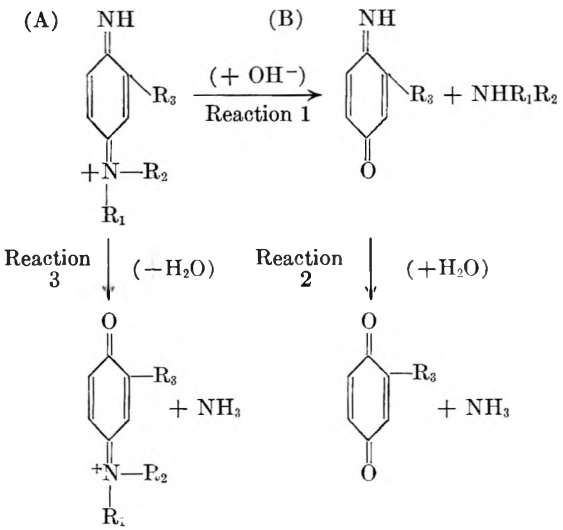

In a given buffer, reactions 1 and 3 combine to remove (A) according to the first-order rate equation

$$\frac{d(A)}{dt} = -(k_1 + k_3)(A) \qquad (3)$$

Upon substitution of (A) from equation 1

$$\frac{d(C)}{dt} = -(k_1 + k_3)(C) \qquad (3')$$

and $(k_1 + k_3)$ can therefore be calculated directly from the concentration change of the "blue" dye. The individual constants can be resolved in this case, owing to the fact that the product of reaction 1, quinone-monoimine (B), couples with α-naphthol to form the "red" dye, while the product of reaction 3 does not couple. Therefore, since the value of k_2 and the variation of (B) with time are known, k_1 and k_3 can be resolved.

The procedure followed was first to measure k_2 in the same buffer, starting with (B) produced by oxidation of the corresponding aminophenols (compounds VIII and IX). It will be shown later that reaction 2 is also first-order with respect to (B). In experiments starting with (A), (B) will therefore vary with time according to the equation

$$\frac{d(B)}{dt} = k_1(A) - k_2(B) \qquad (4)$$

Solving the differential equations 3 and 4, with the boundary conditions at $t = 0$; $(A) = (A)_0$, $(B) = 0$, one obtains

$$(A) = (A)_0 \exp[-(k_1 + k_3)t] \qquad (5)$$

$$(B) = \frac{k_1[(A)_0 \exp(-k_2t) - (A)]}{(k_1 + k_3 - k_2)} \qquad (6)$$

where $(A)_0$ is the initial concentration of the diimine. After substituting equations 1 and 2 into equation 6, one obtains

$$\frac{k_1}{(k_1 + k_3 - k_2)} = \frac{(D)}{(C)_0 \exp(-k_2t) - (C)} \qquad (7)$$

Thus, when (D) is plotted against $(C)_0 \exp(-k_2t) - (C)$, the ratio on the left-hand side of equation 7 is obtained from the slope. The values of k_1 and k_3 can now be calculated from this ratio and the known values of $(k_1 + k_3)$ and k_2.

For *p*-phenylenediamine, deamination at either end-group leads to the same intermediate (B). We have, therefore

$$\frac{d(A)}{dt} = -2k_3(A) \qquad (8)$$

and

$$\frac{d(B)}{dt} = 2k_3(A) - k_2(B) \qquad (9)$$

After integration and substitution of appropriate constants, the following equations are obtained

$$(A) = (A)_0 \exp(-2k_3t) \qquad (10)$$

and

$$(B) = \frac{2k_3(A)_0[\exp(-k_2t) - \exp(-2k_3t)]}{2k_3 - k_2} \qquad (11)$$

In terms of (C) and (D), the last equation becomes

$$(D) = \frac{2k_3(C)_0[\exp(-k_2t) - \exp(-2k_3t)]}{2k_3 - k_2} \qquad (12)$$

For reactions taking place between two mixing chambers and with uniform flow, the reaction time, t, upon reaching the second chamber, is

$$t = Al \times \frac{\Delta t}{\Delta V}$$

where

A = cross-section of the reaction tube (mm.^{2})
l = length of the reaction tube (mm.) (spacer and chamber)
ΔV = vol. of soln. delivered (mm.^{3})
Δt = time required for delivery (sec.)

For a first-order reaction, one obtains the expression

$$k = -2.303 \frac{d \log C}{dt}$$

In the experiments, $A = 2.045$ mm.^{2} and $\Delta V = 2.932 \times 10^4$ mm.^{3}. After substitution of the expression for t with its constants, this equation becomes

$$k = \frac{-3.31 \times 10^4}{l} \frac{d \log (C)}{d\Delta t} \qquad (13)$$

The rate constants were calculated graphically from the slope of log (C) *vs.* Δt plots, using the appropriate value of l for the given spacer.

Results and Discussion

Identification of Reaction Products.—When compound IV was oxidized and allowed to react at *p*H 12 for increasing time intervals, before the reaction

TABLE III

DEAMINATION OF QUINONEDIIMINE FROM COMPOUND IV, *p*H 12

Solution 1 = compound IV (7.5×10^{-4} *M*); solution 4 = acid stop.

Expt. no.	Soln. 2	Soln. 3	Path length, mm. Chambers A-B	Chambers B-C	k_1 (sec.$^{-1}$)
10	$K_3Fe(CN)_6$, 4.8×10^{-3} *M*	Phosphate buffer, *p*H 12	15.3	90.9	12.3
20	$K_3Fe(CN)_6$, 4.8×10^{-3} *M*	Phosphate buffer, *p*H 12	75.0	90.9	12.3
30	$K_3Fe(CN)_6$, 7.5×10^{-4} *M*	Phosphate buffer, *p*H 12	75.0	90.9	11 7
40	H_2O	$Fe(CN)_6^{-3}$, 2.4×10^{-3} *M* in phosphate buffer, *p*H 12	15.3	50.2	12.6

was stopped by reducing to *p*H 6 and the products were allowed to couple with α-naphthol, the resulting dye mixtures gave a series of absorption curves in butyl acetate (Fig. 1) showing a continuous decrease of D_{600} and a continuous increase of D_{510}, resulting in an isosbestic point at 518 mμ. The existence of an isosbestic point suggested an equimolar conversion of the diimine to a product capable of coupling with α-naphthol to produce a red dye. That the red dye was a product of coupling was evidenced by the fact that it was absent in the extract without the addition of α-naphthol. Since coupling would not be likely without the NH_2 group, and dyes of the indophenol type are known to be red in solvents like *n*-butyl acetate, it was speculated that the most probable reaction taking place in the decomposition of the diimine involved the loss of the substituted imino group. This was confirmed by comparing the absorption of butyl acetate solutions of dyes from three sources as follows.

Sample 1 was extracted from the product of coupling between α-naphthol and the deamination product of oxidized compound IV. The molar absorbancies were based on the initial concentration of IV.

Sample 2 was an extract of the product of coupling between α-naphthol and oxidized 2-methyl-4-hydroxyaniline (compound IX). The molar absorbancies were based on the initial concentration of IX.

Sample 3 was a large batch prepared as for sample 1. This was extracted, isolated and recrystallized from a benzene–cyclohexane mixture. The isolated dye had the following analysis (compared with the theoretical composition based on the assumed formula for the indophenol dye): Calcd.: C, 77.6; H, 5.0; N, 5.3. Found: C, 77.6; H, 5.0; N, 5.5.

The molar absorbancies were calculated by using the molecular weight of materials having the same formula. Comparison of molar absorbancies for the visual region for the three samples shows that they were identical.

Further evidence that the deamination product is identical with oxidized compound IX is afforded by the fact that they both underwent further reaction and disappeared at the same rate (Table IV).

Validity of the Method.—Before the results of the kinetics are discussed, the characteristics and performance of the mixing machine upon which the validity of these results depends will first be described. It has been implicitly assumed that the duration of the deamination reaction is the time required for the solution to flow from chamber B to chamber C and that sufficient time has been allowed for the oxidation of the diamine to take place beforehand. These assumptions are supported by the experiments described in Table III. Thus, there was no observable change in the rate either in experiment 20, where the time allowed for oxidation was increased to five times normal (experiment 10) by insertion of a spacer between A and B, or in experiment 40, where ferricyanide was dissolved in the alkaline buffer, so that oxidation and deamination began simultaneously.

The accuracy of the flow method is evidenced from the results plotted on Fig. 4. Although the points below log $k = -1$ were obtained using manual mixing and those above it using machine mixing, it is apparent that they all lie on the same straight line without serious breaks.

In normal runs, the reactions were carried out using an excess of ferricyanide, the diamines were oxidized practically completely to the diimines and, as shown in Fig. 2, the rate was found to be proportional to the diimine concentration. Experiment 30 (Table III) was performed with one-half the amount of ferricyanide theoretically required to oxidize the developer to diimine, additional ferri-

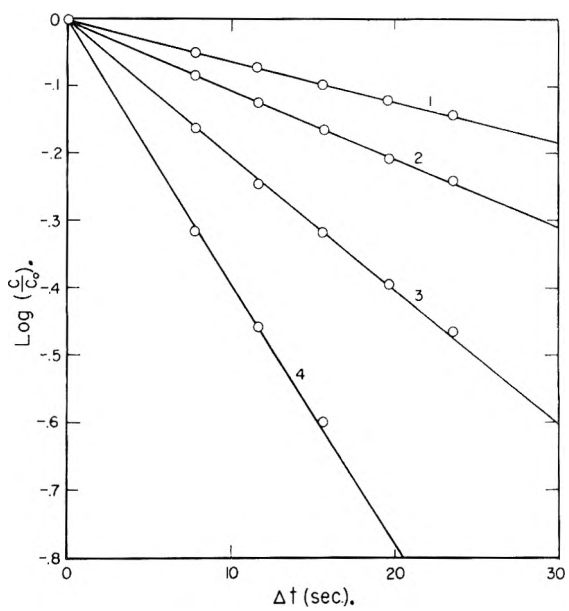

Fig. 2.—Extent of reaction as a function of machine speed and path length. Curves 1, 2, 3 and 4 have spacer lengths of 0, 9.68, 34.68, 84.68, respectively, and slopes of 6.0, 10.3, 20.0, 38.8×10^3, respectively.

cyanide being added to the α-naphthol for analysis. Under this condition, which is most favorable for semiquinone formation, the rate constant, calculated on the basis of a diimine concentration equivalent to the limited ferricyanide used, was the same as when excess ferricyanide was employed. The fact that the rate was found to be the same under the two sets of conditions shows that semiquinone formation is insignificant under these conditions, except for the improbable situation that the rate of deamination of the semiquinone is exactly one-half the rate for the diimine.

Kinetics.—In the analysis of kinetic data, k_2 was first obtained, using compounds VIII and IX, which produce the quinonemonoimines (B) directly upon oxidation. The immediate product for this reaction is suspected to be a quinone; however, in the presence of high *p*H and excess $K_3Fe(CN)_6$, it is likely to undergo further reaction. The rate law for the conversion of B was found to be of the first order in respect to (B) from *p*H 12 down to *p*H 5. At lower *p*H, deviations from the first-order rate equation were noticed. In Table IV, two rate constants are given for compound IX for *p*H 12. In one of the runs, the quinonemonoimine was produced directly by oxidation of IX, while in the other run it was a product of reaction 1, starting with compound IV. The close agreement of the reaction rates supports the conclusion that the reacting compounds are the same in the two cases.

After k_2 and $(k_1 + k_3)$ were independently determined for each *p*H, k_1 and k_3 were resolved by the use of equation 7. From the results given by earlier workers[2] for *p*-phenylenediamine, reaction 3, the predominant reaction in the acid region, is suspected to be the removal of the unsubstituted imino group. It is probable that the product of this reaction also undergoes further reaction in the presence of excess ferricyanide.

As an example of the graphical method used to resolve k_1 and k_3 for the various compounds, the data for compound IV at three different *p*H's are plotted according to equation 7, in Fig. 3.

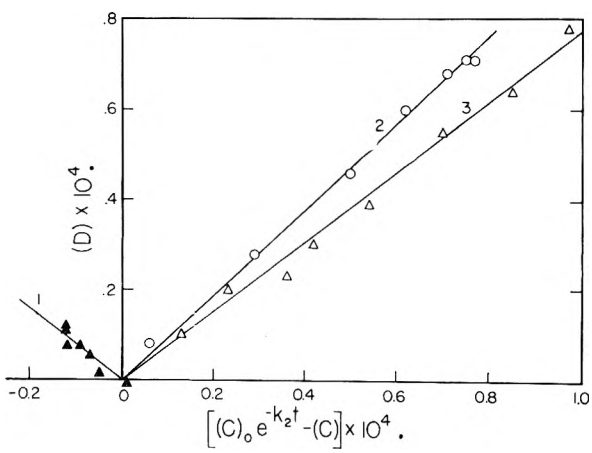

Fig. 3.—Graphical resolution of k_1 and k_2 for compound IV: Curves 1, 2 and 3 have *p*H's 7.03, 8.00 and 8.85, respectively, and slopes of −0.8, 0.95 and 0.77, respectively.

The symmetrical *p*-phenylenediamine (compound I) represents a special case where $2k_3 = (k_1 + k_3)$.

TABLE IV

DEAMINATION OF UNSUBSTITUTED IMINES, 25 ± 0.1°

Compound	$(B)_0$ (moles/l.)	*p*H	k_2 (sec.$^{-1}$)
(a) VIII	2.5×10^{-4} *M*	6.11	1.54×10^{-3}
		7.09	0.55×10^{-3}
		7.95	$.192 \times 10^{-3}$
		8.69	$.131 \times 10^{-3}$
		9.78	$.115 \times 10^{-3}$
		10.95	$.154 \times 10^{-3}$
		11.89	$.384 \times 10^{-3}$
(b) IX	2.5×10^{-4} *M*	6.11	1.62×10^{-3}
		7.08	0.71×10^{-3}
		7.95	$.16 \times 10^{-3}$
		8.75	$.12 \times 10^{-3}$
		9.95	$.08 \times 10^{-3}$
		12.0	$.18 \times 10^{-3}$
		12.0	$.19 \times 10^{-3}$[a]
			k_3 (sec.$^{-1}$)
(c) I	1.25×10^{-4} *M*	6.06	6.34×10^{-3}
		7.03	1.04×10^{-3}
		8.04	0.43×10^{-3}
		8.88	$.35 \times 10^{-3}$
		10.25	$.33 \times 10^{-3}$
		11.30	$.33 \times 10^{-3}$
		12.15	$.33 \times 10^{-3}$
Compound	$(A)_0$ (moles/l.)	*p*H	$(k_1 + k_3)$ (sec.$^{-1}$)
(d) III	1.25×10^{-4}	6.10	0.546×10^{-3}
	1.88×10^{-4}	7.11	1.10×10^{-3}
	1.88×10^{-4}	8.00	6.48×10^{-3}
	1.25×10^{-4}	8.96	57.2×10^{-3}
	1.88×10^{-4}	10.10	1.24
	1.88×10^{-4}	11.10	11.10
	1.88×10^{-4}	11.96	77.6
(e) IV	1.25×10^{-4}	7.02	0.390×10^{-3}
	1.25×10^{-4}	8.00	1.12×10^{-3}
	1.88×10^{-4}	8.85	8.65×10^{-3}
	1.88×10^{-4}	10.04	0.141
	1.88×10^{-4}	11.08	2.00
	1.88×10^{-4}	11.59	5.84
	1.88×10^{-4}	11.93	13.2
(f) II	1.88×10^{-4}	7.10	2.5×10^{-3}
		8.02	16.3×10^{-3}
		10.02	2.53
		11.10	30.4
		11.95	196
(g) V	1.88×10^{-4}	7.98	81×10^{-3}
		8.65	122×10^{-3}
		10.06	0.177
		11.10	.421
		11.96	2.16
(h) VI	1.88×10^{-4}	7.98	21.4×10^{-3}
		8.65	31.9×10^{-3}
		10.06	0.166
		11.02	.519
		11.93	2.86
(i) VII	1.25×10^{-4}	7.05	0.87×10^{-3}
		8.06	5.5×10^{-3}
		8.90	33×10^{-3}
		10.10	0.85
		11.09	7.3
		11.96	5.5

[a] Quinonemonoimine was a product of reaction 1.

The concentration of the intermediate (B) has been calculated from equation 12, using independently

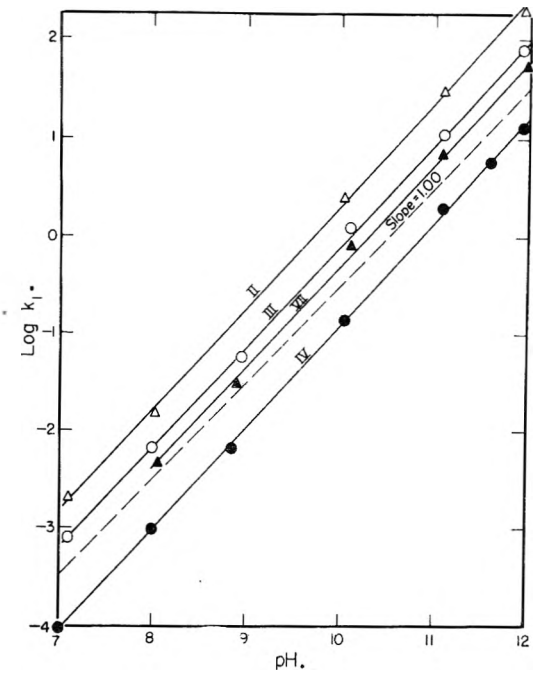

Fig. 4.—Pseudo first-order rate constants for deamination of non-dissociating quinonediimines

determined values of k_2 and k_3. The calculated concentrations plotted *vs.* time agree with the experimental points obtained at *p*H's 7.03 and 8.88. To save space, the figure showing this is not included here.

A summary of the results appears in Table IV and Fig. 4, from which it is evident that, while k_1 is very sensitive to *p*H variations, k_2 and k_3 are not. In Fig. 4, log k_1 was plotted *vs.* *p*H, the data including the majority of compounds studied. For this group, the points for each compound fall on a straight line, with the slope near unity. It is apparent that k_1 is a pseudo first-order rate constant. It was, therefore, converted into a second-order constant, k_4, by the relationship, $k_4 = k_1/OH^-$. For this calculation, (OH^-) was taken as $\log^{-1}(pH - 14)$.

For compounds V and VI, the effect of *p*H on k_1 is twofold; besides the dependence on (OH^-) as shown above, there is an indirect effect due to the change of ionic forms of the diimine.

Both V and VI have ionizable sulfonamido groups. Thus, oxidized V ionizes as

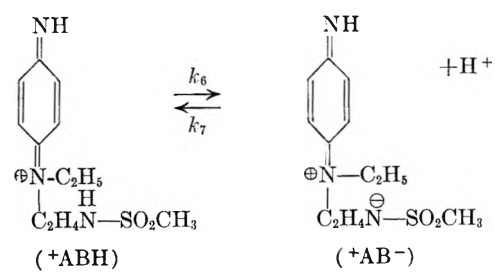

Let (+ABH) represent the ion on the left-hand side and (+AB−) represent the zwitterion on the right-hand side. Let us assume that the two ions

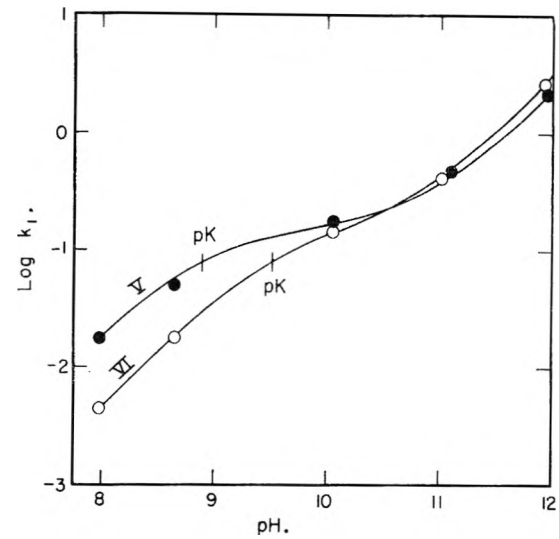

Fig. 5.—Pseudo first-order rate constants for deamination of dissociated quinonediimines. Points are experimental. Curve calculated from equation 15. Compound V, $k_4 = 2 \times 10^4$, $k_4' = 2.2 \times 10^2$ and $K = 1.3 \times 10^{-9}$; compound VI, $k_4 = 4.5 \times 10^3$, $k_4' = 3 \times 10^2$ and $K = 3 \times 10^{-10}$.

deaminate according to the equations

$$^+ABH + OH^- \xrightarrow{k_4} P$$

and

$$^+AB^- + OH^- \xrightarrow{k_4'} P'$$

Also, let us assume that the ionization is in equilibrium, during the reaction, with $K = k_6/k_7$. Then

$$\frac{-d[(^+ABH) + (^+AB^-)]}{dt} = [k_4(^+ABH) + k_4'(^+AB^-)]OH^- \quad (14)$$

where k_4 and k_4' are second-order rate constants. After the substitution of the equilibrium concentrations for (^+ABH) and $(^+AB^-)$, we obtain

$$\frac{-d \ln [(^+ABH) + (^+AB^-)]}{dt} = k_1 = \left\{k_4\left[1 - \frac{K(OH^-)}{K(OH^-) + kw}\right] + k_4'\left[\frac{K(OH^-)}{K(OH^-) + kw}\right]\right\}(OH^-) \quad (15)$$

If the proper values are selected for k_4, k_4' and K, with $kw = 10^{-14}$, the pseudo first-order constant k_1 can be expressed as a function of *p*H. The experimentally determined values of k_1 at different *p*H's are plotted in Fig. 5, along with the curves calculated by the above equation, using the following values for the constants

Compound	V	VI
k_4, l./mole sec.	2×10^4	4.5×10^3
k_4' l./mole sec.	2.2×10^2	3×10^2
K, l./mole sec.	1.3×10^{-9}	3×10^{-10}

It is interesting to note that the pK's (9–10) so obtained for the diimines are lower than those for the corresponding diamine developers (pK *ca.* 11).[6] This is reasonable, because the positively

(6) R. J. Gledhill, private communication.

TABLE V

SPECIFIC RATE CONSTANTS AND STRUCTURES OF QUINONEDIIMINE

Original diamine	II	III	IV	VII
Diimine	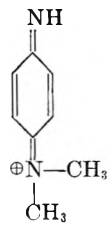	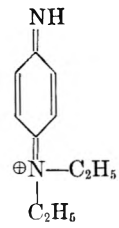	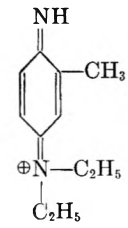	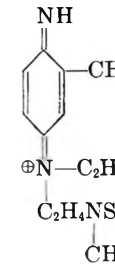
log k_4 or log k_4'	4.40	3.72	3.22	3.78
Original diamine	V	V	VI	VI
Diimine	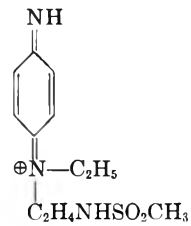	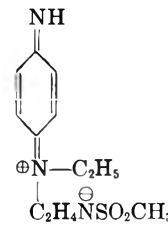	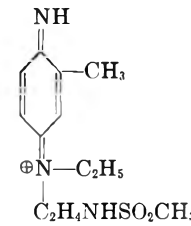	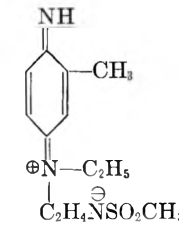
log k_4 or log k_4'	4.30	2.34	3.65	2.48

charged diimine should be a stronger acid than the unoxidized free base. It is also interesting to note the linear relationship between k_1 and *p*H for compound VII. This developer is similar to VI, except that the ionizable H on the sulfonamido group is replaced by a CH_3 group, resulting in behavior similar to that of other un-ionizable developers.

Effect of Structure on the Rate of Deamination. Removal of Disubstituted Imino Group.—For this reaction, comparisons are made of the specific rate constant, k_4. Since, for different compounds, this constant is not exactly independent of (OH^-), extrapolated values at *p*H 12 were used, with the exception of V and VI, where k_4 and k_4' were obtained as described in the previous section. In Table V are listed the structures of the reacting diimines, together with the log of k_4.

The structures in Table V show the charge on the substituted N, but a more complete representation according to the resonance theory should include some of the main contributing structures.

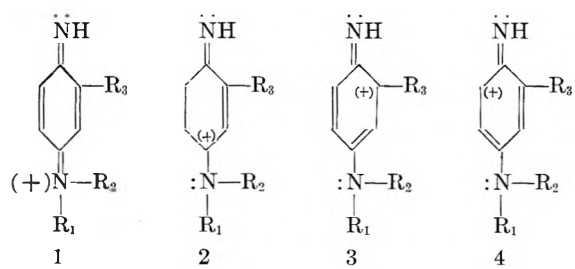

1 2 3 4

The experimental results are consistent with the hypothesis that the rate-determining step is the direct attack by the (OH^-) on the ring carbon to which the substituted N is attached, followed by a rapid scission of R_1R_2N: and H^+, and rearrangement of the C–O bond.

This mechanism pictures the reaction as an attack on the ring carbon by a nucleophilic reagent, and any substituent which effectively makes the reacting carbon atom more positive should increase the rate. Conversely, a substituent which makes the carbon atom more negative should decrease the rate. The results shown in Table V can be interpreted on the basis of this assumption.

The difference in structure between compound III and compound IV is a $-CH_3$ group in the ring. By an inductive effect, this substitution of an electron-repelling $-CH_3$ group deactivates the *meta*-position toward nucleophilic attack. This results in a rate decrease in going from III to IV. Similarly, a decrease in rate was observed in going from V to VI when they are in the acid form.

Inductive effects due to the substituents on the nitrogen atom produce similar results. In going from II to III, there is a rate decrease, which can be explained on the basis that $-C_2H_5$ is more electron-repelling than $-CH_3$. In V, the positive effect of $-C_2H_4-$ is partially neutralized by $-NHSO_2CH_3$ and therefore its rate is higher than that of III. The partial neutralization of $-C_2H_5$ by substitution of $-NHSO_2CH_3$ is again illustrated by the fact that the rate is higher for VI than for IV. The rates for the dissociated (basic) species of V and VI are very much lower than for the undissociated (acid) species, since a formal negative charge on the sulfonamido group must greatly decrease the positive charge of the ring.

Removal of=NH.—The unsubstituted *p*-phenylenediamine differs from the other diamines in that the resulting diimine is probably neutral. Being neutral, its reaction with (OH^-) would be expected to be much slower. Based on this and the additional fact that the rate of deamination for this compound is relatively insensitive to *p*H change, the reaction above *p*H 8 is suspected to be predominantly an uncatalyzed hydrolysis.

In a more acid region, a proton is added to one of the nitrogens to give the positive ion

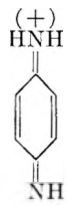

and the rate of hydrolysis of this ion is faster than that of the symmetrical neutral molecule. This accounts for the increase in rate for the acid region. This assumption is not unreasonable because the uncharged molecule, being symmetrical, is stabilized more by resonance. From the similarity among all the values of k_2 and k_3 (except those for V and VI) and the relative insensitivity to variation of pH, one is led to suspect that all of the reactions removing =NH follow the same mechanism, hydrolysis, either uncatalyzed or catalyzed by H^+.

Acknowledgment.—The author wishes to thank Dr. P. W. Vittum for his kind encouragement during the work on this problem, and for his help in the preparation of this manuscript. He also wishes to thank Dr. W. R. Ruby for his helpful discussions.

ON THE PERMEABILITY OF CELLOPHANE MEMBRANES TO SODIUM DODECYL SULFATE SOLUTIONS

BY B. S. HARRAP AND I. J. O'DONNELL

Biochemistry Unit, Wool Textile Research Laboratory, C.S.I.R.O., Melbourne, Australia

Received May 29, 1954

It is shown that purified sodium dodecyl sulfate, on equilibrium dialysis in the presence of salt, does not distribute itself equally across a Cellophane membrane when the total concentration is above the critical micelle concentration. This is considered to support the hypothesis of Yang and Foster that the solution inside the dialysis bag contains micelles plus single ions whereas that on the other side of the membrane contains single ions only. The size of the micelles decreases with decreasing salt concentration to such an extent that, in the absence of salt, diffusion of micelles through the membrane occurs, resulting in equal concentrations of detergent on both sides of the membrane when equilibrium is reached. It is also noted that certain commercial detergents cannot be completely removed from solution by exhaustive dialysis.

Introduction

The work of Yang and Foster[1] with the commercial detergents, Santomerse No. 3 and technical alkyl dimethylbenzylammonium chloride[2] has shown that, on equilibrium dialysis, the detergent ions do not distribute themselves equally across a Cellophane membrane, except at concentrations below the critical micelle concentration. They interpreted this as indicating that on one side of the membrane the solution at equilibrium contains both single ions and micelles whereas on the other side of the membrane it contains single ions only. In a subsequent discussion of this paper Mysels[3] suggested that this apparently non-uniform distribution may be an artifact due to the presence of non-diffusible impurities (such as aromatic oils) in the commercial detergents used.

We had already observed (unpublished work) that solutions of the commercial detergents Duponol C, Santomerse No. 1, etc., could not be completely freed from detergent by exhaustive dialysis against running water. The work on which we were engaged at the time required a detergent which was completely diffusible through Cellophane and a sample of sodium dodecyl sulfate prepared from carefully fractionated dodecyl alcohol was found to fulfil these requirements. In view of the uncertainty of the effects of detergent purity on the interpretation of the results of Yang and Foster, it seemed of interest to establish whether there is a non-uniform distribution of detergent ions across a Cellophane membrane when a pure detergent is used. That this is indeed the case, under certain conditions, is borne out by the results which were obtained from both equilibrium dialysis and osmotic pressure measurements.

Experimental

(a) **Materials.**—Pure sodium dodecyl sulfate was prepared by the method of Dreger, Keim, Miles, Shedlovsky and Ross.[4] The first sample was prepared from carefully fractionated dodecyl alcohol (b.p. 110.9° at 2.00 mm.).[5] Later preparations were made from Eastman Kodak dodecyl alcohol which had not been further purified and this proved to be equally satisfactory. On exhaustive dialysis each sample of detergent used was shown to diffuse completely through the Cellophane bag. This was in contrast to solutions of the commercial detergents where, initially, a considerable proportion of the detergent diffused through the Cellophane bag, but as dialysis proceeded the originally clear solution remaining in the bag became progressively more turbid and diffusion almost ceased. On raising the temperature, the solution in the bag cleared and more detergent diffused through, but a state was reached eventually where even at 60° there was a precipitate in the bag and scarcely any effusion of detergent.[6]

(1) J. T. Yang and J. F. Foster, THIS JOURNAL, **57**, 628 (1953).

(2) The principal components of these detergents are sodium dodecylbenzene sulfonate and *n*-dodecyldimethylbenzylammonium chloride.

(3) K. J. Mysels, THIS JOURNAL, **57**, 633 (1953).

(4) E. E. Dreger, G. I. Keim, G. D. Miles, L. Shedlovsky and J. Ross, *Ind. Eng. Chem.*, **36**, 610 (1944).

(5) This was kindly supplied by Mr. K. E. Murray, Division of Industrial Chemistry, C.S.I.R.O., Melbourne, Australia.

(6) This phenomenon was attributed to the presence of higher homologs in the commercial detergents used. Although the higher homologs have Krafft temperatures above room temperature they would be initially solubilized by the lower homologs present. As these latter are removed by dialysis so the solubility of the higher homologs would decrease and, since the Krafft temperature increases rapidly with chain length, it is not surprising that precipitates should form which are insoluble even at 60°.

Buffer solutions were made with distilled water and Analytical Reagent grade salts.

(b) **Analysis.**—The concentration of detergent on either side of the Cellophane membrane was determined by titration with cetyltrimethylammonium bromide (C.T.A.B.) according to the method of Epton,[7] using methylene blue as indicator. The C.T.A.B. was purified by recrystallizing I.C.I. Cetavlon from aqueous acetone.

(c) **Equilibrium Dialysis.**—Visking Cellophane tubing was freed from soluble material by repeated boiling with distilled water. Aliquots (10 ml.) of detergent solution were placed in Cellophane bags and equilibrated against an equal volume of buffer at either 28 or 38° for two days with shaking. The detergent concentrations on either side of the membrane were then determined by titration.

(d) **Osmotic Pressure Measurements.**—These were carried out on dialyzed solutions in a Hepp-type osmometer as designed by Scatchard, Brown, Bridgeforth, Weeks and Gee.[8] The osmometer was immersed in a bath at 40° so that the detergent remained in solution over the range of ionic strengths used. Measurements were carried out on a 3% solution of detergent in water and in $M/25$ potassium chloride. The membranes were Cellophane 300PT[9] and were thoroughly washed before use by repeated soaking in detergent solution and water to free them from soluble material.

Results

(a) **Equilibrium Dialysis.**—It was of interest first to determine the effect of ionic strength on the ratio of detergent concentrations (C_i/C_0) on the inside (C_i) and outside (C_0) of the bag for the same total concentration level (1%) of detergent. Figure 1 shows the results obtained using *p*H 7.1 phosphate buffers of differing ionic strength. Because of the increase in Krafft temperature with ionic strength, all of these solutions were equilibrated at 38°, a temperature which is above the Krafft temperature corresponding to the highest ionic strength investigated.

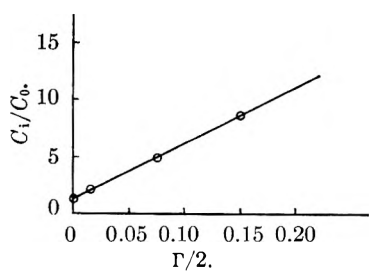

Fig. 1.—The ratio C_i/C_0 as a function of ionic strength; total detergent concentration = 1%, temp. = 38°, *p*H 7.1.

Figure 2 shows the concentration of detergent both inside (C_i) and outside (C_0) the dialysis bag for a series of solutions of varying detergent concentration but constant ionic strength. The buffer used consisted of 0.02 M K_2HPO_4 and 0.02 M KH_2PO_4, *p*H 7.1 and ionic strength $\Gamma/2 = 0.06$. The temperature of equilibrium was 28°.

(b) **Osmotic Pressure.**—In the case of the 3% solution of sodium dodecyl sulfate in water, dialysis led to equal concentrations of detergent on both sides of the membrane and hence there was no osmotic pressure developed. If an undialyzed solution was put in the osmometer the pressure rose quickly to a maximum and then fell off to zero. When the 3% solution of sodium dodecyl sulfate was dissolved in and dialyzed against $M/25$ potassium chloride it was found that a large osmotic pressure (*ca.* 40 cm.) was obtained which only slowly fell off over several days and did not reach zero.

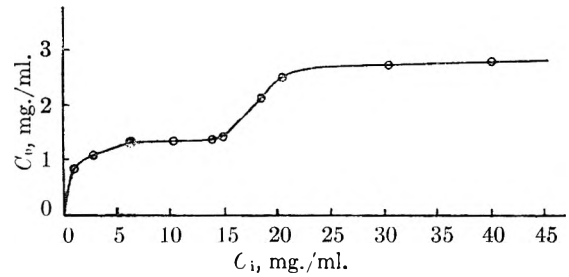

Fig. 2.—C_i as a function of C_0 at constant ionic strength; $\Gamma/2 = 0.06$, temp. = 28°, *p*H 7.1.

Discussion

The results summarized in Fig. 1 establish the main point of Yang and Foster's argument, *viz.*, that under certain conditions detergent does not distribute itself equally across a Cellophane membrane. However, it must be emphasized that this does not occur at low ionic strength. Figure 1 shows clearly that in distilled water there is virtually a uniform distribution of detergent on either side of the membrane, although the concentration used (1%) is well above the critical micelle concentration for sodium dodecyl sulfate in distilled water (approximately 0.23%—Goddard, Harva and Jones[10]). The molecular weight of the micelle at low ionic strength is thought to be in the range 10–15,000 (Philippoff[11]), and it is well known that Cellophane is permeable to particles of this size. Although stable osmotic pressures could not be obtained at low ionic strength using Cellophane as a semi-permeable membrane, an approximate value of 15,000 was calculated for the molecular weight of the micelles at ionic strength $\Gamma/2 = 0.04$ from the osmotic pressure at a concentration of 3%. This assumes no concentration dependence of osmotic pressure and is therefore of doubtful accuracy but shows that the micellar size is of an order which would diffuse through Cellophane.

The decrease in diffusion across the membrane at higher ionic strengths shown in Fig. 1 may be attributed to an increase in the size and molecular weight of the micelles. It should be noted that Debye[12] showed by the light scattering technique that the molecular weight of cationic detergent micelles increases rapidly with chain length.

Figure 2 shows that at detergent concentrations less than about 0.1% the detergent distributes itself uniformly on either side of the membrane even though the ionic strength ($\Gamma/2 = 0.06$) is moderately high. This concentration range is probably below the critical micelle concentration so that only freely diffusible single ions are present in solution. As the detergent concentration increases, the slope C_0/C_i decreases, indicating non-uniform distribution, until a plateau parallel to the C_i axis is reached. This is in contrast to the results of

(7) S. R. Epton, *Trans. Faraday Soc.*, **44**, 226 (1948).

(8) G. Scatchard, *et al.*, *Amer. Scient.*, **40**, 61 (1952).

(9) Cellophane 300PT was supplied by E. I. du Pont de Nemours & Co., Inc., Wilmington, Delaware, U.S.A.

(10) E. D. Goddard, O. Harva and T. G. Jones, *Trans. Faraday Soc.*, **49**, 980 (1953).

(11) W. Philippoff, *Disc. Faraday Soc.*, **11**, 96 (1951).

(12) P. Debye, *Ann. N.Y. Acad. Sci.*, **51**, 575 (1949).

Yang and Foster who found no plateau but simply observed a curve of decreased slope after the initial region where $C_0/C_i = 1$. This is probably accounted for by a distribution of homologs in the material used by later investigators. On the basis of Yang and Foster's discussion, the concentration C_0 at which this plateau occurs would be taken as the critical micelle concentration of the detergent. However, in view of the fact that micelles of sodium dodecyl sulfate are able to diffuse through Cellophane under certain conditions, this assumption is not always justified. For purpose of comparison all results in Fig. 2 were obtained after a standard time of two days. The concentration C_0 corresponding to the plateau (*ca.* 0.14%) thus represents not the CMC but the sum of the critical micelle concentration and the concentration of micelles which have diffused in this time. When the concentration of detergent within the dialysis bag exceeds approximately 1.5%, the concentration C_0 increases with increasing C_i until a further plateau is reached at C_i approximately 2.0%. The concentration C_0 at this plateau is approximately 0.27%. This plateau extends to $C_i = 4.0\%$, the highest concentration investigated. It is difficult to understand the significance of this second plateau. The most likely explanation is that it represents the formation of a second type of micelle, this latter being in equilibrium with a different concentration of single ions. (For a comprehensive discussion of the types of micelles postulated from time to time see McBain.[13]) It is interesting to compare this effect with the results of Ekwall and Passinen.[14] These workers studied the solubilization of decanol in sodium oleate and sodium myristyl sulfate and found that the composition of the detergent–alcohol complex was constant as the detergent concentration was increased above the critical micelle concentration until, at considerably higher concentrations, (*ca.* 5%), the alcohol/detergent ratio increased, again suggesting that the nature of the micelles changes at these higher concentrations.

(13) J. W. McBain, "Colloid Science," D. C. Heath and Co., Boston, Mass., 1950, pp. 255–261.

(14) P. Ekwall and K. Passinen, *Acta Chem. Scand.*, **7**, 1098 (1953).

TERNARY SYSTEMS OF LIQUID CARBON DIOXIDE[1]

By Alfred W. Francis

Contribution from Socony-Vacuum Laboratories, A Division of Socony-Vacuum Oil Co., Inc., Research and Development Department, Paulsboro, New Jersey

Received June 1, 1954

Mutual solubilities of liquid carbon dioxide with each of 261 other substances are reported. Nearly half of these are miscible with carbon dioxide. Some relations to structure are noted. Density observations show contractions of ten to fifteen per cent on mixing.

Triangular graphs are presented for 464 ternary systems involving liquid carbon dioxide. These are of many different types, some of them novel. They include those with three separate binodal curves (and three plait points) and several with a binodal band across two sides of the triangle and a separate binodal curve on the third side. Another system has three plait points although one pair of components is miscible.

Carbon dioxide has a strong homogenizing action upon pairs of other liquids at moderate concentrations, but a precipitating action at higher concentrations. In contrast to most solvents it has a selectivity against dicyclic hydrocarbons. Cosolvents were found necessary to make these unusual properties effective in solvent extraction of hydrocarbon mixtures.

The large collection of unusual graphs provides experimental evidence on methods of merging of binodal curves. External contact of convex curves always occurs at both plait points.

No ternary systems of liquid carbon dioxide have been published. Miscibility relations of this condensed gas with other liquids have now been studied in an investigation of its possibilities for use in solvent extraction.[2] Cosolvents are necessary to make its unusual properties available for that purpose.

Several ternary systems with two separate binodal curves were presented in a recent paper.[3] Graphs with three such curves are suggested in many physical chemistry textbooks, but no actual example is recorded in the chemical literature. For this type two incompletely miscible liquids must become homogenized by addition of a third liquid which is not miscible with either of the other two; and this effect must occur with all three pairs. This would not normally be expected.[4] Liquid carbon dioxide yields many such systems.

Ternary diagrams were observed for 464 systems involving carbon dioxide at or near room temperature. Several of these are of novel types including 21 systems with graphs showing three separate binodal curves, and 38 showing a binodal band across two sides of the triangle and a separate binodal curve on the third side. There are also 76 systems with two separate binodal curves, 82 systems with a binodal band so highly concave on its borders as to indicate that it can be considered as a result of a merger of two binodal curves; and 29 systems with three liquid phases. The only type of ternary all-liquid system observed elsewhere but not among the carbon dioxide systems is that of island curves (ternary miscibility gaps not connected with binary ones).

The property of liquid carbon dioxide which makes these uncommon diagrams possible may be

(1) Presented before the Division of Physical and Inorganic Chemistry of the 126th Meeting of the American Chemical Society, New York, September 15, 1954.

(2) A. W. Francis, U. S. Patents 2,463,482 (1949); 2,631,966; 2,632,030; 2,646,387 (1953); three other U. S. Patents applied for; *Ind. Eng. Chem.*, in press, 1955.

(3) A. W. Francis, *J. Am. Chem. Soc.*, **76**, 393 (1954).

(4) C. R. Bailey, *J. Chem. Soc.*, **123**, 2579 (1923); and several textbooks.

the proximity of its critical temperature, 31°, to the temperature of the observations. Carbon dioxide exhibits dual solubility effects which are apparently antagonistic to each other. At moderate concentrations, up to about 40% by weight, it acts as a dissolved gas and exerts a strong mixing action. Most pairs of partially miscible liquids become homogeneous on dissolving sufficient carbon dioxide in them. At higher concentrations, especially 60 to 90%, liquid carbon dioxide is a relatively poor solvent for many of these same liquids. It exerts a demixing or precipitating effect more intense than that of propane in deasphalting operations.

Hydrogen chloride and bromide are known[3,5] to behave somewhat similarly, being effective in homogenizing water with ether and higher alcohols although the hydrogen halides have limited solubility in water. Probably other condensed gases would have analogous effects. An investigation of nitrous oxide parallel to the present one was considered because of the similarity in physical properties to those of carbon dioxide. It was rejected because of possible explosibility of mixtures of organic compounds with liquid nitrous oxide.

Another respect in which the solubility relations of liquid carbon dioxide are abnormal is its negative selectivity. It is incompletely miscible with dicyclic hydrocarbons both naphthenic and aromatic (even if the rings are separate) but mixes with aliphatic and monocyclic hydrocarbons in the same boiling range as the dicyclics. This relation is the reverse of that with most solvents, in which the more highly cyclic hydrocarbons are more soluble. Fluorocarbons have similar negative selectivity.[6-8]

Liquid carbon dioxide is only weakly acidic, showing no noticeable affinity for moderately basic organic compounds like aniline and pyridine. It does form salts with stronger bases such as ammonia and aliphatic amines. *p*-Phenetidine is a borderline case, permitting observations of metastable liquid-liquid solubilities before solid salt appears. Systems of components forming salts are omitted from the graphs.

The literature abounds with observations on solubility of gaseous carbon dioxide in aqueous and organic liquids at various temperatures and pressures. But quantitative data are meager for the mutual solubilities of liquid carbon dioxide and other liquids. Büchner[9] made qualitative observations of solubility of several substances in liquid carbon dioxide. He stated that no hydrocarbon was known which gives two liquid phases with carbon dioxide. This is no longer true.[10]

Apparatus and Materials.—All of the observations on carbon dioxide miscibility were made in a visual autoclave.[11] This is a Jerguson gage of 116-ml. capacity with narrow Pyrex glass windows about 17 mm. thick, front and back. It has been tested to 400 atmospheres. Incandescent lamps are mounted behind the vertical position. Agitation results from rotation end-over-end within a heat insulated case.

The reagents used were mostly from Eastman Kodak Company, first grade, but not further purified except to dehydrate those suspected of containing water. The inaccuracies due to the amounts of other impurities likely to be present are believed to be less than other experimental errors. The hydrocarbon mixtures mentioned had the following properties

Hydrocarbon mixture	d^{20}_4	$n^{20}D$	Aniline C.S.T., °C.
Gasoline (straight run)	0.723	1.397	58.7
Kerosene (refined)	.796	1.438	61.2
Fuel oil	.853	1.479	62
Transformer oil	.867	1.490	80
Lubricating oil (naphthenic)	.910	1.5076	72
Bright stock (residual, refined)	.948	1.532	73.2
Crystal oil (Nujol)	.891	1.4797	123

Binary Systems.—A "system" in this investigation includes only condensed phases, even though the weight of the vapor phase is appreciable, because, with a few exceptions, it is substantially pure carbon dioxide. The autoclave was charged with liquid reagents from pipets through a small glass funnel inserted through a 4.5 mm. hole in the autoclave. Their weights were calculated from their densities. Liquefied gas reagents were then added in the order of increasing vapor pressure (butane, sulfur dioxide, propane, propylene, hydrogen sulfide, ethane, carbon dioxide) from steel lecture bottles attached through cone joints and a valve. The lecture bottle was detached before agitation.

The weight of carbon dioxide (and those of other condensed gases) added to a system was estimated from the increase in liquid volumes, as indicated by the positions of the meniscuses, and from the apparent density of dissolved carbon dioxide as a function of the concentration. The apparent density was ascertained from the new actual density observed in typical cases by a special technique, and an average value (0.7 to 1.36 depending on concentration) was then used for the various systems. Apparent density is here defined as the ratio of total increase in weight to the total increase in volume.

Liquid Densities of Carbon Dioxide Mixtures.—Several sealed floats were made of thin glass tubing, about 3 × 60 mm., each containing a small quantity of mercury to make it float in a vertical position. The density of each float was found by adjusting a mixture of acetic acid or methanol and water or one of acetone and heptane so that the float would remain stationary while completely submerged in the mixture. The density of the liquid was then determined with a pycnometer. They were used as in the following example.

The visual autoclave was charged with 5.0 ml. or 4.39 g. of pure benzene and three floats of densities 0.8486, 0.8203 and 0.7916, respectively. Carbon dioxide was added. All three floated with a small volume and sank with a large volume. They barely floated at volumes (corrected for volumes of floats) of 30.1, 44.3 and 64.6 ml. corresponding to 25.5, 36.4 and 51.1 g., respectively (using the densities of the floats, which equalled those of the liquid mixtures). These indicated percentages of 82.8, 88 and 91.4% carbon dioxide, respectively. In a single binary system two compositions with the same density were often observed.

Although the floats were necessarily thin walled (less than 0.2 mm.) in order to float, they were sufficiently rugged to stand tumbling in agitating the system. They also had to support an external pressure of 65 atmospheres without crushing. The elastic contraction of the floats due to pressure, which would make density observations too low, must be very slight since a float which just sank (even in water)

(5) A. W. Francis in "Solubilities of Inorganic and Organic Compounds," A. Seidell and W. F. Linke, eds., Suppl. to 3rd ed., D. Van Nostrand Co., New York, N. Y., 1952, pp. 991, 994, 997, 1002, 1018.

(6) J. H. Hildebrand, B. B. Fisher and H. A. Benesi, *J. Am. Chem. Soc.*, **72**, 4348 (1950).

(7) C. J. Egan, U. S. Patent 2,582,197 (1952).

(8) A. W. Francis and G. C. Johnson, U. S. Patent, 2,663,670 (1953).

(9) E. H. Büchner, *Z. physik. Chem.*, **54**, 665 (1906).

(10) E. B. Auerbach, Brit. Patents 277,946 (1926); 285,064 (1927); Can. Patent, 285,782 (1928); U. S. Patent, 1,805,751 (1931).

(11) W. F. Caldwell, *Ind. Eng. Chem.*, **38**, 572 (1946).

was floated by an increase in pressure, showing that the liquid was more compressible than the float. In fact, it was found that a float was compressed less than one part in 10^5 per atmosphere.

Results of density observations for mixtures of carbon dioxide with each of four solvents are shown in Table I and Fig. 1. In each case the dissolved carbon dioxide has an apparent density of about 1.0 g. per ml. at low concentrations, as indicated by the dashed lines tangent to the curves. Straight lines drawn through the zero point and a point of any other selected percentage on each of the four curves converge approximately to the same apparent density for dissolved carbon dioxide. In view of the diversity in structure of the four solvents this measure of carbon dioxide concentration was applied to all solvents tested. In water or glycerol (of low solvent power for carbon dioxide) the initial apparent density is about 1.36. This was calculated from the density of a saturated solution (6%) of liquid carbon dioxide in water at 26° and 65.1 atm., 1.016, in comparison with that of pure water, 0.9999, at the same temperature and pressure.

TABLE I

DENSITIES OF CARBON DIOXIDE MIXTURES AT 26°

Liquid	Wt. % CO_2	d^{26}_4
Acetic acid	0	1.0454
	49.5	0.9914
	65	.9429
	70.5	.9227
	76	.8912
	85.5	.8749
	100	.69
Benzene	0	0.8730
	20	.8952
	35	.8980
	48	.8952
	73	.8749
	82.8	.8486
	88	.8203
	91.4	.7916
Methanol	0	0.7888
	16	.8203
	40	8480
	65	.8480
	73.5	.8413
	76.5	.8250
n-Heptane	0	0.6785
	48	.7605
	88	.7605

The dotted curve on the right of Fig. 1 indicates compositions and corresponding densities calculated for solutions containing the same weight of carbon dioxide per milliliter as that present in pure liquid carbon dioxide, 0.69 g. per ml. On this curve the apparent density of the solvent is infinite. Density observations above this curve show a concentration of carbon dioxide higher than that of pure liquid carbon dioxide.

In all of the observations reported here involving carbon dioxide the pressure was autogenous, that corresponding to vapor–liquid equilibrium. When not otherwise indicated, the temperature was 21 to 26° and the pressure approached 65 atmospheres.

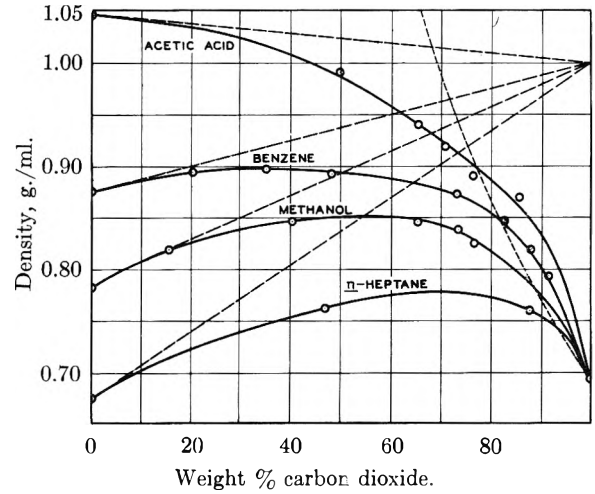

Fig. 1.—Densities of carbon dioxide mixtures at 26°.

Since moderate changes in temperature were found to have little effect on the liquid–liquid miscibility relations, precise temperature control was unnecessary. This was due to compensating factors. The normal increase in solubility with rising temperature is largely balanced by a decrease due to the more gas-like quality of liquid carbon dioxide.

No upper critical solution temperature with carbon dioxide was observed. Lower critical solution temperatures occur only in systems with a narrow miscibility gap. Those observed were α-chloropropionic acid 12°, *p*-nitrotoluene 15°, and ethyl phthalate 25°.

Mutual solubilities of carbon dioxide and another liquid were estimated as in the following example.

The visual autoclave was charged with 20 ml. or 17.9 g. of decahydronaphthalene (decalin) and carbon dioxide until a trace of upper layer remained after agitation. The initial interface was at 34 ml. The 14-ml. increase corresponded to 13 g. or 42% in the lower layer since the converging lines through the zero and 42% points of the curves of Fig. 1 indicate an average apparent density of 0.93. More carbon dioxide was then added until the levels after agitation were 18 and 62 ml. The additional carbon dioxide in the system was 28 ml. or 23.6 g. (apparent density 0.84) a total of 36.6 g. of which 6.9 g. ($^{18}/_{34} \times 13$) was in the lower layer and 29.7 g. in the upper. The latter contained 8.4 g. ($^{16}/_{34} \times 17.9$) or 22% of decalin.

Mutual solubilities of liquid carbon dioxide with each of 261 other substances are presented in Table II. The first column gives an arbitrary code abbreviation for designation of the components on the graphs and in column 2 of Table III. Solids (m.p. given) melt at room temperature in contact with liquid carbon dioxide in those cases in which M or a numerical value is listed under "x" (column 4).

Since ternary systems usually involving hydrocarbons were to be studied, the miscibilities of the liquids with various hydrocarbons are indicated qualitatively in column 3 as explained in the footnotes. The last column lists the graphs showing systems studied involving these components, and with column 2 serves as an alphabetical index for the graphs. A few metal salts were tested because other relations between them and certain hydrocarbons had been noted previously. Of these only stannic chloride was appreciably soluble in liquid carbon dioxide.

TABLE II

MUTUAL SOLUBILITIES WITH LIQUID CARBON DIOXIDE

Each code letter or pair of letters refers only to the substance opposite it. Substances without codes are listed by name in Table III (except those forming solid salts, which are not illustrated in the graphs).

Hydrocarbon miscibilities are at 25° as liquid. A solid is considered miscible with a hydrocarbon or carbon dioxide if it is highly soluble in it without the formation of two liquid layers in equilibrium, and it is probable that the subcooled liquid would mix with the solvent at 25°.

If a substance is miscible with one group of hydrocarbons, as indicated by a footnote letter, it is also miscible with all of the hydrocarbons indicated by letters following this one in the series, *a* to *f*. Thus "*b*" means "*b*, *c*, *d*, *e*, *f*"; "*c*" means "*c*, *d*, *e*, *f*"; "*d*" means "*d*, *e*, *f*"; and "*e*" means "*e*, *f*."

Code (legend in graphs)	Substance	Hydrocarbon miscibility (see footnotes)	Carbon dioxide solubility (M = Miscible) [i] x	y	Graphs
AA	Acetal	*a*	M	...	A64
AB	Acetaldehyde	*b*	M	...	C25
AC	Acetamide (m.p. 82°)	*g*	..	1	B10
AD	Acetic acid	*c*	M	...	A7, 42, 64, B9, 10, C21
...	Acetic anhydride	*e*	M	...	C8, 21
AE	Acetone	*b*	M	...	A26, 49, 50, 52, B51, C11, 22
AF	Acetonitrile	*f*	M	...	A8, C12, 20
AG	Acetophenone	*b*	M	...	B1
AH	Acetyl chloride	*a*	M	...	A64
AJ	Acrolein	*d*	M	...	A65
...	Acrylonitrile	*d*	M	...	C8
AK	Aldol	*d*	31	11	B33, D8, 43, 56
Al	Aluminum chloride (m.p. 190°)	*g*	..	0	A47
...	2-(2-Aminoethylamino)-ethanol	*g*	..	...	Forms salt
...	2-Amino-2-methyl-1-propanol	*f*	..	...	Forms salt
AM	*t*-Amyl alcohol	*a*	M	...	A44
A	Aniline	*c*	20	3	A64, B17, 27, 35, D9, 38, 44, 53, 54
AN	*o*-Anisidine	*e*	20	1	B13, D38
AS	Anisole	*a*	M	...	A64
PE	Benzalacetone (m.p. 42°) (4-Phenyl-3-butene-2-one)	*d*	40	5	C67, D5
BD	Benzaldehyde	*b*	M	...	B1, 49
B	Benzene	*a*	M	...	A16, 32, 36, 37, 43, 45, 51, 64, B1, 4, 19, 34
...	Benzoic anhydride (m.p. 42°)	*e*	20	3	B40, D39
BE	Benzonitrile	*b*	M	...	A60, B62
BF	Benzophenone (m.p. 48°)	*c*	25	4	A31, C65
BH	Benzoyl chloride	*a*	M	...	B6
BI	Benzyl alcohol	*d*	27	8	B18, C34, 41, 46, D11, 37
BJ	Benzyl benzoate	*c*	40	10	A19, C62
BK	Bibenzyl (m.p. 52.5°)	*a*	..	1	A16, C66
...	Biphenyl (m.p. 71°)	*a*	..	2	C66
BL	Bright stock	*a*	15	0.5	B4, 62
...	Bromine	*a*	8	2	A17
BM	Bromoform	*a*	40	30	A13, C26
BN	*n*-Butane	*a*	M	...	A64, B1, 4
BO	*sec*-Butyl alcohol	*b*	M	...	B54
BP	*t*-Butyl alcohol	*b*	M	...	A64
BS	2-Butanone (methyl ethyl ketone)	*a*	M	...	B1, 55
BT	*n*-Butyl ether	*a*	M	...	B1
BU	Butyl oxalate	*a*	M	...	A64
BV	Butyl phthalate	*b*	55	8	C47
BX	Butyl stearate	*a*	55	3	A18
BY	*n*-Butyraldehyde	*a*	M	...	A65, 66
Ca	Calcium nitrate (m.p. 561°)	*g*	..	0	A50
CA	Camphor (m.p. 176°)	*a*	M	...	A38, 61
CB	Caproic acid	*a*	M	...	B1
CC	Caprylic acid	*a*	M	...	A34, B1
DH	Carbitol (see below)	*c*	M	...	A35, B62
CD	Carbon disulfide	*a*	M	...	B6
CE	Carbon tetrachloride	*a*	M	...	A17, B1

TABLE II (*Continued*)

Code (legend in graphs)	Substance	Hydrocarbon miscibility (see footnotes)	Carbon dioxide solubility (M = Miscible) *i* *x*	*y*	Graphs
CF	Castor oil	*d*	15	1	B21, D22
...	Cellosolve (β-ethoxyethanol)	*b*	M	...	B63
...	Chloral hydrate (m.p. 48°)	*e*	..	2	A16
DC	Chlorex (see below)	*c*	M	...	B61, 63, 66
CG	Chloroacetic acid (m.p. 61°)	*f*	..	10	A10, 56, D47, 57
...	Chloroacetone	*e*	M	...	C13
CH	*o*-Chloroaniline	*c*	25	5	D6, 33
CI	*m*-Chloroaniline	*e*	23	1	B35, D38, 49
CJ	Chlorobenzene	*a*	M	...	A65
CK	β-Chloroethanol	*f*	40	10	B31, 32, C30 43, D15, 57
...	β-Chloroethyl acetate	*c*	M	...	C13
CL	Chloroform	*a*	M	...	A65, B50
CM	Chloromaleic anhydride (m.p. 33°)	*f*	M	...	A62
...	α-Chloronaphthalene	*a*	15	1	A29, C49
CO	*o*-Chlorophenol	*c*	M	...	A54, 55, B2, C1
CP	*p*-Chlorophenol (m.p. 43°)	*d*	25	8	B39, D7, 23
CR	2-Chloro-6-phenylphenol	*d*	20	1	B14
CS	α-Chloropropionic acid	*f*	52	26	D2, D55
CT	Cinnamaldehyde	*e*	20	4	B25, D27
CU	Cinnamyl alcohol (m.p. 30°)	*e*	20	5	B40, D59
CV	*o*-Cresol (m.p. 30°)	*b*	30	2	D18
C	*m*-Cresol	*b*	20	4	A28, 30, 33, C42, 45, C49, 61, D16, 33
...	*p*-Cresol (m.p. 36°)	*b*	30	2	D18
CW	Crotonaldehyde	*b*	M	...	A64
CX	Crystal oil	*a*	20	1	C1, 7, D26
CY	Cyclohexane	*a*	M	...	B13, 17, 44, 53
...	Cyclohexanol	*a*	20	4	A28
CZ	Cyclohexanone	*a*	M	...	A60
D	Decahydronaphthalene (decalin)	*a*	42	22	32 Systems
...	1-Decene	*a*	M	...	B17
DA	1-Decyl alcohol	*a*	30	1	D28
HY	Diacetone alcohol (see below)	*c*	M	...	C6
DB	Di-*sec*-butylbenzene	*a*	M	...	A27, B37, 53
...	*p*-Dichlorobenzene (m.p. 53°)	*a*	M	...	B7
DC	β,β′-Dichloroethyl ether (Chlorex)	*c*	M	...	B61, 63, 66
DD	β,β′-Dichloroisopropyl ether	*a*	M	...	A60
DE	2,4-Dichlorophenol (m.p. 45°)	*a*	30	14	A23, C29, 63
DF	α,α-Dichlorotoluene	*a*	M	...	B6
...	Di-(β-cyanoethyl)-amine	*f*	..	...	Forms salt
DG	N,N-Diethylacetamide	*c*	M	...	A1
...	N,N-Diethylaniline	*a*	45	17	C36, 62
...	Diethylene glycol	*g*	10	1	B23, 47, D50
DH	Diethylene glycol monoethyl ether (Carbitol)	*c*	M	...	A35, B62
...	N,N-Diethylformamide	*e*	M	...	A4
DI	*p*-Dimethoxybenzene (m.p. 53°)	*a*	M	...	B7
DJ	N,N-Dimethylacetamide	*e*	M	...	A4
DK	N,N-Dimethylaniline	*a*	M	...	B6
...	N,N-Dimethylformamide	*f*	M	...	C3, 8, 9, 19
DL	Dimethylnaphthalenes (mixed)	*a*	40	2	A21
DM	2,2-Dimethylpentane	*a*	M	...	A30, B32, 35, 39
...	2,5-Dimethylpyrrole	*a*	32	5	C28, 33, 48
DN	2,4-Dinitrochlorobenzene (m.p. 62°)	*f*	15	1	A32, D66
DO	*p*-Dioxane	*b*	M	...	B1
...	Diphenylamine (m.p. 53°)	*c*	..	1	A51, C66
DP	N,N′-Diphenylethylenediamine (m.p. 62°)	*e*	..	1	A36
DT	Diphenylmethane (m.p. 27°)	*a*	30	4	A63
DV	Dipropylene glycol	*e*	15	2	B26, D12, 60

TABLE II (*Continued*)

Code (legend in graphs)	Substance	Hydrocarbon miscibility (see footnotes)	Carbon dioxide solubility (M = Miscible) *i* *x*	*y*	Graphs
DX	*n*-Dodecane	*a*	M	...	A5, 6, 8, 12, 14, 20, 51, B8
...	Ethane	*h*	M	...	C25
...	β-Ethoxyethanol (Cellosolve)	*b*	M	...	B63
EA	Ethyl acetate	*a*	M	...	B1, 51
EB	Ethyl acetoacetate	*d*	M	...	A3, B67
EC	Ethyl alcohol	*b*	M	...	A41, C12
ED	N-Ethylaniline	*a*	35	13	A14, C31
...	Ethyl anthranilate	*b*	40	6	C62
EE	Ethyl benzoate	*a*	M	...	A64
EF	N-Ethyl-N-benzylaniline	*a*	33	4	C58
EG	Ethyl carbonate	*a*	M	...	B1
EH	Ethyl chloroacetate	*b*	M	...	B59
EI	Ethyl chloroformate	*a*	M	...	A64
EJ	Ethylene bromide	*a*	M	...	A64, B48
..	Ethylene diformate	*f*	M	...	A5, C20, 21
E	Ethylene glycol	*g*	7	0.2	A35, B49, 50, 51, D28, 48, 51
EK	Ethylene glycol monobutyl ether (Butyl Cellosolve)	*a*	M	...	A65
EL	Ethyl ether	*a*	M	...	A47, 65
EM	Ethyl formate	*b*	M	...	A64
EN	2-Ethylhexanol	*a*	53	17	C28, 59
EO	Ethyl lactate	*c*	M	...	C6, 14
...	Ethyl maleate	*d*	M	...	C13
...	Ethyl oxalate	*c*	M	...	A2, B67
EP	*p*-Ethylphenol (m.p. 46°)	*b*	8	1	C53, 54
EQ	Ethyl phenylacetate	*a*	M	...	A60, B23
ER	Ethyl phthalate	*d*	60	10	B12, D46
ES	Ethyl salicylate	*a*	M	...	A65
...	Ethyl succinate	*d*	M	...	B67
...	Ethyl sulfate	*e*	M	...	C9, 13
EU	Eugenol	*b*	38	10	C48, D1
FA	Formamide	*g*	10	0.5	B47, D50
FB	Formanilide (m.p. 47.5°)	*f*	10	0.5	A43, B53
FC	Formic acid	*g*	M	...	A11, 12, C10, 16, 24
FO	Fuel oil	*a*	42	18	C9, 23
F	Furfural	*e*	M	...	A5, 63, B56, C3, 8, 17
FU	Furfuryl alcohol	*f*	30	4	B16, 34, C41, 44, D12, 58
...	Gasoline	*a*	M	...	B47
G	Glycerol	*g*	7	0.05	A44, B51, 52, C55, 56, 61, D52
HA	1-Heptaldehyde	*a*	M	...	A65
H	*n*-Heptane	*a*	M	...	62 Systems on A & B
HB	Heptyl alcohol	*a*	38	6.2	C33, 43
HD	*n*-Hexadecane (Cetane)	*a*	38	8	44 Systems (after A53)
...	2,5-Hexanedione	*e*	M	...	C21
HE	Hexyl alcohol	*a*	M	...	B6
HN	Hydrocinnamaldehyde	*c*	55	17	D3, 4, 19
H_2S	Hydrogen sulfide	*a*	M	...	A67
HV	*o*-Hydroxybiphenyl (m.p. 56°)	*d*	..	1	D30
HX	β-Hydroxyethyl acetate	*f*	50	17	D25, 34, 41, 42, 55
HY	4-Hydroxy-4-methyl-2-pentanone (diacetone alcohol)	*c*	M	...	C6
HZ	β-Hydroxypropionitrile	*g*	30	1	B22, 34
IN	Indene	*a*	M	...	B15
I_2	Iodine (m.p. 113.7°)	?	..	0.2	A53
IA	Isocaproic acid	*a*	M	...	B52
IP	Isopropyl alcohol	*b*	M	...	A39, B60
IS	Isopropyl ether	*a*	M	...	A64
K	Kerosene	*a*	M	...	A2, 5, 7, 9, 11, 33, B6, 27

TABLE II (*Continued*)

Code (legend in graphs)	Substance	Hydrocarbon miscibility (see footnotes)	Carbon dioxide solubility (M = Miscible) t x	y	Graphs
...	Lactic acid	*g*	8	0.5	B23
LA	Lauric acid (m.p. 48°)	*a*	40	1	A22, C64
...	Limonene	*a*	M	...	A5, 67
Li	Lithium chloride (m.p. 600°)	*g*	..	0	A48
L	Lubricating oil	*a*	20	0.7	151 Systems
MA	Maleic anhydride (m.p. 57°)	*f*	55	7.5	B57, D65
MC	Mercuric chloride (m.p. 282°)	*g*	..	0	A52
MD	Mesityl oxide	*a*	M	...	A64
ME	Methanol	*f*	M	...	A6, 9, 35, 40, 46, 48, B11, C8, 9, 12, 16, 23
...	2-Methoxybiphenyl (m.p. 29°)	*a*	20	5	A28
MF	β-Methoxyethanol	*e*	M	...	B64, C4, 5, 19
MG	α-Methoxynaphthalene	*a*	15	1	A29, C37
...	Methyl acetate	*b*	M	...	A67
MH	Methylal	*a*	M	...	B1
MI	N-Methylaniline	*b*	40	20	A14, C36, 40, 50, 62, D26, 48
MJ	Methyl benzoate	*a*	M	...	A65
MK	Methylcyclohexane	*a*	M	...	B28, 45
ML	*p*-Methylcyclohexanol	*a*	20	4	A25
MM	Methylene iodide	*e*	30	30	B44, 45, 46
BS	Methyl ethyl ketone (2-butanone)	*a*	M	...	B1, 55
...	Methyl formate	*c*	M	...	C11
M	α-Methylnaphthalene	*a*	30	6	A27, 55, 56, 58, 62, B5, C16, 43, 44, 45, 46, 52, C54, 59, D34, 35, 50
MN	β-Methylnaphthalene (m.p. 35°)	*a*	29	9	A59
MP	Methyl phthalate	*e*	43	6	B30, D17, 40
...	Methyl salicylate	*a*	M	...	B2, 23
...	Methyl sulfate	*f*	M	...	C18, 21
MT	Monoacetin	*g*	10	1	A26
...	Morpholine	*c*	..	...	Forms salt
...	Naphthalene (m.p. 80°)	*a*	..	2	A51, C57, 66
NA	α-Naphthylamine (m.p. 52°)	*e*	20	1	B43
...	*o*-Nitroanisole	*e*	35	2	B34, D58
N	Nitrobenzene	*c*	M	...	A53, 54, 57, B5, 6, 61, 62, 63, C7
NB	*o*-Nitrobiphenyl (m.p. 37°)	*e*	15	2	B41, D39
NC	*o*-Nitrochlorobenzene (m.p. 32°)	*d*	42	21	C32, 52, D14, 20
...	Nitroethane	*d*	M	...	B64, C13
NM	Nitromethane	*f*	M	...	A5, 54, 58, 59, C9, 18, 21
NN	α-Nitronaphthalene (m.p. 58°)	*e*	..	1	D32
NP	*o*-Nitrophenol (m.p. 45°)	*d*	M	...	C2
...	1-Nitropropane	*b*	M	...	B60
NS	*o*-Nitrotoluene	*b*	M	...	B6
NT	*p*-Nitrotoluene (m.p. 51°)	*b*	56	20	C27
O	*n*-Octadecane (m.p. 28°)	*a*	30	3	C9, 15, 18, 20, 50
...	1-Octadecene	*a*	26	10	D8
ON	2-Octanone	*a*	M	...	A60
...	Oleic acid	*a*	22	2	A33
...	Oleum (20%)	*f*	6	0.1	A42
...	Olive oil	*a*	20	4	A28
OX	*p*-Oxathiane (thioxane)	*a*	M	...	A60
PA	Paraffin wax (m.p. 52°)	*a*	..	1	B8
PB	Paraldehyde	*b*	M	...	A64
...	*p*-Phenetidine	*e*	12	1	Forms salt
P	Phenol (m.p. 41°)	*d*	..	3	A38, B29, C56, D29, 31, 67
PC	Phenylacetic acid (m.p. 77°)	*c*	..	0	A34
PD	Phenylacetonitrile	*e*	52	13	B24, D36
PE	4-Phenyl-3-butene-2-one (benzalacetone) (m.p. 42°)	*d*	40	5	C67, D5
PF	Phenylcyclohexane	*a*	35	8	C30

TABLE II (*Continued*)

Code (legend in graphs)	Substance	Hydrocarbon miscibility (see footnotes)	Carbon dioxide solubility (M = Miscible)[i] x	y	Graphs
PG	Phenylethanol	*d*	15	3	B36, D22
...	Phenylethanolamine	*f*	15	1	A45, D60
PH	Phenyl ether (m.p. 28°)	*a*	35	8	C51
...	Phenylhydrazine	*f*	..	...	Forms salt
PI	Phenyl isocyanide	*a*	M	...	B1
...	Phenyl phthalate (m.p. 70°)	*e*	..	1	A37
PJ	Phenyl salicylate (m.p. 43°)	*b*	38	9	A23
PK	Phosphorus trichloride	*a*	M	...	B1
PL	Phthalyl chloride	*d*	33	4	B20, D21
PM	2-Picoline	*a*	M	...	A60
PN	Pinacol (m.p. 38°)	*c*	23	2	A24, D23
PO	Pinene	*a*	M	...	B16
PP	Piperonal (m.p. 37°)	*f*	45	10	B28, 42
PR	Propane	*h*	M	...	B3, 4
PT	Propionaldehyde	*a*	M	...	A64
PV	Propylene	*a*	M	...	B58
PX	Propylene glycol	*g*	10	0.5	A35, B23, 38, 48, D61
PY	Pyridine	*b*	M	..	A60
R	Resorcinol (m.p. 109°)	*g*	..	0.1	A40
..	Salicylaldehyde	*d*	M	...	B67
...	Saligenin (m.p. 86°)	*f*	..	0.1	A40
SN	Silver nitrate (m.p. 212°)	*g*	..	0	B58
...	Stannic chloride	*a*	M	...	A1
SU	Succinonitrile (m.p. 54.5°)	*g*	20	2	B19, D64
S	Sulfur dioxide	*c*	M	...	A2, 55, C5, 13, 15
...	Sulfuric acid (95%)	*g*	6	0.1	A41, 42
...	Sulfuryl chloride	*a*	M	...	A54
TB	Tetrabromoethane	*c*	10	1	D24
T	*n*-Tetradecane	*a*	50	16	C4, 10, 28, 35, 37, 58, 66, D3, 6, 7, 11, 16, 17, 24, 41, 51, 61
TD	Tetrahydrofurfuryl alcohol	*e*	20	3	B25, D10, 38
TE	Tetrahydronaphthalene (tetralin)	*a*	41	12	A14, 54, 57, C41, 42, C60, D25, 63
TF	Thiophene	*a*	M	...	A60, B22, 23, 38
OX	Thioxane (*p*-oxathiane)	*a*	M	...	A60
TH	Thymol (m.p. 51.5°)	*a*	41	9	A15
...	Toluene	*a*	M	...	B36
TK	*o*-Toluidine	*c*	37	7	D8, 45
TL	*m*-Toluidine	*c*	40	15	D8, 52
TM	*p*-Toluidine (m.p. 45°)	*c*	37	7	C55, D13
TN	Tolunitriles (mixed)	*b*	M	...	A60
TO	Transformer oil	*a*	14	2	A64, 66, B63, 66, C14, 17, 19, 22, D54
TP	Triacetin	*f*	M	...	B65, C8, 17, 18
...	Tri-*sec*-butylbenzene	*a*	M	...	B17
TQ	α,α,α-Trichlorotoluene (benzotrichloride)	*a*	20	2	A17, C38, 42
TR	Triethylene glycol	*f*	12	2	A45, B15, 36, 37, D35, 60, 61, 62, 63
TT	2,2,3-Trimethylbutane (triptane)	*a*	M	...	A5, 28, 33, B31, 34, 35, 39
U	Urea (m.p. 132.7°)	*g*	..	0	B9, 11
V	Valeraldehyde	*a*	M	...	A64
W	Water	*g*	6	0.104	A39, 41, 42, 46, 49, B54, 55, 56, D64, 67
X	3,5-Xylenol (m.p. 68°)	*a*	..	1	A37, 51, C35, 57
XY	3,4-Xylidine	*b*	33	9	C39

[a] Miscible with all liquid hydrocarbons. [b] Miscible with *n*-dodecane and lower liquid paraffins. [c] Miscible with *n*-heptane. [d] Miscible with methylcyclohexane and lower naphthenes. [e] Miscible with di-*sec*-butylbenzene and lower aromatics. [f] Miscible with benzene. [g] Not miscible with any hydrocarbon. [h] Propane is miscible with liquid hydrocarbons except those with three or more condensed aromatic rings. Ethane is miscible with liquid paraffins including *n*-octadecane, but not with the four heaviest oils mentioned. [i] M, complete miscibility; x, solubility of liquid carbon dioxide in substance in weight per cent. of the solution; y, solubility of the substance in liquid carbon dioxide in weight per cent. of the solution.

TABLE III

ADDITIONAL TERNARY SYSTEMS DESCRIBED BY THE GRAPHS
(Indicated there by plus signs)

Graph[a]	Left hand components[b]	Right hand components
A1	Stannic chloride	*n*-Heptane
A2	Ethyl oxalate	*n*-Heptane
A4	Diethylformamide	*n*-Heptane
A5	Ethylene diformate	*n*-Heptane, limonene, or triptane
A5	Nitromethane	*n*-Dodecane, *n*-heptane, or triptane
A12	Formic acid	*n*-Dodecane
A14	Ethylaniline or methylaniline	*n*-Heptane
A16	Chloral hydrate	Benzene
A17	Bromine	Carbon tetrachloride
A23	2,4-Dichlorophenol	*n*-Heptane
A28	*m*-Cresol, cyclohexanol, 2-methoxybiphenyl or olive oil	*n*-Heptane
A29	α-Chloronaphthalene	*n*-Heptane
A33	Oleic acid	*n*-Heptane or triptane
A35	Propylene glycol	Methanol
A37	Phenyl phthalate	Benzene
A40	Saligenin	Methanol
A41	Sulfuric acid	Ethyl alcohol
A42	Oleum or sulfuric acid	Acetic acid
A45	Phenylethanolamine	Benzene
A51	Diphenylamine	*n*-Heptane
A51	Naphthalene	Benzene or *n*-dodecane
A54	*o*-Chlorophenol or nitrobenzene	Decalin
A54	Sulfuryl chloride	*n*-Hexadecane
A55	*o*-Chlorophenol	*n*-Hexadecane
A60	BE, CZ, DD, EQ, ON, OX, PM, TF, or TN	Lubricating oil
A64	AA, AH, AS, BP, BU, CW, EE, EI, EJ, EM, IS, MD, PB, PT, or V	Lubricating oil
A64	Benzene or *n*-butane	Transformer oil
A65	AJ, BY, CJ, EK, EL, ES, HA, or MJ	Lubricating oil
A67	Limonene or methyl acetate	Lubricating oil
B1	AG[c], BD[c], BN, BS, BT, CB, CC, CE[c], DO, EA, EG, MH, PI, or PK[c]	Lubricating oil
B2	Methyl salicylate	Lubricating oil
B4	*n*-Butane or propane	Bright stock
B6	BH, CD, DF, DK, HE, K, or NS	Lubricating oil
B7	*p*-Dichlorobenzene	Lubricating oil
B17	Aniline	1-Decene or tri-*sec*-butylbenzene
B23	Diethylene glycol	Methyl salicylate
B23	Lactic acid	Thiophene
B25	Cinnamaldehyde	*n*-Heptane
B32	β-Chloroethanol	2,2-Dimethylpentane
B34	Furfuryl alcohol	*n*-Heptane or triptane
B34	*o*-Nitroanisole	*n*-Heptane
B35	Aniline	*n*-Heptane, triptane, or 2,2-dimethylpentane
B36	Triethylene glycol	Toluene
B39	*p*-Chlorophenol	*n*-Heptane or triptane
B40	Benzoic anhydride	*n*-Heptane
B47	Diethylene glycol	Gasoline or *n*-heptane
B51	Ethylene glycol	Ethyl acetate
B53	Formanilide	Cyclohexane
B60	1-Nitropropane	Lubricating oil
B61	Chlorex	*n*-Hexadecane
B62	Benzonitrile or nitrobenzene	Bright stock
B63	Chlorex or β-ethoxyethanol	Lubricating oil
B64	Nitroethane	Decalin
B67[c]	Ethyl oxalate, ethyl succinate, or salicylaldehyde	Lubricating oil
C3	Dimethylformamide	Decalin
C5	β-Methoxyethanol	*n*-Hexadecane
C6	Ethyl lactate	Lubricating oil
C8	Acetic anhydride	Decalin
C8	Acrylonitrile, dimethylformamide, furfural or triacetin	*n*-Hexadecane
C9	Methanol	Fuel oil
C9	Ethyl sulfate	*n*-Hexadecane
C9	Dimethylformamide	*n*-Octadecane
C11[c]	Methyl formate	Lubricating oil
C12	Acetonitrile or ethyl alcohol	Lubricating oil
C13[c]	Chloroacetone, β-chloroethyl acetate, ethyl maleate, ethyl sulfate, or nitroethane	Lubricating oil
C16[c]	Methanol	*n*-Hexadecane
C17[c]	Furfural or triacetin	Lubricating oil
C18[c]	Methyl sulfate or nitroethane	*n*-Hexadecane
C19[c]	Dimethylformamide	Lubricating oil or transformer oil
C20[c]	Acetonitrile or ethylene diformate	*n*-Hexadecane
C21[c]	Acetic acid, acetic anhydride, ethylene diformate, 2,5-hexanedione, or methyl sulfate	Lubricating oil
C23[c]	Methanol	50% *n*-Hexadecane 50% Fuel oil
C25	Ethane at 15°	Lubricating oil
C28	2,5-Dimethylpyrrole	*n*-Tetradecane
C33	2,5-Dimethylpyrrole	Decalin
C36	Diethylaniline	Decalin
C41	Benzyl alcohol	Tetralin
C42	α,α,α-Trichlorotoluene	*n*-Hexadecane
C43	Heptyl alcohol	α-Methylnaphthalene
C48	2,5-Dimethylpyrrole	Lubricating oil
C49	α-Chloronaphthalene	Lubricating oil
C54	*p*-Ethylphenol	*n*-Hexadecane
C57	Naphthalene	*n*-Hexadecane

TABLE III (*Continued*)

Graph[a]	Left hand components	Right hand components
C58	Ethylbenzylaniline	Decalin
C62	Benzyl benzoate, diethylaniline, or ethyl anthranilate	Lubricating oil
C66	Biphenyl, diphenylamine, or naphthalene	*n*-Tetradecane
D8	*o*-Toluidine	*n*-Hexadecane
D8	*m*-Toluidine	1-Octadecene
D12	Dipropylene glycol	Decalin
D18	*p*-Cresol	*n*-Hexadecane
D22	Castor oil	Lubricating oil
D23	Pinacol	Lubricating oil
D33	*o*-Chloroaniline	*n*-Hexadecane
D38	*o*-Anisidine, *m*-chloroaniline, or tetrahydrofurfuryl alcohol	Lubricating oil
D39	Benzoic anhydride	Lubricating oil
D41	β-Hydroxyethyl acetate	Decalin
D50	Diethylene glycol	α-Methylnaphthalene
D53	Aniline at 0°	Lubricating oil
D55	Chloropropionic acid	Lubricating oil
D57	Chloroacetic acid	Lubricating oil
D58	*o*-Nitroanisole	Lubricating oil
D60	Dipropylene glycol or phenylethanolamine	Lubricating oil
D61	Propylene glycol	*n*-Tetradecane

[a] The temperature observed for all graphs was 21 to 26° except those noted, as follows: C25, below 17.6° the minimum critical temperature of ethane and carbon dioxide mixtures; D53, at 0° to permit merging of band and bite. D57, at 37° to melt chloroacetic acid in contact with carbon dioxide. [b] Capital letters refer to first column of Table II. [c] These systems have isopycnics or twin density lines (17).

Nearly half (127) of the 261 substances tested were miscible with liquid carbon dioxide (M in column 4). In nine other cases of incomplete miscibility the carbon dioxide *poorer* phase contained over 50% of carbon dioxide. It will be noted from Table II that the solubility of carbon dioxide in another liquid is (with one exception) much greater than that of the other liquid in carbon dioxide, and that the ratio of these two solubilities is greatest for those liquids of low miscibility with carbon dioxide. The solubilities in and for water were taken from the work of Wiebe and Gaddy[12] and that of Stone,[13] respectively; and those for lubricating oil, naphthalene, iodine and glycerol in carbon dioxide from the work of Quinn and Jones.[14]

From Table II the miscibilities of many other solvents with carbon dioxide may be predicted. Homologs differ only slightly in miscibility. With increasing molecular weight, solubilities may increase at first and then steadily decrease (*e.g.*, aniline–toluidines–xylidine). Halogen atoms and carbonyl and ether groups also have slight effects (carbon tetrachloride, 2-octanone and *n*-butyl ether are all miscible with carbon dioxide); but hydroxyl, amino and nitro groups diminish solubility, especially if two or more are present. Complete mixing is prevented also by a bicyclic structure in derivatives (*e.g.*, methoxynaphthalene) as well as in hydrocarbons. These effects are similar to but not quite parallel with those involved in hydrocarbon miscibilities.[15]

Ternary Systems.—Mutual binary solubilities of two normally liquid components, usually a hydrocarbon and a non-hydrocarbon, were observed in graduated test-tubes if not already known. They are indicated approximately in the graphs by miscibility gaps on the base line. Then various charges of the two liquids were placed in the autoclave and carbon dioxide was added as before. With increasing amounts the composition of the system follows a straight line (isologous line or line with a constant binary ratio) toward the apex (carbon dioxide corner) of the triangular diagram from a point on the base line corresponding to the relative weights of liquid reagents charged. Whenever a new interface appeared (after agitation), or one disappeared, the weight of carbon dioxide added, when plotted as percentage on the isologous line gave a point on a binodal curve of the diagram.

Sometimes with increasing amounts of carbon dioxide two liquid phases became miscible; and with further additions of carbon dioxide another two layers appeared which did not mix on agitation. It is even possible for the second pair of layers to mix at compositions higher up on the same isologous line. The diagrams (*e.g.*, graph D38) clarify the reasons for this peculiar behavior.

After proceeding up the isologous line as far as was practicable (when the autoclave was full), the carbon dioxide was released, sometimes gradually so as to check the previous observations. If the other two reagents were sufficiently non-volatile so that no loss was feared, more of one of them was added and a new isologous line was studied. Otherwise, the whole system was discharged, and a new proportion of reagents was charged. Sometimes one or two isologous lines were sufficient to define the system adequately, provided they were chosen judiciously with respect to the expected diagram. In other cases a dozen of them might be required, depending on the complexity of the diagram.

Graphs.—The 464 systems studied are presented in 268 graphs numbered 1 to 67 on each of pages A to D. Carbon dioxide is assigned the top corner in each graph. The other components are indicated by code letters under the appropriate corners, referring to the first column of Table II. The left hand component or "solvent" is the more polar one, usually the non-hydrocarbon.

A considerable saving in number of graphs results from the close similarity in many of the simpler systems. Additional ternary systems illustrated by a single graph are listed in Table III. Indication that there is an alternate component for either position is by means of a plus sign after the code letters. Thus, graph A64 illustrates 18 systems with a binodal curve on the right side. One of these is acetic acid–aniline as indicated by the codes AD and A on the graph. Plus signs after

(12) R. Wiebe, *Chem. Revs.*, **29**, 475 (1941); R. Wiebe and V. L. Gaddy, *J. Am. Chem. Soc.*, **61**, 315 (1939); **62**, 815 (1940); **63**, 475 (1941).

(13) H. W. Stone, *Ind. Eng. Chem.*, **35**, 1285 (1943).

(14) E. L. Quinn, *ibid.*, **20**, 735 (1928); *J. Am. Chem. Soc.*, **50**, 677 (1928); E. L. Quinn and C. L. Jones, "Carbon Dioxide," Reinhold Publ. Corp., New York, N. Y., 1936, pp. 109–10.

(15) A. W. Francis, *Ind. Eng. Chem.*, **36**, 764, 1096 (1944).

these codes refer to Table III which lists the other 17 systems, namely, 15 solvents designated by code letters, each with lubricating oil, and also benzene or *n*-butane, each with transformer oil. The curve has an altitude of about 30% solvent, and the tie lines are nearly parallel to the side line, as indicated by the position of the plait point near the apex of the curve. This multiple representation by graphs results in compromises and minor inaccuracies in drawing. Binary solubilities with carbon dioxide should be taken from Table II in preference to scaling the graphs.

The tie lines shown as shading on the binodal areas were not observed; but their orientations were estimated from observed plait points and phase boundaries. They serve to clarify the differences in those areas.

The graphs are arranged in order of number, positions and altitudes of binodal curves. In graph A1 all components are miscible. It would represent an unlimited number of systems not tested because of no interest. However, a few ternary systems with three pairs of consolute components were tested in an unsuccessful search for a system with an island curve. In graphs A2 to A12 carbon dioxide is miscible with each of the other two components, which are not mutually miscible. They are miscible in the systems of graphs A13 to B11, but carbon dioxide is incompletely miscible with the solvent in graphs A13 to A53 and with the hydrocarbon (or other right hand component) in the others. In graphs B12 to B58 only the carbon dioxide and right hand component, and in graphs B59 to C25 only the carbon dioxide and solvent are miscible. In C26 to C66 the liquid components are miscible with each other, but neither with carbon dioxide. In the systems of graphs C67 to D67 no pair of components is miscible. In the first 18 of this group of graphs (21 systems) the three binodal curves are separate, and there are three plait points.

Solids are considered "miscible" for this purpose if it is probable that subcooling of melted solid would not give two-liquid phases in metastable equilibrium. However, solid phase equilibria are shown in the graphs. Some are isolated from the binodal curves (58 systems in which solid–liquid tie lines radiate from a base corner of the diagram, *e.g.*, A15, 56); some submerge probable binodal curves (no plait point, graphs A51, 52, 53, B11); and some intersect the curves or bands (39 systems, *e.g.*, A10). The last occurrence gives a triangular three phase area (a solid and two liquids) one corner of which is at a base corner of the graph. These are shown in black with white crosshatching. Graph B58 is a special case of this type in which some of the phase boundaries coincide with the side lines. It is virtually identical with that published[16] for silver nitrate–propane–propylene. In graphs D30, 32 two S-L_1-L_2 triangles appear, one across each binodal area.

Systems with three liquid phases (29 systems, graphs C10, 24, D48 to D67) are shown as usual with an internal triangle not quite touching any border line, though often close to some of them. These triangles are crosshatched. The last three graphs contain triangular areas of both types. Graph C10 is almost unique in having three plait points although one pair of components is miscible.

In 45 systems (especially those of graphs C13 to C23) a change in the amount of carbon dioxide present caused a reversal in the relative densities of the phases, so that the layers inverted. These isopycnics or twin density lines[17] are marked on the graphs with straight dashed lines though in some systems they should be slightly curved. An inversion is interesting to watch but has no theoretical significance. Quinn[14] considered it pertinent that the greatest solubility of a lubricating oil in carbon dioxide occurred at the temperature, 10°, at which the densities of the two liquid phases were equal (binary twin density line). This was probably coincidental. In two graphs (C22, 23) two twin density lines are shown.

The "dual solubility effects" of liquid carbon dioxide at different concentrations mentioned above are shown in 99 graphs with a binodal curve on the bottom side and other binodal curves on the left or right side or both, and also in 23 graphs (D18 to D40) with a binodal curve on the bottom side and a band across the other two sides. Thus in graph D39, *o*-nitrobiphenyl, a solid, and lubricating oil (of only moderate mutual miscibility) are mixed by adding about 30% carbon dioxide to the system. Yet carbon dioxide dissolves only about 2% of *o*-nitrobiphenyl and less than 1% of the oil. Neither is it very soluble in either of them nor much more so in their mixture.

The homogenizing action of carbon dioxide, evident in almost every graph, is common to many solvents. The precipitating action is recognized in at least seven patents.[18] In the fourth of these, for example, Lantz states "an increase in the quantity of the carbon dioxide actually reduces the amount of oil dissolved. . ."

Merging of Curves.—The existence of 97 systems with separate binodal curves and 118 systems with concave bands apparently resulting from coalescence of such curves affords an opportunity for testing the validity of conflicting speculations[19–21] as to the manner of merging.

Examples were sought but not found of two separate convex binodal curves approaching each other externally at points other than both plait points, or of a three phase area resulting from such a merger.[20,21] In the only graph suggestive of this postulate, that for formic acid–*n*-hexadecane (C24), the triangular area was shown to be present as in graph C10 before the band was formed by direct plait point merger of two small binodal curves.

(16) A. W. Francis, *J. Am. Chem. Soc.*, **73**, 3710 (1951).

(17) A. W. Francis, *Ind. Eng. Chem.*, **45**, 2789 (1953).

(18) U. S. Patents, 2,130,147; 2,165,503; 2,188,013; 2,188,051; 2,246,227; 2,315,131; 2,346,639.

(19) Reference 5, pp. 829–31; A. W. Francis in "Physical Chemistry of Hydrocarbons," A. Farkas, ed., Academic Press, Inc., New York, N. Y., 1950, pp. 251–4.

(20) J. E. Ricci, "The Phase Rule and Heterogeneous Equilibrium," D. Van Nostrand Co., New York, N. Y., 1951, pp. 215, 244.

(21) A. E. Hill in "Treatise on Physical Chemistry," H. S. Taylor, ed., D. Van Nostrand Co., New York, N. Y., 1931, pp. 574–575; R. E. Treybal, "Liquid Extraction," McGraw-Hill Book Co., Inc, New York, N. Y., 1951, p. 17; and several other textbooks.

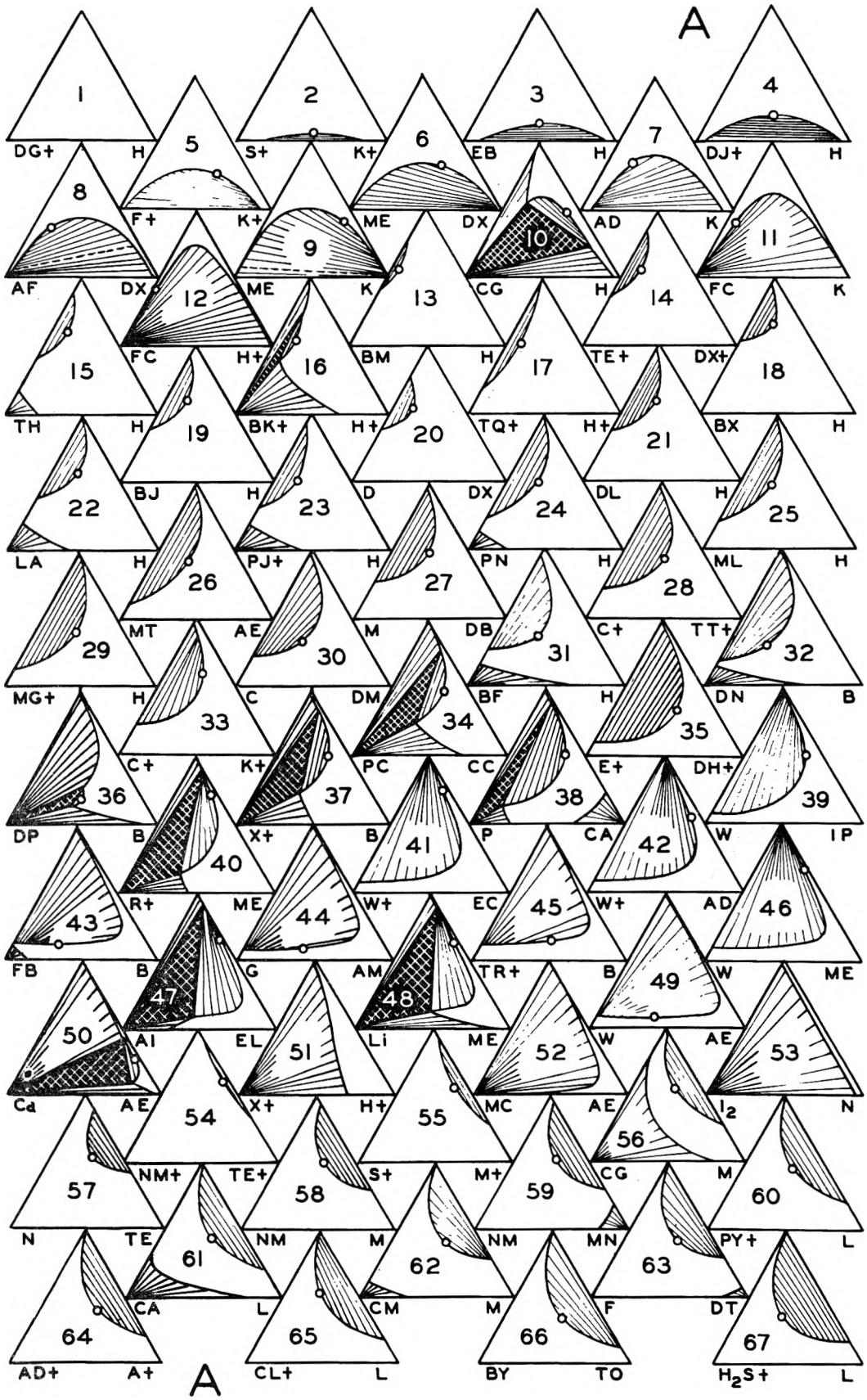

Components: Carbon dioxide is assigned the top corner in each graph. The other components are indicated by letters referring to the first column of Table II. Additional systems are indicated by plus signs after one or both sets of the code letters. These are listed in Table III.

Shading: White areas indicate homogeneous compositions. Oriented shading indicates two phases. It is solid-

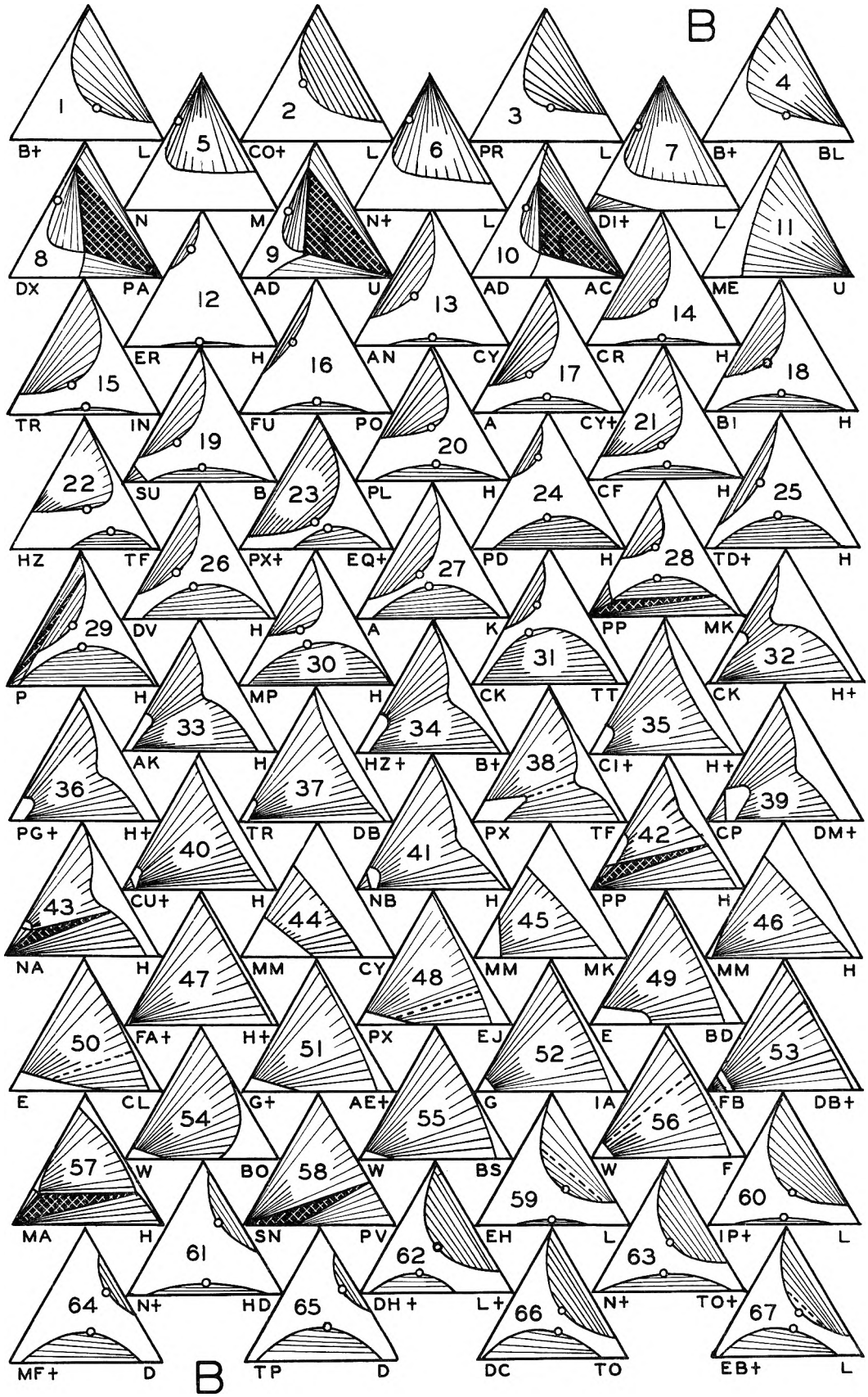

liquid if the lines radiate from a base corner of the graph. Otherwise it is a binodal or two liquid phase area. A cross-hatched triangle indicates three phases. Black on white shows three liquid phases. White on black (with a corner at a base corner of the graph) indicates a solid and two liquid phases. No solid phases other than the pure compound are shown on these graphs. A dashed line across a binodal area is an isopycnic or twin density line.

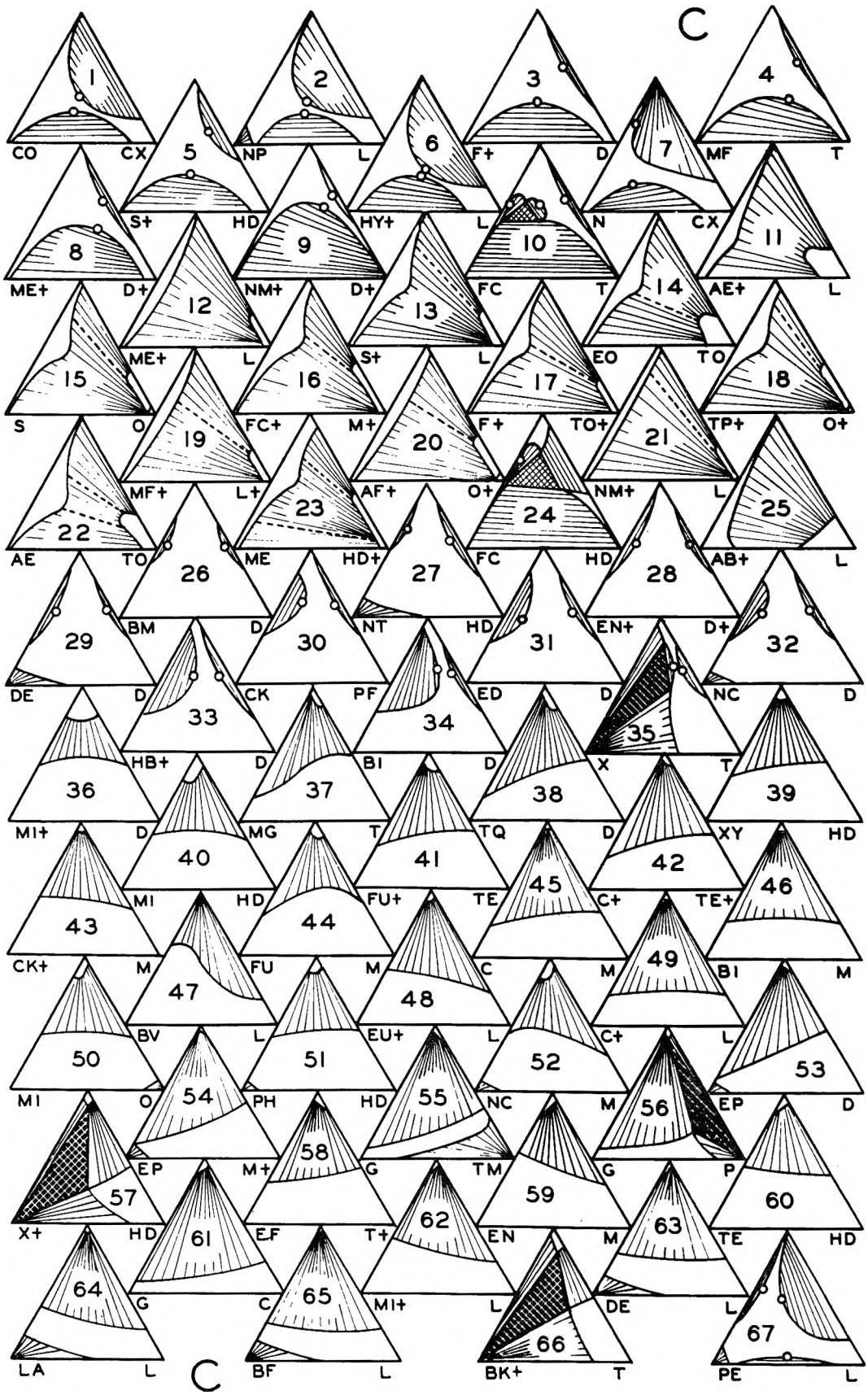

As in the systems reported previously,[3] *external contact of convex curves always occurs at both plait points.* Two separate curves do not necessarily meet at all. Thus in graph C7 the upper curve probably would contact the side line instead.

On the other hand, meeting of a band with a bite

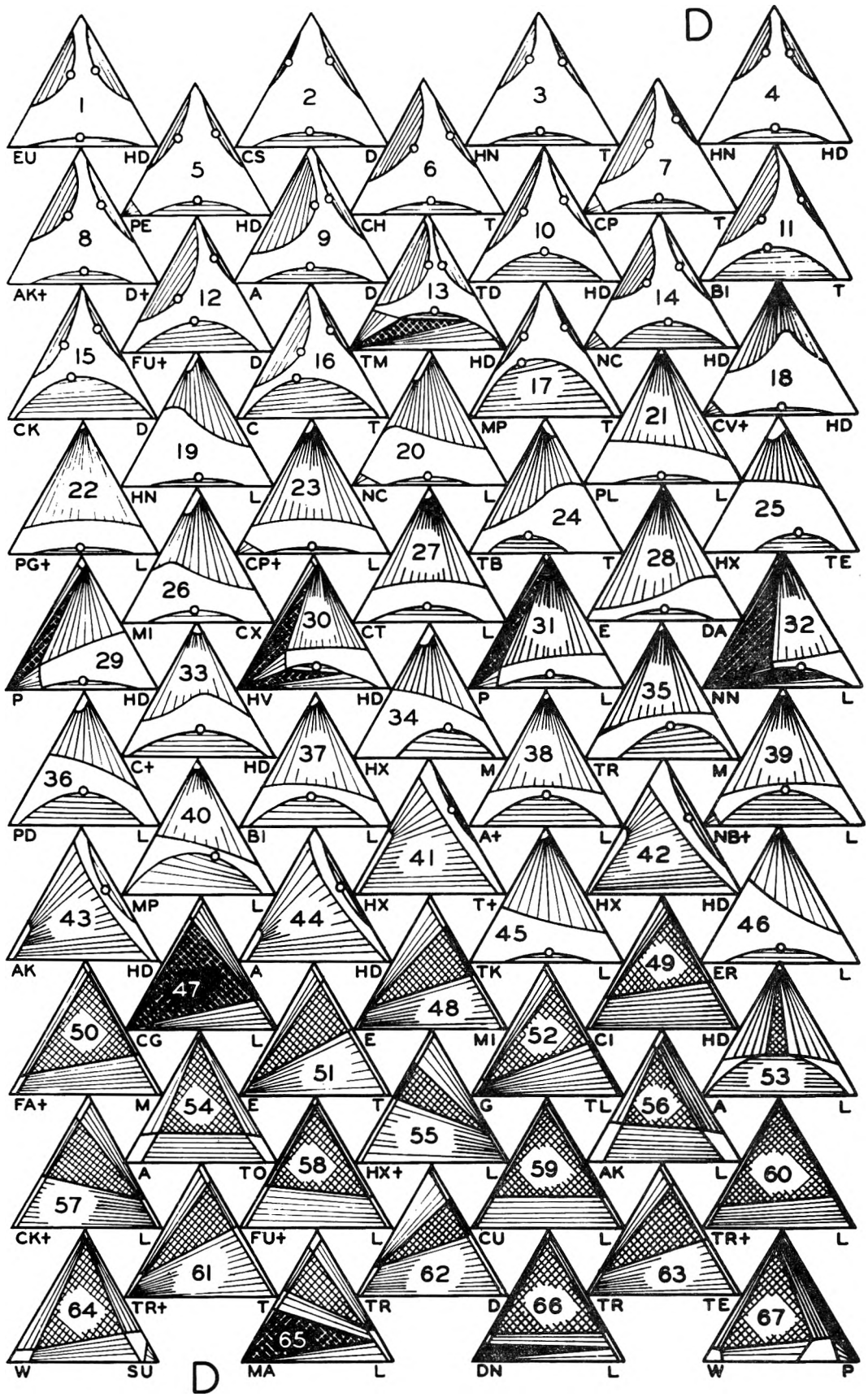

(free binodal curve) is possible although there is only one plait point. The system aniline–lubricating oil (graph D38) was cooled to about 0° (or diluted with a little hexadecane) to accomplish the merger as in graph D53. The result was a triangular three-liquid phase area, as predicted.

However, at the point of contact (which occurred at the plait point of the bite) the border of the band just before contact was distinctly concave. This is a theoretical requirement to satisfy Schreinemakers' rule[19,20] with respect to triangular areas representing three phases. That rule would prohibit the more usual illustration of merger of convex curves.[20,21]

The three-liquid phases in some of the carbon dioxide systems result from the above mechanism. Those of the others, including the formic acid systems mentioned above, and probably all of the published systems with three liquid phases[22] result from eruption of a second binodal curve from *within* another one at a point other than the latter's plait point. This is possible, and is the type cited by Hill[21] in support of his hypothetical diagram.

(22) Reference 5, pp 847, 977, 1009, 1015, 1029-31, 1035-6, 1070.

A STUDY OF THE EQUATION OF STATE FOR EDNA[1]

By Melvin A. Cook, Robert T. Keyes, G. Smoot Horsley and Aaron S. Filler

Explosives Research Group, University of Utah, Salt Lake City, Utah

Received June 1, 1954

Thermohydrodynamic calculations were made by the "inverse" method (measured detonation velocity–density equation included in the solution) for EDNA using three fundamentally different equations of state leading to widely different internal pressures ($(dE/dv)_T$). Two sets of measured velocity data were used with each equation of state. The results show that all the calculated thermodynamic quantities except temperature are less sensitive to the form of the equation of state than to errors in the determination of detonation velocity. Hence, temperature alone provides an adequate criterion of an objective evaluation of the equations of state when one approaches the problem solely from detonation theory. However, so far reliable detonation temperature measurements have not been possible, and this criterion cannot therefore be applied. A corollary of this conclusion is that any reasonable equation of state provides, through detonation theory and measured velocities, as reliable thermodynamic data as any other. Objective detonation equation of state studies must evidently await more accurate velocity–density measurements and the development of methods for measuring some detonation property with sufficient accuracy to allow one to evaluate the various forms of the equations of state unambiguously.

Numerous equations of state of various forms have been used in thermohydrodynamic calculations. In spite of wide differences in form and character of these equations of state the thermodynamic quantities computed, either by direct use of experimental detonation velocity *vs.* density data or by adjustment of parameters to give best agreement with observed velocities, have been in surprisingly close agreement, except for computed detonation temperatures. Temperature alone turns out to be strongly dependent upon the nature of the equation of state. This situation led one of us[2] to conclude that the detonation temperature is the only factor where a comparison between computed and observed values could be used to evaluate the accuracy of the equation of state. Unfortunately, even such a comparison with detonation temperatures is inadequate in view of the great limitations of temperature measurements. It was therefore considered advisable to make a thorough theoretical study of the influence of the form of the equation of state on the various thermodynamic quantities computed from the thermohydrodynamic theory and also to study theoretically the influence of experimental errors in velocity.

The explosive EDNA (Haleite)[3] was selected for this study since it appeared to be well suited both from the viewpoint of reliability of computed products of detonation and from measured velocities. In fact, two sets of velocities have been obtained showing good agreement at high densities but differing considerably in the velocity at low density and in the slope of the velocity-density curve. These were as follows[4]

$$D = 5650 + 3860(\rho_1 - 1.0) \quad (1a)$$

$$D = 5960 + 3275(\rho_1 - 1.0) \quad (1b)$$

(See Appendix I for definitions of symbols)

The general equation of state

$$pv = nRT\varphi \quad (2)$$

was adopted for this study. Specific forms of φ were selected such as to exaggerate differences in the equation of state, using the specific definition

$$\varphi = e^x \quad (3)$$

where

$$x = K(v)\frac{T^c}{v}$$

Three cases were treated using the following values of c

$$c = -0.25 \quad (3a)$$

$$c = 0 \quad (3b)$$

$$c = +0.1 \quad (3c)$$

Definition 3a leads to an equation of state of much the same form as that of Kistiakowsky–Wilson–Brinkley,[5] although K is here allowed to vary with density (experimental velocities being used to determine K) whereas in the KWB equation it is a constant. Also here $\varphi = e^x$, but in the KWB case $\varphi = 1 + xe^x$. One will, however, note that these two forms are not radically different. Definition 3b is equivalent to the $\alpha(v)$ approximation used by Cook[2] and in different form by Caldirola[6a] and Paterson.[6b] Definition 3c is probably completely

(1) This project was supported by Office of Naval Research (Contract Number N7-onr-45107, Project Number 357 239).

(2) M. A. Cook, *J. Chem. Phys.*, **15**, 518 (1947).

(3) Ethylenedinitramine $O_2NHNCH_2CH_2NHNO_2$.

(4) Measured at Bruceton, Pennsylvania (NDRC, Division 8).

(5) OSRD No. 69, 905, 1231, 1510, 1707, NDRC Division 8 Staff.

(6) (a) P. Caldirola, *J. Chem. Phys.*, **14**, 738 (1946); (b) S. Patterson, *Research*, **1**, 221 (1948).

erroneous since it leads to an internal pressure which apparently is inconsistent with detonation conditions.

Derivation of Equations and Methods of Solution. —The fundamental equations of the hydrodynamic theory are:

(Conservation laws)

$$D = v_1 \left(\frac{p_2 - p_1}{v_1 - v_2}\right)^{1/2} \tag{4a}$$

$$W = (v_1 - v_2) \left(\frac{p_2 - p_1}{v_1 - v_2}\right)^{1/2} \tag{4b}$$

$$E_2 - E_1 = {}^1/_2(p_2 + p_1)(v_1 - v_2) \tag{4c}$$

(C-J condition)

$$\frac{p_2 - p_1}{v_1 - v_2} = -\left(\frac{\mathrm{d}p_2}{\mathrm{d}v_2}\right)_S \tag{4d}$$

Using equation of state 2 (with $\varphi = e^x$, and $x = K(v)T^c v^{-1}$) one obtains the relations

$$D^2 = nRT_2e^x(1 + \theta)^2/\theta \tag{5}$$

where

$$\theta = \frac{V_2}{v_1 - v_2} = 1 + (cx + 1)\frac{nRe^x}{C_v}\left[(1 + cx) + \frac{T_2}{n}\left(\frac{\mathrm{d}n}{\mathrm{d}T_2}\right)_v\right] - x\left(\frac{v_2}{K}\frac{\mathrm{d}K}{\mathrm{d}v_2} - 1\right) - \frac{v_2}{n}\left(\frac{\mathrm{d}n}{\mathrm{d}v_2}\right)_S \tag{6}$$

$$C_v = C_v^* - nRc\left[e^x(1 + cx) - 1 - \int_{K(\infty)}^{K(v)}(1 + c + cx)xe^x\frac{\mathrm{d}K}{K}\right] \tag{7}$$

(T_2 = constant)

$$\bar{C}_v = \bar{C}_v^* - \frac{cnRT_2}{T_2 - T_1}(e^x - 1) + \frac{cnRT_2}{T_2 - T_1}\int_{K(\infty)}^{K(v)} xe^x\frac{\mathrm{d}K}{K} \tag{8}$$

(T_2 = constant)

$$W^2 = nRT_2\frac{e^x}{\theta} \tag{9}$$

$$T_2 = (Q + \bar{C}_vT_1)/(\bar{C}_v - nRe^x/2\theta) \tag{10}$$

(Derivations are given in Appendix II.)

The $K(v)$ function can be evaluated, in lieu of any fundamental basis for it, only by introducing the experimental $D(\rho_1)$ data given by equation 1. In solving these equations one needs also to know the composition of the products of detonation for the particular conditions corresponding to detonation.

In studies of detonation it is necessary to solve a relatively large number of equilibria simultaneously for various specific conditions. The problem is complicated and arduous since iteration of the numerous generally non-linear simultaneous equations is required. Moreover, in the completion of a single problem, *i.e.*, a single explosive calculation, solutions of the problem for many different sets of conditions are required. For instance, in the problem of obtaining reliable thermodynamic data from the hydrodynamic theory by the "inverse" method, one requires a minimum of about one hundred separate solutions each involving an iterative solution of about twenty-five simultaneous equations. Furthermore, in many specific applications, numerous additional solutions are required for the various specific conditions for which data are desired. After extensive study of this problem it is suggested that perhaps the most efficient method in many cases of providing the necessary product compositions is to compute for the explosive a series of composition *vs.* fugacity isotherms covering a broad enough range to include the real solution in order to have the necessary composition data available for use in the much easier thermohydrodynamic calculations. This more systematic method will here be illustrated for EDNA. Defining the equilibrium constants K_i in the manner suggested by Brown,[7] using the equation of state given by equations 2 and 3 following the recent methods,[8] one obtains

$$K_i = \frac{\prod_i A_i^{\nu_i}}{\prod_j B_j^{\nu_j}}\left(\frac{\varphi}{v}\right)^{\Delta\nu}\exp\Delta\nu\int_0^p(\varphi - 1)\,\mathrm{d}\ln p = \frac{\prod_i A_i^{\nu_i}}{\prod_j B_j^{\nu_j}}F^{\Delta\nu} \tag{11}$$

(T_2 = constant)

where

$$F = \frac{\varphi}{v}\exp\int_0^p(\varphi - 1)\,\mathrm{d}\ln p \tag{12}$$

(T_2 = constant)

Introducing equation 3, equation 12 becomes

$$F = \frac{e^x}{v}\exp\left\{e^x - 1 + x^2\left(\frac{1}{2\cdot 2!} + \frac{x}{3\cdot 3!} + \frac{x^2}{4\cdot 4!}\cdots\right) - \int_{K(\infty)}^{K(v)}(e^x - 1)\frac{\mathrm{d}K}{K} + \int_{n(\infty)}^{n(v)}(e^x - 1)\frac{\mathrm{d}n}{n}\right\} \tag{12a}$$

(T_2 = constant)

Figures 1 to 5 give the various isotherms needed to carry out the thermohydrodynamic solution by the simultaneous solutions of equations 5 to 12. Incidentally, one will note from Fig. 1 that the equilibrium $CO + 2H_2 \rightleftarrows CH_3OH$ not previously considered was found to be important at large F. This will be discussed in a future article where the necessary heat and statistical mechanical data to justify the use of this and other previously ignored possible products of detonation and their influence in determining over-all composition of detonation products will be discussed.

In the first approximation, one may neglect $\mathrm{d}K/\mathrm{d}v_2$ and the integrals in equations 7, 8 and 12a, and ignore the variation of n with F shown in Fig. 2. It is convenient to solve the equations for various values of x (or φ) noting that the term in the exponential of equation 12a is then completely determined (see Table I). The next approximation can now make use of these first approximation plots of $K(v)$ *vs.* v_2 and $n(v)$ *vs.* v_2 allowing one to determine as a next approximation the integrals and $\mathrm{d}K/\mathrm{d}v_2$ neglected in the first approximation. This process is then repeated as often as necessary for complete stabilization of the approximation variables. The solution in which one takes into account the factor $(\mathrm{d}n/\mathrm{d}T_2)_v$ in θ is actually non-tractable. However, this is evidently not serious since one can show that the term involving this

(7) F. K. Brown, Bureau of Mines Technical Paper No. 632.

(8) M. A. Cook, *J. Chem. Phys.*, **16**, 1081 (1948).

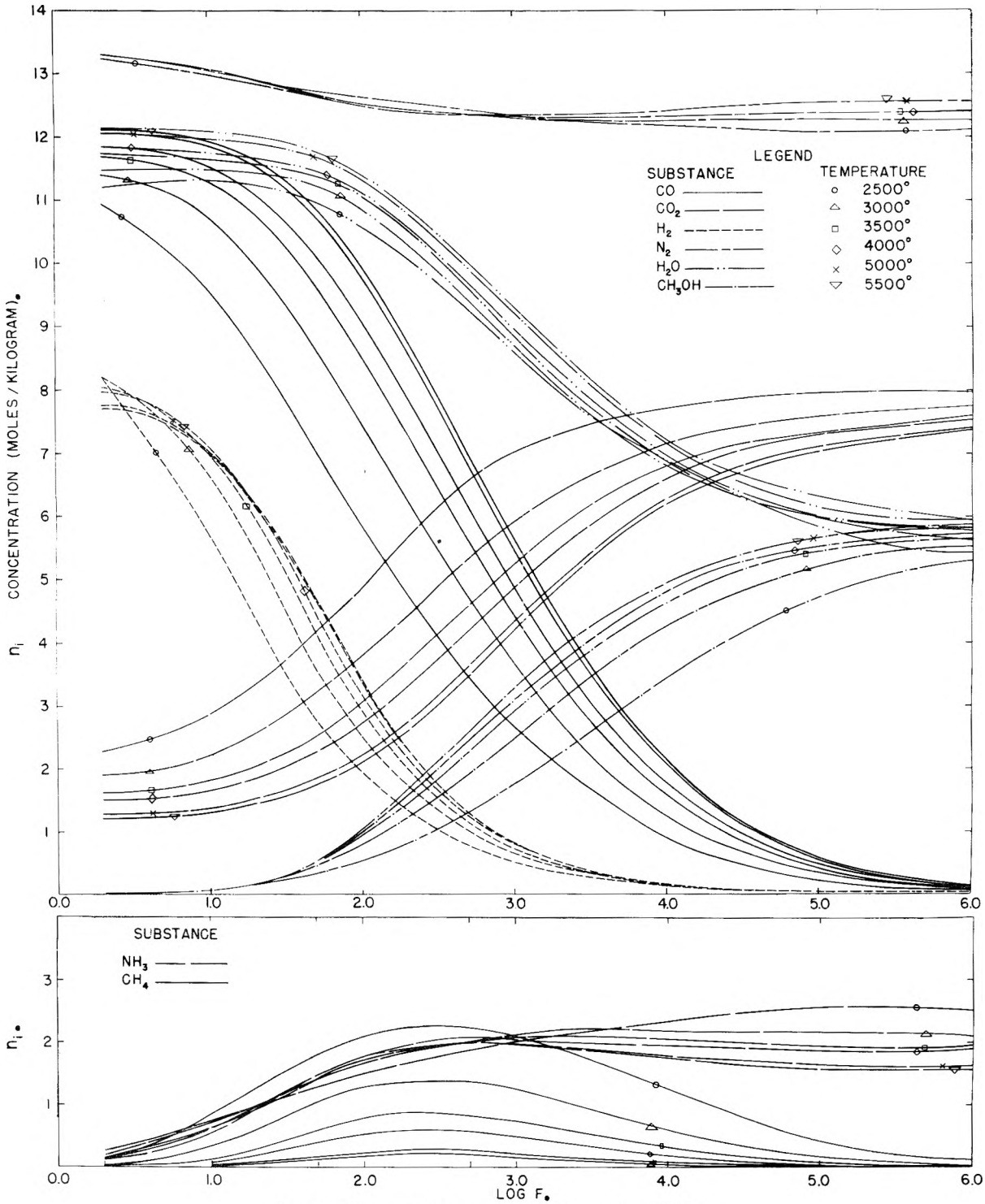

Fig. 1.—Concentration *versus* F isotherms for EDNA.

factor, at least in the case of EDNA, is negligible, *e.g.*, at $F = 10^4$ and 3500°K., $T_2/n\ (\mathrm{d}n/\mathrm{d}T_2)_v$ is about 0.05 which is its maximum value. If $(\mathrm{d}n/\mathrm{d}T_2)_v$ were not negligible, one could not of course drop the subscript S in the factor $(\mathrm{d}n/\mathrm{d}v_2)_S$. In this study, however, $(\mathrm{d}n/\mathrm{d}T_2)_v$ was taken as zero, and $\mathrm{d}n/\mathrm{d}v_2$ evaluated from successive plots of n *vs.* v_2. In one set of calculations $(\mathrm{d}n/\mathrm{d}v_2)_S$ was neglected as has been done in all previous theoretical treatments, *i.e.*, in all previous work n has (tacitly) been taken to be constant. The influence of treating n as a constant as compared with the assumption $n = n(v)$ is illustrated in the calculated results of this article.

The integrals in equations 7, 8 and 12a should be evaluated at constant temperature. Actually they were computed at the calculated detonation temperatures. The error so introduced is small for the equation of state determined by (3a) since then the detonation temperature is almost con-

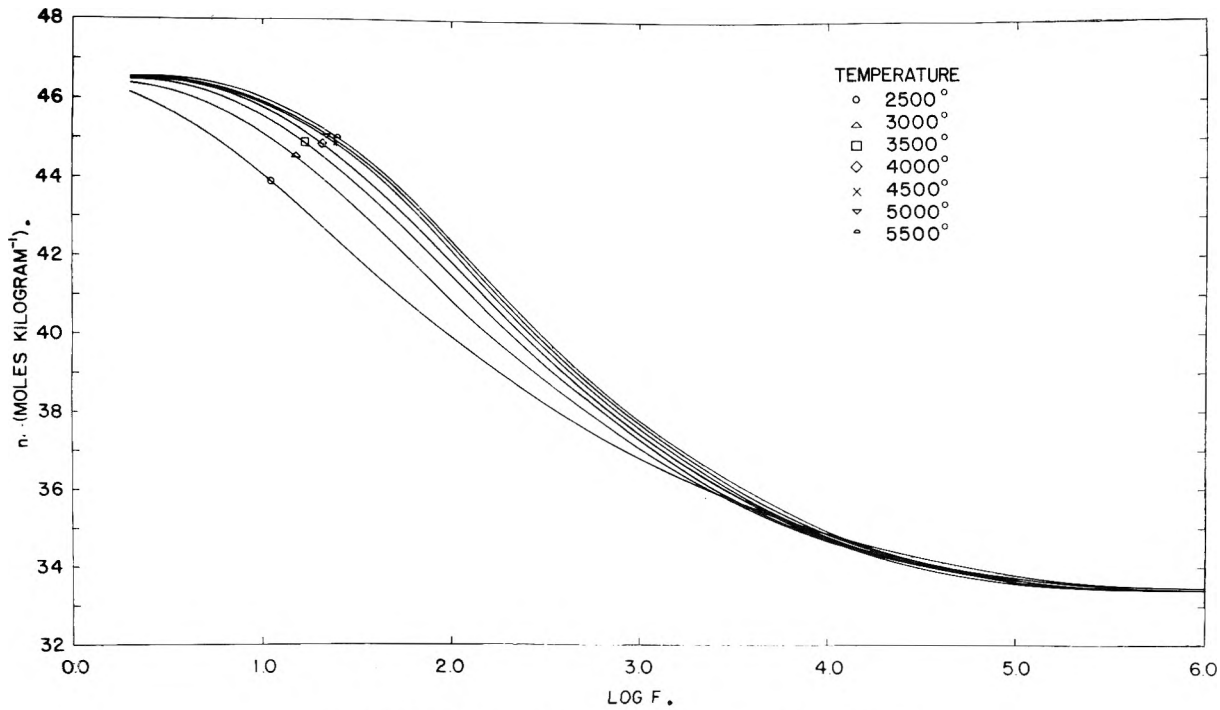

Fig. 2.—Total moles of gas per kilogram *versus* F isotherms.

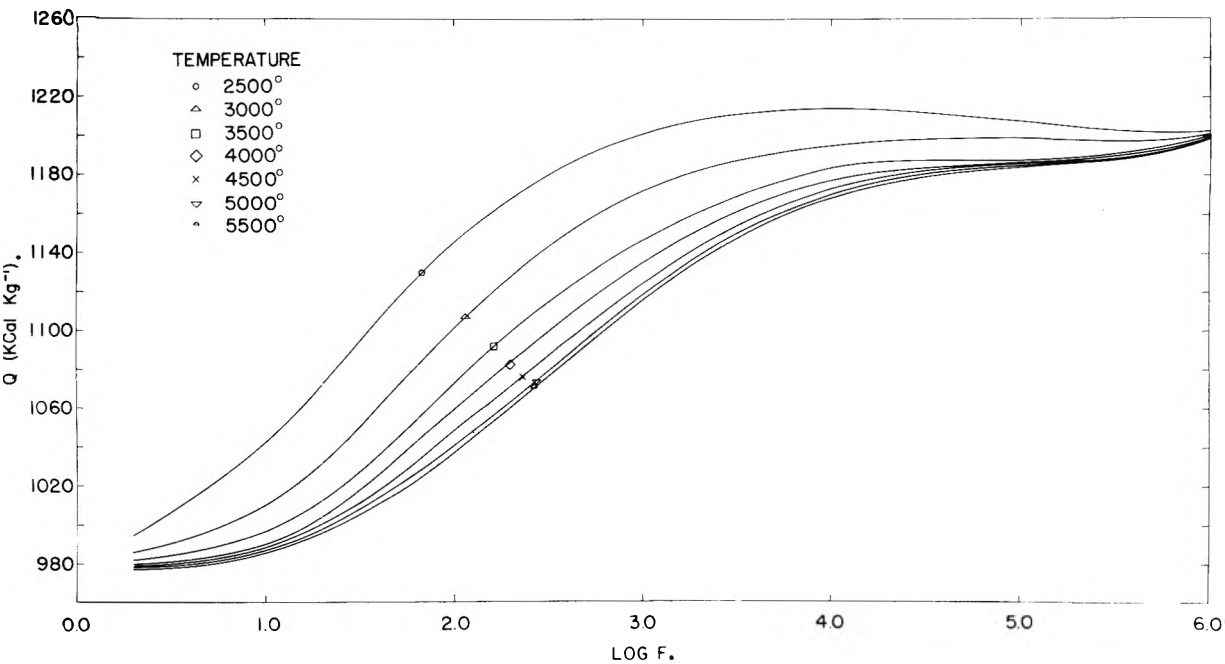

Fig. 3.—Heat of explosion *versus* F isotherms.

stant. In the case of the equation of state determined by (3b), since the integrals in (7) and (8) are multiplied by c, which is zero, the only error is in (12a). In the case of the equation of state determined by (3c) there will be error in all three equations 7, 8 and 12a. One of the advantages of the type of equation of state given by equation 3 is that the major parts of the equations 7, 8 and 12a are given in analytical form. The analytical parts are more important than the parts given by the integral, and the effects of errors in the integrals are thus reduced.

Results of Calculations

Calculations were first carried through with the three equations of state defined by equations 2 and 3 for the velocity data given by equation 1a. In these calculations the $n = n(v)$ approximation was employed. To show the influence of this more refined treatment, calculations were also carried through for equation of state (3b), $pv = nRTe^{K(v)/v}$, treating n as a constant. Then to show the influence of measured velocities on these calculations, results were repeated with two of the equations of state (x defined by 3a and 3b) and the set of

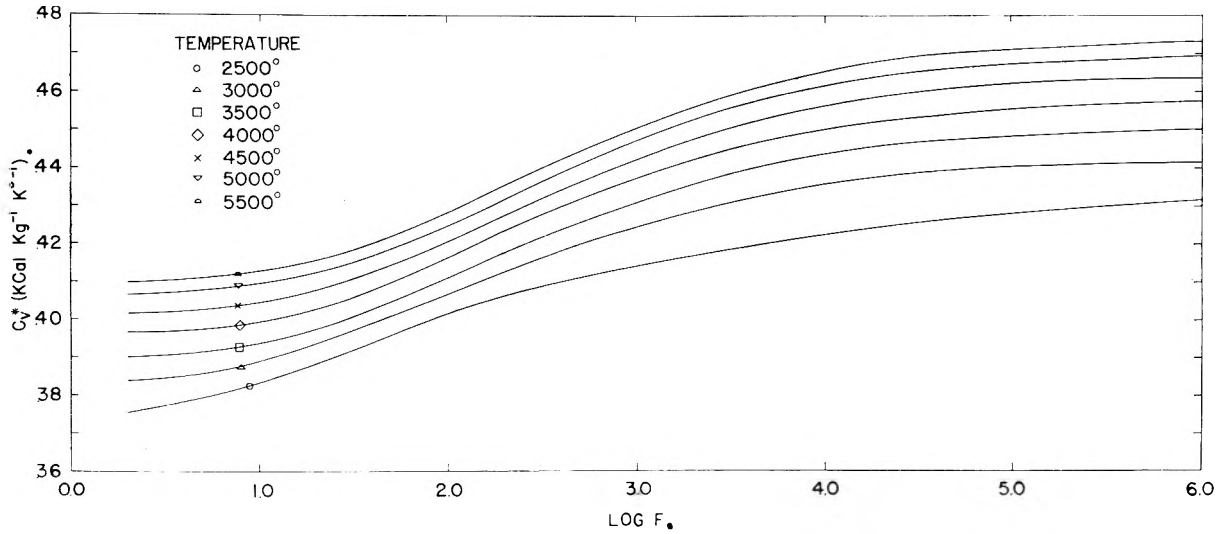

Fig. 4.—Constant volume heat capacity *versus* F isotherms.

TABLE I

TABLE OF $e^x - 1 + \sum_{n=1}^{\infty} \frac{x^n}{n \cdot n!} = x + J - Y$

In equation (12a) and (viiic) $\log_{10} F$ is conveniently calculated using the entries in the second column

$$\log_{10} F = M(x + J - Y) + MY - \log_{10} v_2$$

where

$$M = \log_{10} e = 0.4342945$$

and

$$Y = -\int_{K(\infty)}^{K(v)} (e^x - 1)\frac{dK}{K} + \int_{n(\infty)}^{n(v)} (e^x - 1)\frac{dn}{n}$$

x	$M(x + J - Y)$	x	$M(x + J - Y)$
0.05	0.04426	1.55	2.67003
.10	.09022	1.60	2.82775
.15	.13796	1.65	2.99254
.20	.18756	1.70	3.16474
.25	.23911	1.75	3.34469
.30	.29269	1.80	3.53277
.35	.34841	1.85	3.72939
.40	.40635	1.90	3.93494
.45	.46663	1.95	4.14987
.50	.52935	2.00	4.37462
.55	.59462	2.05	4.60967
.60	.66256	2.10	4.85552
.65	.73330	2.15	5.11270
.70	.80697	2.20	5.38175
.75	.88370	2.25	5.66327
.80	.96364	2.30	5.95784
.85	1.04694	2.35	6.26611
.90	1.13375	2.40	6.58875
.95	1.22425	2.45	6.92645
1.00	1.31860	2.50	7.27998
1.05	1.41699	2.55	7.65006
1.10	1.51961	2.60	8.03754
1.15	1.62665	2.65	8.44326
1.20	1.73834	2.70	8.86813
1.25	1.85489	2.75	9.31306
1.30	1.97652	2.80	9.77906
1.35	2.10349	2.85	10.26715
1.40	2.23606	2.90	10.77843
1.45	2.37448	2.95	11.31403
1.50	2.51904	3.00	11.87515

velocity data given by equation 1b. The two sets of velocities (1a) and (1b) are in good agreement at high densities, but differ considerably at low densities. It is possible to obtain super-velocities at low densities in explosives of very high chemical reaction rate and coarse granulation; that is, the detonation wave can conceivably propagate independently in the individual grains such that the effective density is not the average over-all density, but somewhere between this density and the individual grain density. By this means velocities 200 to 300 m./sec. higher than normal were observed by one of us in unpublished studies of loose-packed RDX. Perhaps because of effects of this sort as well as difficulties in density control it has not been possible to reproduce velocities at low density with much better accuracy than is indicated by the differences between sets (1a) and (1b). It therefore seemed desirable in this study to determine the relative importance of the form of the equation of state on one hand and differences of velocity in the range of such experimental error on the other.

Discussion of Results

The functions p_2, T_2 and the CO/CO_2 ratio are plotted against the explosive density in Figs. 7–9, inclusive, for each of the sets calculated in this study. Figure 6 reproduces K *vs.* v_2 plots for the various sets. These seem to represent the most significant differences of all quantities determined. (Detailed data on the calculations are available upon request.) The results of these studies show that the equation of state actually influences all the calculated thermodynamic quantities in addition to temperature appreciably, the influence on temperature being, however, greatest. For instance, definition (3a) for x leads to 15–20% higher pressures than definition (3c) and 10–15% higher pressures than definition (3b) in the range of operating densities. However, except for temperature, the form of the equation of state is seen to have less effect than changing from the one set of velocity data (1a) to the other (1b). For example, using one particular equation of state but

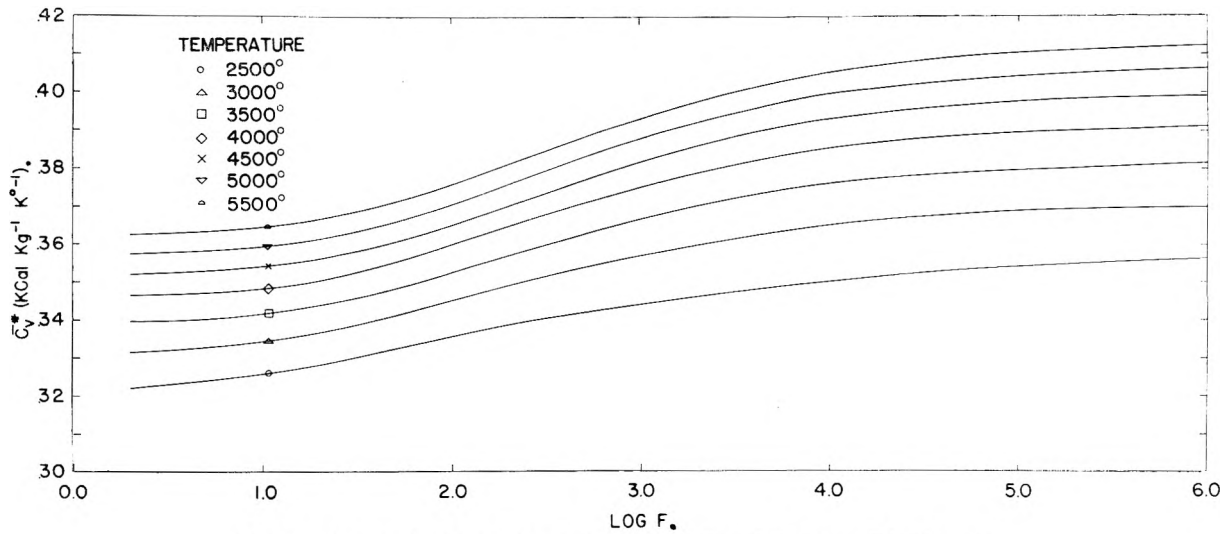

Fig. 5.—Average heat capacity (between 300°K. and T) *versus* F isotherms.

different velocities one calculates pressures differing by as much as 30% (at the density of maximum difference). The calculated temperature is enough more sensitive to the form of the equation of state than to experimental errors in velocity that it could readily be used to ascertain the correct equation of state if it could be measured. Unfortunately, this has not yet been possible as far as the detonation temperature T_2 is concerned.

From the results of this study, it may be concluded that fundamental theoretical–experimental evaluations of the equation of state applicable in detonation must await (1) reliable and accurate measurements of temperature, and/or (2) the developments of techniques which will allow one to determine detonation velocity *vs.* density dependent parameters not only at high densities, but also at low densities with an experimental error of 0.5% or less, together with experimental techniques for the measurement of pressure, composition, density, and/or particle velocity with suitable precision. For instance, if it were possible to measure detonation pressures within 2% and velocities within 0.5%, one could distinguish satisfactorily between the three equations used here.

Available techniques for velocity determinations are already adequate, the limitation being wholly in obtaining reproducible densities at low density,

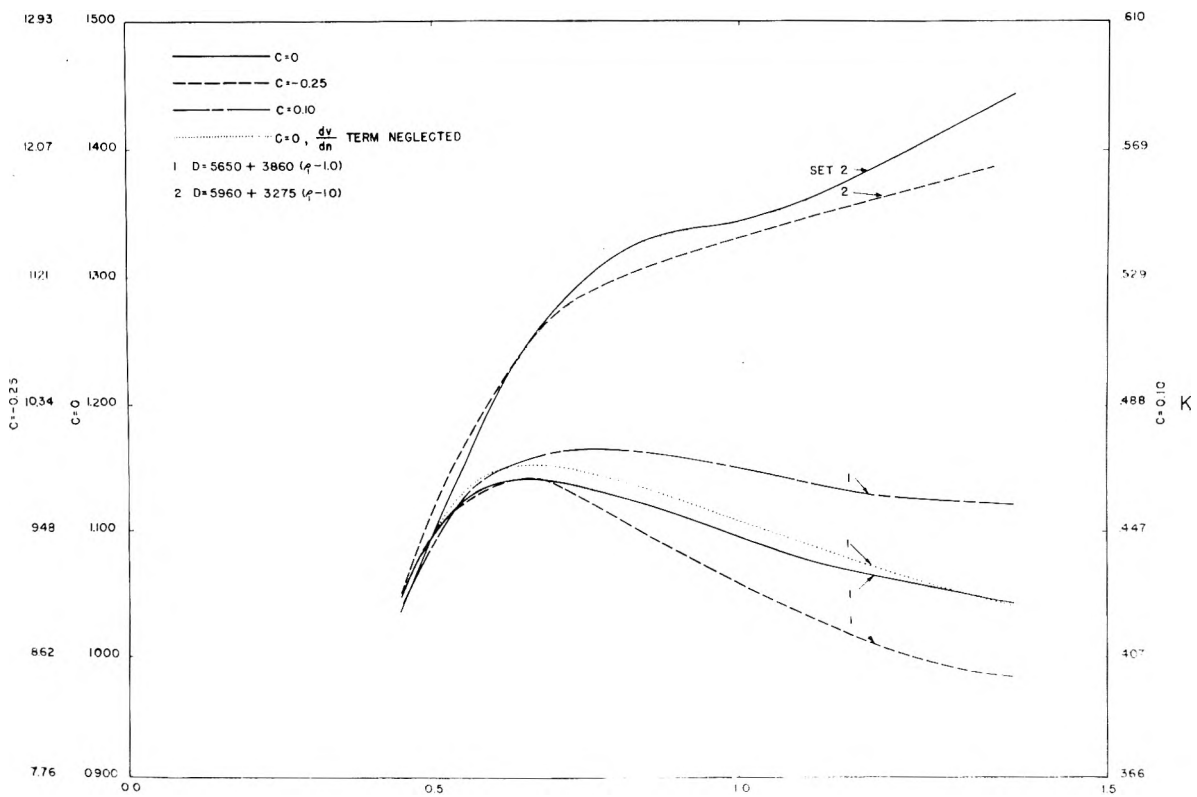

Fig. 6.—The K(v) curve for different equations of state and two sets of $D(\rho_1)$ data.

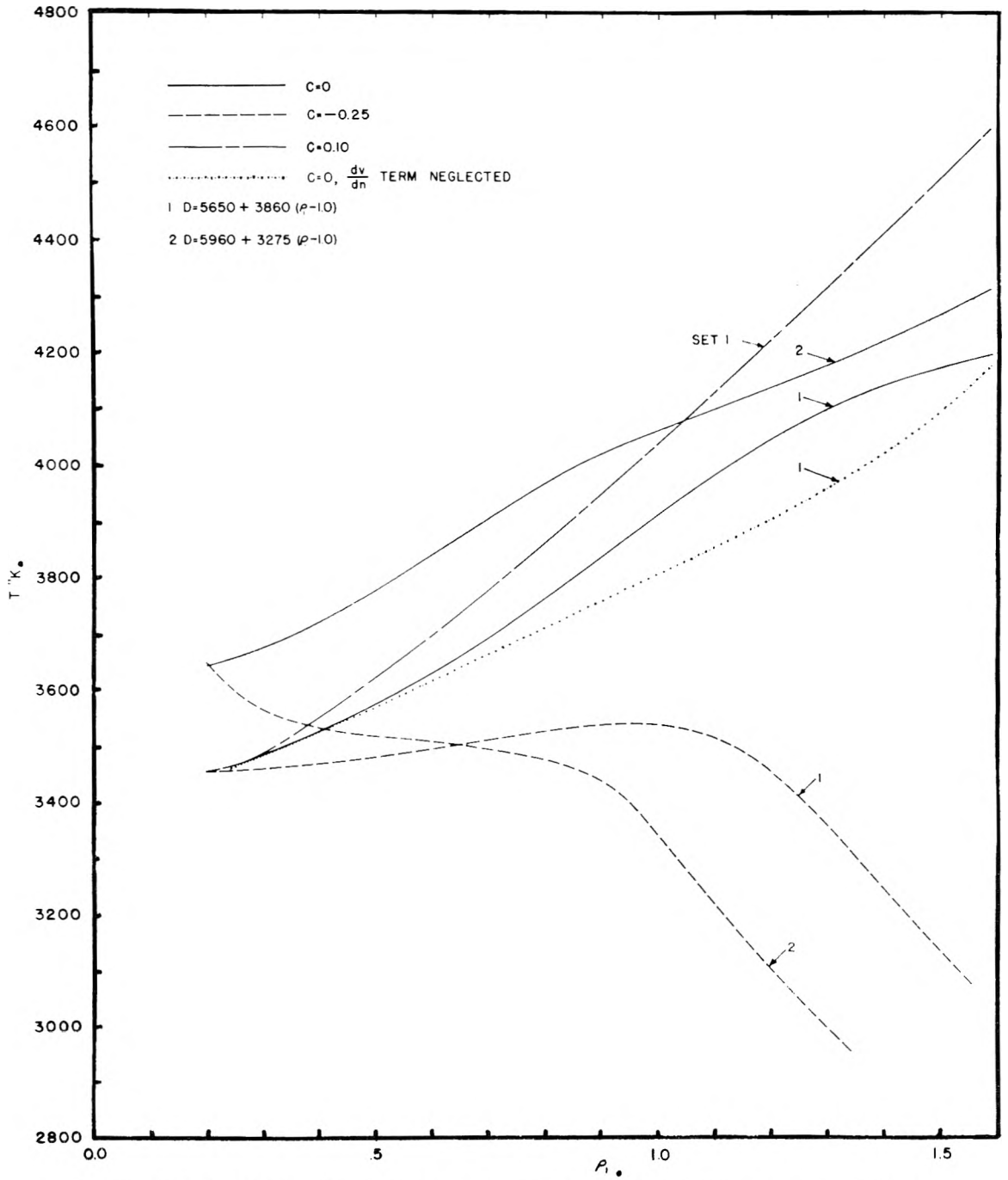

Fig. 7.—Variation of detonation temperature with explosive density for different equations of state.

and in regulating particle size such as to avoid the influence of the heterogeneous distributions of density within the charge. So far no experimental methods are available for measurement of any of the thermohydrodynamic quantities or composition factors with accuracy sufficient to allow one to distinguish between the various equations of state even if velocities and densities could be measured with sufficient accuracy. However, this task does not appear hopeless. For instance, one might develop an X-ray technique capable of measuring densities in the original explosive (ρ_1) and at the C–J plane (ρ_2), or the ratio ρ_1/ρ_2, with sufficient accuracy to accomplish this purpose. This would require velocity measurements of greater accuracy than $^1/_2\%$, and ρ_1/ρ_2 ratios within about 1%. To be sure such precision measurements are difficult in explosives technology.

Another conclusion of the present study is that any convenient equation of state is suitable for calculating thermodynamic and composition data (except temperature) in detonation within the limits of objective study with present techniques. Hence one should adopt for such purposes the most convenient (yet reasonable) equation of state available. Therefore, even if no other arguments were available these considerations justify completely the use of the most tractable but, of course,

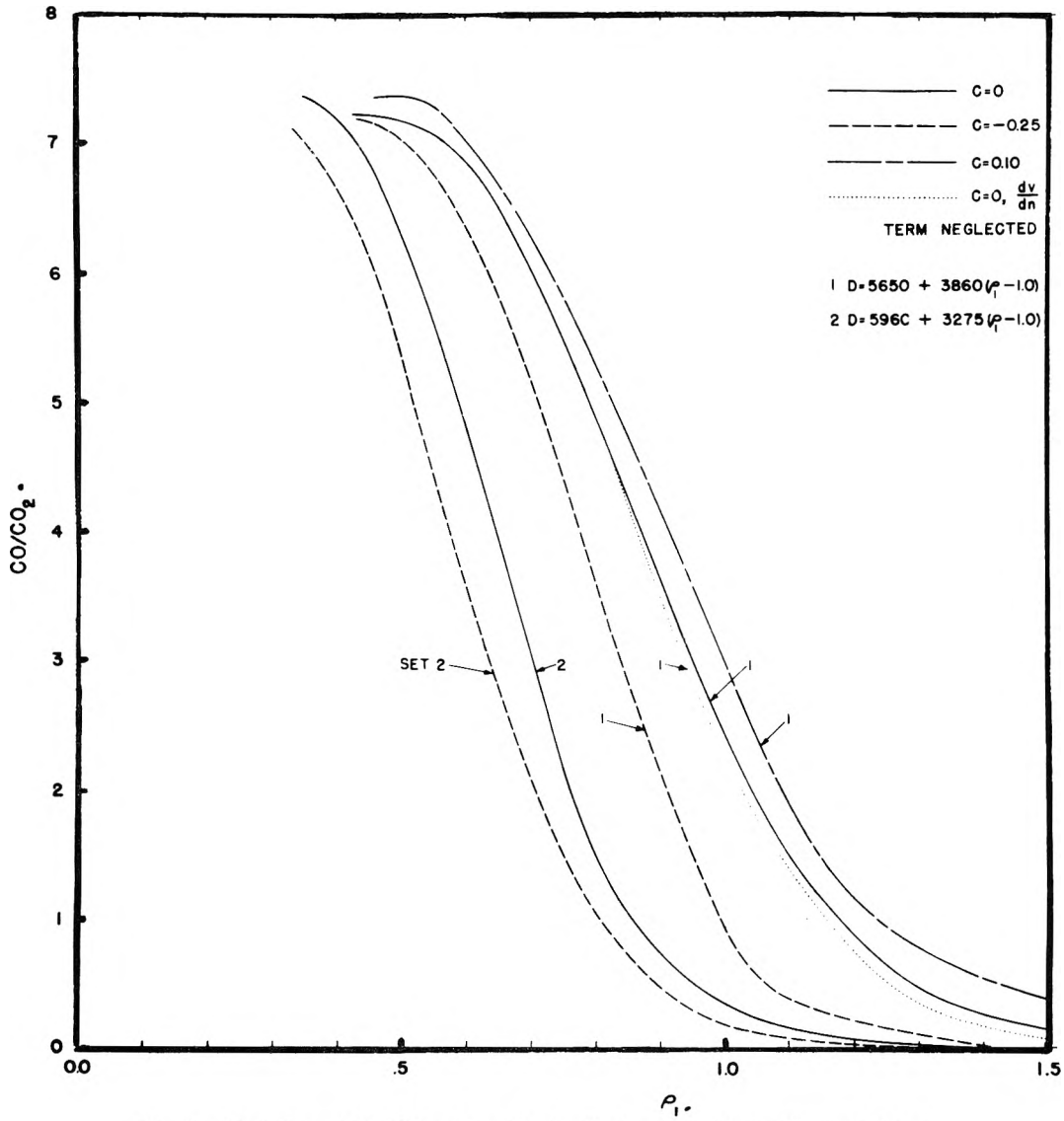

Fig. 8.—Variation of CO/CO_2 ratio with density for different equations of state.

reasonable equation of state available, *e.g.*, $pv = nRT + \alpha(v)p$, or the equivalent equation $pv = nRTe^{K(v)/v}$. This is an important consideration in any fundamental study of explosives because one frequently needs to know the thermodynamic quantities under various specific conditions.

Finally, it is worthy of note that a successful study of reaction rates of explosives at low and high densities has the potentiality of providing, as a by-product, a solution to the equation of state through absolute reaction rate theory. Thus, one will note from Fig. 7 that, whereas at very low densities all equations of state lead to the same detonation temperature, at high densities the temperature is very sensitive to the form of the equation of state. Reaction rate theory would provide the temperature coefficients of rates if temperatures were known. Conversely, if rates were known, one might compute temperatures by the inverse process. The reaction rate studies carried out at this Laboratory have indeed already provided crucial evidence favoring $c = 0$ in the equation 3. This however, is an extensive subject requiring detailed study and will not be discussed in this article.

Appendix I

Definitions of Symbols and Units.—

p	=	pressure
v	=	specific volume (l./kg.) of explosive
n	=	(moles/kg.) of explosive
R	=	gas constant
T	=	temperature, °K.
ρ	=	density, g./cc.
f	=	Lewis fugacity
E	=	internal energy
C_v	=	actual heat capacity, kcal./kg. °K.
C_v^*	=	ideal heat capacity, kcal./kg. °K.
$\bar{C}_v$	=	av. actual heat capacity (kcal./kg. °K.) from 300°K. to T
$\bar{C}_v^*$	=	av. ideal heat capacity (kcal./kg. °K.) from 300°K. to T
Q	=	chemical energy released in detonation, kcal./kg.
D	=	detonation velocity, m./sec.
W	=	particle velocity, m./sec.
F	=	defined in equation 12
φ	=	defined in equation 3
x	=	defined in equation 3
$K(v)$	=	defined in equation 3
θ	=	defined in equation 6
c	=	defined in equations 3a, 3b, 3c

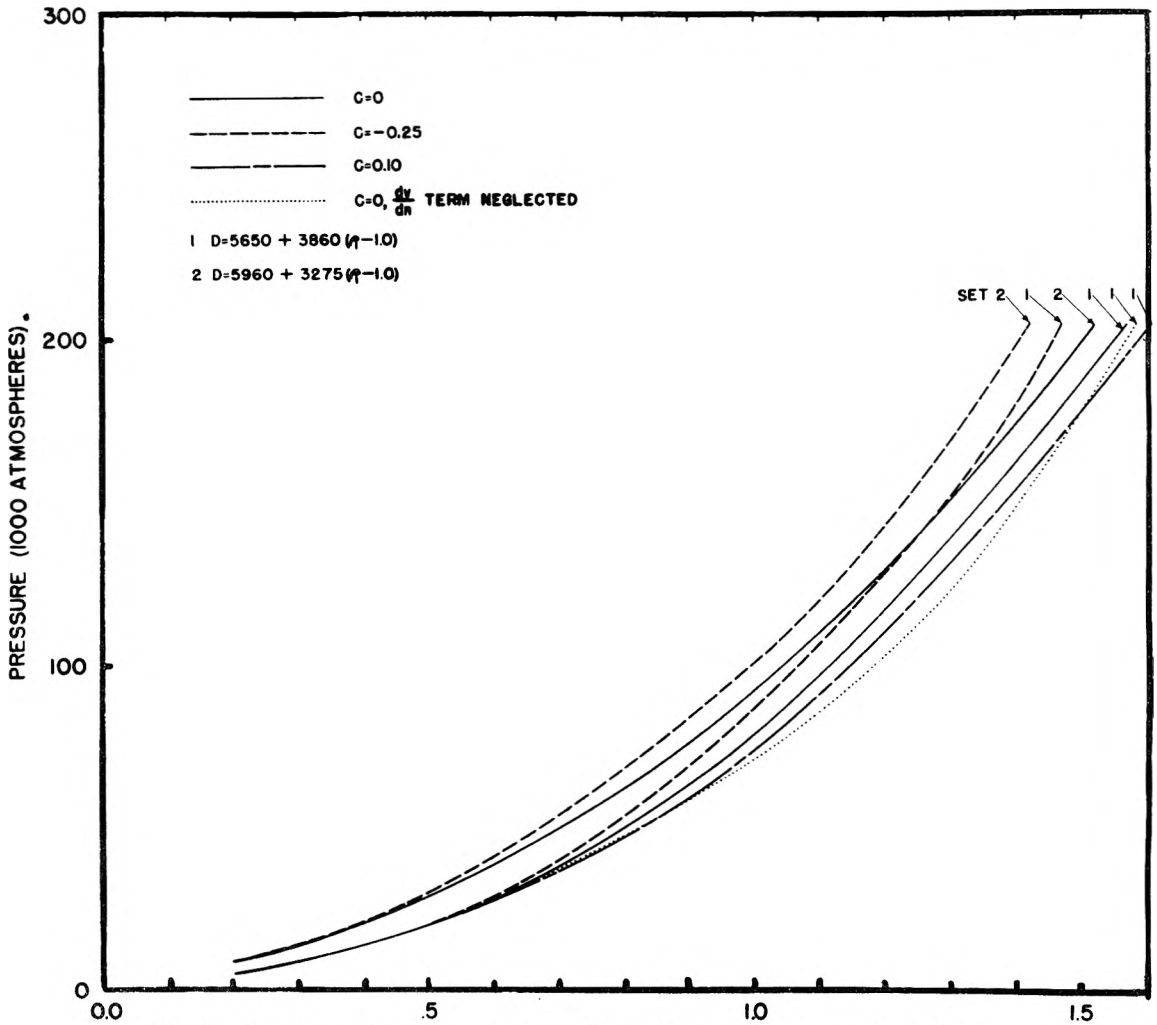

Fig. 9.—Variation of detonation pressure with density for different equations of state.

The symbol (CO), etc., indicates the concentration of CO in moles/kg. of detonated explosive.

Note: A subscript 1 on any of the above symbols refers to initial conditions in the undetonated explosive, and a subscript 2 refers to detonation conditions.

Appendix II

Derivation of Equations.—From the hydrodynamic theory using the conservation laws one has

$$D^2 = v_1^2 \frac{p_2 - p_1}{v_1 - v_2} \qquad \text{(ia)}$$

$$E_2 - E_1 = {}^1/_2(p_2 + p_1)(v_1 - v_2) \qquad \text{(ib)}$$

$$W^2 = (v_1 - v_2)^2 \frac{p_2 - p_1}{v_1 - v_2} \qquad \text{(ic)}$$

and the C–J condition

$$\frac{p_2 - p_1}{v_1 - v_2} = -\left(\frac{dp_2}{dv_2}\right)_S \qquad \text{(id)}$$

Using the definition $\theta = v_2/(v_1 - v_2)$ and the fact that $p_2 >> p_1$ in condensed explosives equation (ia) becomes

$$D^2 = \frac{p_2}{v_2} v_1^2 \theta \qquad \text{(iia)}$$

Introducing the equation of state $pv = nRT\varphi(T,v)$; $\varphi = e^x$; $x = K(v)T^c/v$ (where $n = n(v,T)$ and c = constant) and realizing that $v_1/v_2 = (1 + \theta)/\theta$ one obtains from (iia)

$$D^2 = nRT_2 e^x \frac{(1 + \theta)^2}{\theta} \qquad \text{(iib)}$$

(This is equation 5 of the article.)

Using equation (ia) and the C–J condition (id) one has

$$-D^2 = v_1^2 \left(\frac{dp_2}{dv_2}\right)_S \qquad \text{(iic)}$$

Comparing this with (iia) one gets the result

$$\theta = -\frac{v_2}{p_2}\left(\frac{dp_2}{dv_2}\right)_S \qquad \text{(iiia)}$$

Differentiating the equation of state holding the entropy constant one obtains

$$p_2 + v_2\left(\frac{dp_2}{dv_2}\right)_S = nRT_2\left(\frac{d\varphi}{dv_2}\right)_S + nR\varphi\left(\frac{dT_2}{dv_2}\right)_S + RT_2\varphi\left(\frac{dn}{dv_2}\right)_S$$

Hence

$$\theta = \frac{-v_2}{p_2}\left(\frac{dp_2}{dv_2}\right)_S = 1 - \left[\frac{v_2}{\varphi}\left(\frac{d\varphi}{dv_2}\right)_S + \frac{v_2}{T_2}\left(\frac{dT_2}{dv_2}\right)_S + \frac{v_2}{n}\left(\frac{dn}{dv_2}\right)_S\right] \qquad \text{(iiib)}$$

The term $v_2/\varphi(d\varphi/dv_2)_S$ can be evaluated from the

equation of state and the definitions of φ and x as

$$\left(\frac{d\varphi}{dv_2}\right)_S = e^x\left(\frac{dx}{dv_2}\right)_S = e^x\left[\frac{T_2^c}{v_2}\left(\frac{dK}{dv_2}\right)_S - \frac{K}{v_2^2}T_2^c + \frac{cKT_2^{c-1}}{v_2}\left(\frac{dT_2}{dv_2}\right)_S\right]$$

thus

$$\frac{v_2}{\varphi}\left(\frac{d\varphi}{dv_2}\right)_S = \frac{xv_2}{K}\left(\frac{dK}{dv_2}\right)_S - x + \frac{cxv_2}{T_2}\left(\frac{dT_2}{dv_2}\right)_S \quad \text{(iiic)}$$

The term $(dT_2/dv_2)_S$ can be evaluated as follows: For a constant entropy process the first and second laws of thermodynamics give

$$C_v\,dT = -\left[\left(\frac{dE}{dv}\right)_T + p\right]dv = -(p_i + p)\,dv$$

thus

$$\left(\frac{dT_2}{dv_2}\right)_S = -\frac{p_2}{C_v}\left(\frac{p_i}{p_2} + 1\right) \quad \text{(iiid)}$$

But from thermodynamics

$$T\left(\frac{dp}{dT}\right)_v = p_i + p$$

Again using the equation of state one obtains

$$\left(\frac{dp_2}{dT_2}\right)_v = \frac{nR\varphi}{v_2} + \frac{nRT_2}{v_2}\left(\frac{d\varphi}{dT_2}\right)_v + \frac{RT_2\varphi}{v_2}\left(\frac{dn}{dT_2}\right)_v = \frac{nRe^x}{v_2} + \frac{cnRxe^x}{v_2} + \frac{RT_2e^x}{v_2}\left(\frac{dn}{dT_2}\right)_v$$

Hence

$$\frac{p_i}{p_2} = \frac{T_2}{p_2}\left(\frac{dp_2}{dT_2}\right)_v - 1 = cx + \frac{T_2}{n}\left(\frac{dn}{dT_2}\right)_v \quad \text{(iiie)}$$

From equation (iiib) using (iiic), (iiid) and (iiie) one obtains finally

$$\theta = 1 + \frac{nRe^x}{C_v}(1 + cx)\left[(1 + cx) + \frac{T_2}{n}\left(\frac{dn}{dT_2}\right)_v\right] - x\left[\frac{v_2}{K}\left(\frac{dK}{dv_2}\right)_S - 1\right] - \frac{v_2}{n}\left[\frac{dn}{dv_2}\right]_S \quad \text{(iiif)}$$

(This is equation 6 of the article.)

The actual heat capacity is obtained from the thermodynamic formula

$$C_v = C_v^* + T_2\int_\infty^{v_2}\left(\frac{d^2p_2}{dT_2^2}\right)_v dv_2 \quad \text{(iva)}$$

(T_2, n constant)

using the equation of state

$$\left(\frac{dp_2}{dT_2}\right)_v = \frac{nRT_2}{v_2}\left(\frac{d\varphi}{dT_2}\right)_v + \frac{nR\varphi}{v_2} = \frac{nRe^x}{v_2}(cx + 1)$$

and

$$\left(\frac{d^2p_2}{dT_2^2}\right)_v = \frac{nRe^x}{v_2}(1 + c + cx)\left(\frac{dx}{dT_2}\right)_v = \frac{nRe^x}{v_2}(1 + c + cx)\frac{cx}{T_2} \quad \text{(ivb)}$$

Using (ivb) and the fact that at T_2 constant $dv_2/v_2 = dK/K - dx/x$, equation (iva) becomes

$$C_v = C_v' + cnR\int_{K(\infty)}^{K(v)} xe^x(1 + c + cx)\frac{dK}{K} - \int_0^x xe^x(1 + c + cx)\frac{dx}{x} \quad \text{(ivc)}$$

(T_2, n constant)

The last integral can be evaluated explicitly, leaving finally

$$C_v = C_v^* - cnR[e^x(1 + cx) - 1] + cnR\int_{K(\infty)}^{K(x)} xe^x(1 + c + cx)\frac{dK}{K} \quad \text{(ivd)}$$

(T_2, n constant)

(This is equation 7 of the article.)

The average heat capacity is obtained from the thermodynamic formula

$$\bar{C}_v = \bar{C}_v^* + \frac{1}{T_2 - T_1}\int_\infty^{v_2} p_i dv_2 \quad \text{(va)}$$

(T_2, n constant)

which becomes using (iiie)

$$\bar{C}_v = \bar{C}_v^* + \frac{c}{T_2 - T_1}\int_\infty^{v_2} p_2 x dv_2 \quad \text{(vb)}$$

(T_2, n constant)

Using the equation of state to eliminate p_2 and the relation $dv_2/v_2 = dK/K - dx/x$ at T_2 constant (vb) becomes

$$\bar{C}_v = \bar{C}_v^* + \frac{cnRT_2}{T_2 - T_1}\int_{K(\infty)}^{K(v)} xe^x\frac{dK}{K} - \int_0^x xe^x\frac{dx}{x} \quad \text{(vc)}$$

(T_2, n constant)

The integral involving x can again be evaluated, leaving

$$\bar{C}_v = \bar{C}_v^* - \frac{cnRT_2}{T_2 - T_1}(e^x - 1) + \frac{cnRT_2}{T_2 - T_1}\int_{K(\infty)}^{K(v)} xe^x\frac{dK}{K} \quad \text{(vd)}$$

(This is equation 8 of the article.)

Introducing the equation of state, using the definition $\theta = v_2/(v_1 - v_2)$, and neglecting p_1 since $p_2 >> p_1$ (ic) becomes

$$W^2 = nRT_2\frac{e^x}{\theta} \quad \text{(xia)}$$

(This is equation 9 of the article.)

The detonation temperature is derived from the fundamental equation

$$Q + E_2 - E_1 = \int_{T_1}^{T_2} C_v dT = \bar{C}_v(T_2 - T_1) \quad \text{(viia)}$$

Using (ib), neglecting p_1 with respect to p_2, and introducing the equation of state to eliminate p_2 together with the definition of θ, (viia) becomes

$$Q + \frac{nRTe^x}{2\theta} = \bar{C}_v(T_2 - T_1)$$

or

$$T_2 = \frac{Q + \bar{C}_vT_1}{\bar{C}_v - \frac{nRe^x}{2\theta}} \quad \text{(viib)}$$

(This is equation 10 of the article.)

The relation for the fugacity factor

$$F = \frac{\varphi}{v_2}\exp.\int_0^{p_2}(\varphi - 1)\frac{dp_2}{p_2} = \frac{\varphi}{v_2}e^J \quad \text{(viiia)}$$

(T = constant); $J = \int_0^{p_2}(\varphi - 1)\frac{dp_2}{p_2}$

is evaluated by means of the equation of state as follows.

At constant T_2

$$\frac{dp_2}{p_2} = \frac{dn}{n} + \frac{d\varphi}{\varphi} - \frac{dv_2}{v_2}$$

Using the definition of φ and the relation $\frac{dv_2}{v_2} = \frac{dK}{K} - \frac{dx}{x}$ at T_2 constant J may be expressed

$$J = \int_{n(\infty)}^{n(v)} (e^x - 1)\frac{dn}{n} + \int_0^x (e^x - 1)\,dx + \int_0^x \frac{e^x - 1}{x}\,dx - \int_{K(\infty)}^{K(v)} (e^x - 1)\frac{dK}{K} \quad \text{(viiib)}$$

(T_2 = constant)

The second term in (viiib) can be integrated and the third term can be expanded in an infinite series and integrated term by term giving

$$J = e^x - 1 + x^2\left[\frac{1}{2\cdot 2!} + \frac{x}{3\cdot 3!} + \frac{x^2}{4\cdot 4!} + \ldots\right] - \int_{K(\infty)}^{K(v)} (e^x - 1)\frac{dK}{K} + \int_{n(\infty)}^{n(v)} (e^x - 1)\frac{dn}{n} \quad \text{(viiic)}$$

(This is equation 12 of the article.)

HEATS OF SOLUTION OF SOME ALKYL SULFATES IN WATER[1,2]

BY ERIC HUTCHINSON, KENNETH E. MANCHESTER AND LORRAINE WINSLOW

Department of Chemistry, Stanford University, Stanford, California

Received June 1, 1954

The heats of solution of three alkyl sulfates in water have been obtained by direct calorimetry and from solubility measurements. A relationship is deduced between the turbidity of the solution and the factor required to convert the apparent heats of solution obtained from solubility measurements made above the Krafft point.

Theoretical

Particular interest is attached to a knowledge of the heats of solution of detergents since from a knowledge of this quantity above and below the critical concentration for micelle formation it is possible to derive the heat effect associated with the formation of micelles. This latter affords valuable information on the structure of the micelles. A number of papers[3] have been published on the subject of heats of micellization, derived by indirect means, but so far as we know no direct calorimetric data have been published.

Conflicting views have been expressed[4] about the structure of detergent micelles, some suggesting that a micelle is similar to a crystalline bimolecular leaflet, others suggesting that the micelle is a loose aggregate of spherical or spheroidal shape. Since the extreme views differ greatly in the degree of organization involved in the micelle it may be expected that measured heat and entropy effects associated with micelle formation will help to resolve the difficulties of deciding which model is the more accurate representation. A further point of interest is that these detergent solutions become highly non-ideal even at low concentrations owing to micelle formation, and consequently offer a good case for testing the theories of non-ideal behavior.

Stainsby and Alexander,[5] in a paper interpreting the solubility data obtained by Tartar and his coworkers[6] have put forward a thermodynamic argument about non-ideal solutions which is incorrect, and we present below an accurate thermodynamic interpretation of the solubility relations in non-ideal solutions which differs somewhat from that given by Williamson,[7] and which is of interest in that it is related to the theory of light scattering by solutions.[8]

For the equilibrium between a pure solute and its saturated solution we have, in general, that the chemical potential of the solvent (component 1) is a function of four variables

$$\mu_1 = \mu_1(P, T, n_1, n_2)$$

where

T = Kelvin temperature
P = pressure
n_1 and n_2 = the numbers of moles of solvent and solute, respectively

Hence

$$d\mu_1 = \left(\frac{\partial\mu_1}{\partial P}\right)_{T,n_1,n_2} dP + \left(\frac{\partial\mu_1}{\partial T}\right)_{P,n_1,n_2} dT + \left(\frac{\partial\mu_1}{\partial n_1}\right)_{P,T,n_2} dn_1 + \left(\frac{\partial\mu_1}{\partial n_2}\right)_{P,T,n_1} dn_2$$

Imposing the conditions of constant pressure and n_1

$$\left(\frac{\partial\mu_1}{\partial T}\right)_{P,n_1} = \left(\frac{\partial\mu_1}{\partial T}\right)_{P,n_1,n_2} + \left(\frac{\partial\mu_1}{\partial n_2}\right)_{P,T,n_1}\left(\frac{\partial n_2}{\partial T}\right)_{P,n_1} \quad (1)$$

Now $(\partial\mu_1/\partial T)_{P,n_1,n_2} = -\bar{S}_1$ = partial molal entropy of the solvent in solution. From the Gibbs–Duhem equation for the solution at constant pressure, we have

$$d\mu_1 = -\frac{1}{n_1}\{S\,dT + n_2\,d\mu_2\}$$

and

$$\left(\frac{\partial\mu_1}{\partial T}\right)_{P,n_1} = -\frac{1}{n_1}\left\{S + n_2\left(\frac{\partial\mu_2}{\partial T}\right)_{P,n_1}\right\} \quad (2)$$

Since the solute is in equilibrium with pure excess solute we also have

$$\mu_2^{\text{solution}} = \mu_2^{\text{solid}}$$

$$\therefore \left(\frac{\partial\mu_2}{\partial T}\right)_{P,n_1} = \left(\frac{\partial\mu_2^{\text{solid}}}{\partial T}\right)_{P,n_1} = -\bar{S}_2^{\circ} \quad (3)$$

(1) This work was carried out with the support of the Office of Naval Research under Contract N60NR 25130 with Stanford University.

(2) Presented at the September 1953 meeting of the American Chemical Society.

(3) (a) G. S. Hartley, *Kolloid Z.*, **88**, 33 (1939); (b) B. D. Flockhart and A. R. Ubbelohde, *J. Colloid Sci.*, **8**, 423 (1953).

(4) W. Philippoff, *ibid.*, **5**, 169 (1950).

(5) G. Stainsby and A. E. Alexander, *Trans. Faraday Soc.*, **46**, 587 (1950).

(6) H. C. Tartar and K. A. Wright, *J. Am. Chem. Soc.*, **61**, 539 (1939).

(7) A. T. Williamson, *Trans. Faraday Soc.*, **40**, 421 (1944).

(8) E. Hutchinson, Technical Report No. 3, ONR Contract N6ONR 25130.

where $\bar{S}_2^\circ$ is the molal entropy of pure solid solute. Substituting in equation 1 we have

$$-\frac{1}{n_1}\{S - n_2\bar{S}_2^\circ\} = -\bar{S}_1 + \left(\frac{\partial\mu_1}{\partial n_2}\right)_{P,T,n_1} \times \left(\frac{\partial n_2}{\partial T}\right)_{P,n_1} \quad (4)$$

But by definition

$$S = n_1\bar{S}_1 + n_2\bar{S}_2$$

where $\bar{S}_2$ is the partial molal entropy of the solute in solution. Thus on rearranging terms

$$-\frac{n_2}{n_1}\{\bar{S}_2 - \bar{S}_2^\circ\} = \left(\frac{\partial\mu_1}{\partial n_2}\right)_{P,T,n_1} \times \left(\frac{\partial n_2}{\partial T}\right)_{P,n_1} \quad (5)$$

If $\bar{H}_2$ and $\bar{H}_2^\circ$ are the partial molal heat content of solute in solution and in the pure state, respectively

$$\bar{S}_2 - \bar{S}_2^\circ = \frac{\bar{H}_2 - \bar{H}_2^\circ}{T} = \frac{\bar{L}_2}{T}$$

where $\bar{L}_2$ is, conventionally, the differential heat of solution of the solute. Thus

$$\frac{\bar{L}_2}{T} = -n_1\left(\frac{\partial\mu_1}{\partial n_2}\right)_{P,T,n_1} \times \left(\frac{\partial \ln n_2}{\partial T}\right)_{P,n_1} \quad (6)$$

Writing

$$L_{app} = RT^2\left(\frac{\partial \ln n_2}{\partial T}\right)_{P,n_1}$$

$$L = \frac{n_1}{RT}\left(\frac{\partial\mu_1}{\partial n_2}\right)_{P,T,n_1} \times L_{app}$$

In which L_{app} is the apparent differential heat of solution.[9] It is readily shown that since

$$\mu_1 = \mu_1^\circ(P, T) + g_1RT \ln N_1$$

where g_1 is the osmotic coefficient of the *solvent*, and N_1 is the mole fraction of the solvent, defined by the relation

$$N_1 = \frac{n_1}{n_1 + \nu n_2}$$

where

ν = 1 for a non-electrolyte solute

$\nu = \nu_+ + \nu_-$ for an electrolyte $A_{\nu_+}\cdot B_{\nu_-}$

Then

$$\frac{n_1}{RT}\left(\frac{\partial\mu_1}{\partial n_2}\right)_{P,T,n_1} = -\nu\left\{g_1 + \left(\frac{\partial g_1}{\partial \ln n_2}\right)_{P,T,n_1}\right\} \quad (7)$$

to a very close approximation. In the case of an electrolyte which is ideal, ($g_1 = 1$), L_{app} is defined as $\nu RT^2\{(\partial \ln N_2/\partial T)_{P,n_1}\}$ so that

$$L = L_{app}\left\{g_1 + \left(\frac{\partial g_1}{\partial \ln n_2}\right)_{P,T,n_1}\right\}$$

for both electrolytes and non-electrolytes. Hutchinson[8] has shown that

$$g_1 + \left(\frac{\partial g_1}{\partial \ln n_2}\right)_{P,T,n_1} = \frac{Hc_2}{\tau} \quad (8)$$

where

τ = the turbidity of the solution
c_2 = the molal concn. of solute
H = the conventional light scattering constant

Thus

$$L = L_{app} \times \frac{Hc_2}{\tau}$$

For dilute solutions which are ideal the differential and integral heats of solution are almost identical. For detergent solutions above the critical micelle concentration the deviations from ideality are almost entirely ascribable to association into micelles, which are approximately ideal *considered as micelles*, so that below the critical micelle concentration we may expect the calorimetrically determined heat to agree with the differential heat of solution obtained from solubilities. Above the critical micelle concentration we may expect the calorimetric heat to agree reasonably well with the above theoretical result.

Because sodium tetradecyl and hexadecyl sulfates have a limited solubility in water at room temperature, we have not been able to obtain light scattering data for these solutions. The measured solubilities are included in the tables below, however, since the results themselves are of some empirical value apart from the calculation of heats of solution. The light scattering data for sodium dodecyl sulfate are taken from the work of Hutchinson.[8]

Experimental

The sodium dodecyl, tetradecyl and hexadecyl sulfates were prepared as described by Dreger, *et al.*[10] The cetylpyridinium chloride was supplied by the Wm. S. Merrill Company.

Solubilities were determined by a method similar to that used by Tartar.[6] Analysis for solute was carried out by drying known weights of solution at 100°, which caused a faint yellowing of the solute but no appreciable change in weight when prolonged. Since it is, as Tartar[6] points out, very difficult to ensure that true equilibrium is established, it is possible that some of the solubilities quoted may be in error by as much as 10% in the worst cases. All data are the average of at least three determinations.

For the measurements of integral heat of solution the calorimeter consisted of a dewar flask of 500-ml. capacity with a tightly fitted Bakelite lid. It contained a stainless steel stirrer with a Bakelite section to minimize heat leakage, a heating element which was made of manganin wire and enclosed in a cylindrical brass jacket which in turn was coated with glyptal, a stainless steel platform for breaking the sample bulb, and a spring-loaded Bakelite shaft which held the sample bulb in position. The sample was contained in a thin-walled glass bulb which was sealed by the insertion of a tapered Teflon plug in the neck. This latter unit was screwed to the Bakelite shaft. The dewar vessel was surrounded by a constant temperature bath which showed a variation of ±0.005°. The bath was housed in a plywood box insulated with about two inches of fiberglass. Temperature measurements inside the calorimeter were made with a five-junction copper–constantan thermel in conjunction with a White double potentiometer. A change of 1.5×10^{-4}° could be detected.

The electrical energy necessary to restore the original temperature of the calorimeter after dissolution of the sample was measured by determining the current in the heating circuit, the potential drop across the heater, and the time of current flow. The current and potential drop were measured on the "P" scale of the White potentiometer, and the heating period was determined with an electric timer. Current and potential drop measurements were reproducible to 1 part in 15000 or 0.007%, but errors in the time of heating varied from 0.11% in the case of the smallest temperature changes to 0.05% in the case of the largest changes.

Samples were weighed to 0.0001 g. in all cases.

The procedure for a typical run was to assemble the calorimeter and heat the contents to a predetermined temperature. The system was then allowed to equilibrate for at least 30 minutes before time–temperature readings were started. The initial heating rate was observed for about eight minutes and the bulb broken. Time–temperature readings were continued until a constant heating rate was attained and then the heater was turned on for whatever period was necessary to raise the temperature to the original value. Current and potential readings were taken during

(9) Except as noted below.

(10) E. E. Dreger, *et al.*, *Ind. Eng. Chem.*, **36**, 610 (1944).

this period. After the heating period the final heating rate was observed for a period of about ten minutes. The observed temperature changes were corrected for heat of stirring and heat transfer, and the heat of solution was then calculated by the equation

$$\Delta H = \frac{Eit}{4.183(1000)} \times \frac{H_1 M}{H_2 w}$$

where

E = potential drop across the heater in international volts
i = current in international amp.
t = time in seconds
H_1 = temp. change due to dissolution of the solute
H_2 = temp. change during the heating period
w = weight of the sample
M = the molecular weight of the sample (g. formula wt.)

The quantity $Eit/4.183$ multiplied by H_2 is termed the calorimeter constant.

In order to determine the accuracy of the apparatus we measured the heat of solution of one mole of potassium chloride in 200 moles of water at 25°. We also measured the heat of solution of one mole of potassium chloride in 2000 moles of water at 25°, in order to determine the precision of our measurements for small temperature changes. The average value of five determinations for the heat of solution at the higher concentration was found to be 4.200 ± 0.003 kcal./mole/200 moles water at 25°. This result is in excellent agreement with the value given in the literature[11] as 4.201 kcal./mole/200 moles water. For the dilute solutions the average of three determinations was found to be 4.179 ± 0.005 kcal./mole/2000 moles water. The heat of solution at this concentration, determined by extrapolation of the values given in the literature,[11] is 4.177 kcal./mole/2000 moles water.

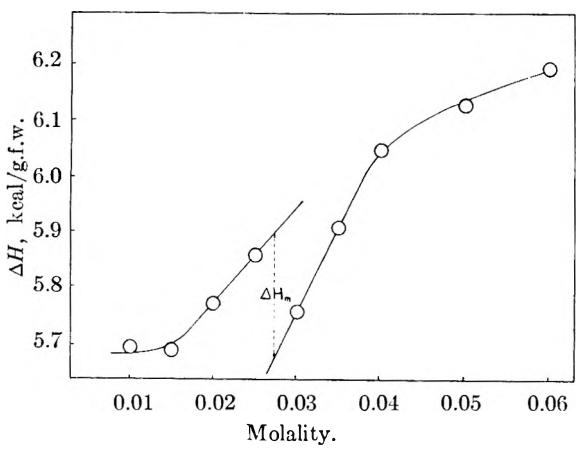

Fig. 1.—The heat of solution of sodium decyl sulfate in water as a function of the concentration.

Results

The solubilities of sodium dodecyl, tetradecyl and hexadecyl sulfates in water at a series of temperatures are given in Tables I-III. In the case of the dodecyl sulfate the values[8] of Hc_2/τ are also given, together with the product of L_{app} and Hc_2/τ. The calorimetric work has been carried out mainly with sodium decyl sulfate, but values for sodium octyl sulfate, sodium dodecyl sulfate and cetylpyridinium chloride, over more restricted ranges of concentration, have been determined. These are given in Tables IV-VII, while Fig. 1 shows a plot of heat of solution of sodium decyl sulfate as a function of concentration.

(11) "Selected values of chemical thermodynamic properties," Circular of the Bureau of Standards, 500, U. S. Government Printing Office, Washington, D. C., Feb. 1, 1952, p. 487.

TABLE Ia

THE SOLUBILITY OF SODIUM DODECYL SULFATE IN WATER

Temp., °K.	Solubility, g./1000 g. water	$L_{app.}$, kcal./mole	Temp., °K.	Solubility, g./1000 g. water	$L_{app.}$, kcal./mole
274.8	1.73	8.64	289.4	72.0	55.6
278.8	2.16	8.89	291.6	144.0	47.5
282.1	2.59	9.10	293.2	216.0	40.1
286.9	28.8	58.8	294.4	288.0	40.1

TABLE Ib

THE HEAT OF SOLUTION OF SODIUM DODECYL SULFATE IN WATER

Solution, m	$L_{app.}$	Hc_2/τ	L, kcal./mole
6×10^{-3}	8.64	0.862	7.62
1×10^{-1}	58.8	.125	7.35
2.5×10^{-1}	55.6	.20	11.12
5.0×10^{-1}	47.5	.20	9.5

TABLE II

THE SOLUBILITY OF SODIUM TETRADECYL SULFATE IN WATER

Temp., °K.	Solubility, g./1000 g. water	$L_{app.}$, kcal./mole
297.5	1.896	112.6
297.9	2.528	112.9
303.5	31.6	75.0
305.2	63.2	75.9
306.2	94.8	76.4

TABLE III

THE SOLUBILITY OF SODIUM HEXADECYL SULFATE IN WATER

Temp., °K.	Solubility, g./1000 g. water	$L_{app.}$, kcal./mole
310.4	3.44	103.6
311.7	6.88	104.5
314.9	34.4	64.9
316.5	51.6	39.4

TABLE IV

HEAT OF SOLUTION OF SODIUM DECYL SULFATE IN WATER

No. of determinations	Final soln., m	Temp., °C.	$\Delta H^{25°}$, kcal./g.f.w.
3	0.0100	25.01	5.699 ± 0.019[a]
3	.0150	25.00	5.692 ± 0.021
3	.0200	25.01	5.775 ± 0.005
3	.0250	25.00	5.862 ± 0.030
2	.0275	25.00	5.842 ± 0.058
3	.0300	25.01	5.762 ± 0.015
1	.0325	25.00	5.871 ± 0.010
3	.0350	25.00	5.912 ± 0.011
3	.0400	25.01	6.050 ± 0.009
3	.0500	25.00	6.130 ± 0.016
3	.0600	25.01	6.193 ± 0.023

[a] Errors are estimated by the method of F. D. Rossini, *Chem. Revs.*, 18, 233 (1936).

TABLE V

HEAT OF SOLUTION OF CETYLPYRIDINIUM CHLORIDE IN WATER

No. of determinations	Final soln., m	Temp., °C.	$\Delta H^{25°}$ kcal./g.f.w.
3	0.0099	25.01	14.00 ± 0.03
4	.0199	25.02	14.17 ± 0.04
3	.0299	25.02	13.95 ± 0.17
3	.0399	25.00	13.98 ± 0.03

TABLE VI

HEAT OF SOLUTION OF SODIUM OCTYL SULFATE IN WATER

No. of determinations	Final soln., m	Temp., °C.	$\Delta H^{25°}$, kcal./g.f.w.
2	0.0200	25.02	3.868 ± 0.081
2	.0400	25.02	3.967 ± 0.096
2	.0600	25.01	4.062 ± 0.010
2	.0800	25.01	4.128 ± 0.040

TABLE VII

HEAT OF SOLUTION OF SODIUM DODECYL SULFATE IN WATER

No. of determinations	Final soln., m	Temp., °C.	$\Delta H^{25°}$, kcal./g.f.w.
2	0.0060	25.00	7.63 ± 0.11
5	0.0500	25.02	7.64 ± 0.09

Discussion

To deal with the solubility data first: the results for sodium dodecyl sulfate may be regarded as providing good confirmation of the theory outlined earlier, particularly when the possibility for error in both the light scattering and solubility determinations is borne in mind. It is clear, however, that if differential heats of solution obtained from solubility are to be of any value in interpreting the structure of detergent solutions in detail a considerable improvement in experimental accuracy is required, and it is questionable whether such improvements are worth striving for in view of the relative ease of making direct determinations by calorimetry.

The calorimetric results obtained in the case of sodium decyl sulfate show that there is an abrupt change in the integral heat of solution between 0.025 and 0.030 molal concentration. (The critical micelle concentration as determined by light scattering[8] is in the region 0.030 to 0.035 molal and as determined by electrical conductance[2] is 0.031 molal.) From Hess's law the heat of micellization is readily deduced to be of the order −0.21 kcal./mole, and if there is true equilibrium between micelles and single species the corresponding entropy of micellization is 0.70 cal./mole/degree. Although the data for cetylpyridinium chloride are more restricted they are sufficient to indicate that the heat effect is about −0.3 kcal./mole and the entropy change about 1 cal./mole/degree. The apparent critical micelle concentration for this solute is in fair agreement with the value 0.029–0.035 molal derived from solubility data.[12]

Sodium octyl sulfate and sodium dodecyl sulfate present problems of experimental technique for these studies in terms of the large amount of solute required to exceed the critical micelle concentration, in the first case, and the small quantity required to fall below the critical concentration, in the second case. It is of interest to note that Flockhart and Ubbelohde[3b] determined the heat of micellization of sodium dodecyl sulfate by measuring the temperature coefficient of the critical micelle concentration determined by electrical conductance, and found values varying between +0.8 kcal./mole at 5° and −1.9 kcal./mole at 45°. These results are in better accord with our direct measurements than are those of Stainsby and Alexander.[5]

It will be seen from the data for the octyl, decyl and dodecyl sulfates that the heat of solution of a $-CH_2-$ group is of the order of 0.9 kcal./mole. This value may be compared to the value 0.64 to 0.71 kcal./mole derived by Langmuir[13] as the heat of adsorption of a $-CH_2-$ group on water, and with the value 1.18 kcal./mole derived by Herington[14] from solubility measurements for hydrocarbons in water.

Stainsby and Alexander have attempted to break down the heat of micellization into a number of terms, accounting for changes in surface energy, changes in rotational energy, etc. On this basis we are led, from our results, to conclude that micellization is a process in which there is a very delicate balance between the kinetic energy on the one hand and end group interactions on the other. Whatever the details may be, our results show that micellization is certainly not a process comparable to a phase change, in the concentration range studied. From light scattering data[8] we know that the micelles of sodium decyl and dodecyl sulfates contain some 60 or so single species, and the small heat and entropy effects are in good agreement with the loose structure which such an aggregation would involve on the basis of a spherical or spheroidal micelle. The results certainly rule out, in the solutions examined, the existence of the bimolecular leaflet lamellar micelle, which is essentially a micro-crystallite. Such a structure would involve entropy changes far in excess of the measured values.

Acknowledgment.—It is a pleasure to acknowledge the kind advice of Dr. F. O. Koenig, and the generosity of Dr. G. S. Parks in making available to us the White potentiometer and auxiliary equipment used in our calorimetric work.

(12) N. K. Adam and K. G. Pankhurst, *Trans. Faraday Soc.*, **42**, 523 (1946).

(13) I. Langmuir, *J. Am. Chem. Soc.*, **39**, 1883 (1917).

(14) E. F. G. Herington, *ibid.*, **73**, 5883 (1951).

INTERACTION OF CUPRIC IONS WITH POLYACRYLIC ACID[1]

BY FREDERICK T. WALL AND STANLEY J. GILL

Noyes Chemical Laboratory, University of Illinois, Urbana, Illinois

Received June 3, 1954

The interaction of cupric ions with polyacrylic acid has been investigated spectroscopically, polarographically and by *p*H titration curves. The absorption spectra suggest the formation of a complex between copper and polyacrylic acid. The polarographic studies also show that the copper is associated in some way with the polyanion. Finally, the *p*H titration curves demonstrate that each cupric ion replaces two hydrogens, thus suggesting the formation of a chelate. The interaction of copper ions with polyacrylic acid is not a simple electrostatic phenomenon, since the behavior of copper is markedly different from that of the alkaline earths. Other ions like those of nickel, cobalt and zinc exhibit to a small extent tendencies to form complexes with polyacrylic acid.

Introduction

When polyacrylic acid (PAA) is partially neutralized with sodium hydroxide, it is found that an appreciable number of the sodium ions become bound to the polymer anion in such a way that they are carried along with the anion during electrical transference, diffusion, etc.[2-4] When divalent ions, such as those of calcium or strontium, are introduced into such a system, it is found that they are preferentially taken up by the polyanions, which appear to act as miniature ion-exchange systems. The binding of ions like sodium or calcium appears to be essentially electrostatic in character, since ordinary equilibrium considerations cannot account for the binding quantitatively.[5] However, when cupric ions are substituted for the alkaline earths, it is found that a different kind of binding takes place. By investigating the interaction of copper ions with polyacrylic acid, we have obtained evidence for the formation of complex structures which appear to involve intramolecular pairs of carboxyl groups associated with copper ions. The experiments consisted of the measurement of absorption spectra, polarographs and *p*H titration curves.

Experimental

Reagent grade materials were used throughout. Copper perchlorate was prepared by dissolving copper oxide in perchloric acid, filtering and crystallizing the salt from a concentrated solution. The *p*H of the copper solutions used was never less than 4.5.

The polyacrylic acid was made by the organic preparations section at the University of Illinois, and its solutions were standardized by drying aliquot portions.

A Cary Recording Spectrophotometer with a 1-cm. length quartz cell was used for obtaining absorption data. Solutions were maintained at an approximate ionic strength of 0.084 by the addition of sodium perchlorate.

Polarographic studies were made at 25° using a Sargent XXI Polarograph. A conventional "H" cell was used with the solution under investigation in both sides. Connection to the external saturated calomel reference electrode was made through an agar–saturated potassium chloride salt bridge. The diffusion current values were taken as $^6/_7$ of the maximum diffusion currents with no damping. The capillary had the following characteristics: h = 91 cm. and $m^{2/3}t^{1/6}$ = 1.766 mg.$^{2/3}$ sec.$^{-1/2}$ at −0.200 volt.

*p*H readings were obtained with a Beckman *p*H meter model G. Temperatures of the solutions were in the range 23 ± 2°.

Discussion

A strong absorption peak is observed at 2570 Å. for aqueous mixtures of polyacrylic acid and copper perchlorate. This is significant because the optical density of the separate solutions is negligible at this wave length. An effect can also be observed without instruments because the mixtures exhibit an intense blue color, which is, of course, readily borne out by absorption spectra measurements. However, the visual band is much less intense than that at 2570 Å. The absorption can be intensified by increasing the copper perchlorate or polyacrylic acid concentration, or, more markedly, by neutralizing the polyacrylic acid with a base that does not give appreciable absorption at 2570 Å. with polyacrylic acid alone. Figure 1 illustrates this effect of neutralization upon the copper ion–polyacrylic acid absorption peak when the ratio of copper ion to carboxyl group concentration is about one to ten. It is worth noting that the height of this absorption peak rises with increasing neutralization and passes through a maximum at about 45% neutralization; this effect disappears for smaller ratios of copper ion to carboxyl and is entirely absent for ratios below one to twenty, when the polyacrylic acid concentration is of the order of 4×10^{-3} N. Ratios higher than one to five result in precipitation upon partial neutralization.

Absorption spectra on related systems were examined to provide comparison with the copper–polyacrylic acid data. These included spectra of partially neutralized sodium polyacrylate, strontium polyacrylate and zinc polyacrylate, none of which showed any absorption comparable to the copper mixtures. Therefore we conclude that the intense band at 2570 Å. is peculiar to copper in the presence of polyacrylic acid. Cupric solutions with simple monobasic and dibasic acids, such as propionic, glutaric, succinic, adipic and citric, show weak absorption peaks below 2500 Å. when the acids are partially neutralized. No maxima in absorption peak heights were observed for neutralizations less than 100%, nor was precipitation encountered for large ratios of copper to acid concentrations.

The above facts are consistent with the following picture for the interaction of copper with polyacid chains. When there is a large ratio of copper to carboxyl groups, intramolecular associa-

(1) The work discussed herein was performed as a part of the research project sponsored by the Reconstruction Finance Corporation, Office of Synthetic Rubber, in connection with the Government Synthetic Rubber Program.

(2) J. R. Huizenga, P. F. Grieger and F. T. Wall, *J. Am. Chem. Soc.*, **72**, 2636 (1950).

(3) J. R. Huizenga, P. F. Grieger and F. T. Wall, *ibid.*, **72**, 4228 (1950).

(4) F. T. Wall, J. J. Ondrejcin and M. Pikramenou, *ibid.*, **73**, 2821 (1951).

(5) F. T. Wall and J. W. Drenan, *J. Poly. Sci.*, **7**, 83 (1951).

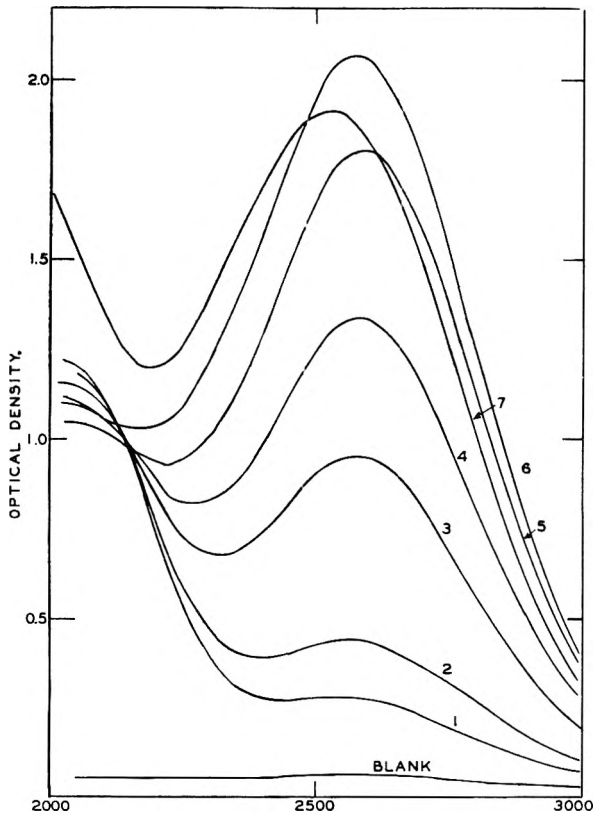

Fig. 1.—Absorption spectra of solutions with total copper concentration of 4.32×10^{-4} M and polyacrylic acid concentration of 4.05×10^{-3} N, neutralized to the following extents with NaOH: (1) 0%; (2) 4.9%; (3) 14.7%; (4) 21.2%; (5) 40%; (6) 49%; and (7) 97% (0.08 M $NaClO_4$ present).

tion through copper occurs to such an extent that the chain is partially constricted. This constriction will be opposed by the increasing net ionic charge that attends increasing neutralization. A maximum in absorption is therefore quite likely if enough copper is present to distort the polymer configuration without producing precipitation. Presumably some kind of copper complex is formed, such as a chelate, which could distort the polymer chain.

To test this hypothesis, polarographic measurements were carried out to investigate the stoichiometry of the complex. The reduction wave of the complexed copper proved to be irreversible, thus prohibiting detailed interpretation. However, two effects were noted, namely, a marked shift of the wave to a negative potential (−0.08 volt *vs.* S.C.E.), and a marked reduction in wave height. Assuming the wave height to be controlled by diffusion, the Ilkovic equation[6] can be used to calculate diffusion coefficients which at 25° appeared to have the following values.

Solution	D cm.^{2} sec.$^{-1}$
$Cu(ClO_4)_2$ ($1.072 \times 10^{-4} M$)	0.71×10^{-5}
$Cu(ClO_4)_2$ ($1.072 \times 10^{-4} M$)	$(1.97 \pm 0.05) \times 10^{-7}$
84% neutralized PAA (0.12 N)	
$Cu(ClO_4)_2$ ($1.072 \times 10^{-4} M$)	$(1.34 \pm 0.05) \times 10^{-7}$
84% neutralized PAA (0.24 N)	
(Supporting electrolyte: 1 M $NaClO_4$)	

(6) I. M. Kolthoff and J. J. Lingane, "Polarography," Interscience Pub. Inc., New York, N. Y., 1941, p. 55.

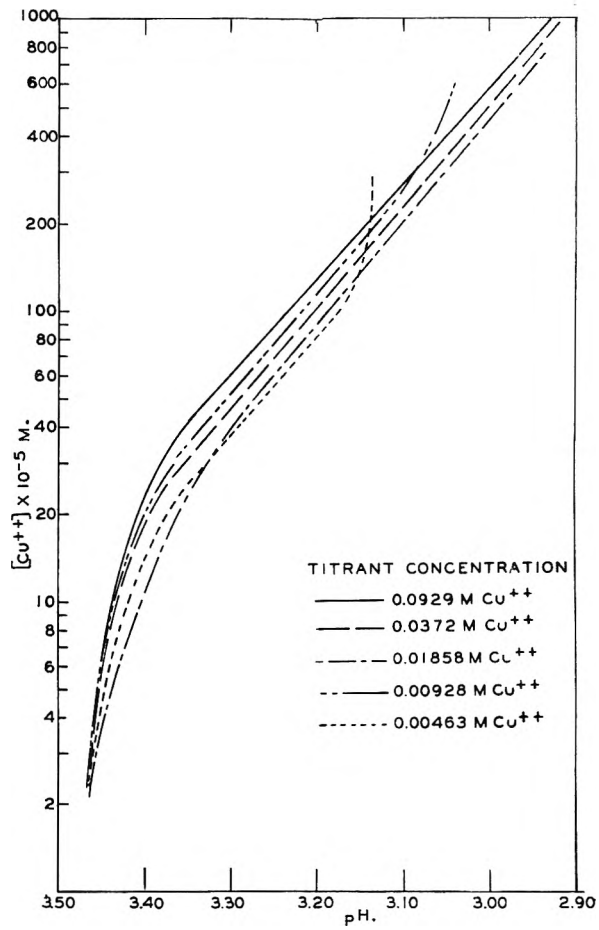

Fig. 2.—Titration of 20 ml. of 0.01041 N PAA with copper nitrate solutions.

The difference between the last two values might be attributed to viscosity effects. The small diffusion coefficient of copper in the presence of polyacrylic acid is attributed to the large size of the polymer coil.

Final evidence for the formation of a copper complex was gained from *p*H curves as shown in Fig. 2. Data for these curves were obtained by titrating copper nitrate solutions of different concentrations into 20 ml. of 0.01041 N polyacrylic acid. It should be noted that the position of the curves with respect to titrant concentration could not be ascertained precisely because of experimental errors in *p*H measurements made on different days. (Copper nitrate was found to give results identical to those of copper perchlorate.) For *p*H values below 2.9, precipitation occurs with the more concentrated copper solutions. When log $[H^+]$ is plotted *versus* the log of the total copper concentration, straight lines are obtained with slopes of 3.1 to 3.3 over wide ranges of copper concentration. The curves of Fig. 2 are consistent with the reaction

$$Cu^{++} + (COOH)_2 \longrightarrow (COO)_2Cu + 2H^+ \qquad (1)$$

which has the equilibrium constant

$$K = \frac{[(COO)_2Cu][H^+]^2}{[Cu^{++}][(COOH)_2]} \qquad (2)$$

At this point we should explain why the carboxyl groups are indicated as $(COOH)_2$ instead of

2COOH. This is done to emphasize the fact that intramolecular carboxyls appear to react with copper and not just any two carboxyls from different molecules that get close enough together. Evidence for this is obtained from the fact that the equilibrium constant expression is found to vary inversely with the first power of the acid concentration and not with the square of that concentration. The inverse first power thus implies that the pairs of carboxyls involved come from the same molecule, and that they might even be adjacent. If enough copper has been added to the solution so that self-ionization of the acid is replaced by reaction 1, we can write that

$$[(COO)_2Cu] = \frac{1}{2}[H^+] \quad (3)$$

Moreover, from the experimental conditions we note that the following approximations can be made for the straight portion of the curves

$$[Cu^{++}] \cong [Cu]_T = \text{total copper concn.} \quad (4)$$

and

$$[(COOH)_2] = \frac{1}{2}\text{ equivalent concn. of PAA} \quad (5)$$

Equation 2 can now be simplified to

$$K = \frac{[H^+]^3}{[Cu]_T[PAA]} \quad (6)$$

Since PAA remains essentially constant for the titrations with the higher concentrations of copper nitrate, a log log plot between $[H^+]$ and $[Cu]_T$ should have a slope of approximately 3, as confirmed by experiment.

Other salts such as potassium nitrate, strontium nitrate, zinc nitrate and even nickel perchlorate and cobalt perchlorate do not show nearly as strong a tendency for replacement of hydrogen in polyacrylic acid as copper ion does. This behavior is consistent with the behaviors of these ions in forming other complexes.

The *p*H results thus corroborate the polarographic and absorption spectra observations which suggest that a copper polyacrylate complex exists, presumably a chelate structure involving adjacent carboxylate groups.[7]

Acknowledgment.—Acknowledgment is made for the assistance given by Robert L. Rebertus in obtaining the polarographs.

(7) Professor Paul J. Flory recently reported (private communication) that a decrease in viscosity occurs when copper salts are added to polyacrylic acid. This fact can also be explained by the formation of a complex: see P. J. Flory and J. E. Osterheld, THIS JOURNAL, **58**, 653 (1954).

BURNING RATE STUDIES. I. MEASUREMENT OF THE TEMPERATURE DISTRIBUTION IN BURNING LIQUID STRANDS

BY D. L. HILDENBRAND, A. G. WHITTAKER AND C. B. EUSTON

Chemistry Division, U. S. Naval Ordnance Test Station, Inyokern, China Lake, California

Received June 14, 1954

Fine wire thermocouples (0.0003 inch diameter) carefully prepared by micromanipulative techniques have been used to explore the temperature distribution in several burning liquid systems as an aid in the theoretical approach to liquid combustion. The experimental temperature–time records were combined with simultaneously determined liquid consumption rates to give the steady-state temperature distance curves. Work to date has been chiefly concerned with the liquid phase profiles and the effect of variables such as liquid viscosity on the shape of the profile. High-speed motion pictures of the burning process have been synchronized with the temperature–time records to determine the relative positions of the thermocouple and the liquid surface. The three liquid systems studied thus far have been the two component systems 2-nitropropane–nitric acid, metriol trinitrate cooled with triacetin, and ethyl nitrate. Emphasis has been on interpretation of the data and their application to determining surface temperature.

Introduction

A knowledge of the temperature distribution in a combustion wave is essential for understanding the mechanism of propagation of the wave. Ideally, the experimental temperature profiles will give such valuable information as the distribution of heat sources and a characterization of the modes of energy flow within the system. These data will, in turn, be helpful in working out the detailed chemical kinetic processes taking place in the combustion wave.

This study has been primarily concerned with the liquid phase temperature distribution in the hope of acquiring information about chemical reactions occurring in this region and the possibility of their influencing the over-all rate of burning. The data would also be useful for checking the validity of theoretical treatments such as that developed for solid powders by Rice and Ginell[1] which is based on a rate of burning controlled by the surface temperature. However, it is the intent to present only the experimental method and some of the preliminary results in this paper. Details of the results and conclusions reached in this work will be published at a later date.

Experimental Procedure

The temperature profiles were obtained with thermocouples prepared from a 0.0003 inch diameter platinum and platinum–10% rhodium Wollaston wire. In the early work, the thermocouples were made by dissolving off about one-half inch of the silver coating and passing the crossed wire ends through a gas-oxygen flame as described by Klein, *et al.*[2] Using this method, the size of the bead at the junction could not be closely controlled and the bead diameter varied from three to six times that of the wire. When it became apparent from the early records that at least a portion of the temperature–time trace was much steeper

(1) O. K. Rice and R. Ginell, THIS JOURNAL, **54**, 885 (1950).

(2) R. Klein, M. Mentser, G. Von Elbe and B. Lewis, *ibid.*, **54**, 877 (1950).

than anticipated, it was decided to use micromanipulative techniques in preparing the thermocouples. In this way, the bead could be kept at a small, uniform size, thereby reducing thermal lag to a minimum.

A deFonbrune Micro-forge was modified slightly and used as a micromanipulator. The thermocouples were then made in the following manner. About 1/4 inch of the silver coating was dissolved from a short length of platinum Wollaston wire. The 0.0003 inch diameter platinum wire was then brazed to a 0.004 inch diameter platinum lead wire with a gas–oxygen microtorch and the small wire cut off to the appropriate length. The process was repeated for the platinum–10% rhodium wire. The two large lead wires were then mounted in opposite arms of the micromanipulator and brought together until the tips of the 0.3 mil wires were just touching. By bringing the tip of the microtorch into the field of the microscope, the welding operation could be very carefully controlled; the flame was removed as the two wires just fused together. Using this method, essentially a butt-weld was obtained with the junction about 70% larger in diameter than the wire. To remove any uncertainties regarding the temperature–e.m.f. relation, one of the 0.3 mil diameter couples was compared with a Bureau of Standards calibrated platinum, platinum–10% rhodium thermocouple in the temperature range 25–1000°. The behavior of the fine thermocouple was entirely normal and it followed the standard couple within ±1° over the whole range. For most of the work, bare thermocouples were used. However, a few runs made using couples coated with a very thin Teflon film gave profiles identical to those obtained with bare couples, indicating a lack of catalytic activity by the platinum.

The thermocouples were mounted in Pyrex tubes by drilling two holes with a hot tungsten wire and stretching the couple diametrally across the tube using additional micromanipulators. A wax seal held the thermocouple firmly in position, with the junction located as closely as possible in the center of the tube. Conduction errors were minimized by this type of mounting since the couple lay essentially in an isothermal region.

For the temperature profile measurements, the liquid filled tube was placed in a two-window bomb and pressurized with nitrogen gas. Thermocouple leads and igniter wires were brought out through the bomb head by high-pressure insulated connectors. The liquid was ignited by passing a current through a length of iron wire on which was threaded a small piece of ballistite. By locating the thermocouple sufficiently far down the tube, any igniter effects were completely damped out by the time the combustion wave reached the vicinity of the couple. As the liquid burned past the thermocouple, the temperature rise was recorded. A mask could be attached to the tube to provide reference marks a known distance apart for measuring consumption rates. The thermocouple output was amplified with a Tektronix Type 112 direct coupled amplifier and fed to an Electronic Tube Corp. Model H-21 dual beam cathode ray oscilloscope; the scope pattern was photographed on continuous strip film with a Fairchild Type 314 Oscillograph Record Camera. One of the scope beams was modulated at 250 c.p.s. and used as a baseline while the other was modulated at 1000 c.p.s. and used to record the thermocouple signal. At the same time, motion pictures of the combustion wave traveling down the tube were taken with an Eastman high-speed camera at a rate of about 400 frames per second. Signals from a time base pulse generator were used to Z-axis modulate the oscilloscope and to actuate the high-speed camera timing light in order to synchronize the two film records and provide a common zero time reference. By means of appropriate lenses, the high-speed camera covered a field of view about 1/2 inch square in which the thermocouple could be clearly seen. Before and after each run several known voltages were impressed on the oscilloscope to calibrate the record. The sensitivity of the instrument was usually such that a full scale deflection corresponded to a temperature rise of about 600°. A traveling microscope was used for assessing the temperature record. Separate experiments showed the time lag in the electronics of the temperature measuring system to be less than two milliseconds, which was entirely negligible in this work. The actual frequency response of the thermocouple was not determined. However, since the couple readily recorded changes of fifty to one hundred thousand degrees centrigrade per second obtained as described later, it was felt that the response would be adequate for recording the rise in the liquid preheat zone which had a maximum rate of change of one to three thousand degrees per second.

Results and Discussion

Thus far, profile data have been obtained for three liquid systems—the stoichiometric mixture (for complete combustion) 2-nitropropane–95% nitric acid, metriol trinitrate[3a] (82%)–triacetin,[3b] and ethyl nitrate. The temperature records for all three systems have the same general shape. The various features of the profile appear to be related to the combustion wave in the following way. As the burning surface approaches the couple, there is a rapid exponential rise of 100–300°, depending on the system, which is from 0.1 to 0.3 millimeter in depth. High-speed motion pictures show that the couple is visible beneath the liquid surface in this region. This is followed by a very gradual rise of some 20–50° extending over a region 0.3 to 1 millimeter in length in which the couple is no longer visible. The length of this plateau was not entirely reproducible and was shown by the motion pictures to be caused by the thermocouple pulling up a film of liquid as it works against the surface forces. At the end of the plateau there is an extremely abrupt rise of over 1000° in about 10 milliseconds. The start of the abrupt rise was shown to coincide exactly with the breaking of the liquid film as seen in the high-speed pictures. Because of this filament pull-out effect, the couple finds itself well up into the hot gases above the surface when the film breaks. There is a further gradual rise until the thermocouple reaches the hottest portion of the flame. Only a part of the gas phase profile can be obtained, of course, if the flame temperature exceeds the melting point of platinum, as it did in the case of the nitropropane–nitric acid mixture. In this study, however, the liquid preheat region and the surface temperature were of primary interest.

It is clear that because of the filament pull-out effect, the present method does not yield the correct gas phase profile in the region directly above the surface. However, the effect is helpful in determining the actual liquid surface temperature. The thermocouple is interpreted as reading the "true" surface temperature when it becomes tangent to the liquid surface and just begins pulling up the liquid film. This corresponds to the point on the profile at which the exponential rise breaks over into the gradual plateau, as indicated at point A of Fig. 1. In calculating the temperature–distance curves from the experimental data, the temperature distribution was assumed to move down the tube at the steady-state consumption rate and only enough points were included to show the shape of the curve. By comparing data obtained from a series of runs made under identical conditions it was found that the exponential liquid phase temperature rise was reproducible to well within ±10° and that surface temperatures may likewise be obtained within the same limits.

High-speed photographs pointed out a striking

(3) (a) Methyl trimethylol methane trinitrate; (b) glycerol triacetate.

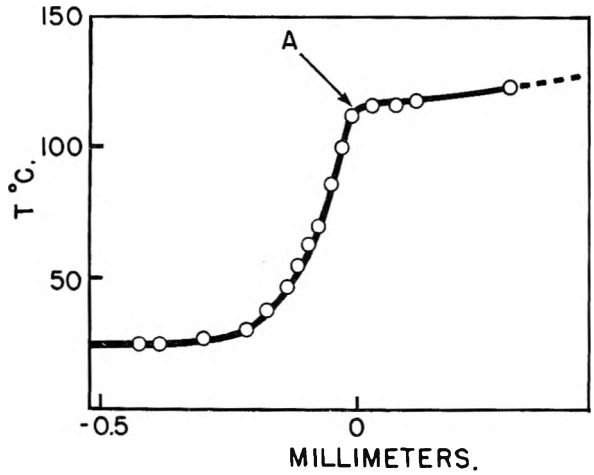

Fig. 1.—Temperature *versus* distance from burning surface for ethyl nitrate burning at 100 p.s.i.g.; consumption rate 0.052 cm./sec.

feature in the combustion behavior of the 2-nitropropane–nitric acid system. There is a great deal of random motion or turbulence in the liquid preheat region beneath the surface, presumably due to convection currents caused by the large thermal gradients and possibly by heat generated in exothermic chemical reactions near the surface. Because of these disturbances the profiles for this system were quite erratic in the liquid preheat region as shown in Fig. 2. Addition of 0.5%

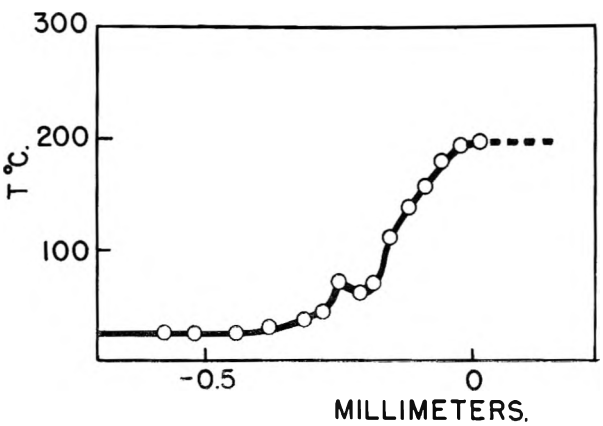

Fig. 2.—Temperature *versus* distance from burning surface for 2-nitropropane–95% nitric acid burning at 300 p.s.i.g.; consumption rate 0.160 cm./sec.

Lucite by weight increased the viscosity from 0.7 to 18 centipoises and damped out completely the irregularities in the profile as seen in Fig. 3. Unfortunately, the Lucite itself did not burn completely and a considerably higher surface temperature was recorded, probably because of a polymer-rich film on the surface. The experiment does serve to show, however, that the "thermal noise" can be damped out by increasing the viscosity sufficiently. Photographs of the burning Lucited mixture tended to confirm this by revealing a greatly reduced amount of activity in the preheat zone. The other two liquid systems, metriol trinitrate and ethyl nitrate, with viscosities of 25 and 0.6 centipoises, respectively, both yielded smooth and very reproducible liquid phase profiles with the photographs showing only a very thin region of extremely mild convection currents in the preheat zone. This would seem to indicate that with the two nitrate esters any liquid phase reactions must be occurring to a much lesser extent than in the nitropropane–nitric acid system and they must be occurring in a region much closer to the surface if they occur at all.

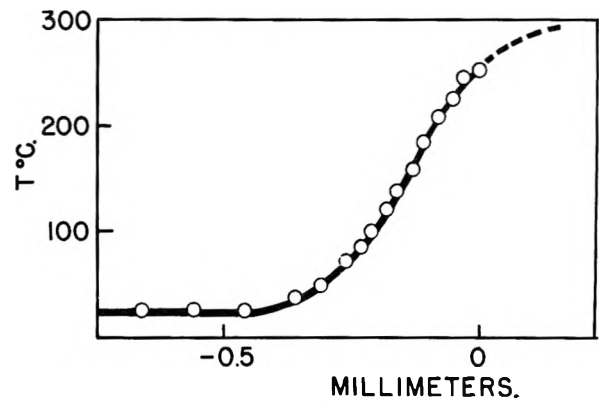

Fig. 3.—Temperature *versus* distance from burning surface for 2-nitropropane–95% nitric acid plus 0.5% lucite burning at 300 p.s.i.g.; consumption rate 0.132 cm./sec.

A detailed theoretical treatment of the combustion process cannot be made until more is known about the chemistry involved. However, some useful information may be gained from an analysis of the experimental profiles according to treatments such as that developed by Reid.[4] He has proposed an expression for the steady-state temperature distribution in a burning liquid or solid resulting from heat conduction and radiation absorption by treating a region sufficiently far below the surface so that heat generated by chemical reaction is negligible. Exclusion of the chemical reaction term, of course, allows the heat flow equation to be solved analytically. The temperature distribution may then be expressed by the equation

$$v^2(T - T_\infty) = h^2 \left(\frac{\partial T}{\partial t}\right)_x + A \frac{v}{\rho c} \exp(-\alpha r)$$

where v is the steady-state consumption rate, T and T_∞ are temperature recorded by the thermocouple and initial temperature, respectively, h^2 is the thermal diffusivity, t is time, A is the radiation intensity at the burning surface, ρ and c are density and specific heat, α is the radiation absorption coefficient and r is the distance below the surface at which T and $\partial T/\partial t$ are measured. All but A, α and h^2 are known from the experiment. From three sets of data taken at three different times, simultaneous solution of the resulting three equations will yield these quantities. As an example, the following values for these parameters were obtained from an analysis of a metriol trinitrate–triacetin liquid phase profile: $\alpha = 121$ cm.$^{-1}$, $A = 17$ cal./cm.^{2} sec. and $h^2 = 3.6 \times 10^{-4}$ cm.^{2}/sec. None of these quantities have been determined independently so that a comparison

(4) W. P. Reid, THIS JOURNAL, **57**, 242 (1953).

can be made, but the calculated values do appear to be reasonable. By applying the treatment to other systems, it may be possible to classify them according to certain models, *e.g.*, a radiation and conduction model or a conduction only model. Work of this type is planned.

STUDIES ON COÖRDINATION COMPOUNDS. XII. CALCULATION OF THERMODYNAMIC FORMATION CONSTANTS AT VARYING IONIC STRENGTHS[1]

BY REED M. IZATT, CHARLES G. HAAS, JR., B. P. BLOCK AND W. CONARD FERNELIUS

Contribution from the College of Chemistry and Physics, The Pennsylvania State University, State College, Pa.

Received June 16, 1954

Molarity quotients determined potentiometrically at varying ionic strengths have been converted to stepwise thermodynamic formation constants in aqueous solution for the reactions of Zn^{++}, Ni^{++}, Ce^{3+}, and Pr^{3+} (as the perchlorates) with the acetylacetonate ion at 30° by means of activity coefficients calculated from the Debye–Hückel equation. Agreement of the several thermodynamic constants calculated for each metal ion is good. The molarity quotients in the literature for the Pb^{++}-citrate[8] and the Cu^{++}-, Ni^{++}-, Cd^{++}-, and Mg^{++}-malonate[4] systems may be satisfactorily converted to thermodynamic constants by the same procedure.

Introduction

Much of the quantitative work in the determination of formation "constants" of coördination compounds has been done in solutions containing a large excess of neutral salt, which was added to maintain the activity coefficients of the various species constant throughout the determination. This procedure allows comparisons to be made among different metal ions, if the same medium is employed in each case. Unfortunately, however, work on different coördination systems has been done at various ionic strengths and often with different anions. It would be more desirable if the "constants" were true thermodynamic constants and therefore theoretically comparable.

The present investigation was undertaken to determine for a given chelating agent, the acetylacetonate ion, the practicability of obtaining thermodynamic constants by correcting molarity quotients with theoretically calculated activity coefficients. The data obtained also indicate the range of ionic concentration in which such a calculation procedure yields concordant values. A further object of the investigation was to illustrate the desirability of the use of the method by applying it to data for molarity quotients already available in the literature and noting the agreement obtained.

Theoretical.—The calculation of thermodynamic formation constants requires that the activity coefficient term of equation 1 be known.

$$K_f = Q_f \times \frac{y_{(MCh_x)^{(n+)-xz}}}{(y_{M^{n+}})(y_{Ch^{z-}})^x} \qquad (1)$$

where

K_f = the thermodynamic formation constant
Q_f = the molarity quotient
y = the molar activity coefficient of the ionic species, as indicated, present in the soln.
x and y refer to the number of ligands, Ch, attached to M^{n+} and the charge on the ligand, respectively

It may be learned by (i) making determinations near infinite dilution (as in conductivity methods), (ii) determining Q_f at several ionic strengths and extrapolating the plot of ionic strength or square root of ionic strength *vs.* Q_f to infinite dilution, or (iii) calculating activity coefficients from theoretical relationships (*e.g.*, the Debye–Hückel theory). Procedure (i) yields thermodynamic constants so that no correction is necessary. Procedure (ii) gives accurate values if one is able to determine the Q_f values at sufficiently dilute concentrations so that the error involved in the extrapolation from the last point to infinite dilution is minimized. This error is usually large since the curve is steepest at the last points measured. Procedure (iii) eliminates the necessity of making the large number of determinations required to define the curve because the activity coefficients enable one to determine the value of the thermodynamic constant from the molarity quotient at some concentration, C.

Ionic strength is defined by Lewis and Randall[2] as

$$\mu = {}^1/_2 \Sigma m_i Z_i^2$$

Harned and Owen[3] give the expression for the activity coefficient of an ion, f_i, based on the Debye–Hückel theory as

$$\log f_i = -Z_i^2 \left(\frac{\pi N \epsilon^6}{1000(DKT)^3}\right)^{1/2} \sqrt{\Gamma} \qquad (2)$$

where

(a) all terms have their usual significance (for a complete definition of terms see ref. 3)
(b) the expression in the parentheses is constant for a given solvent and temperature, and is referred to hereafter as H
(c) $\Gamma = 2\mu$

Equation 2, then, makes possible the calculation of the activity coefficient of an ion in dilute solutions. Since the work reported in this paper was performed in fairly concentrated solutions, it was

(1) From a dissertation presented by Reed M. Izatt in partial fulfillment of the requirements for the degree of Doctor of Philosophy, August, 1954.

(2) G. N. Lewis and M. Randall, "Thermodynamics and The Free Energy of Chemical Substances," 1st ed., McGraw-Hill Book Co., Inc., New York, N. Y., 1923, pp. 373–74.

(3) H. S. Harned and B. B. Owen, "Physical Chemistry of Electrolytic Solutions," 2nd Ed., Reinhold Publ. Corp., New York, N. Y., 1950, pp. 35–42, equation 3-4-4, 117–121.

necessary to introduce a term, A, which takes into account the effect of the diameter of the ions on the activity coefficient. This has been done in equation 3, below, which was used to calculate all constants reported in this paper.

$$\log f_j = -\frac{Z_j^2 H \sqrt{\Gamma}}{1 + A\sqrt{\Gamma}} \qquad (3)$$

where[3] $A = f(a^\circ, D, T, \Gamma)$.

No method is available to calculate an exact value for a°, the diameter of an ion in a solution. A discussion of the problem is given by Glasstone[4] who states that for most electrolytes this ionic diameter is about 3 to 4 $\times 10^{-8}$ cm. McIntyre[5] calculated values of a° from data given by Harned and Owen[3] for activity coefficients of KCl and HCl over a range of concentrations from 0.0010 to 1.0 M. He found that these a° values ranged from zero at the lowest concentrations to 5 or 6 Å. at 0.10 to 0.50 M. The value 10 Å. has been used for a° in all calculations in this paper since the acetylacetonate ion is appreciably larger than K^+ or Cl^-.

At the present time there is no way known to verify experimentally activity coefficients of single ions except by indirect evidence such as the agreement of a large number of calculations made at different ionic concentrations. At infinite dilution $f\pm$ becomes equal to $y\pm$, the ionic molar activity coefficient. At moderate dilutions these terms differ by a factor involving the densities of the pure solvent and the solution. Throughout this paper $y\pm$ is used to denote the activity coefficient and is taken as equal to $f\pm$ throughout the concentration range used.

Experimental Procedure

Potentiometric determinations of the Ni^{2+}–, Zn^{2+}–, Pr^{3+}– and Ce^{3+}–acetylacetone systems were made at several metal ion concentrations and in the cases of Zn^{2+} and Ni^{2+} at several ionic strengths (metal ion concentration constant and of the order of 0.0010 M, standard $NaClO_4$ added to give Γ = 0.10, 0.20, etc.).

Weighed quantities of Pr_2O_3 (98%) (obtained from Research Chemicals, Inc., Burbank, California), and Ce_2O_3 (prepared from G. Frederick Smith $Ce(ClO_4)_3$ hydrated) were dissolved in known amounts of standard $HClO_4$. The $Zn(ClO_4)_2$ and $Ni(ClO_4)_2$ solutions were prepared by dissolving the metal salt (obtained from the G. Frederick Smith Chemical Co.) in water and standardizing the resulting solutions. The acetylacetone was obtained from Eastman Kodak Company.

A stock solution of the metal ion and acetylacetone was prepared in each case and varying amounts of this solution were taken for analysis except in two cases (designated by * in Table I) in which the metal ion and acetylacetone were added separately to the titrating vessel. These portions containing varying amounts of metal ion, acetylacetone and water were titrated with standard NaOH (1.0 to 0.0060 N depending on the metal ion concentration). An excess of about one equivalent of acetylacetone over the amount necessary to chelate the metal ion completely was present in each titration.

A glass electrode (Beckman, Type E. No. 1190-80) and a saturated calomel electrode (Beckman No. 1170) were placed in the solution, and the pH was measured with a Beckman Model G pH meter. The pH meter was checked periodically against Beckman standard buffer solutions (pH 4.01 and 6.98). The solutions were stirred continuously and the temperature was maintained at 30.0 ± 0.1° during the titrations.

Calculations.—The formation molarity quotients were calculated by means of simultaneous equations.[6]

The thermodynamic dissociation constant of acetylacetone, $K_D = (H^+)(Ch^-)/(HCh)$, was found to be 1.12 $\times 10^{-9}$. This constant was transformed to the corresponding concentration constant for the particular ionic strength at which the titration was made by means of activity coefficients.

$$Q_D = \frac{K_D y_{HCh}}{y_{H^+}\, y_{Ch^-}}$$

where y_{HCh} is assumed to equal 1, y_{H^+} is assumed to equal y_{Ch^-}.

The pH reading was converted by means of an activity coefficient to $[H^+]$ before calculating $\bar{n}$ and $[Ch^-]$. From sets of $\bar{n}$ and $[Ch^-]$ values, molarity quotients, Q_{f_i}, were calculated for the reactions neglecting in each case hydration of the ions:

$$MCh_i^{(n-i)+} + Ch^- \rightleftharpoons MCh_{i+1}^{(n-i-1)+}$$

$$Q_{f_i} = \frac{[MCh_{i+1}^{(n-i-1)+}]}{[MCh^{(n-i)+}][Ch^-]} \qquad (4)$$

Values were calculated for Q_{f_1} and Q_{f_2} in the cases of Ni^{2+}, Zn^{2+}, Pr^{3+} and Ce^{3+}, and also for Q_{f_3} in the case of Pr^{3+}. No value for Q_{f_3} was calculated for Ce^{3+} because precipitation occurred above $\bar{n} \sim 2.0$. These molarity quotients were utilized to calculate the concentration of the ionic species present in the solution at the pH's at which the $\bar{n}$ and $[Ch^-]$ values were taken. Values of Γ were calculated at the various pH's. Activity coefficients were then calculated and utilized to convert (4) to (5). It was assumed that the activity coefficients of all neutral species were unity.

$$K_{f_i} = Q_{f_i} \times \frac{y^{(n-i-1)+}}{y^{(n-i)+}\, y^-} \qquad (5)$$

Discussion

The constants obtained are tabulated in Table I. The average value is given in each case. The indicated range is the 95% confidence interval calculated from the individual values for each constant by the method indicated by Youden.[7] It is seen that values of log K_{f_i} in the cases Ni^{2+}, Zn^{2+}, Ce^{3+} and Pr^{3+} are reasonably constant throughout the concentration range used. As would be expected, the value of the molarity quotient in each case is dependent upon the ionic strength. Thus, whether this ionic strength is made up of neutral salt or metal ion or both, the activity constants calculated by means of activity coefficients (the values of which are a function of Γ) are constant throughout the concentration ranges investigated. Considerable work which has been reported in the literature is within the range of ionic strength values given in this study. If desired, these values readily could be converted to activity constants using equation 3.

(4) S. Glasstone, "An Introduction to Electrochemistry," D. Van Nostrand Co., Inc., New York, N. Y., 1942, pp. 145–146.

(5) G. H. McIntyre, Jr., Ph.D. Thesis, Pennsylvania State University, pp. 13–15 (1953).

(6) B. P. Block and G. H. McIntyre, *J. Am. Chem. Soc.*, **75**, 5667 (1953).

(7) W. J. Youden, "Statistical Units of Measurement," National Bureau of Standards Report 1539, March 26, 1952.

TABLE I

THERMODYNAMIC LOG K VALUES FOR THE REACTION OF Zn^{2+}, Ni^{2+}, Ce^{3+} AND Pr^{3+} WITH THE ACETYLACETONATE ION AT SEVERAL M^{n+} CONCENTRATIONS AND SEVERAL IONIC STRENGTHS, TEMPERATURE = 30°

Metal ion	$[M^{n+}]$	Γ	log Q_{f_1}	log K_{f_1}		log Q_{f_2}	log K_{f_2}		log Q_{f_3}	log K_{f_3}	
	2×10^{-3}	0.0098	4.90	5.02		3.77	3.82				
	5×10^{-3}	.024	4.82	4.99		3.72	3.80				
	1×10^{-2}	.049	4.74	4.95		3.68	3.78				
	2×10^{-3}	.10	4.70	4.96	4.98	3.62	3.76	3.83			
Zn^{2+}	2.5×10^{-2}	.122	4.70	4.98	± 0.05	3.70	3.83	± 0.07			
	2×10^{-3}	.20	4.66	4.98		3.67	3.83				
	5×10^{-2}	.25	4.64	4.98		3.68	3.84				
	2×10^{-3}	.30	4.61	4.96		3.63	3.81				
	1×10^{-1}	.487	4.61	5.00		3.80	3.98[a]				
	4×10^{-4}	0.00197	5.82	5.89		4.44	4.47				
	1×10^{-3}	.0053	5.86	5.95		4.46	4.50				
	3×10^{-3}	.0141	5.80	5.93	5.92	4.36	4.43	4.46			
Ni^{2+}	1×10^{-2}	.043	5.75	5.95	± 0.05	4.40	4.49	± 0.11			
	1×10^{-3}	.10	5.59	5.86		4.21	4.35				
	2×10^{-2}	.119	5.62	5.90		4.33	4.46				
	1×10^{-1}	.482	5.56	5.94		4.32	4.49				
	7.5×10^{-4}	0.0055	5.10	5.24		3.95	4.04				
	[b] 9.2×10^{-4}	.011	5.09	5.29	5.28	3.99	4.12	3.98			
Ce^{3+}	2.0×10^{-3}	.026	5.06	5.31	± 0.11	3.71	3.90	± 0.20			
	4.5×10^{-3}	.053	4.96	5.28		3.69	3.92				
	7.5×10^{-3}	.108	4.86	5.28		3.64	3.92				
	[b] 1×10^{-3}	0.0182	5.23	5.46		4.00	4.15		3.26	3.32[a]	
	2.3×10^{-3}	.0338	5.17	5.45	5.43	3.96	4.15	4.13	2.90	2.99	2.96
Pr^{3+}	4.8×10^{-3}	.069	5.09	5.44	± 0.13	3.91	4.15	± 0.10	2.84	2.96	± 0.13
	[b] 1×10^{-2}	.132	4.91	5.38		3.77	4.09		2.78	2.93	

[a] The calculated average does not include these values. [b] See Experimental.

Since the tervalent ions require calculation of a $y \pm$[9] term, one would not expect good agreement of the activity constants to be maintained at as high Γ values as in the case of the M^{2+} species. However, in Table I agreement is seen to be good throughout the concentration range used (to $\Gamma \sim 0.20$).

Two examples are given below in which activity coefficients have been used to change molarity quotients to activity constants. Stock and Davies[8] determined, by a method involving the colorimetric measurement of pH, molarity formation quotients of several bivalent metal ions with malonate ion, $^{-}OOCCH_2COO^{-}$. They then calculated activity coefficients and thermodynamic constants in a similar manner to that given above, and compared these thermodynamic constants with values determined by different investigators using conductivity measurements.[9,10,11] Good agreement was observed in all cases.[8] The metal salt used was the chloride in the determinations made by Stock and Davies, whereas the metal malonate was employed in the conductivity measurements. This is of interest since one would expect more than the observed deviation in the log K_f values of the two cases due to Cl^{-} coördination with the metal ion. From these data it appears that good values of the thermodynamic constants are obtainable in metal chloride solutions as well as in the metal perchlorate solutions.

(8) D. I. Stock and C. W. Davies, *J. Chem. Soc.*, 1373 (1949).

(9) R. W. Money and C. W. Davies, *Trans. Faraday Soc.*, **28**, 609 (1932).

(10) H. L. Riley and N. L. Fisher, *J. Chem. Soc.*, 2006 (1929).

(11) D. J. G. Ives and H. L. Riley, *ibid.*, 1998 (1931).

S. S. Kety[12] has determined Q, the molarity dissociation quotient, for the reaction

$$Pb\ Citrate^{-} \rightleftharpoons Pb^{2+} + Citrate^{3-}; \qquad (10)$$

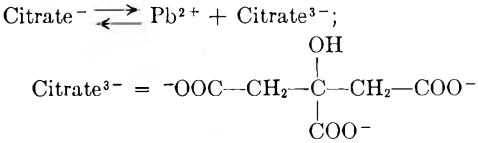

at several different concentrations of excess neutral salt (NH_4NO_3). He has plotted pQ *vs.* Γ and extrapolated from $\Gamma \sim 0.03$ to $\Gamma = 0$. (Kety's symbol μ apparently corresponds to Γ as Γ is defined in this paper. This was shown to be the case by calculating activity coefficients for charge type ± 2 at several values of Γ between 0.05 and 0.005. These calculated activity coefficients showed excellent agreement with activity coefficients of Pb^{2+} which were experimentally determined by Kety[12]). His value for pQ at infinite dilution is 6.50. However, he states that, since this value is obtained by extrapolation from a portion of the curve where experimental error is the greatest, the value obtained is only approximate. If one takes values for Γ and pQ from his graph, calculates activity coefficients for the ions involved in (10) and from these activity coefficients and pQ values calculates values for pK, the internal agreement is good. These values are summarized in Table II. The values calculated appear to fit the experimental curve of pQ *vs.* Γ as well as does Kety's extrapolated value, 6.50.

The deviation of a molarity quotient from the corresponding thermodynamic constant increases

(12) S. S. Kety, *J. Biol. Chem.*, **142**, 181 (1942).

TABLE II

CALCULATION OF pK VALUES FROM pQ AND 2 μ VALUES AS GIVEN BY KETY[11]

All pQ and 2 μ values except the last (marked*) are interpolations from a plot of pQ *vs.* 2 μ. The (*) values are given by Kety.

2 μ	(−) log dissn. quotient, pQ (from Kety) pQ	pQ	pK calcd. from pQ of Kety (eq. 3)
0	6.50	...	...
0.028	...	6.20	6.72
.0876	...	5.95	6.71
.138	...	5.82	6.68
.164*	...	5.74*	6.64

with (1) increasing ionic strength, and (2) increasing charge on the metal ion or ligand or both. A consideration of the effect of these two factors on the magnitude of the molarity quotient illustrates the desirability of using thermodynamic constants when making comparisons of published data. For example, consider the reactions of Zn^{2+} and Ce^{3+} with acetylacetone at $\Gamma = 0.121$ (Table I) and Pb^{2+} with citrate ion at $\Gamma = 0.138$ (Table II). Comparing log Q_{f_1} values in the cases of Zn^{2+} and Ce^{3+} with pQ for Pb^{2+} one observes that the differences between molarity quotients and thermodynamic constants are 0.28, 0.42 and 0.86 log unit, respectively. The corresponding differences for (1) a univalent metal ion with a univalent ligand and (2) a ter- or quadri-valent metal ion with a ter- or quadri-valent ligand would be less than 0.29 and greater than 0.86 log unit, respectively, at $\Gamma \sim 0.12$. The resulting uncertainty in any comparison of such data especially where different ionic strengths and/or different ionic charge types are represented is likely to be very great.

Acknowledgment.—The authors gratefully acknowledge financial support furnished for this work by the United States Atomic Energy Commission through Contract AT(30-1)-907.

THE EFFECT OF ALCOHOLS ON THE CRITICAL MICELLE CONCENTRATIONS OF FATTY ACID SOAPS AND THE CRITICAL MICELLE CONCENTRATION OF SOAP MIXTURES

BY KŌZŌ SHINODA

Department of Physical Chemistry, Faculty of Engineering, Yokohama National University, Minamiku, Yokohama, Japan

Received June 18, 1954

The effect of various alcohols on the critical micelle concentrations (CMC) of potassium octanoate, decanoate, dodecanoate and tetradecanoate was determined by the change in color of pinacyanol chloride. It was found that (a) the CMC of fatty acid soaps is a linear function of the alcohol concentration, (b) the logarithm of the rate of change of CMC with alcohol concentration is a linear function of the number of carbon atoms in the alcohol molecule, and (c) the logarithm of the rate of change of CMC with the concentration of a given alcohol is a linear function of the number of carbon atoms in the soap molecule. These relationships are explained by a decreased charge density on the micelle surface and a decrease in the free energy of mixing resulting from the penetration of alcohol molecules into the palisade layer of the micelle. The energy change per methylene radical, ω, passing from the aqueous phase into the hydrocarbon environment is estimated as $1.1kT$, on a gram mole basis it is 620 cal./mole at 10°. The CMC of several ternary soap mixtures were determined and a theoretical equation derived for the CMC of multi-component soap mixtures; the experimental results are in good agreement with the calculated values.

Introduction

The effect of alcohols on the critical micelle concentrations (CMC) of some long chain salts has been investigated by several authors.[1-6] Corrin and Harkins[7] measured the CMC of dodecyltrimethylammonium bromide and dodecylammonium chloride in the presence of the lower alcohols. Herzfeld, Corrin and Harkins,[8] who measured the effect of hexanol-1, heptanol-1, decanol-1 and undecanol-1 on the CMC of dodecylammonium chloride, found that the rate of change of CMC with alcohol concentration, dC/dC_a, is constant for a given alcohol; for alcohols with chain lengths of three to ten carbon atoms

$$\log_{10}(dC/dC_a) = 0.5017m' - 3.7024 \qquad (1)$$

where m' is the number of carbon atoms in the alcohol molecule. We have determined the CMC of a series of fatty acid soaps in the presence of a series of alcohols which permits a determination of the effect of chain lengths of either components. The data fitted the equation

$$\log dC/dC_a = -0.69m + 1.1m' + \text{Const.}$$

where m is the number of carbon atoms in the soap chain. The inaccuracy of the individual CMC values is believed to be less than 50% which is a small error when compared to the hundred thousandfold range covered.

The CMC of binary soap mixtures has been investigated by several authors.[9-11] We have deter-

(1) A. F. H. Ward, *Proc. Roy. Soc. (London)*, **A176**, 412 (1940).
(2) A. W. Ralston and C. W. Hoerr, *J. Am. Chem. Soc.*, **68**, 851 (1946); *ibid.*, **68**, 2460 (1946).
(3) E. C. Evers and C. A. Kraus, *ibid.*, **70**, 3049 (1948).
(4) P. F. Grieger and C. A. Kraus, *ibid.*, **70**, 3803 (1948).
(5) G. L. Brown, P. F. Grieger and C. A. Kraus, *ibid.*, **71**, 95 (1949).
(6) A. W. Ralston and D. N. Eggenberger, *ibid.*, **70**, 983 (1948).
(7) M. L. Corrin and W. D. Harkins, *J. Chem. Phys.*, **14**, 640 (1946).
(8) S. H. Herzfeld, M. L. Corrin and W. D. Harkins, THIS JOURNAL, **54**, 271 (1950).
(9) K. Shinoda, *ibid.*, **58**, 541 (1954).
(10) H. B. Klevens, *J. Chem. Phys.*, **14**, 742 (1946); THIS JOURNAL, **52**, 130 (1948).
(11) H. Lange, *Kolloid-Z.*, **131**, 96 (1953).

mined the CMC of ternary soap mixtures and compared them with the values calculated from the equation for multi-component soap mixtures. The data fitted the equation

$$C_{m1}^{1+K}x_1 + C_{m2}^{1+K}x_2 + C_{m3}^{1+K}x_3 = C_{mix.}^{1+K}, (x_1 + x_2 + x_3 = 1)$$

in which C_{m1}, C_{m2}, C_{m3} and $C_{mix.}$ are the CMC of the respective soaps and the soap mixture in moles per liter. Mole fractions of the soaps are denoted by x_1, x_2 and x_3, the value of K determined experimentally is 0.56.[12,13]

Experimental

The soap solutions, prepared by neutralizing a known quantity of carbonate-free potassium hydroxide solution with the fatty acid, were made up in boiled-out distilled water and contained 2 equivalent per cent. excess of potassium hydroxide to suppress hydrolysis. These solutions were then diluted to the proper concentrations with the dye solution, alcohol (or aqueous alcohol) and water.

Aliquot portions containing varying amounts of alcohol were then titrated with water containing the dye in the same concentration, 5×10^{-5} mole/liter, as the soap solution; the original soap solution was used as a blank.[14] The first visible change of color from blue to reddish-violet was taken as the end-point.[12] Then, various amounts of dye solution, approximating that necessary to reach the end-point, were added to a series of vessels which contained a definite quantity of soap solution. In the course of two hours the colors change gradually and a series of solutions results ranging from blue to reddish-violet. The end-point, which is always at a somewhat higher concentration than in the preliminary test, was determined 2 to 4 hours after the mixing as the concentration in the vessel at the boundary between the blue and reddish-violet solutions. Both the CMC and the concentration of alcohol were calculated from the titration end-point.

Propanol-1 and butanol-1 were purified by distillation through a 2-ft column; b.p. 97.5 and 117°, respectively. Isoamyl alcohol, hexanol-1, octanol-1, decanol-1 and octanoic acid were purified by distillation through a 3-ft glass-packed column; b.p. 131, 156, 96° (16 mm.), 101° (5 mm.) and 120° (9 mm.), respectively. Nonanol-1 was synthesized from enanthol and purified by distillation through a 1-ft column; b.p. 96–96.5° (8 mm.), decanoic acid (m.p. 31.5°) and dodecanoic acid (m.p. 44.5°) were "Nihonyushi" purest grade materials. Heptanol-1 (b.p. 176°) and tetradecanoic acid (m.p. 54°) were "Kahlbaum" pure grade materials. The pinacyanol chloride was not purified since it was used in very low concentration.

The CMC of ternary mixtures, which were made up from these soap solutions, were determined by the procedure previously described.[9]

Results

The CMC of potassium octanoate are given as a function of various alcohols in Figs. 1–3; the corresponding values for potassium decanoate[15] are given in Figs. 4–6; those of potassium dodecanoate in Figs. 7–9; and those of potassium tetradecanoate in Figs. 10–12.

Within the error of the determinations and the alcohol concentrations employed, the rate of change of critical concentration with alcohol concentration, dC/dC_a, is constant for a given alcohol. The values of dC/dC_a for the various alcohols and soaps investigated are listed in Table I.

The logarithms of dC/dC_a *versus* the number of carbon atoms in the alcohol and the soap chain are plotted in Figs. 13 and 14, respectively.

(12) S. H. Herzfeld, THIS JOURNAL, **56**, 959 (1952).

(13) M. L. Corrin and W. D. Harkins, *J. Am. Chem. Soc.*, **69**, 683 (1947).

(14) M. L. Corrin and W. D. Harkins, *ibid.*, **69**, 679 (1947).

(15) The CMC of this soap are in good agreement with the values obtained by conductivity measurements.

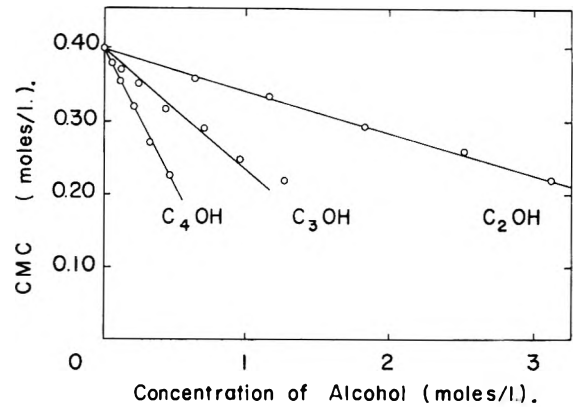

Fig. 1.—The effect of ethanol, propanol-1 and butanol-1 on the CMC of potassium octanoate at 10°.

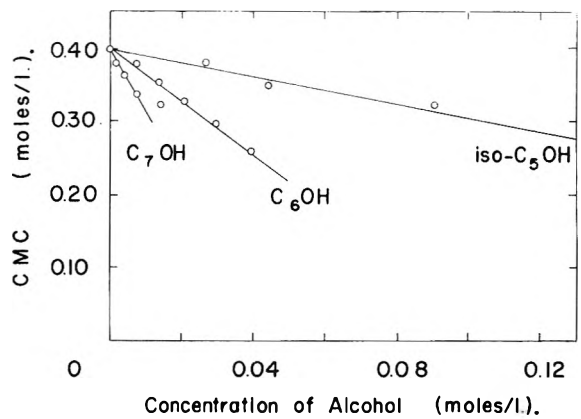

Fig. 2.—The effect of isoamyl alcohol, hexanol-1 and heptanol-1 on the CMC of potassium octanoate at 10°

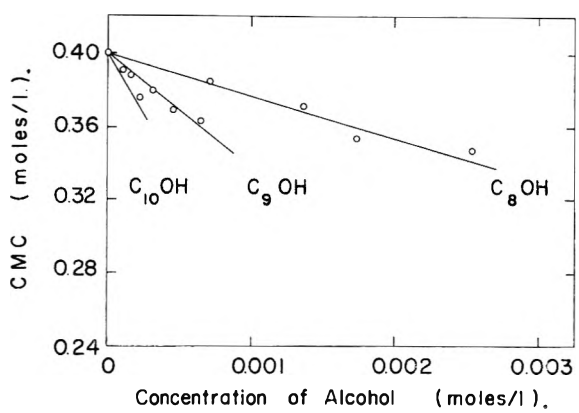

Fig. 3.—The effect of octanol-1, nonanol-1 and decanol-1 on the CMC of potassium octanoate at 10°

TABLE I

THE RATE OF CHANGE OF THE CMC OF FATTY ACID SOAPS WITH THE CONCENTRATION OF ALCOHOL, dC/dC_a

Alcohol	dC/dC_a			
	C_7COOK	C_9COOK	$C_{11}COOK$	$C_{13}COOK$
Ethanol	0.057	0.020	0.0048	0.0010
Propanol-1	.14	.065	.012	.0032
Butanol-1	.38	.19	.038	.0098
Isoamyl alcohol	.78	.43	.091	.025
Hexanol-1	3.6	1.3	.37	.098
Heptanol-1	8.3	4.4	1.0	.32
Octanol-1	23	8.3	3.5	1.0
Nonanol-1	57	29	8.1	2.6
Decanol-1	112	55	18	8.1

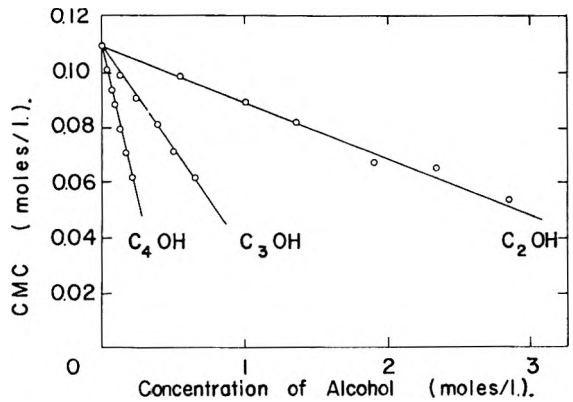

Fig. 4.—The effect of ethanol, propanol-1 and butanol-1 on the CMC of potassium decanoate at 10°.

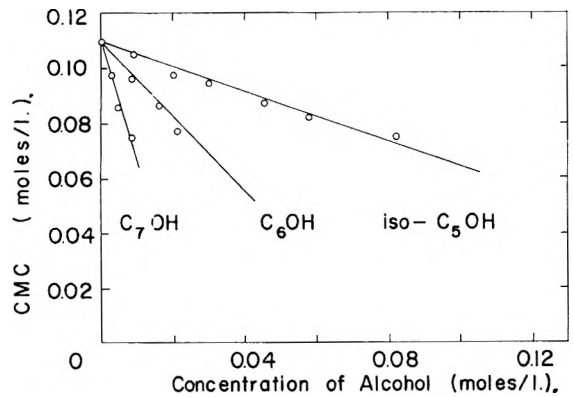

Fig. 5.—The effect of isoamyl alcohol, hexanol-1 and heptanol-1 on the CMC of potassium decanoate at 10°.

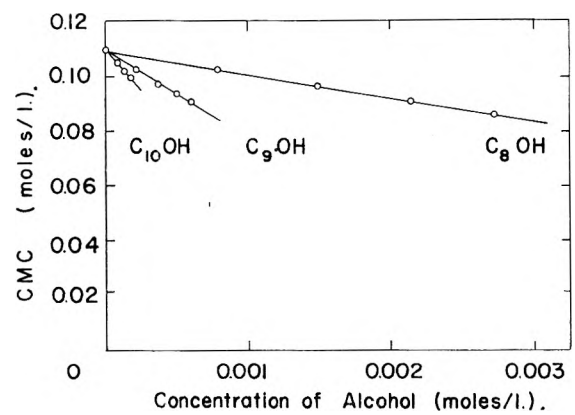

Fig. 6.—The effect of octanol-1, nonanol-1 and decanol-1 on the CMC of potassium decanoate at 10°.

Figure 13 shows that the logarithm of dC/dC_a is a linear function of the number of carbon atoms, m', in the alcohol molecule. The slope in Fig. 13 is about 1.1 per carbon atom on a natural logarithm basis. Figure 14 indicates that the logarithm of dC/dC_a for a given alcohol is proportional to the number of carbon atoms in the soap chain, m, and/or that dC/dC_a is proportional to the CMC of the respective soaps. The slope in Fig. 14 is 0.69 per carbon atom on a natural logarithm basis.

These relations may be expressed in one equation

$$\log \frac{C - C'}{C_a} = \log \frac{dC}{dC_a} = -0.69m + 1.1m' + \text{Const.}$$
$$= \log C + 1.1m' + \text{Const.} \quad (2)$$

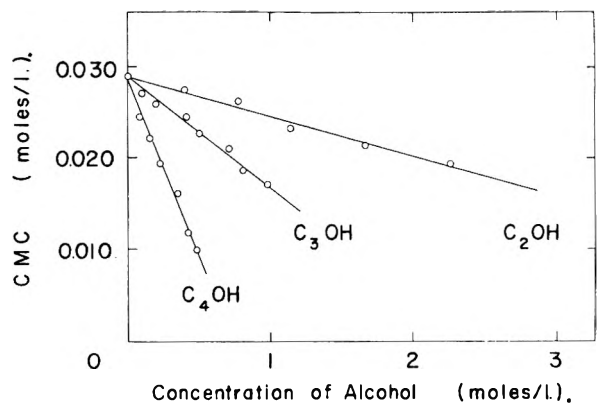

Fig. 7.—The effect of ethanol, propanol-1 and butanol-1 on the CMC of potassium dodecanoate at 10°.

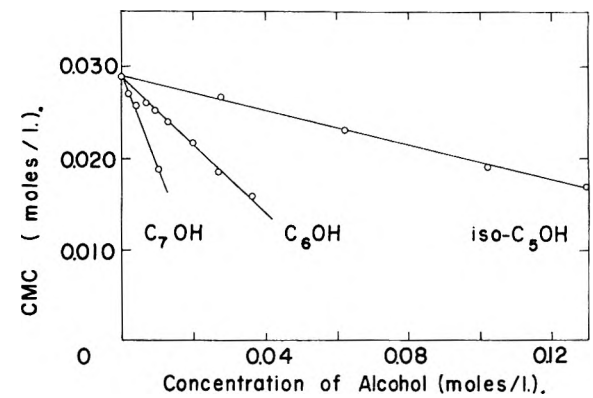

Fig. 8.—The effect of isoamyl alcohol, hexanol-1 and heptanol-1 on the CMC of potassium dodecanoate at 10°.

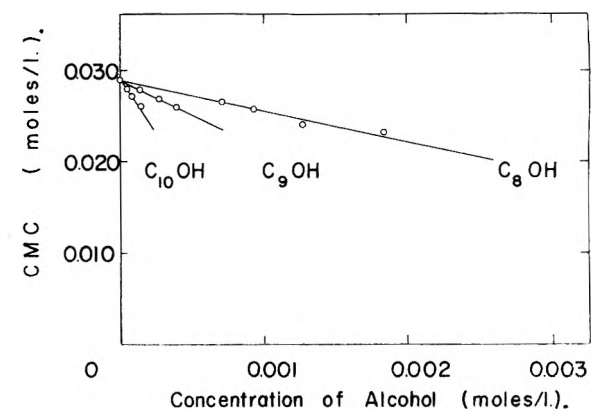

Fig. 9.—The effect of octanol-1, nonanol-1 and decanol-1 on the CMC of potassium dodecanoate at 10°.

The deviation of dC/dC_a from the logarithmic relationship for the longer chain alcohols mixed with the shorter chain soaps indicates some incompleteness or difficulty in the penetration of the non-polar portion of the alcohol molecules into the interior of the micelle. This presumably results from the relative shortness of the hydrocarbon chain of the micelle forming ions. Values in the case of alcohols having chain lengths longer than that of the soap are excluded from the calculation of the slope in Figs. 13 and 14. The other deviations may be attributed to experimental error.

The CMC of the following ternary soap mixtures were determined: potassium hexanoate, heptanoate and octanoate; potassium decanoate, undecanoate

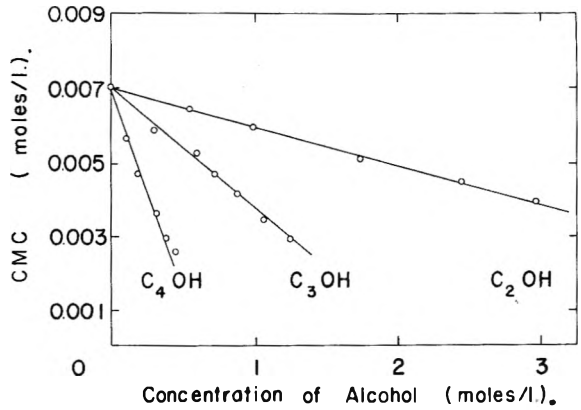

Fig. 10.—The effect of ethanol, propanol-1 and butanol-1 on the CMC of potassium tetradecanoate at 18°.

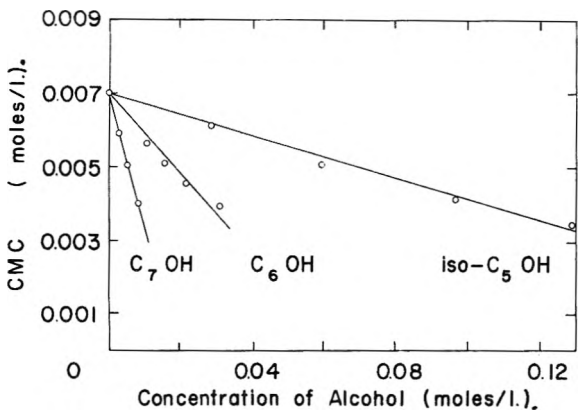

Fig. 11.—The effect of isoamyl alcohol, hexanol-1 and heptanol-1 on the CMC of potassium tetradecanoate at 18°.

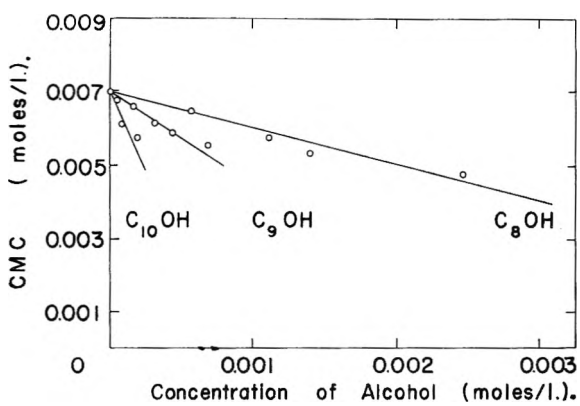

Fig. 12.—The effect of octanol-1, nonanol-1 and decanol-1 on the CMC of potassium tetradecanoate at 18°.

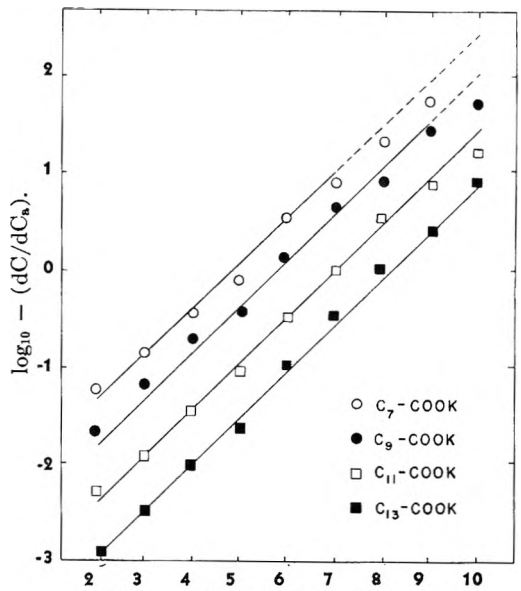

Fig. 13.—The logarithmic relation between the rate of change of CMC with alcohol concentration, dC/dC_a, and the number of carbon atoms in the alcohol.

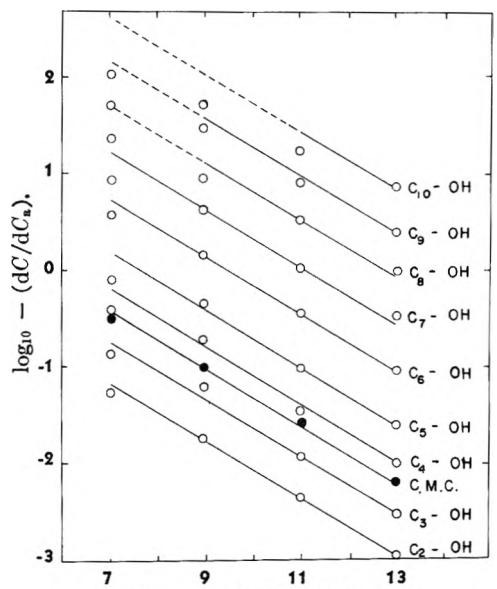

Fig. 14.—The logarithmic relation between the rate of change of CMC with alcohol concentration, dC/dC_a, and the number of carbon atoms in the soap chain.

and dodecanoate; potassium octanoate, decanoate and dodecanoate; potassium decanoate, dodecanoate and tetradecanoate. Some of these data are illustrated on the equilateral triangle in Figs. 15 and 16 together with the calculated equi-CMC lines.

In all the cases studied the CMC of soap mixtures lie between the highest and lowest CMC value of the individual soaps. When the differences in the number of carbon atoms of the mixed soaps are the same, the variation of the CMC is similar.

Discussion

In the process of micelle formation two energy factors are of major importance: a decrease in free energy which is brought about by the transfer of the non-polar portion of the long chain ion from the aqueous environment to the interior of the micelle; and an increase in free energy which is brought about by the aggregation of long chain ions in the micelle.

The addition of alcohol was found to depress the critical concentration according to the equation 2, it is also known that alcohol molecules penetrate the oriented structure of the micelle,[16] forming the mixed micelle. An attempt was made to explain the effect of alcohols on the critical concentration by the decreased charge density on the micelle surface and the decrease in free energy of mixing.

(16) W. D. Harkins, R. W. Mattoon and R. Mittelmann, *J. Chem. Phys.*, **15**, 763 (1947).

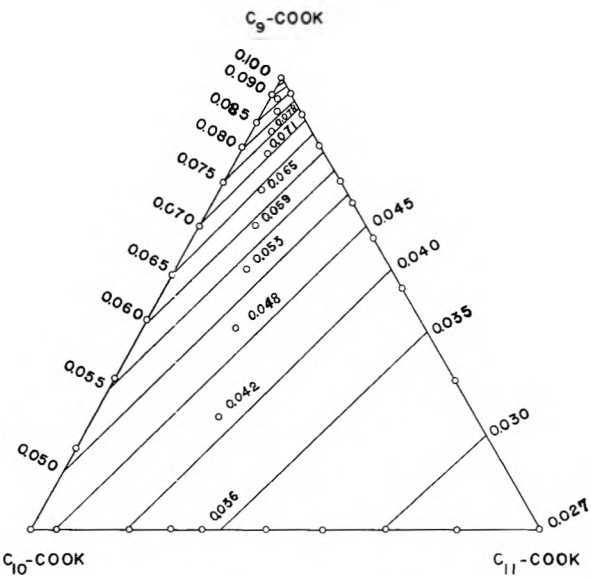

Fig. 15.—Equi-CMC lines of the ternary system potassium decanoate, undecanoate and dodecanoate at 25°.

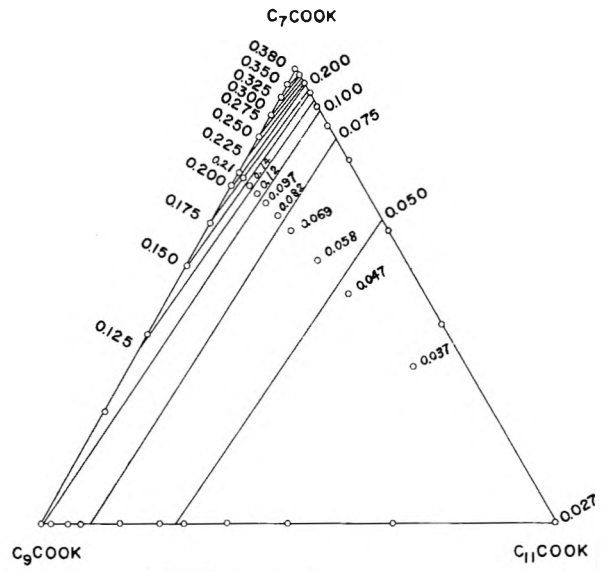

Fig. 16.—Equi-CMC lines of the ternary system potassium octanoate, decanoate and dodecanoate at 25°.

The addition of salt likewise depresses the critical concentration,[12,13] however, this decrease is a result of a decrease in the electronic work per micelle-forming ion.[17,18]

The relationship between the critical micelle concentration and the surface charge density on the micelle is given in the equation[17,18]

$$\log C = K_1\{\log \sigma^2 - \log C_a\} + \text{Const.} \qquad (3)$$

where C is the critical micelle concentration in moles per liter; σ is the surface charge density; C_a is the concentration of counterions in gram equivalents per liter and is equal to the critical micelle concentration in case no salt is added; K_1 is a constant which has a value of 0.56 for fatty acid soaps.[12,13]

Let the mole fractions of alcohol and soap in the mixed micelle be x and $1 - x$, respectively, the critical micelle concentration of this mixed micelle is

$$\log C' = K_1\{\log (1 - x)^2\sigma^2 - \log C_a'\} + \log (1 - x) + \text{Const.} \qquad (4)$$

The difference between equations 3 and 4 is the decrease of surface charge density from σ to $(1 - x)\sigma$ and the addition of the mixing term.

Substituting $K_1 = 0.56$ in equations 3 and 4, we obtain

$$\log C' = \log C + 1.36 \log (1 - x) \qquad (5)$$

or

$$C' \approx C(1 - 1.36x) \qquad x \ll 1 \qquad (6)$$

On the other hand if the energy decrease in the non-polar portion of the alcohol molecule passing from the aqueous environment into the micelle is proportional to the number of carbon atoms in the alcohol, the following expression of the law of partition may be applied

$$C_a/x = K_2 \exp(-m'\omega/kT) \qquad C_a \ll 1 \qquad (7)$$

where K_2 is a constant and ω is the surface energy per methylene radical passing from the aqueous phase into the interior of the micelle. Since at the critical concentration there are few micelles, the fall in alcohol concentration in the aqueous phase due to penetration of alcohol molecules into the micelle is negligible.

Substituting (7) into (6), we obtain

$$C' = C\{1 - K_3C_a \exp(m'\omega/kT)\} \qquad (8)$$

From equation 8, we derive

$$(C - C')/C_a = K_3C \exp(m'\omega/kT) \qquad (9)$$

or

$$\log \frac{(C - C')}{C_a} = \log C + \frac{m'\omega}{kT} + \text{Const.} \qquad (10)$$

Equation 10 corresponds to equation 2; the surface energy change per methylene radical, passing from the aqueous phase into the hydrocarbon environment, ω, is about $1.1kT$, on a gram mole basis it is 620 cal. per mole at 10°.

Extension of the treatment of binary mixtures[9] gives the following equation for the CMC of multicomponent soap mixtures

$$\Sigma C_{m_i}^{1+K} x_i = C_{mix.}^{1+K} \qquad (11)$$

$$\Sigma C_{m_i}^{1+K} \frac{x'_i \exp(m_i\omega/kT)}{\Sigma x'_i \exp(m_i\omega/kT)} = C_{mix.}^{1+K} \qquad (12)$$

where x_i, x_i' are the mole fractions of mixed soaps in the micelle and in the bulk of the solution, respectively; m_i is the number of carbon atoms in the respective soap chain; ω is the surface energy change per methylene radical passing from the aqueous phase into the interior of the micelle, the value of which is $1.1\ kT$[9,18,19]; K is a constant for each homologous series of long chain salts, the value of which in this case is 0.56.[12,13]

It follows from (11) and (12) that all the CMC values fall between the highest CMC and the lowest CMC of the pure soaps. As the logarithm of the CMC is a linear function of the number of carbon atoms in the chain, it is apparent from (11) and (12) that the nature of the equi-CMC lines on the equilateral triangle is similar when the

(17) M. E. Hobbs, THIS JOURNAL, **55**, 675 (1951).
(18) K. Shinoda, *Bull. Chem. Soc. Japan*, **26**, 101 (1953).
(19) J. T. Davis, *Trans. Faraday Soc.*, **48**, 1052 (1952).

differences in the number of carbon atoms of the mixed soaps are the same.

According to the above treatment equi-CMC lines on the triangular diagram are straight. This can be shown as follows: let the three apexes of an equilateral triangle be A, B, and C. Consider a point D(a, o, 1-a) on line BC and another point E(o, b, 1-b) on line AC which give the same values of CMC on the triangle, (a, o, 1-a), etc., express the mole fractions of the respective soaps. Then consider an arbitrary point P on line DE. If we assume DP/DE = λ and PE/DE = $1 - \lambda$, the mole fractions of point P are $a\lambda$, $b(1 - \lambda)$ and $(1 - a)\lambda + (1 - b)(1 - \lambda)$.

Let the number of carbon atoms in the individual soaps which are represented by A, B, and C, be m_1, m_2 and m_3, respectively. From the definition of D and E, it follows that

$$C_{m_1}^{1+K} a + C_{m_3}^{1+K}(1 - a) = C(E)_{mix.}^{1+K} = C(D)_{mix.}^{1+K} = C_{m_2}^{1+K} b + C_{m_3}^{1+K}(1 - b) \quad (13)$$

On the other hand the CMC at point P is, according to (11)

$$C_{m_1}^{1+K} a\lambda + C_{m_2}^{1+K} b(1 - \lambda) + C_{m_4}^{1+K}\{(1 - a)\lambda + (1 - b)(1 - \lambda)\} = C(P)_{mix.}^{1+K} \quad (14)$$

Substituting (13) into (14), we obtain

$$C(P)_{mix.}^{1+K} = C(E)_{mix.}^{1+K}\lambda + C(D)_{mix.}^{1+K}(1 - \lambda) = \text{Const.} \quad (15)$$

Thus all points of the straight line DE have the same CMC values.

Figures 15 and 16 show equi-CMC straight line calculated from equation 12 and experimental values for points of the ternary system. The agreement is within experimental error.

Acknowledgment.—The author is greatly indebted to Prof. K. Kinoshita and Prof. H. Akamatsu for encouragement and kind advice. Some of the experiments were carried out by M. Nōmi.

THE STRUCTURE OF AMORPHOUS MATERIALS

BY MAURICE L. HUGGINS

Communication No. 1666 from the Kodak Research Laboratories, Research Laboratories, Eastman Kodak Company, Rochester, N. Y.

Received June 23, 1954

A theory is presented, according to which various extensive properties (*e.g.*, the volume) of amorphous materials can be computed additively from contributions characteristic of the types of "structon" present, a structon consisting of an atom (or group of atoms or molecule) surrounded by close neighbors in a given way. If the possible types of structon differ sufficiently in stability, the number of such types present in appreciable quantities in a sample at equilibrium is small. If it is the minimum number required to give the correct over-all composition, the sets of structon types present change as suddenly as the composition changes. The property–composition curve then consists of a series of straight-line segments, with sharp breaks between them. Detailed consideration is given to the volumes (and densities) of two-component silicate glasses, especially those in the Na_2O–SiO_2 system. Reasonable sets of structon types account quantitatively for the locations of the observed breaks. In some composition ranges, definite conclusions can be drawn regarding the structon types present, their relative numbers, and their individual contributions to the total volume. In other composition ranges, the possibilities are greatly limited, but alternative interpretations remain.

Introduction

Liquids, solutions and amorphous solids all possess a high degree of randomness of *long-range* structure. There is much more regularity, however, in their *short-range* structure, especially in the distribution of closest neighbors around each of the component units. In certain cases (*e.g.*, in ionic solutions), considerable progress has been made in deducing, theoretically and experimentally, the closest-neighbor arrangements, but much more remains to be done.

Theory and Definitions.—Many extensive properties of condensed systems, amorphous or crystalline, can reasonably be treated as additively constituted of terms characteristic of the different types of neighbor-to-neighbor contact or of terms characteristic of the different types of *structon*, a "structon" being defined, for this purpose, as a single atom (or ion or molecule) surrounded in a specified manner by others.

For example, structon types existing in sodium silicate glasses, according to evidence presented below, include those represented by the following formulas, among others

Si(4O) Na(6O) O(2Si) O(2Si, Na) O(2Si, 2Na) O(Si, 3Na).

The (fractional) numbers of structons of these types, per atom of oxygen in the structure ($N_{Si(4O)}$, $N_{Na(6O)}$, etc.) are easily computed [1–3] from the percentage composition of the material. The sum of the numbers of the oxygen structons must obviously equal one.

Knowledge of the structure of an amorphous material and of the relations between its structure and its properties can be advanced considerably if one can determine what structons are present, their relative numbers, and their individual contributions to the properties of interest. The present paper deals with this problem. To illustrate the assumptions made, methods used and results obtained, the structures and densities of sodium silicate glasses are especially dealt with.

If the free energy of a given quantity of amorphous material, such as an inorganic glass, could accurately be considered as the sum of terms involving only nearest-neighbor arrangements, it might be possible to deduce the free-energy contributions of the structon types under

(1) M. L. Huggins, *J. Opt. Soc. Am.*, **30**, 420 (1940).
(2) M. L. Huggins, *Ind. Eng. Chem.*, **32**, 1433 (1940).
(3) M. L. Huggins and K.-H. Sun, *J. Am. Ceramic Soc.*, **26**, 4 (1943).

consideration and then to compute, for a given composition, which set of structon types would give the lowest free energy. *Approximate* additivity of this sort does in fact exist,[4-6] for the energies, and presumably also for the free energies, of oxygen-containing glasses, but since the entropy and the coulomb energy contributions must depend, not negligibly, on the relative arrangements of (and interactions between) atoms and groups which are not closest neighbors, it seems unlikely that the degree of additivity is sufficient to distinguish between alternative sets of structon types which are energetically not very different. In the present instance, free-energy considerations will be used only in a very general way, to limit the structon types to be considered to those which are energetically possible or probable, distinguishing between these by other means. For this purpose, the entropy differences associated with changes of types of structon may be neglected. Non-neighbor coulomb energies will be considered as favoring structons having small or zero *structon charges* (on the oxygens, in silicate glasses) over those having structon charges which are larger in magnitude. This is similar to, but slightly more general than, Pauling's "electrostatic valence rule."[7] The "structon charge" on an oxygen in a silicate glass is computed by adding algebraically the valence number (-2) of the oxygen and, for each contact between that oxygen and one of its electropositive neighbors, the quotient of the valence number of that neighbor atom, divided by the number of *its* contacts to oxygens. The structon charge is thus computed as if the structure were completely ionic.

For example, if all the silicon and sodium atoms in a glass are surrounded by 4 and 6 oxygens, respectively (*i.e.*, if the only silicon and sodium structons are of the types in the list given above), the structon charges of the other structons listed are, in order: 0, $+1/6$, $+1/3$, and $-1/2$.

The requirement that the glass be neutral may be expressed mathematically by the equation

$$\sum_M \frac{\nu_M}{2} N_M = 1 \qquad (1)$$

where M designates one of the electropositive elements present, ν_M is its valence number, and N_M is the number of atoms of this element per atom of oxygen.

To be definite—probably more so than the assumptions warrant—it can be assumed that, other things being equal, the most stable set of structons is that giving the lowest sum of structon charges, obtained by adding together the product of the structon charge for each type and the number of such structons present.

Aside from the longer-range coulomb energies just dealt with, one can consider the total energy (or the total stability) as additively made up of contributions of the structons present, each depending only on nearest-neighbor interactions. In considering the relative contributions of different types of structon, covalent bond requirements and coördination number limitations are especially important. Knowledge of the structon types existing in comparable crystals and molecules is often helpful. In certain systems (*e.g.*, the sodium silicate glasses), experimental evidence regarding the limits of concentration ranges, each corresponding to a set of structon types, can be very useful in distinguishing between different hypothetical sets, as will be shown.

The numbers and kinds of structon present in a given material under given conditions are, of course, limited by the relative numbers of atoms of the different elements present. If equilibrium exists at a given temperature and if one set of types is sufficiently more stable than any other which is possible with the same over-all compositions, then the most stable set will be present to the practical exclusion of all others. If, however, alternative sets of types have nearly the same (free) energy, structons of both sets will be present. The higher the temperature, the greater the energy difference between the most stable set and the next most stable set which is required to make the former predominate.[8,9] With silicate glasses, the temperature concerned is the lowest temperature at which equilibrium exists, *i.e.*, at which changes from less stable to more stable structons can occur in the time available. In a silicate glass melt, it is probable that many structons are present other than those corresponding to the most stable set. Quenching freezes in these non-equilibrium structures. Lowering the temperature slowly, on the other hand, gradually changes the less stable structons to those which are more stable, until the temperature range is reached in which the atomic shifts necessary for these changes can no longer occur in the time available. The most stable set of structons may or may not be the only ones remaining and persisting as the glass is cooled to still lower temperatures. Evidence will be presented to show that in certain well-annealed sodium silicate glasses structon equilibrium has been practically completely attained, with only the structons of the most stable set present to any appreciable extent in each glass. It is probable, however, that in many other cases, even of well-annealed glasses, this state of affairs does not exist.

It is convenient to deal with the quantity of glass which contains one gram-atom of oxygen. The volume of this quantity (in ml. at 20°) will be designated as V_O. The structon volumes (*i.e.*, the contributions of the various structon types to the total volume per gram-atom of the central atom) will be represented as $v_{Si(4O)}$, $v_{Na(6O)}$, etc. Assuming additivity

$$V_O = \Sigma N_{\ldots} v_{\ldots} \qquad (2)$$

The magnitudes of the individual structon volumes (v) cannot be determined, other than by arbitrary definition. One may use, instead, the

(4) M. L. Huggins and K.-H. Sun, *J. Am. Ceramic Soc.*, **28**, 149 (1945).

(5) M. L. Huggins and K.-H. Sun, THIS JOURNAL, **50**, 319 (1946).

(6) K.-H. Sun and M. L. Huggins, *ibid.*, **51**, 438 (1947).

(7) L. Pauling, "The Nature of the Chemical Bond," 2nd ed., Cornell Univ. Press, Ithaca, New York, N. Y., 1940, p. 384.

(8) M. L. Huggins, THIS JOURNAL, **47**, 502 (1943).

(9) M. L. Huggins, K.-H. Sun and A. Silverman, in "Colloid Chemistry, Theoretical and Applied," Vol. V, edited by J. Alexander, Reinhold Publ. Corp., New York, N. Y., 1944, pp. 308–326.

cell volumes (v^*. . .), each being defined as the sum of the structon volume [$v_{O(\ .\ .\ .)}$] of an oxygen structon and its share of the structon volumes of the neighboring structons. Thus

$$v^*_{2Si} = v_{O(2Si)} + \frac{1}{2} v_{Si(4O)} \quad (3)$$

$$v^*_{2Si,Na} = v_{O(2Si,Na)} + \frac{1}{2} v_{Si(4O)} + \frac{1}{6} v_{Na(6O)}, \text{ etc.} \quad (4)$$

The cell volumes can be evaluated experimentally. The sum of the appropriate cell volumes, each multiplied by the number (per oxygen) of the corresponding oxygen structon, equals V_O.

Pure Silica.—In crystalline silica, *e.g.*, quartz, as first shown by the writer,[10] each silicon atom is surrounded tetrahedrally by four oxygen atoms and each oxygen atom has two silicon neighbors. The only structons present are Si(4O) and O(2Si).

A structure of the same sort, but possessing long-range randomness, would be expected for vitreous silica. The X-ray diffraction data obtained from this material conform to this expectation.[11]

There being only one type of oxygen structon in (crystalline or vitreous) silica

$$N_{O(2Si)} = 1 \quad (5)$$

From the formula, SiO_2

$$N_{Si(4O)} = N_{Si} = 1/2 \quad (6)$$

From the additivity assumption

$$V_O = N_{Si(4O)} v_{Si(4O)} + N_{O(2Si)} v_{O(2Si)} = v^*_{2Si} \quad (7)$$

For well-annealed silica glass, this volume is 13.63 ml. at 20°.[12] We shall assume this same value to hold in all silicate glasses.

Two-component Silicate Glasses.—The density of well-annealed sodium silicate glasses is not a smooth function of the composition; the curve representing this dependence exhibits definite discontinuities.[1,13–15] This is strikingly shown, for example, by Fig. 1. The data are well represented by a series of connected straight lines.

Other two-component silicate glasses exhibit a similar behavior, although the data which can be used for determining the quantitative relationships are much less satisfactory than in the sodium silicate case.

The hypothesis that the breaks found experimentally are at compositions of specific compounds, a glass having a composition between those of two breaks consisting of a solid solution of two of these compounds, is contradicted by a large amount of X-ray diffraction evidence.[11]

The writer[1] has proposed that the straight-line regions and breaks are related to the types of structure of the silicon–oxygen units (silicate "ions," if, as a convenient approximation to the truth, one considers the oxygen atoms to be covalently bonded to each adjacent silicon atom, but to no atoms of other elements). Suggestions have been made[1,9,16] with regard to the compositions and structures of some of the silicate "ions" present in the different composition ranges, but no thorough study of the situation has previously been published.

Range I.—Consider two-component silicate glasses having relatively small amounts of the non-silica component. Reasoning either from knowledge of the structures of crystalline silicates or from the principle of minimum effective charge sum (to give minimum coulomb energy), the following seem the most likely structon types

Set I: Si(4O) M(zO) O(2Si) O(2Si, M) O(Si, yM)

The first and third of these structon types exist in pure silica and would certainly be expected in glasses having, in addition, only small amounts of other components. The second is to be expected from energy considerations and is always found in crystalline silicates. (Here "z" denotes the coördination number of the M atom or ion; for the present, we consider it an unknown, but constant within this composition range.) The last (with y a constant integer) is to be expected on similar grounds. One might conceive of a structure containing, instead, structons of the type O(xM), but these would be energetically unreasonable and are not found in the structures of comparable crystals.

The charges on the oxygen structons listed above are 0, $+ \nu/z$, and $y\nu/z - 1$, respectively.[17] The last becomes zero if $y = z/\nu$. In such a case, structons of the type O(2Si, M) would be absent if conditions are such as to permit the minimum number of structons. For most components of interest, however, values of y and z conforming to this requirement are impossible, or at least unreasonable, requiring high van der Waals repulsion energies.

Assuming the structon types of set I to be the correct ones (and the only ones) in a well-annealed glass in this composition range, it is easy to calculate the limits of the range (one, of course, being $N_{Si} = 1/2$; $N_M = 0$) and, within these limits, the relative numbers of the different structon types. The sum of the numbers of oxygen structons equals unity

$$N_{O(2Si)} + N_{O(2Si,M)} + N_{O(Si,yM)} = 1 \quad (8)$$

The number of O → Si contacts equals the number of Si → O contacts

$$2N_{O(2Si)} + 2N_{O(2Si,M)} + N_{O(Si,yM)} = 4N_{Si(4O)} = 4N_{Si} = 2 - \nu N_M \quad (9)$$

The number of O → M contacts equals the number of M → O contacts

$$N_{O(2Si,M)} + yN_{O(Si,yM)} = zN_{M(zO)} = zN_M = \frac{2z}{\nu} - \frac{4z}{\nu} N_{Si} \quad (10)$$

From these equations, one obtains the following

$$N_{Si(4O)} = N_{Si} = \frac{1}{2} - \frac{\nu}{4} N_M \quad (11)$$

(10) M. L. Huggins, *Phys. Rev.*, **19**, 363 (1922).

(11) B. E. Warren, *J. Applied Phys.*, **8**, 645 (1937); *J. Am. Ceramic Soc.*, **24**, 256 (1941).

(12) R. B. Sosman, "The Properties of Silica," Reinhold Publ. Corp., New York, N. Y., 1927.

(13) F. W. Glaze, J. C. Young and A. N. Finn, *J. Research Natl. Bur. Standards*, **9**, 799 (1932).

(14) J. C. Young and A. N. Finn, *Glass Industry*, **19**, 172A (1938).

(15) M. L. Huggins and K.-H. Sun, *ibid.*, **24**, 472 (1943).

(16) M. L. Huggins, K.-H. Sun and A. Silverman, *J. Am. Ceramic Soc.*, **26**, 393 (1943).

(17) Here, and in the remainder of this paper, the valence of the electropositive element, other than silicon, is represented merely by ν, without a subscript. In treating glasses of more than two components, subscripts are of course needed.

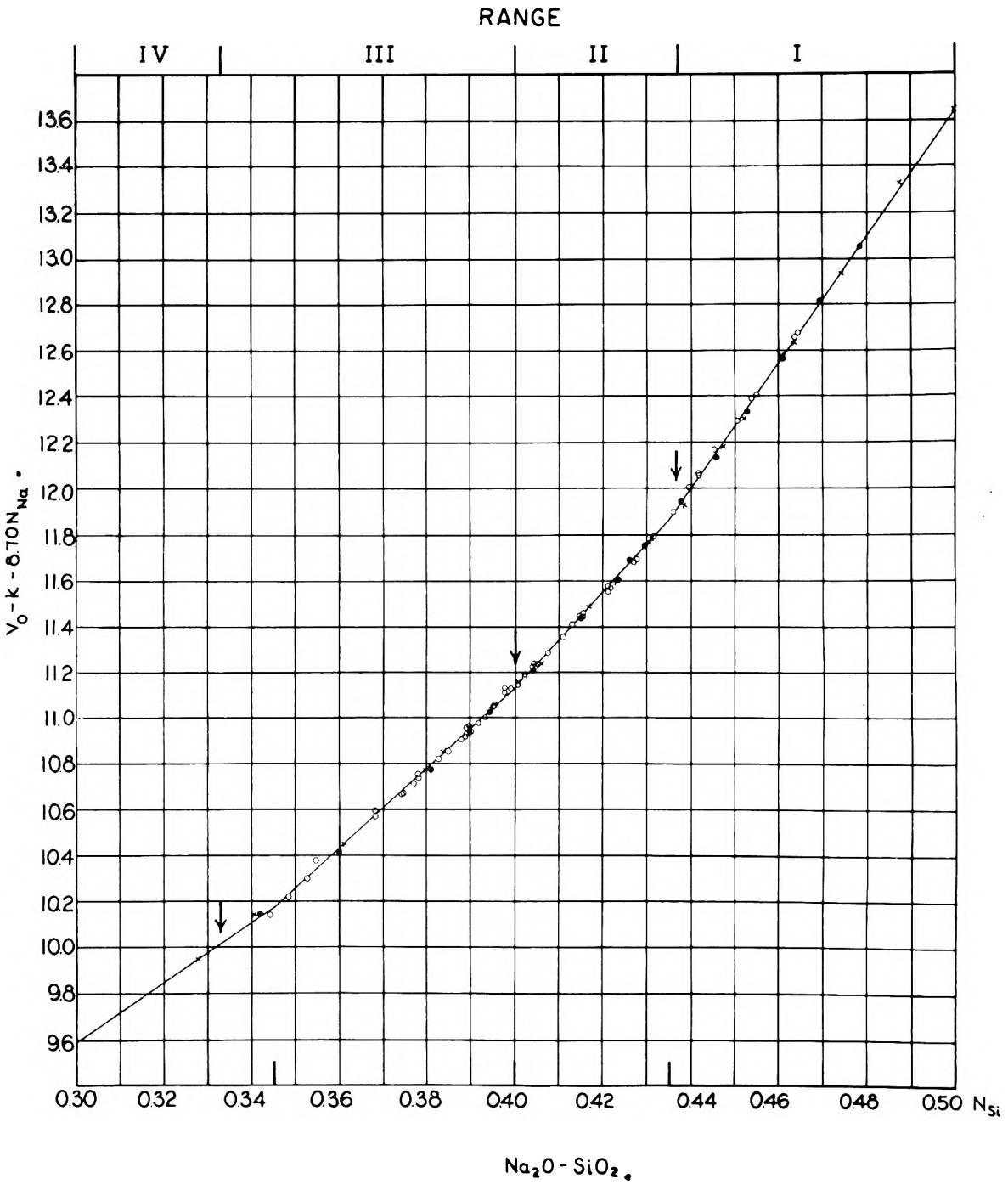

Fig. 1.—Volume–composition dependence for sodium silicate glasses (k is a small constant inserted to allow for differences in annealing techniques[1]): ×, Morey and Merwin, *J. Opt. Soc. Am.*, **22**, 632 (1932); ○, Glaze, Young and Finn, *J. Research Natl. Bur. Standards*, **9**, 799 (1932); ●, Winks and Turner, *J. Soc. Glass Tech.*, **15**, 185 (1931).

$$N_{M(zO)} = N_M = \frac{2}{\nu} - \frac{4}{\nu} N_{Si} \qquad (12)$$

$$N_{O(2Si)} = (-2w - 1) + (4 + 4w)N_{Si} = 1 - \nu(w + 1)N_M \qquad (13)$$

$$N_{O(2Si,M)} = 2w - 4wN_{Si} = \nu w N_M \qquad (14)$$

$$N_{O(Si,yM)} = 2 - 4N_{Si} = \nu N_M \qquad (15)$$

For convenience the abbreviation

$$w = z/\nu - y \qquad (16)$$

is here introduced.

At one limit (pure SiO_2) of this composition range $N_{M(zO)}$, $N_{O(2Si,M)}$ and $N_{O(Si,yM)}$ are all equal to zero, and

$$N_{Si} = 1/2; \quad N_M = 0 \qquad (17)$$

The other limit of Range I is at the composition (highest N_{Si}) at which the number of structons of any of the characteristic types first becomes zero. Inspection of eq. (11) to (15) shows that O(2Si) is the first to disappear. From eq. (13), then

$$N_{Si} = \frac{1 + 2w}{4 + 4w} \qquad (18)$$

or

$$N_M = \frac{1}{\nu(w+1)} \quad (19)$$

The volume per gram-atom of oxygen in the structure is

$$V_O = [(-1-2w)v^*_{2Si} + (2w)v^*_{2Si,M} + 2v^*_{Si,yM}] + [(4+4w)v^*_{2Si} - (4w)v^*_{2Si,M} - 4v^*_{Si,yM}]N_{Si} \quad (20)$$

or, equivalently

$$V_O = v^*_{2Si} + [-\nu(w+1)v^*_{2Si} + (\nu w)v^*_{2Si,M} + \nu v^*_{Si,yM}]N_M \quad (21)$$

These equations represent a straight-line dependence of V_O on N_{Si} (or on N_M), as found experimentally for the Na_2O–SiO_2 system. The slope and the (lower N_{Si}) limit of this composition range (in which the structon types listed can coexist, without others) both depend on w, hence on y and z.

From the sodium silicate data (Fig. 1), the lower limit of this range is at an N_{Si} value of about 0.43_5. This is in excellent agreement with eq. 18, giving, for this limit[18]

$$N_{Si} = \frac{7}{16} = 0.4375 \text{ (or } N_{Na} = 0.250) \quad (22)$$

provided w is given the value 3.

This can be considered as confirmation of the present theory and of the set of structon types listed above for range I. No other set which could be considered at all reasonable yields this result. In this system at least, careful annealing produces glasses in which these types are present to the practical exclusion of all others. Moreover, from the value of w (equal to $z - y$ in this system) which has been deduced one can conclude that z is equal to 6 and y is equal to 3, these values being more reasonable than any other combination of z and y values (giving w equal to 3), on the basis of present knowledge of the structures of crystalline silicates and related compounds containing sodium.

Substituting into eq. (20) and (21), we obtain

$$V_O = (-95.41 + 6v^*_{2Si,Na} + 2v^*_{Si,3Na}) + (218.08 - 12v^*_{2Si,Na} - 4v^*_{Si,3Na})N_{Si} \quad (23)$$

or

$$V_O = 13.63 + (-54.52 + 3v^*_{2Si,Na} + v^*_{Si,3Na})N_{Na} \quad (24)$$

Using the constants previously deduced[1] empirically for this range

$$V_O = 27.26N_{Si} + 8.7N_{Na} = 17.4 - 7.54\,N_{Si} = 13.63 + 1.88_5N_{Na} \quad (25)$$

Hence

$$v^*_{Si,3Na} = 56.405 - 3v^*_{2Si,Na} \quad (26)$$

The volume of glass per gram-atom of oxygen at $N_{Si} = 0.4375$, the lower limit of range I, obtained by substituting eq. (22) into eq. (25), is 14.10_{125}.

Throughout this range, the Si–O structure is essentially a network. Although some relatively small silicate "ions," *e.g.*, of the composition $Si_4O_{10}^{-4}$ and structure like that of the P_4O_{10} molecule,[19] are possible without contradicting our postulates, one can conclude from probability considerations that these would not be numerous. The chance that any given oxygen atom does not bridge between two silicons is given by the value of $N_{O(Si,yM)}$, eq. (15). This varies (for sodium silicates) from zero to one-fourth. Of the four oxygens around each Si, the average number which are non-bridging is

$$\frac{N_{O(Si,3M)}}{N_{Si}} = \frac{2}{N_{Si}} - 4 \quad (27)$$

varying from zero to 4/7, in this range.

Range II.—For the next composition range, all sets of structon types which, on other grounds, appear at all reasonable, have been tested, by methods similar to those used for range I. The only set which is satisfactory for the sodium silicates, accounting for the break experimentally found at $N_{Si} = N_{Na} = 0.40$, is

Set II: Si(4O) M(zO) O(2Si, M) O(2Si, 2M) O(Si, yM)

with w (equal to $z - y$) again equal to 3, hence, probably, z equal to 6 and y equal to 3.

Using the experimental value of V_O at the break

$$V_O = 19.89_{67} - 13.24_{67}N_{Si} = 13.27_{33} + 3.31_{17}N_{Na} \quad (28)$$

In this range, as in range I, the Si–O structure is essentially of a network type. The chance that an oxygen atom is non-bridging varies from $^1/_4$ to $^2/_5$. From $^4/_7$ to 1 of the four atoms of each SiO_4 group, on the average, are non-bridging. The chance of the existence of small silicate ions, such as the $Si_4O_{10}^{-4}$ ions already mentioned, increases as N_{Si} decreases.

Range III.—Proceeding to glasses of lower silica content, reasonable sets of structon types are

Set IIIa: Si(4O) M(zO) M[(z − 1)O] O(2Si, 2M) O(Si, yM)

valid between $N_{Si} = 0.400$ and $N_{Si} = 0.375$, and

Set IIIb: Si(4O) M[(z − 1)O] M[(z − 2)O] O(2Si, 2M), O(Si, yM),

valid for $0.375 > N_{Si} > 0.333$.

The experimental data show no obvious break at $N_{Si} = 0.375$. This is readily accounted for by the not unreasonable assumption that

$$v_{M(zO)} - v_{M[(z-1)O]} \approx v_{M[(z-1)O]} - v_{M[(z-2)O]} \quad (29)$$

Another possible pair of structon sets for range III would include O[Si, (y + 1)M] and O[Si, (y + 2)M], instead of M[(z − 1)O] and M[(z − 2)O]. These would give the same range limits.

Still a third pair of sets would include the structon types O(2Si, 3M) and O(2Si, 4M). This pair would result in a possible slight break at $N_{Si} = 0.375$ (as for the others), but a lower limit of 0.357. Still other possibilities are conceivable, at least for the range below 0.375. The experimental data now available do not suffice to distinguish between these.

Regardless of which set of structon types is the correct one, the fraction of oxygen atoms which are non-bridging is equal to νN_M or $2-4N_{Si}$; as N_{Si} changes from 0.40 to 0.33, this fraction changes from 0.40 to 0.67. Of the four oxygens around each Si, the average number which are non-bridging varies from 1 to 2. At the high-silica end of the range, the silicon–oxygen structure is still essentially a network. At the low-silica end, it would

(18) According to this interpretation, the limit of this range is at the composition of the hypothetical compound $2Na_2O{\cdot}7SiO_2$, not, as previously supposed,[1] at the composition of $3Na_2O{\cdot}10SiO_2$, for which $N_{Si} = 10/23 = 0.4348$.

(19) G. C. Hampson and A. J. Stosick, *J. Am. Chem. Soc.*, **60**, 1814 (1938).

better be described as primarily a chain structure, with some cross-links. At the lower limit (taken as $N_{Si} = 1/3$), the number of branch junctions equals the number of chain ends (counting each silicon surrounded by one non-bridging and three bridging oxygens as a *single* junction and each silicon surrounded by four bridging oxygens as *two* junctions). Although the over-all composition and the requirements of the present analysis would be satisfied if all the silicons in the glass were tied together by oxygens into a single macro-ion

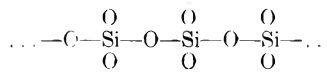

this would be statistically improbable.

Range IV.—Various sets of structon types are also possible, on the basis of our present knowledge, for glasses having still lower N_{Si} values (less than 0.33, in the Na_2O–SiO_2 system). One such set would be

Set IV: Si(4O) M[(z − 2)O] O(2Si, 2M) O(Si, yM) O[Si, (y + 1)M].

The lower limit of its range of existence would be (for the sodium silicates)

$$N_S = 0.25; \quad N_{Na} = 1.00 \qquad (30)$$

Glasses in this range can be considered as composed primarily (as regards their silicons and oxygens) of chain ions, of various lengths. Neglecting branching, the average number ($\bar{n}$) of silicon atoms per chain ion is given by the relation

$$\bar{n} = \frac{N_{Si}}{1 - 3N_{Si}} \qquad (31)$$

At the limit given by eq. 30, the average value of $\bar{n}$ is 2. A sodium silicate of this composition would be expected to consist primarily of $Si_2O_7^{-6}$ ions and sodium ions, with some SiO_4^{-4} ions and some $Si_3O_{10}^{-8}$ and a few even larger ions.

The Structon Number Rule.—Let us consider the relationship between the minimum number (S) of structon types possible for a given system, the number (C) of components (Na_2O, SiO_2, in the sodium silicate glasses), and the number (F) of degrees of freedom (considering composition variables only). To specify the number of structons of each type, one needs S numbers, hence S independent equations to determine them. For each component, there is an equation expressing the fact that, for the metal atom concerned (Na or Si), the total number of metal–oxygen contacts equals the total number of oxygen–metal contacts. There is also an equation to express the fact that the total number of oxygen-centered structons equals unity, and another to express the neutrality relationship. If the number of structon types equals the number of these equations, the composition is obviously fixed, hence $F = 0$. If the number of structon types is greater than the number of equations (of the kinds just discussed), the excess gives the number of degrees of composition freedom. Hence

$$S = C + F + 2 \qquad (32)$$

For sodium silicate glasses, there are two components. For each of the composition ranges considered, F equals 1. Hence, the minimum number of structon types in each set is 5. At the joints between ranges, F is zero and S is 4.

In those special cases in which all the structon charges are individually zero, as in pure SiO_2 itself, the neutrality requirement reduces to 0 = 0. This cannot be used to compute the numbers of the different kinds of structons, hence, in place of eq. (32)

$$S = C + F + 1 \qquad (33)$$

These two equations, together, may be designated as the *structon number rule*, by analogy with the phase rule.

Summary and Conclusions

It has been assumed that many extensive properties, such as the volume, of amorphous substances can be treated as additively composed of contributions of their "structons," also that this is approximately true of their stability (the negative of the free energy). As a result of this, one would expect a relatively small number of types of structon to exist in a sample which is at equilibrium, as regards the distribution of the component units, or which has had an equilibrium situation frozen in (as in a glass), especially if the relative stabilities of the different structon types differ sufficiently.

If the number of structon types present is the *minimum* number required to give neutrality and the correct over-all composition, the additivity postulate requires that the property–composition curves be series of connected straight lines, as observed experimentally for well-annealed sodium silicate glasses. For any assumed set of structon types, their relative numbers and the existence limits of the set are readily calculated. It has been shown that reasonable sets will account quantitatively for the locations of these limits (the breaks in the volume–composition curve). From the experimental slopes, one can compute relationships between the volume contributions of the different types of structon, but their absolute values cannot be deduced from a study of this one system alone.

The minimum number of structon types needed for any given composition or composition range has been shown to be derivable from the number of components by a relationship, analogous to the phase rule, which has been designated the *structon number rule*.

The procedures to be used in extending the application of the theory to other properties and to other glass systems, other amorphous solids (*e.g.*, certain types of high polymers), liquids and solutions, should be obvious. In many cases, unfortunately, the required experimental data are not now available and must be obtained by new research. Also, such quantitative results as those obtained in the present study of sodium silicate glasses can hardly be expected, except in those cases in which the interactions between the atoms, groups of atoms, or molecules concerned can be classified into a sufficiently small number of types, with these differing sufficiently in stability. At a later date, the author hopes to present examples of the application of the theory to such cases.

THE ABSORPTION AND LIGHT SCATTERING OF VANADIUM PENTOXIDE HYDROSOLS[1]

BY MILTON KERKER, GEORGE L. JONES, JR., JAMES B. REED, CYNTHIA N. P. YANG AND MELVIN D. SCHOENBERG

Department of Chemistry, Clarkson College of Technology, Potsdam, New York

Received June 28, 1954

Vanadium pentoxide hydrosols, prepared by the hydrolysis of *t*-amyl orthovanadate, have been studied by optical absorption, light scattering and electron microscopy. These sols consist of long needle-like particles. Absorption is due to both scattering and true absorption within the particles. Electron microscopy shows that as the sol ages, the micelles are redistributed from numerous small rods to a smaller number of large filaments. This change is accompanied by up to thirty-fold increase in the optical density and more than one hundred-fold increase in light scattering. The magnitude of the increase in absorption is larger than anticipated by available theory. Gans' theory, applicable to small ellipsoids, predicts a very small increase in absorption. Mie's theory, applicable to spheres, does predict an appreciable increase in absorption but not of the magnitude observed for this system. A satisfactory theory of scattering by ellipsoids must account for these increases quantitatively and should differentiate the effect of size from shape. The vertical component of the scattered light is more intense than the horizontal. The scattering is more intense in the forward than in the backward direction. The vanadium pentoxide hydrosols are dissolved by dilution of the sol, and this is followed by slow fading of the optical density and scattering. Electron microscopic observations show that partial solution of the colloidal particles and not homogeneous ionic processes, as previously reported, causes this fading. A new value of the solubility of vanadium pentoxide, differing by more than 35% from the most recent value in the literature is reported (*i.e.*, our value, 0.0296 g./100 cc. at 25°). The molar extinction coefficient of homogeneously dissolved vanadium pentoxide is reported from λ 268 mμ to λ 470 mμ.

1. Introduction

The scattering of electromagnetic waves by particles of the same or somewhat smaller order of magnitude as the wave length of the radiation has been widely used in recent years to obtain information about the scattering particles. The direct information sought is the particle size and shape, and from these such dynamic processes as the growth, coagulation or settling of a system of particles can be followed. Colloidal systems such as aerosols, hydrosols and solutions of high molecular weight substances have been investigated by light scattering,[2] whereas, short wave length radio waves (radar) have been used to study atmospheric rain, snow, and clouds.[3]

The interpretation of scattering data is usually based either upon the work of Mie[4] or that of Smoluchowski,[5] Einstein,[6] and Debye.[7] The Mie theory treats the scattering of a parallel, linearly polarized electromagnetic wave by a spherical, optically homogeneous particle. There are no restrictions upon the size of the sphere or the optical constants. The solution follows rigorously from Maxwell's theory of electromagnetism and gives the intensity of radiation scattered in a given direction as a function of the size and optical constants of the particle, and the wave length and polarization of the incident radiation. The absorption of radiation by the particle can also be determined.

The Mie equations are complicated, and the computation of scattering functions is tedious. The equations become simpler as the particle size relative to the wave length decreases, and for a particle radius less than one-twentieth the wave length of the radiation, the Mie theory coincides with the Rayleigh equation for scattering by small particles.[2a] The Rayleigh equation is the basis of the treatment of scattering by Smoluchowski and Einstein. Their results have been extended by Debye to the determination of the molecular weights of high polymeric materials.

This paper will present the results of an experimental investigation of the scattering and absorption of light by a system of non-spherical particles, the ester hydrosol of vanadium pentoxide. Besides being non-spherical, these particles are further characterized by their appreciable absorption of light. The sols were also studied by electron microscopy in order to correlate the scattering and absorption with the size and shape of the particles.

There is no rigorous solution of scattering by non-spherical particles, although attempts have been made.[8,9,10] Approximate solutions have been carried out by Gans,[11] Debye,[7] and Montroll and Elliot.[12] Gans' treatment for small ellipsoids of revolution is applicable to absorbing as well as dielectric media and was used to analyze our data.

2. Experimental Procedure

A. Preparation of Vanadium Pentoxide Hydrosols.—Vanadium pentoxide hydrosols are usually prepared by the peptization of vanadium pentoxide by washing through a filter paper and subsequent dialysis (Biltz sols). Huber and Zbinden[13] have investigated the size distribution of such sols with the electron microscope and have found that they are relatively more polydispersed than those formed by the hydrolysis of the esters of orthovanadic acid. We have accordingly prepared our sols by the latter procedure.

A number of esters of orthovanadic acid were explored including the ethyl, *n*-propyl, isopropyl, *n*-butyl, isobutyl, *n*-amyl and *t*-amyl esters. The lower molecular weight esters hydrolyzed extremely rapidly and decomposed in the presence of small amounts of moisture. The *t*-amyl ester was sufficiently stable so that it could be stored for

(1) Supported in Part by N.A.C.A. Contract NAw-6206.

(2) (a) G. Oster, *Chem. Revs.*, **43**, 319 (1948); (b) D. Sinclair and V. K. La Mer, *ibid.*, **44**, 245 (1949).

(3) D. Atlas, M. Kerker and W. Hitschfeld, *J. Atm. and Terrest. Phys. (London)*, **3**, 108 (1953).

(4) G. Mie, *Ann. phys.*, **25**, 377 (1908).

(5) M. Smoluchowski, *ibid.*, **25**, 205 (1908).

(6) A. Einstein, *ibid.*, **33**, 1275 (1910).

(7) P. Debye, *J. Appl. Phys.*, **15**, 338 (1944).

(8) F. Moglich, *Ann. phys.*, **83**, 609 (1927).

(9) F. W. Schultz, Report UMM-42, March 1, 1950, Aeronautical Research Center, Engineering Research Institute, University of Michigan.

(10) Since the preparation of this paper, a paper by A. F. Stevenson, *J. Appl. Phys.*, **24**, 1134 (1953), may provide a method of obtaining an exact solution of scattering by non-spherical particles.

(11) R. Gans, *Ann. phys.*, **37**, 881 (1912).

(12) E. W. Montroll and R. Hart, *J. Appl. Phys.*, **22**, 1278 (1951).

(13) K. Huber and H. Zbinden, *Z. anorg. Chem.*, **258**, 138 (1949).

extended periods without decomposition. It was used to prepare all the sols upon which we report light scattering results.

The ester was prepared by refluxing dry V_2O_5 with *t*-amyl alcohol and purified by distillation between 125–130° under 2–3 mm. pressure.

The hydrosol was formed by adding the ester dropwise to 100 ml. of triply-distilled water maintained at 30°. A special dropping apparatus was constructed which delivered a uniform drop of ester weighing 0.0103 ± 0.0003 g. The ester formed a surface layer which hydrolyzed at the interface, the vanadium pentoxide diffusing throughout the solution aided by gentle stirring.

The sols were analyzed for vanadium content by reduction to tetravalent vanadium with sulfur dioxide and subsequent titration with potassium permanganate to quinquevalent vanadium.[14]

B. Light Scattering.—Light scattering measurements were taken with an Aminco light scattering microphotometer. A cylindrical light scattering cell with a flat entrance window was used. The cell was 12 mm. in radius and 55 mm. high. The mercury vapor lamp normally used in the instrument was replaced by a tungsten filament projection lamp. The 4 × 8 mm. beam forming nosepiece, and the 10° solid angle receiver nosepiece were used.

With no polaroids in the optical path, the intensity of scattered light was designated U. When the scattered beam passed through a polaroid which transmitted light whose electric vector was perpendicular to the plane of observation, its intensity was designed V. With the polaroid oriented to transmit light whose electric vector vibrated in the plane of observation, the scattered light was designated H. U, V and H were determined at several angles of observation, γ. γ is defined as the angle formed by the scattering direction and the direction of propagation of the incident beam.

C. Optical Density and Differential Refractive Index.—The optical density of the sols was obtained with a model D. U. Beckman quartz spectrophotometer, using 1-cm. fused silica cells. The differential refractive index was determined with a Phoenix Differential Refractometer.

D. Electron Microscopy.—The electron microscope used was an RCA Model EMT. All photographs were taken with the 3000× pole piece in position. The actual magnification on the 2″ × 2″ lantern slide as calibrated with a ruled grating was 2570×.

Samples for the electron microscope were prepared by depositing a droplet of sol upon a grid coated with a water cast collodion film and withdrawing the excess sol. This gave better separation of colloidal particles than a spray technique which utilized a capillary spray gun. Some samples were shadow cast with gold in an RCA type EMV-6 Shadowing Unit at a shadowing angle of 12°. Although polystyrene gave clear shadows it was not possible to detect shadows associated with the vanadium pentoxide particles. This may have been due to the lower resolving power of our instrument since pictures taken with the Type EMU microscope in another laboratory did show shadows which indicated that the particles were lying flat on the film. Since the vanadium pentoxide scatters electrons sufficiently to give a clear picture, and the particles were lying down, there was no particular advantage to shadowing. Therefore, it was omitted in the work reported here.

3. The Absorption and Light Scattering of Aging Sols

Although Huber and Zbinden had found that the sols prepared by ester hydrolysis stabilized somewhat after a month, they did not report their behavior during the first month after preparation. We found that the sols were not at all stable during this initial period. This aging of vanadium pentoxide sols can be attributed to growth from small rods to long filaments. We have followed the aging spectrophotometrically and by light scattering in order to determine the effect of the changing particle size and shape upon absorption and scattering.

The change in particle form is clearly apparent upon electron microscopic examination.[15] Fresh sols consist of small rods, practically all of which are under 1000 Å. in length, whereas, as progressively older samples are examined, the length of the particles increases. Thus, a sol whose concentration is 0.285% V_2O_5 by weight shows very few particles shorter than 15,000 Å. 48 hours after preparation. The particle concentration is correspondingly smaller in the aged sols.

Assuming that solution equilibrium is established shortly after preparation of the sol, the total volume of vanadium pentoxide in the colloidal state should be constant throughout this growth process. As we will presently show, the absorption and scattering of a sol increases markedly as it ages, thus demonstrating the dependence of absorption and scattering upon particle size and shape rather than upon the total volume of colloidal material.

The behavior of three sols, designated as sol I (0.095%), sol II (0.190%), and sol III (0.285%) will be examined. The optical density of each of these at various times after their formation is presented in Table I. The optical density increases rather rapidly at first and then levels off after several days. This increase is depicted graphically in Fig. 1 for the three sols at three convenient wave lengths. Sol III, the most concentrated, levels off after about ten days, whereas sol I is still increasing at an appreciable rate after 39 days. The corresponding elongation of the particles shown by the electron micrograph suggests that this increasing absorption is due to the growth of the colloidal particles. That the increase in absorption is actually due to the colloidal material and not to the formation of molecular species dissolved in the homogeneous phase, can be shown by filtering a dark red, aged sol through a micro filter. The filtrate has the light yellow color of a homogeneous solution of vanadium pentoxide.

The total absorption in a colloid is the result of two factors, the true absorption of energy within the particle which is dissipated as heat, and the lateral scattering of radiation. Before attempting to interpret the darkening of the aging sols, let us consider whether there is also an influence of particle size and shape upon the light scattering alone.

The true absorption of light by these sols is considerable and has an influence upon the scattered light observed. Even in the aged sols, the scattering contributes only a small fraction to the total attenuation of light. In an absorbing system, the incident beam is attenuated en route to a potential scatterer, and after being scattered continues to be attenuated on the way out of the solution. Therefore, the light actually scattered will be greater than that observed. We have corrected the observed intensities of scattered light for this absorption effect by the following procedure.

If the transmission of a sol at wave length λ is T_λ, and the diameter of the cylindrical scattering cell is δ, a beam of light scattered at the center of

(14) W. Hillebrand, G. Lundell, H. Bright and J. Hoffman, "Applied Inorganic Analysis," John Wiley and Sons, Inc., New York, N. Y., 1953, p. 458.

(15) A more complete report, obtainable from the National Advisory Committee for Aeronautics, includes electron micrographs.

TABLE I

INCREASE OF OPTICAL DENSITY WITH TIME

Sol	Age, days	Wave length, mμ 470	490	510	530	546	560	580	600	625	350
	0	1.736	0.753	0.257	0.086	0.056					
	1	2.4	1.273	0.571	0.284	0.196					
	2		1.479	0.719	0.367	0.249					
I	6			1.194	0.701	0.494	0.382				
	8			1.597	0.890	0.630	0.496	0.373			
	14				1.237	0.881	0.715	0.549	0.454	0.406	
	22				1.475	1.102	0.882	0.698	0.596		0.518
	39				1.697	1.263	1.027	0.815	0.709	0.640	0.621
	0		1.450	0.558	0.208	0.108		0.044			
	3				1.645	1.072	0.744	0.436			
II	12						1.680	1.082	0.643	0.373	0.272
	18						1.825	1.210	0.753	0.453	0.337
	38						1.984	1.351	0.839	0.506	0.384
	0				1.255	0.760	0.504	0.290	0.160		0.053
	2							1.745	0.962		0.319
III	9								1.725	1.039	0.799
	17								1.728	1.095	0.873
	36								1.761	1.132	0.900

the cell will emerge reduced in intensity over its value for a non-absorbing system by the factor $T\delta$.[16] If the product of the intensity of the light source and the sensitivity of the phototube at wave length λ is P_λ, then the signal recorded by the phototube will be reduced by the factor

$$\frac{\int_\lambda (T_\lambda P_\lambda \delta) d\lambda}{\int_\lambda P_\lambda d\lambda} \qquad (1)$$

The integration is carried out over all wave lengths. For monochromatic radiation, the reduction factor is obviously $T_\lambda\delta$. The observed signal must be multiplied by the reciprocal of this factor in order to compensate for the loss in the medium. T_λ can be computed from the optical density data in Table I. The values of P_λ are given in Table II.

TABLE II

$P\lambda$ *versus* WAVE LENGTH

Wave length, mμ	Relative response of 1P21 phototube[a]	Relative output of tungsten lamp[b]	$P\lambda$
700	0	200	0
650	3	165	495
600	10	130	1300
580	20	115	2300
560	30	100	3000
540	40	87	3400
527	50	76	3800
513	60	68	4080
500	70	60	4200
480	80	49	3920
450	90	33	2920
400	100	15	1500

[a] From spectral sensitivity curve supplied by manufacturer. [b] J. O. Kraehenbuehl, "Electric Illumination," John Wiley and Sons, Inc., New York, N. Y., 1951, p. 87.

An incandescent tungsten lamp was used as a light source because the solutions absorbed so strongly in the blue and green that it was not possible to obtain an appreciable scattering signal for the aged sols with the monochromatic lines of the mercury vapor lamp. The tungsten lamp provided sufficient intensity at the red end of the spectrum to avoid this difficulty.

(16) This of course assumes that the law of scattering would be the same in both cases. Since, in general, this is not so, what we are doing is merely correcting for the attenuation and not reproducing the scattering situation for this particle in a non-absorbing medium.

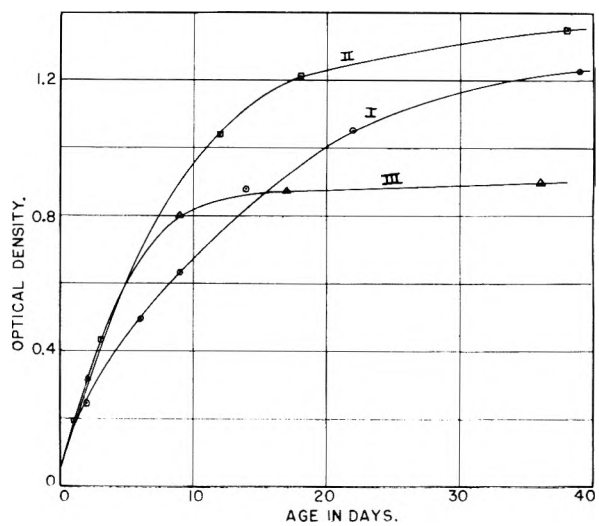

Fig. 1.—Increase of optical density upon aging: sol I, 0.095%, λ 546 mμ; sol II, 0.190%, λ 580 mμ; sol III, 0.285%, λ 650 mμ.

The unpolarized, vertically polarized and horizontally polarized components of the light scattered by the three typical sols are presented in Tables III, IV and V. The units are arbitrary galvanometer readings corrected to a standard incident intensity and have also been corrected for absorption as described above.

The uncorrected scattering for sol I observed at 45° from the forward direction is plotted together with the corrected values in Fig. 2. Whereas the former shows a rapid increase with time and then a decay, the scattering corrected for absorption continues to increase with aging until it finally levels off.

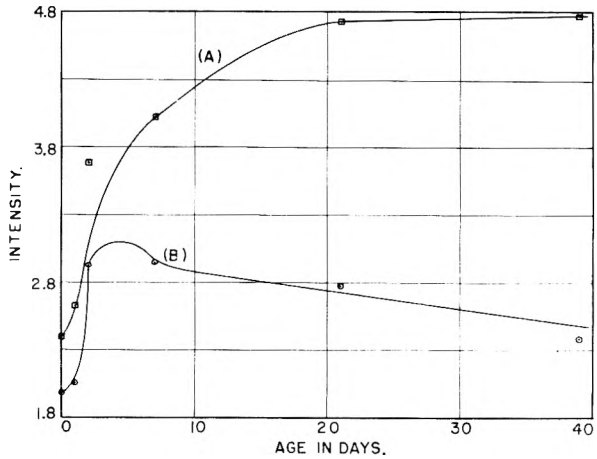

Fig. 2.—Increase with age of the intensity of the vertical component of light scattered at $\gamma = 45°$ by a 0.095% sol: A, corrected for absorption; B, uncorrected.

TABLE III

INTENSITY OF SCATTERED LIGHT AT VARIOUS ANGLES OF OBSERVATION (U)

Sol	Age, days	45°	60°	90°	120°	135°
	0	545	180	71.7	75.9	
	1	817	226	82.3	90.0	
I	2	10,300	5,370	3,030	3,670	
	7	27,400	13,900	7,900	8,580	
	21	95,000		28,600		42,100
	39	103,000		31,900		43,500
	0	317	134	62.3	73.9	
	3	4,127	2,500	1,600	1,990	
II	8	12,000	7,380	4,550	5,560	
	18	45,000		14,800		25,300
	38	42,000		16,700		22,800
	0	532	222	75	83	
	1	8,130	4,900	3,240	4,000	
III	4	11,900	9,900	4,430	5,940	
	16	13,500		5,520		7,550
	36	12,300		4,600		7,300

TABLE IV

INTENSITY OF SCATTERED LIGHT AT VARIOUS ANGLES OF OBSERVATION (VERTICAL COMPONENT OF SCATTERED LIGHT —V)

Sol	Age, days	45°	60°	90°	120°	135°
	0	249	101	46	40	
	1	425	141	51	58	
I	2	4,810	3,150	2,010	1,910	
	7	12,600	8,020	4,770	4,380	
	21	54,700		18,300		19,000
	39	60,000		20,900		21,000
	0	177	82	40	50	
	3	1,812	1,330	980	1,140	
II	8	6,520	4,630	3,180	3,200	
	18	24,100		11,200		11,700
	38	22,400		9,830		10,700
	0	368	132	31	42	
	1	3,900	2,660	1,990	2,090	
III	4	5,310	3,800	2,760	2,790	
	16	6,900		3,540		3,680
	36	6,150		2,780		3,520

TABLE V

INTENSITY OF SCATTERED LIGHT AT VARIOUS ANGLES OF OBSERVATION (HORIZONTAL COMPONENT OF SCATTERED LIGHT—H)

Sol	Age, days	45°	60°	90°	120°	135°
	0	139	38	9.0	17.5	
	1	219	45	7.1	19.2	
I	2	2,100	704	204	672	
	7	4,680	1,310	506	1,740	
	21	13,800		1,850		11,200
	39	15,800		2,300		13,100
	0	108	27	4.3	16.0	
	3	1,040	464	164	435	
II	8	3,180	1,280	517	1,230	
	18	10,200		1,790		6,800
	38	9,140		1,730		6,550
	0	127	37	5.7	15.4	
	1	2,000	800	290	860	
III	4	2,780	1,480	650	1,230	
	16	3,710		817		2,390
	36	3,300		640		2,300

4. Discussion of the Increase in Absorption and Light Scattering of Aging Sols

It is obvious from these data that the larger particles are much more efficient both as scatterers and absorbers of radiation than the smaller ones. The optical density increases as much as thirty-fold, and the scattering increases in some cases by more than two orders of magnitude. This greater efficiency in both scattering and absorption is probably due to a combination of two factors, *i.e.*, the increase in eccentricity in particle shape as the rods become filaments and the over-all increase in size as the particles grow.

Unfortunately, the present state of scattering theory is unable to differentiate these two factors. The Mie theory is capable of predicting the variation of absorption and scattering with size, but it is limited to spherical particles. The Gans theory can predict the influence of shape, but it is restricted to particles which are small compared to the wave length.

Let us examine, first of all, just what the influence of shape alone would be upon the true absorption if the Gans theory were applicable, *i.e.*, how would the absorption vary if a particle were to be extended from a sphere to a long rod maintaining constant volume. We have assumed for the index of refraction, $m = 1.60 - 0.22i$ at $\lambda = 0.546$ mμ. The real part is in the range for crystals of the type of vanadium pentoxide. The imaginary part was obtained by assuming that the molar extinction coefficient of solid vanadium pentoxide is the same as that of vanadium pentoxide in solution. This latter is reported below in Section 7. The refractive index relative to the medium which is water is $m' = 1.20 - 0.17i$.

The total cross-section[17] predicted by the Gans theory for particles of this refractive index is practically independent of shape. For particles of fixed volume it increases 2% as the shape is varied from a sphere to an infinitely long rod. This shape influ-

(17) The cross-section is the ratio of energy attenuated from the incident beam to the energy density of the incident beam.

TABLE VI

ABSORBING AND SCATTERING EFFICIENCY OF SPHERICAL PARTICLES AS A FUNCTION OF PARTICLE SIZE: $m = 1.46 - 4.30i$

1 $\alpha = \frac{2\pi r}{\lambda}$	2 Total cross-section	3 Scattering cross-section	4 Absorption cross-section	5 Scattering cross-section unit vol.	6 Absorption cross-section/ unit vol.
0.01	0.0_61125	$0.0_{10}1498$	0.0_61125	0.0_41498	0.1125
.05	$.0_4265$	$.0_7264$	$.0_4265$	$.0_3211$	.212
.10	$.0_3220$	$.0_51705$	$.0_3218$	.001705	.218
.20	.00210	$.0_31136$	.00199	.01420	.249
.40	.0308	.00845	.0224	.1320	.359
.60	.212	.1129	.0988	.518	.453
.80	.851	.594	.257	1.160	.501
1.00	1.749	1.357	.392	1.357	.392
1.20	2.40	1.925	.471	1.130	.273
1.35	2.81	2.25	.557	0.915	.226
1.50	3.37	2.69	.686	.796	.203
2.00	6.45	5.35	1.100	.668	.1375
2.50	9.18	7.47	1.712	.478	.1100
3.00	11.45	10.20	1.257	.378	.0715
4.00	22.6	18.68	3.89	.292	.0608
5.00	36.3	30.3	6.04	.242	.0483

ence is somewhat greater for higher refractive indexes, but even for a value of $m = 1.95 - 0.80i$, the increase is only 13%.

According to Gans' theory, the attenuation due to true absorption for a fixed shape is directly proportional to the particle volume so that for a system such as ours in which the particles are becoming larger and more elongated while the total volume of colloidal material remains fixed, the increase in true absorption would follow the same pattern as for the model described in the previous paragraph. Clearly, the Gans theory cannot even qualitatively account for the large increases in absorption which we have observed.

On the other hand, the scattering, according to Gans' theory, depends on the square of the volume so that it would increase as the particles grow. The growth observed with the electron microscope could account for the increase in scattering actually observed. However, since the scattering itself accounts for only a small fraction of the total attenuation, the Gans theory is at a loss to explain the major part of the increase in optical density which must be ascribed to the effect of either particle shape or particle size, or both, upon the true absorption within the particle.

We now propose to examine the increase of absorption of spherical particles with size as predicted by the Mie theory. It would seem reasonable that since deviation from sphericity does cause some increase in absorption, a particle which is both increasing in size and becoming less spherical should increase in absorption to at least the same extent as a growing spherical particle.

Spherical scattering functions for the refractive index we have used for vanadium pentoxide were not available, but since only qualitative conclusions are to be drawn, we utilized computations recently completed in this Laboratory for another absorbing material of index of refraction $m = 1.46 - 4.30i$. The results are presented in Table VI. The parameter, α, tabulated in column 1 is the ratio of the particle circumference to the wave length of the radiation. The cross-sections in columns 2, 3 and 4 when multiplied by $\lambda^2/2\pi$, give the ratio of energy attenuated from the incident to the energy density of the incident beam. In order to obtain columns 5 and 6, the scattering and absorption cross sections were divided by α^3 so that the volume units are arbitrary.

If we compare the attentuation on the basis of unit volume, it is obvious that the smallest particles are much less efficient both as scatterers and absorbers than those of an intermediate size. For a material of this refractive index, a particle of $\alpha = 1.0$ would scatter 10^5 times as much light as the same amount of material distributed as one million particles of $\alpha = 0.01$. The dependence of the absorption on size is not as marked. A particle of $\alpha = 0.8$ will absorb only four and a half times as much radiation as the same amount of material distributed among particles of $\alpha = 0.01$. As the particle continues to grow further, the scattering and absorption cross-sections per unit volume decrease. In fact, when $\alpha = 2.5$ the large particles become less efficient absorbers than the small ones.

One would expect considerable variation in the quantitative aspects of these results with different indexes of refraction; however, it is reasonable to expect that the direction of the trend should be the same, *i.e.*, as very small particles grow they scatter and absorb light more efficiently.

We have already seen that the Gans theory which is applicable to small particles does not predict a dependence of absorption on the size distribution of the particles, but only upon the total volume of colloidal material. If scattering by ellipsoids is to follow the pattern for spheres, as an ellipsoidal particle grows it also should become a more efficient absorber of radiation, at least up to some optimum size.

The increase in absorption which we have observed for aging vanadium pentoxide particles is surprisingly large and the extent to which this can be differentiated between the influence of shape and the influence of size is something an exact theory of scattering would have to predict. Since both size and shape are changing simultaneously in our system, it is not obvious how each of these factors behaves individually.

5. Polarization and Angular Dependence of the Scattered Light

One would expect that the polarization of the scattered light would also be dependent upon *both* the size and the shape of the scattering particles. The Mie theory shows that for spherical particles there is a marked dependence of polarization on size, and this has been observed experimentally.[18] The Gans theory indicates that for spheroidal particles the polarization is dependent upon shape, but it does not predict any size dependence.

The polarization ratio, ρ, the ratio of the intensity of horizontally to vertically polarized scattered light is defined by

$$\rho = H/V \qquad (2)$$

Thus, for Rayleigh scattering at angle of observation, $\gamma = 90°$, $\rho = 0$. When V and H are developed for the Gans theory, ρ has a non-zero value.

For randomly oriented rods of infinite length and relative index of refraction chosen for vanadium pentoxide, $m' = 1.20 - 0.0191i$, ρ at 90° is 0.0066. ρ increases to unity as the angle of observation goes to $\gamma = 0°$. The values for 30, 45 and 60° are 0.752, 0.503, and 0.255, respectively. The values for angles greater than 90° are symmetrical. These values do not differ significantly from the values of 0.750, 0.500 and 0.250 for these angles predicted by Rayleigh theory.

The values of ρ obtained experimentally are presented in Table VII. They differ from those predicted by the Gans theory. The Mie theory shows that for spherical particles the polarization ratio at 90° may have a large non-zero value and that ρ varies with both size and angle of observation in a complicated manner. The fact that our data indicate no simple trend of ρ with growth suggests that the dependence in this case may be equally complicated.

TABLE VII

POLARIZATION RATIO

Sol	Age, days	Angle 45°	60°	90°	120°	135°
	0	0.56	0.37	0.20	0.44	
	1	.53	.32	.17	.33	
I	2	.44	.22	.10	.35	
	7	.37	.16	.11	.40	
	21	.25		.10		0.60
	39	.26		.11		0.62
	0	0.61	0.33	0.11	0.32	
	3	.57	.35	.17	.38	
II	8	.49	.28	.16	.38	
	18	.42		.16		0.58
	38	.41		.17		0.61
	0	0.41	0.28	0.18	0.37	
	1	.51	.30	.15	.42	
III	4	.52	.39	.23	.44	
	16	.54		.23		0.65
	36	.54		.24		0.65
Gans theory		0.503	0.254	0.066	0.254	0.503
Rayleigh theory		0.5	0.25	0.0	0.25	0.5

(18) (a) M. Kerker and V. K. La Mer, *J. Am. Chem. Soc.*, **72**, 3516 (1950); (b) M. Kerker, *J. Coll. Sci.*, **5**, 165 (1950); (c) M. Kerker and M. Hampton, *J. Opt. Soc. Amer.*, **43**, 370 (1953).

The situation is very much the same when considering the variation of the intensity of scattering with angle of observation. Here again the Gans theory differs only slightly from the Rayleigh theory. In both cases it is only H which varies with angle of observation. The scattering intensity is symmetrical around 90°.

On the other hand, our data in Table VIII show that both V and H vary in a complicated manner with angle of observation, being more intense in the forward than the backward direction. As the sols age the ratio of backward to forward scattering increases. Again, we are unable to determine to what extent this is due either to increasing size or eccentricity of the particles.

6. The Fading of Diluted Sols

After a vanadium pentoxide hydrosol has been diluted, the optical density of the resulting sol decreases with time for a rather extended period. This fading phenomenon was studied by Lange[19] who attributed it to the slow solution of the vanadium pentoxide micelles. He attempted to study the kinetics of the solution by analysis of the spectrophotometric data. Lange assumed that the colloidal vanadium pentoxide was absorptive, but that the molecularly-dissolved vanadium was colorless. He further assumed that the absorption by a colloidal particle of vanadium pentoxide was directly proportional to the mass of the particle, and hence that the decrease in optical density with time was a direct measure of the rate of solution. The first assumption was not based upon any observation of his and seems to have been completely *ad hoc*. The second assumption ignored the influence of particle size and shape upon scattering and absorption.

Rabinovich and Kargin[20] studied the fading with a view to explaining the buffering action of vanadium pentoxide and tungsten trioxide sols.

Donnet and his co-workers[21] have recently investigated this problem. They claim that the average length of the colloidal particle as determined by electron microscope count does not decrease even after a twenty-fold dilution. They propose that the color is due to ions of polyvanadic acid adsorbed upon the surface of the vanadium pentoxide particles, and that the effect of dilution is to slowly hydrolyze these to some hypothetical uncolored species. This mechanism seems no less *ad hoc* than the colorless vanadium ions of Lange.

We believe that we have been able to demonstrate that the fading is due to solution of the colloidal particles as Lange has proposed, but that it is unnecessary to invoke his colorless ions in the homogeneous phase. We have observed the particles of the fading sols with the electron microscope and found that they slowly decrease in size.[22] It has already been demonstrated that more light is extinguished by vanadium pentoxide in colloidal form than in homogeneous solution. This does not depend upon a change in optical constants, but only

(19) B. Lange, *Kolloid-Z.*, **59**, 162 (1932).

(20) J. Rabinovich and V. Kargin, *Z. physik. Chem.*, **A152**, 24 (1931).

(21) J. Donnet, H. Zbinden, H. Benoit, M. Daune, N. Dubois, J. Pouyet, G. Scheibling and G. Vallet, *J. chim. phys.*, **47**, 52 (1950).

(22) A more complete report, obtainable from the National Advisory Committee for Aeronautics, includes electron micrographs.

TABLE VIII

RATIO OF INTENSITIES OF LIGHT SCATTERED AT VARIOUS ANGLES

Sol	Age, days	Intensity at 90° / Intensity at 45°			Intensity at 90° / Intensity at 60°			Intensity at 120° / Intensity at 60°		
		U	V	H	U	V	H	U	V	H
I	0	0.13	0.19	0.05	0.40	0.43	0.24	0.42	0.37	0.46
	1	.10	.12	.03	.36	.36	.16	.40	.41	.43
	2	.29	.42	.10	.56	.64	.29	.68	.61	.95
	7	.29	.38	.11	.57	.60	.39	.62	.55	1.33
	21	.30	.34	.13						
	39	.31	.35	.15						
II	0	0.20	0.23	0.04	0.46	0.49	0.16	0.55	0.61	0.60
	3	.39	.54	.16	.64	.74	.35	.79	.86	.94
	8	.38	.50	.16	.62	.69	.40	.76	.69	.96
	18	.33	.46	.67						
	38	.40	.48	.72						
III	0	0.14	0.10	0.04	0.34	0.24	0.16	0.37	0.32	0.42
	1	.40	.51	.15	.66	.75	.36	.82	.79	1.07
	4	.37	.52	.23	.45	.73	.44	.60	.74	0.83
	16	.41	.51	.22						
	36	.37	.45	.19						

upon the state of aggregation of the material. Colloidal particles are more efficient scatterers and absorbers than homogeneously dispersed molecules. Furthermore, large colloidal particles scatter and absorb more efficiently than small ones so that it is to be expected that the solution of vanadium pentoxide particles will be accompanied by a decrease in optical absorption.

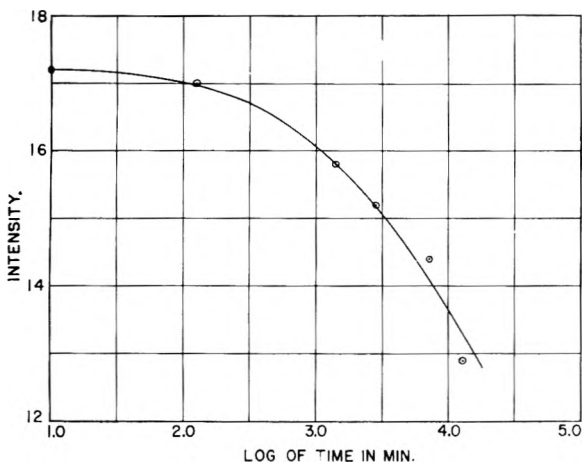

Fig. 3.—Decrease with age of the intensity of light scattered at $\gamma = 90°$ by a 0.190% sol after fivefold dilution.

We have taken light scattering in addition to absorption measurements on the fading sols, and these further confirm that solution is occurring. The decrease in absorption and light scattering for an aged 0.190% sol diluted fivefold is presented in Tables IX and X and in Figs. 3 and 4. The uncorrected scattering readings show that the observed scattering is actually stronger for the faded solutions. This is because in the concentrated solution the scattered light is strongly attenuated before escaping from solution, a condition that has been discussed above. When this attenuation is taken into account, the corrected scattering actually decreases markedly as the fading proceeds. This is consistent with a partial solution of the colloid and a corresponding decrease in average size.

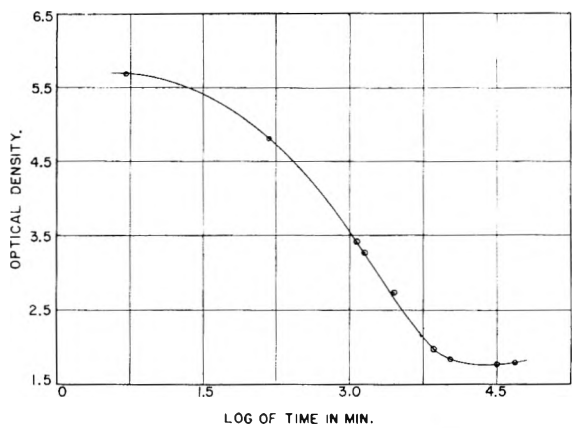

Fig. 4.—Decrease with age of the optical density of a 0.190% sol. after fivefold dilution (λ 5460 Å.).

TABLE IX

LIGHT SCATTERING BY AN AGED 0.190% SOL DILUTED FIVEFOLD

Time after dilution, min.	Intensity at 90° U	V	H
10	17.2	11.0	1.03
120	17.0	10.9	1.47
1,440	15.8	9.8	1.37
2,880	15.2	9.5	1.35
7,200	14.4	9.2	1.31
12,960	12.9	8.1	1.05

TABLE X

OPTICAL DENSITY OF AN AGED 0.190% SOL DILUTED FIVEFOLD

Time after dilution, min.	Optical density λ 5460 Å.	λ 5300 Å.	λ 5100 Å.
150	0.569	0.752	1.402
1,200	.480	.631	0.970
1,440	.343	.453	.713
2,880	.274	.361	.591
7,200	.197	.261	.439
12,960	.184	.241	.411
31,680	.177	.230	.398
48,960	.179	.236	.395

It is evident from all three types of measurement, light scattering, electron microscopy and optical density, that the mechanism for the fading of the vanadium pentoxide sols involves solution of colloidal particles as Lange proposed. However, it is unnecessary to invoke hypothetical ionic processes to account for the color changes. These are due to the much greater scattering and absorbing efficiency of large colloidal particles as compared with small ones. As the particles become smaller they scatter and absorb less light.

7. Solubility of Vanadium Pentoxide

The formation of a vandium pentoxide hydrosol, as the orthovanadic ester is added dropwise to a volume of water, was followed by measuring the optical density, differential refractive index and the intensity of scattered light. The vanadium pentoxide goes into true solution until its concentration exceeds a critical concentration after which additional material precipitates to form the colloid.

The optical density increases linearly with concentration up to a 0.029% solution, after which the curve bends upwards (Fig. 5). This would seem to correspond to the point of formation of the colloid, the increased slope beyond being due to the greater extinction coefficient of vanadium pentoxide in the colloidal form. The dilute solutions which we consider homogeneous do not display the aging characteristics of the colloids.

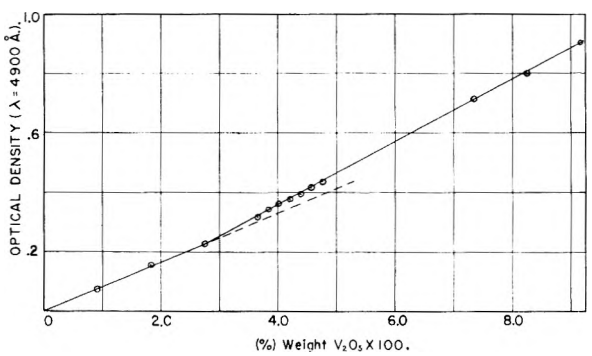

Fig. 5.—Increase of the optical density of a fresh sol with V_2O_5 concentration.

The differential refractive index (Fig. 6) behaves similarly, exhibiting an initial linear section corresponding to the homogeneous solution after which the slope increases presumably due to the presence of colloidal particles.

The light scattering (Fig. 7) is somewhat irregular due to the optical absorption of the vanadium pentoxide. A colorless material would be expected to exhibit a small increase in scattering as the concentration of the homogeneous solution increases, and then a sharp increase upon the formation of colloid. The vanadium pentoxide shows a decrease in scattering from the zero concentration value which is due to background scattering by the water. The decrease is due to the attenuation of the scattered light on passing through the colored vanadium pentoxide. It has been pointed out previously how this attenuation can be corrected for. This correction has been omitted here since the intensity of scattered light at these concentrations is quite small, and the precision considerably less than for

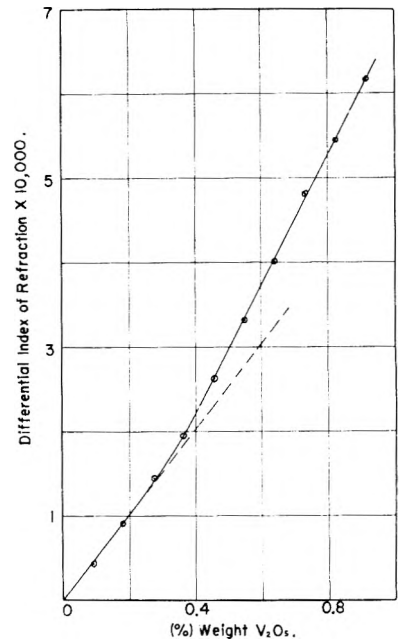

Fig. 6.—Increase of the differential refraction index of a fresh sol with V_2O_5 concentration.

the optical density and differential refractive index measurements. It is sufficiently obvious from the uncorrected data that there is a sharp increase in scattering at about 0.02 to 0.03% concentration.

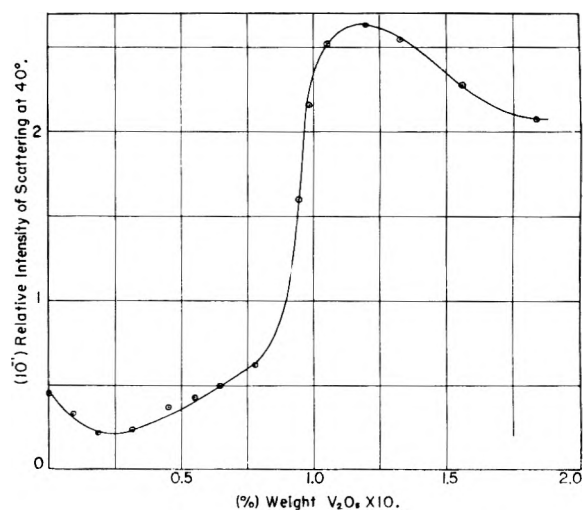

Fig. 7.—Increase of intensity of scattering at $\gamma = 40°$ of a fresh sol with V_2O_5 concentration.

The solubility of vanadium pentoxide as determined from the breaks in the growth curves is considerably lower than that heretofore reported. Meyer and Aulich[23] give a solubility of 0.07% at 25°. Their procedure was to shake some vanadium pentoxide with water and to analyze the supernatant solution by reduction with sulfur dioxide and subsequent titration of the tetravalent vanadium with potassium permanganate. Their value is cited by Seidell.[24] The Handbook of Physics and Chem-

(23) J. Meyer and M. Aulich, *Z. anorg. allgem. Chem.*, **194**, 278 (1930).

(24) A. Seidell, "Solubilities of Inorganic and Metal Organic Compounds," 3rd Ed., John Wiley and Sons, Inc., New York, N. Y., 1940.

istry,[25] Lange,[26] and Perry,[27] give a solubility of 0.8%, a value that would strike anyone who has worked with colloidal vanadium pentoxide as being completely out of line. The most recent determination of the solubility of vanadium pentoxide that we know of is that of Donnet and co-workers.[21] Using an ultrafiltration technique they obtained a solubility of 0.048%, a value in good accord with those of Freundlich and Leonhardt[28] and Gessner.[29]

The discrepancy between our value of 0.03% obtained from the growth curves and the higher values cited above led us to redetermine the solubility of vanadium pentoxide in water. This was done by ultracentrifuging a month-old colloidal sol of 0.194% concentration at 60,000 r.p.m.[30] The upper half of the supernatant was carefully removed from the ultracentrifuge cell and diluted to provide sufficient volume for a transmission cell. The optical transmission was determined and compared with a solution of comparable transmission which had been prepared by dilution from a homogeneous stock solution. The concentration of the stock solution was 0.0199%, well below the suspected solubility. Beer's law was used to determine the relative concentrations of the two dilute solutions and from their dilution ratios and the concentration of the stock solution, the concentration of the ultracentrifugate was evaluated as 0.0296 g./100 cc.

The molar extinction coefficient[31] for homogeneous vanadium pentoxide was calculated from the optical density data of the 0.0199% stock solutions. It was necessary to use dilutions of this solution at the lower wave lengths. At 350 mμ the deviation from Beer's law was less than 3% for a ninefold dilution. Results are presented in Table XI.

TABLE XI

MOLAR EXTINCTION COEFFICIENT OF V_2O_5

Wave length, mμ	Molar extinction coefficient × 10^{-3}	Wave length, mμ	Molar extinction coefficient × 10^{-3}
268	8.00	325	2.78
270	7.84	330	2.68
274	7.40	340	2.45
276	7.08	350	2.24
278	6.84	360	2.04
280	6.48	370	1.79
284	5.87	380	1.66
287	5.39	390	1.52
290	4.97	400	1.34
295	4.37	410	1.15
300	3.87	420	0.98
303	3.63	430	0.81
305	3.54	440	0.69
307	3.39	450	0.56
310	3.25	460	0.44
315	3.04	470	0.31

For the calculations in Part 4 it was necessary to estimate the complex index of refraction for solid vanadium pentoxide, $m = n - i\kappa$.[32] n is the Snell's law refractive index. κ is related to the molar extinction coefficient, E, the molar concentration, C, and the wave length, λ, by

$$\kappa = \frac{\lambda}{4\pi} 2.303Ec \qquad (3)$$

For solid vanadium pentoxide whose density is 4, $C = 22\ M$. We only have values of E up to λ 470 mμ. We can arrive at a rough estimate of E at 546 mμ by assuming that it decreases from 470 to 546 mμ in the same ratio as the optical density of sol I (see Table I) between these wave lengths. This results in the assignment of $\kappa = 0.220$.

(25) C. Hodgman, "Handbook of Chemistry and Physics," 34th Ed., Chemical Rubber Publishing Co., Cleveland, Ohio, 1952.

(26) N. Lange, "Handbook of Chemistry," 7th Ed., Handbook Publishers, Inc., Sandusky, Ohio, 1949.

(27) J. Perry, "Chemical Engineers' Handbook," 2nd Ed., John Wiley and Sons, Inc., New York, N. Y., 1941.

(28) H. Freundlich and W. Leonhardt, *Kolloid Chem. Beih.*, **7**, 172 (1915).

(29) H. Gessner, *ibid.*, **19**, 213 (1924).

(30) We are indebted to Professor Harold Scheraga of Cornell University who kindly carried out this ultracentrifugation.

(31) The molar extinction coefficient, E, is defined by $\log_{10}(I/I_0) = -Elc$, where I/I_0 = transmission, c = molar concentration based upon V_2O_5 as the molecular species, and l = light path in centimeters.

(32) J. Morgan, "Introduction to Geometrical and Physical Optics," John Wiley and Sons, Inc., New York, N. Y., 1953.

SELF-DIFFUSION OF CATIONS, NON-EXCHANGE ANIONS AND SOLVENT IN A CATION EXCHANGE RESIN SYSTEM

BY MARVIN TETENBAUM[1] AND HARRY P. GREGOR

Contribution from the Department of Chemistry of the Polytechnic Institute of Brooklyn, New York, and the Naval Research Laboratory, Washington, D. C.

Received July 12, 1954

The rate of self-diffusion in a polystyrenesulfonic acid cation-exchange resin (12% cross-linked) system of the exchange cation (potassium), non-exchange anion (chloride) and solvent (water) were measured using isotopic techniques. The rate of flow in the shallow bed system was varied over a wide range, up to and including that where the rate was constant; comparable experiments were also performed with stirring in a limited bath system. At a high rate of flow in the shallow bed system, the calculated thickness of the unstirred film (δ) was 1.2 μ, and an excellent fit of calculated curves to data was obtained in the concentration range 0.0001–0.1 M using a diffusion coefficient of potassium which was 21% of the value in free solution. The diffusion coefficient for non-exchange chloride was 37% and of deuterated water 85% of the corresponding values in free solution. At a high rate of stirring in a limited bath, δ was 11 μ, and good correspondence was obtained between the two methods. At higher salt concentrations (0.2–1 M) the experimentally determined self-diffusion coefficients for potassium were higher than the calculated values. These discrepancies are explained in terms of a resin model.

This paper describes rate experiments performed on a polystyrenesulfonic acid cation-exchange resin system, where the self-diffusion of the exchange cation (potassium), the non-exchange anion (chloride) and the solvent (water) were measured using isotopic techniques. The principal variables studied included the rate of flow in a shallow bed system and the concentration of electrolyte in the solution phase.

Experimental Procedures

Resin.—Polystyrenesulfonic acid resins were used, supplied by the courtesy of the Dow Chemical Company, Midland, Michigan. Samples from two different batches were first wet screened, and those particles retained in the interstices were then conditioned over a period of weeks, and the perfect spheres selected. Most of the experiments were performed with both resin samples, but only relative comparisons are possible because of differences in cross-linking. The data reported in this paper are for resin sample A, which was light tan in color and corresponded to about 12% DVB on the swelled volume scale,[2] and for resin sample B which was somewhat larger (30% greater diameter) and more highly cross-linked (15%).

The external volume of the solution equilibrated resin was measured using the centrifugation technique,[2] and the capacity by titration of the hydrogen form resin in an excess of neutral salt.[3] The exchange capacity per ml. of swelled volume of resin A beads in 0.1 M potassium chloride was 3.62 mmoles/ml. The diameter of each particle of this resin in the potassium state was 0.1083 cm. in water, 0.1079 in 0.1 M and 0.1071 in 1 M potassium chloride.

Shallow Bed Technique.—The apparatus used was similar to that of Boyd, Adamson and Myers,[4] and consisted of 60-mesh platinum screen sealed in a 10-mm. i.d. section of glass tubing, separating two 10-mm. bore stopcocks, the latter being fitted with a special clamp arrangement to keep the stopcocks from popping out as a result of the high pressures used to maintain high flow rates. The bed system was connected by ground glass joints and rubber tubing to a 20-l. Pyrex bottle which contained the eluting solution, and which in turn was connected through a reducing valve to a tank of nitrogen gas.

Runs were made using two somewhat different techniques. For cation-exchange processes, the resin (about 0.2–0.3 g.) was equilibrated with potassium chloride solution of a given molarity containing radioactive potassium, then slurried into the cell, which was then completely filled with this same solution between the two stopcocks. The radioactive solution above the upper stopcock was rinsed free of activity, and the entire line to the storage bottle filled with the eluting solution, which consisted of potassium chloride solution of exactly the same concentration as the equilibrating solution. Pressure was applied to the system from the gas tank, and the start of the run initiated by opening the stopcocks. Usually air bubbles were removed from the system, but this was not really necessary since at the high rates of flow employed any air present was rapidly forced through the bed at the start of the run.

Several runs were made to establish the fact that the flow rate was constant during the run. All experiments were performed at 25 ± 0.5°.

Linear rates of flow in cm./sec. were calculated as being four times the volumetric rate of flow, divided by the bed area. The factor of four is used because for a bed of close-packed spheres of uniform size, the bed voids are about 25% of the bed volume.

Experiments were timed by collecting all of the effluent in a series of beakers at periodic intervals, the total interval of the run being timed accurately. From a knowledge of the volume of each sample collected, the total volume and the elapsed time, the amount of activity eluted from the resin could be calculated as a function of time. At the end of each run, the activity remaining in the resin was eluted with a concentrated solution and determined.

When the rate of elution of non-exchange anions (chloride) was measured, the above technique was not used because so little of the activity of the equilibrating solution entered the resin phase itself, due to Donnan effects as described by Gregor, Gutoff and Bregman.[2] In these experiments the radioactive chloride equilibrated resin was either centrifuged,[2] blotted,[5] or placed wet into a shallow bed system, and eluted as described above.

For experiments using deuterated water, the resin was equilibrated as before, using 20% deuterium oxide as solvent, and placed wet into the shallow bed system. Here, however, the rate of elution was followed by stopping the flow of eluate at different times, extracting the isotopic water from the resin phase itself with small volumes of water, and analyzing the extracts.

It should be emphasized that in all of these experiments, unless specifically stated otherwise, the equilibrium condition of the resin system was not disturbed throughout the run because the eluting solutions were virtually identical with the equilibrating solutions.

Limited Bath Technique.—The resin was equilibrated with radioactive potassium (chloride) solution, the excess solution removed by suction using a fritted disc, and the resin placed rapidly into a beaker containing a large volume of inactive eluting solution which was stirred rapidly by means of a simple bent rod stirrer. The rate of stirring was varied, the general technique being similar to that used by Kressman and Kitchener.[6]

(1) A portion of this work is abstracted from the dissertation of Marvin Tetenbaum, submitted in partial fulfillment of the requirements for the degree of Doctor of Philosophy in Chemistry, Polytechnic Institute of Brooklyn, June, 1954. Present address: Nucleonics Division, Naval Research Laboratory, Washington, D. C.

(2) H. P. Gregor, F. Gutoff and J. I. Bregman, *J. Colloid Sci.*, **6**, 245 (1951).

(3) H. P. Gregor and J. I. Bregman, *J. Am. Chem. Soc.*, **70**, 2370 (1948).

(4) G. E. Boyd, A. W. Adamson and L. S. Myers, *ibid.*, **69**, 2836 (1947).

(5) H. P. Gregor, K. M. Held and J. Bellin, *Anal. Chem.*, **23**, 620 (1951).

(6) T. R. E. Kressman and J. A. Kitchener, *Disc. Faraday Soc.*, **7**, 90 (1949).

In contrast to the situation that prevails with the shallow bed experiments, where the composition of the eluting solution remains constant, the use of limited bath means that active, eluted material will diffuse back into the resin. This back-diffusive process was virtually eliminated by using a large volume of solution, so that the total resin capacity was a very small fraction (<2%) of the amount of eluting ions in the solution. The solution phase was therefore infinite for practical purposes, and the more simple equations that obtain were used.

Radio-potassium and Chloride Determination.—Standard radio-chemical techniques were utilized in assaying the activities of the radioactive elements present in trace amounts. Effluents containing radio-potassium (K^{42}) were determined by dip-counter, radio-chloride (Cl^{36}) by evaporation and subsequent determination.

Deuterium Determinations.—The deuterated solutions were analyzed at the Bureau of Standards by the method developed by Broida[7,8] which involves optical spectroscopy with photoelectric detection to scan the hydrogen and deuterium spectra which result from dissociation in a high frequency electrodeless discharge. The accuracy of the determinations reported in this paper was ±5%.

Calculations

The general theory of diffusive processes as applied to ion-exchange resin systems has been described by Boyd, Adamson and Myers,[3] by Kressman and Kitchener[6] and by Grossman and Adamson[9]; the treatment given here is essentially the same as used by these authors. There are essentially two different mechanisms involved. First, consider the case where the rate determining step is transport across a film which surrounds a spherical, homogeneous particle of radius r_0, and where the flux is proportional to the concentration gradient across the film. In treating these systems, it is assumed that there is an unstirred film of thickness δ, that a linear concentration gradient exists in the film, that the solution concentration C is constant for $r > (r_0 + \delta)$, and that diffusion within the particle is sufficiently rapid so that the concentration in the particle C^r is constant for $< 0\ r < r_0$. The coefficient for the distribution of the diffusible species between resin and solution phase is $k = C^r/C^r_0$, where C^r_0 is the concentration in the film section adjacent to the particle; for isotopic exchange k is constant, and its numerical value is determined under equilibrium conditions. Further, it is assumed that the diffusion coefficient in the film is the same as in the solution phase, and is designated D. The application of Fick's law to this model yields the expression

$$1 - Q/Q_0 = \exp\left(-\frac{3Dt}{r_0\delta k}\right)$$

where Q_0 is the amount of diffusible substance present initially in the sphere, and Q the amount which has diffused *out* in time t.

Letting $F = 3D/r_0\delta k$, one first plots Q/Q_0 for assumed values of Ft; from experimental values of Q/Q_0 one then reads off values of Ft, and calculates F. Knowing D, r_0 and k, the value of δ is calculated. The applicability of film diffusion (F mechanism) is ascertained from the constancy of F at different values of t. The plot of Q/Q_0 *vs.* t at small values of Q/Q_0 (< 0.1) is substantially linear.

(7) H. P. Broida and A. Moyers, *J. Opt. Soc. Amer.*, **42**, 37 (1952).
(8) H. P. Broida and G. H. Morgan, *Anal. Chem.*, **24**, 799 (1952).
(9) J. J. Grossman and A. W. Adamson, THIS JOURNAL, **56**, 97 (1952).

It should be emphasized that the term D/δ arises directly from the postulate that it is diffusion across an unstirred layer which is responsible for the film effect. Obviously, any calculated value of δ depends upon the assumed value of D, and a fit of experimental data to the F mechanism plot does not of itself constitute proof that the unstirred film postulate is correct.

Next, consider diffusion out of the spherical particle where the concentration C of diffusible substance in the ambient solution phase is maintained constant for all values of t and radius $r > r_0$, and therefore diffusion within the particle is rate determining. The equation that applies is

$$1 - Q/Q_0 = 6/\pi^2 \sum_{n=1}^{n=\infty} \exp\left(-\frac{D^r\pi^2n^2t}{r_0^2}\right)$$

where D^r is the diffusion coefficient in the resin phase. This equation is used by defining a quantity $P = D^r\pi^2/r_0^2$, assuming a series of values for Pt, and making a theoretical plot of Pt *vs.* Q/Q_0. Then, for each experimental value of Q/Q_0, one reads from the calculated curve a value of Pt, and knowing t obtains P. If the process is as defined in the theory, *i.e.*, controlled by diffusion within the particle (P mechanism), this will be evidenced by the constancy of P for different values of t. D^r is calculated from P and the experimentally determined value of r_0.

Third, both film and particle diffusion mechanisms can be operative, in which case the following is assumed: the solution concentration C is constant; the film thickness is δ and the gradient across it is linear; the diffusion coefficient in the film is D; the diffusion coefficient in the resin in D^r; the distribution coefficient is $k = C^r/C^r_0$. Two new parameters are introduced

$$\theta = \frac{D}{D^r\delta k} \text{ and } u = r(Q_0 - Q)$$

where θr_0 is a dimensionless constant for a particular system. The general solution which obtains is

$$1 - Q/Q_0 = \frac{6\theta^2}{r_0^2} \sum_{n=1}^{n=\infty} \frac{A_n \sin^2(m_n r_0)}{m_n^4} \exp(-D^r m_n^2 t)$$

where

$$A_n = \frac{m_n^2 r_0^2 + (\theta r_0 - 1)^2}{m_n^2 r_0^2 + (\theta r_0 - 1)\theta r_0}$$

and

$$m_n r_0 = (1 - \theta r_0) \tan m_n r_0$$

From a set of values for θr_0, a series of values of $m_n r_0$ and m_n can be calculated which satisfy the transcendental equation. It was found that the first 5 eigen values were sufficient to give a reasonably exact solution to the general equation.

The coupled film and particle diffusion equation (F–P mechanism) obviously reduces to the F mechanism when θr_0 is small. For given values of r_0 and D, F mechanism operates: (a) when D^r is large or diffusion into the interior is rapid; (b) when δ is large or the film thickness is appreciable; (c) when $k = C^r/C^r_0$ is large or the adjacent solution phase is dilute. For a given system with presumably a constant value of δ and D^r, film diffusion will then be rate controlling for dilute solution phases.

The F–P equation is used by taking experimentally derived values of r_0, D, k and δ (obtained from very dilute solution data where the F mechanism is operative) and calculating a series of curves (Q/Q_0 *vs.* t) for assumed values of D^r. The true value of D^r is determined by fitting experimental and calculated curves. The range of assumed D^r values is ascertained by calculating an approximate D^r value from data obtained using concentrated solutions where the P mechanism is largely operative.

Experimental Results

Self-diffusion of Potassium—Typical Results from Shallow Bed Data.—Typical results for three experiments, one at a relatively high concentration where particle diffusion predominates (0.1 M), one at a low concentration where film diffusion is rate controlling (0.0001 M), and one where both mechanisms operate (0.01 M) are shown in Tables I, II and III, respectively. Resin A was used, and approximately the same high flow rate was maintained.

The data presented in Table I where the eluting solution was 0.1 M potassium chloride show that P is reasonably constant, being $14.3 \pm 0.3 \times 10^{-3}$ sec.$^{-1}$ for at least 60% of the elution process. It should be noted that the first value of Q/Q_0, which corresponds to the first portion of eluate, is given in parentheses. The specific activity in the first eluate fraction collected was usually not counted because it contained part of the active solution in equilibrium with the resin in the cell. The true value of Q was obtained by plotting the cumulated, eluted activity Q as a function of $t^{1/2}$, neglecting the first fraction, extrapolating the linear portion of the curve to $t = 0$, and reading off the true value of Q. The accuracy of this calculation could be checked from a knowledge of the total resin capacity, the activity of the equilibrating solution, and the activity in the assembled eluate with the exception of the first sample. Excellent material balance checks were obtained. It should be noted that this extrapolation is valid only when the P mechanism is virtually rate controlling.

From Table I it is seen that here the film mechanism is not rate controlling, as F varies by a factor of three.

TABLE I

POTASSIUM SELF-DIFFUSION

Shallow bed—flow rate 346 cm./sec., 0.1 M potassium chloride.

t, sec.	V, ml.	Resin A Q/Q_0	$P \times 10^3$, sec.$^{-1}$	$F \times 10^3$, sec.$^{-1}$
1.14	100	(0.110)	(13.8)	(103)
2.79	245	.185	14.9	74.4
4.66	410	.244	14.8	60.6
6.94	610	.297	14.2	51.2
9.22	810	.341	14.3	45.6
11.5	990	.376	13.8	41.3
16.0	1400	.438	13.9	36.4
20.4	1785	.489	14.1	32.8
32.0	2815	.588	14.5	27.8
			14.3 ± 0.3	

For very dilute solutions film diffusion is rate controlling, as shown in Table II. Here F is $0.314 \pm 0.001 \times 10^{-3}$ sec.$^{-1}$ when the eluting solution is 0.0001 M potassium chloride. Because of the slowness of the elution process even at high flow rates, and the practical necessity of using a limited volume of solution, the highest value of Q/Q_0 reached was 0.04. The F mechanism is also operative with 0.001 M solutions. For example, with a flow rate of 197 cm./sec. an F value of $2.34 \pm 0.02 \times 10^{-3}$ was obtained. The data of Table II show that the P mechanism is not rate controlling, as P varies by over an order of magnitude.

TABLE II

POTASSIUM SELF-DIFFUSION

Shallow bed—flow rate 253 cm./sec., 0.0001 M potassium chloride.

t, sec.	V, ml.	Resin A Q/Q_0	$P \times 10^3$, sec.$^{-1}$	$F \times 10^3$, sec.$^{-1}$
7.16	460	(0.00225)	6.12	(0.314)
14.2	915	.00446	12.1	.313
21.2	1365	.00662	17.7	.312
28.3	1823	.00890	24.1	.314
36.6	2353	.0115	31.3	.314
44.2	2841	.0139	38.2	.315
52.3	3361	.0165	44.6	.316
59.6	3831	.0187	50.8	.314
66.8	4291	.0210	57.2	.315
82.8	5321	.0259	69.8	.312
98.8	6351	.0310	83.5	.314
116.6	7491	.0366	99.2	.314
134.4	8641	.0423	113	.314
150	9641	.0473	127	.314
				0.314 ± 0.001

The F–P mechanism is operative at intermediate concentrations. In Table III it is seen that neither the parameter F nor P is constant. This is as expected from the theory, since the mechanism is neither pure P nor pure F controlled.

TABLE III

POTASSIUM SELF-DIFFUSION

Shallow bed—flow rate 230 cm./sec., 0.01 M potassium chloride.

t, sec.	V, ml.	Resin A Q/Q_0	$P \times 10^3$, sec.$^{-1}$	$F \times 10^3$, sec.$^{-1}$
1.19	69	(0.034)	(0.86)	(29.0)
2.69	159	.065	1.45	24.7
4.11	239	.089	2.26	22.6
5.90	343	.119	3.12	21.5
8.02	466	.155	3.74	21.0
12.6	734	.208	4.13	18.7
19.5	1134	.281	4.56	16.9
26.8	1554	.345	5.00	16.0
40.0	2324	.440	5.61	14.5

Self-diffusion of Potassium—Calculation of δ from Shallow Bed Data.—The thickness δ of the assumed film is calculated, as described previously, from data obtained at large values of the distribution coefficient k, corresponding to low solution concentrations, since C^r is sensibly constant in ion-exchange systems. The rate of elution and thus the calculated value of δ is a function of the flow rate, as will be discussed later in more detail. Table IV shows values of δ calculated from data

TABLE IV

CALCULATED FILM THICKNESS AT VARIOUS FLOW RATES

Soln. concn., M	Flow rate, cm./sec.	$\delta \times 10^4$, cm.	Soln. concn., M	Flow rate, cm./sec.	$\delta \times 10^4$, cm.
	Resin A			Resin B	
0.0001	238	1.2	0.0001	301	1.4
.0001	253	1.0	.0001	339	1.3
.001	161	2.5	.001	170	2.0
.001	199	1.3	.001	222	1.6
.001	282	1.3	.001	334	1.3
			.001	392	1.2

obtained with both resin samples at different flow rates. The diffusion coefficient of potassium in the solution phase was taken from self-diffusion data for potassium chloride at the same solution concentration.[10] Table IV shows that δ is $1.2 \pm 0.1 \times 10^{-4}$ cm. with resin A and $1.3 \pm 0.1 \times 10^{-4}$ cm. with resin B, which is as expected for similar resins, and with the same high flow rates. Also, δ increases with decreasing flow rate. It is particularly significant that the same value of δ is calculated from rate data using both 0.001 and 0.0001 M solutions, although the actual rate of elution is ten times as great at the higher concentration. The magnitude of δ is about the same as calculated values for unstirred films in other systems; the approach of δ to a minimum value is similarly consistent.

It should be pointed out that under these experimental conditions (*i.e.*, very dilute solutions) the contribution of particle diffusion is negligible. This can be shown by applying the coupled F–P equation to processes in this concentration range, using the value of D^r that obtains, and recalculating δ; the same value of δ is obtained by this iterative process.

Self-diffusion of Potassium—Calculation of D^r from Shallow Bed Data.—The self-diffusion coefficient of potassium in the resin phase was calculated as described earlier. First, an approximate value of D^r was calculated directly from the P constant using 0.1 M solution data. Then by an iterative process, using the δ-value calculated earlier and the F–P equation, the true value of D^r was calculated. At high flow rates (> 150 cm./sec.) with the shallow bed system, the uncorrected value of D^r as calculated from P was $4.25 \pm 0.1 \times 10^{-6}$ cm.^{2} sec.$^{-1}$, while the corrected value was 4.68×10^{-6} for resin A and 0.1 M solution data. Then theoretical curves were calculated using δ (from 0.0001 M data) and D^r (from δ and 0.1 M data) for elution processes with 0.001, 0.01, 0.2 and 1.0 M solutions. Figure 1 shows a plot of $1 - Q/Q_0$ *vs.* t for a series of theoretical curves, with corresponding experimental points.

Figure 1 shows that the data obtained at a concentration where both F and P mechanisms contribute about equally, namely, 0.01 M, fit the calculated curve almost exactly. One can conclude that at this concentration δ is the same as in more dilute solutions, and D^r as in more concentrated (0.1 M) solutions. However, the rate of elution at solution concentrations of 1 M is considerably greater than that predicted from the theory and the assumed values of δ and D^r. This curve was calculated using the values of C^r and r_0 which apply to this system.

Similar data and fits of theoretical and experimental curves were obtained with resin B. The film thickness δ is approximately the same, but D^r is 40% less than with resin A. Figure 2 shows calculated and experimental curves for data obtained using solutions 0.1 M and higher. The rate of the process is significantly faster with 0.2 M solutions than the calculated rate, and with 1 M solutions it is very much faster. The data for both resins are strictly comparable in that in comparing rates at 0.1 M with those at 1 M, the same, proportional increase in rate is found.

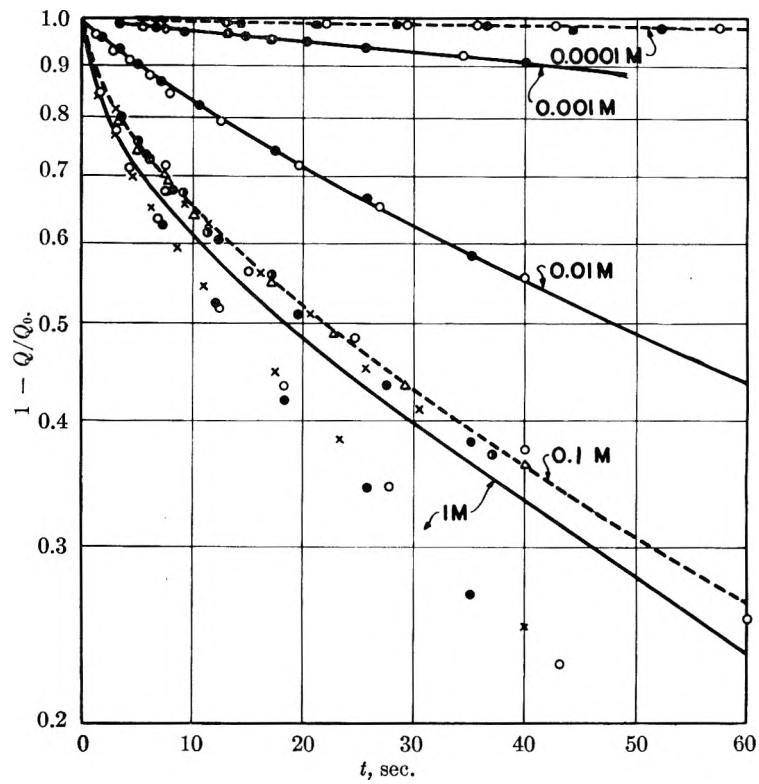

Fig. 1.—Theoretical and experimental curves for the potassium ion self-diffusive process with resin A in a shallow bed system. Curves calculated based on a coupled film-particle diffusion mechanism using $\delta = 1.1 \times 10^{-4}$ cm. and $D^r = 4.68 \times 10^{-6}$ cm.^{2} sec.$^{-1}$ are shown as solid lines; these parameters were obtained from the data for 0.0001 and 0.1 M solutions. Experimental points with corresponding flow rates are as follows: 0.0001 M, 238 cm./sec. (○), 253 (●); 0.001 M, 199 (○), 282 (●); 0.01 M, 156 (●), 230 (○); 0.1 M, 149 (×), 201 (△), 206 (●), 263 (○), 343 (◑); 1 M, 167 (×), 206 (○), 227 (●).

Self-diffusion of Potassium—Comparison of Shallow Bed and Limited Bath Techniques.—It may be seen from Figs. 1 and 2 that the rate of flow in a shallow bed system may be varied from about 150 to 420 cm./sec. without appearing to affect the rate of exchange when 0.1 M solutions

(10) H. S. Harned and B. B. Owen, "The Physical Chemistry of Electrolytic Solutions," Reinhold Publ. Corp., New York, N. Y., 1950.

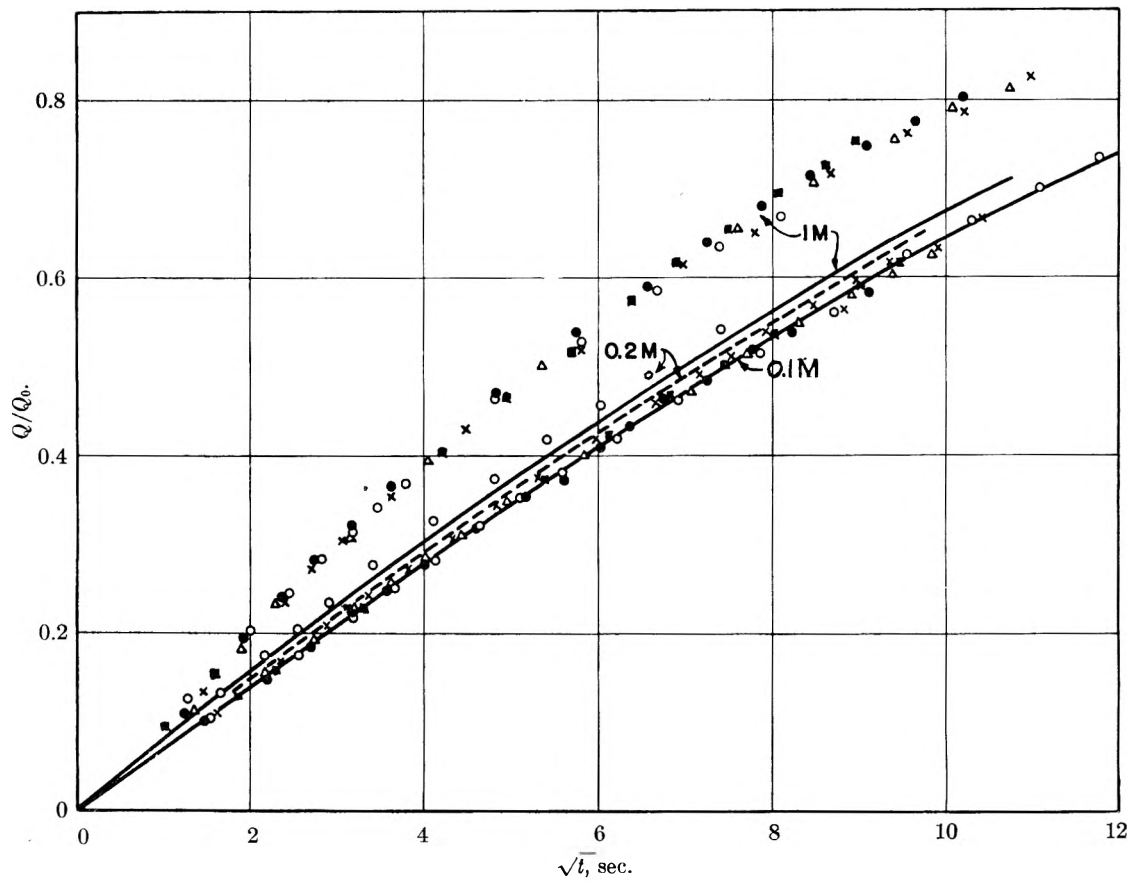

Fig. 2.—Theoretical and experimental curves for the potassium ion self-diffusive process with resin B in a shallow bed system. Curves calculated based on a coupled film-particle diffusion mechanism using $\delta = 1.3 \times 10^{-4}$ cm. and $D^r = 2.90 \times 10^{-6}$ cm.^{2} sec.$^{-1}$. Experimental points with corresponding flow rates are as follows: 0.1 M, 252 cm./sec. (○), 369 (×), 370 (△), 408 (●), 421 (■); 0.2 M, 264 (○); 1 M, 239 (△), 262 (×), 361 (●), 366 (○), 420 (■).

are used. However, the film thickness δ measured using dilute (0.0001–0.001 M) solutions does vary with the rate of flow, reaching a low, constant value at flow rates of about 200 cm./sec., as seen in Table IV. Obviously, δ is sensitive to flow rate, while D^r is presumably independent of rate of flow. Therefore where F mechanism predominates, the rate of exchange can be a function of the rate of flow, while for pure P mechanism processes it cannot.

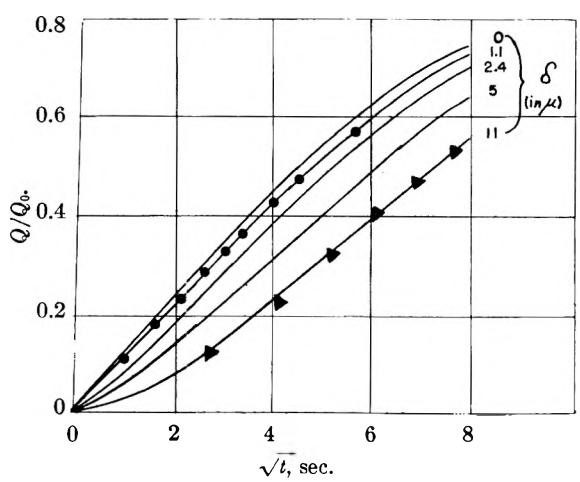

Fig. 3.—Potassium self-diffusion with resin A in a limited bath system. Data for 0.1 M solutions at 725 r.p.m. (▼). Curves calculated based on a coupled film-particle diffusion mechanism using different values of δ and $D^r = 4.68 \times 10^{-6}$ cm.^{1} sec.$^{-2}$ (from shallow bed data) are shown. Results with the shallow bed system shown (●).

Using the limited bath method, the rate of potassium self-diffusion was measured at stirring rates of 500–750 r.p.m. (in which range δ appears to be constant) with various solutions. In the concentration range 0.001 to 0.01 M, the film mechanism predominated, F for each run was quite constant, and the same, calculated value of δ ($10.8 \pm 0.4 \times 10^{-4}$ cm.) was obtained; this is shown in Table V. This value of δ is almost 10 times that of the calculated film thickness from the shallow bed runs.

TABLE V

CALCULATED FILM THICKNESS AT VARIOUS STIRRING RATES —LIMITED BATH METHOD

Resin A, 500–750 r.p.m.

Soln. concn., M	$F \times 10^3$, cm.$^{-1}$	$\delta \times 10^4$, cm.
0.001	0.57 ± 0.01	10.7
.003	0.82 ± .01	11.1
.006	1.84 ± .04	10.1
.010	2.74 ± .11	11.1

Using the limited bath technique, the rate with 0.1 M concentrations was found to be neither particle nor film controlled, *i.e.*, F–P mechanism. Data for an experiment at this concentration carried out at 725 r.p.m. are given in Fig. 3. In-

cluded also in Fig. 3 is a curve calculated using the F–P mechanism, taking the value of δ calculated from the lower concentration runs using the same limited bath technique ($\delta = 10.8 \times 10^{-4}$ cm.), and the value of D^r determined using the *shallow bed technique* ($D^r = 4.68 \times 10^{-6}$ cm.^{2} sec.$^{-1}$). It is seen that the calculated and experimental curves agree closely. Curves calculated using the same value of D^r_K and different values of δ are also shown in Fig. 3.

The effect of rate of flow in the shallow bed system using resin B and 0.1 M solutions is given in Fig. 4. Here $t_{1/2}$, the half time ($Q/Q_0 = 0.5$), is plotted against the linear rate of flow. It is seen that only at slow rates of flow (<100 cm./sec.) does the rate of the process decrease sharply. The range of flow rates used by Boyd and others[4] is also shown by an arrow in Fig. 4. For purposes of comparison, part of the data of Kressman and Kitchener[6] who varied the rate of stirring using a limited bath technique are also shown in Fig. 4. The half-time is shown as a function of r.p.m. of stirring using a simple bent glass stirrer and also a spinning basket device which contained the resin.

Self-diffusion of Diffusible Electrolyte (Chloride).—The rate of elution of non-exchange or diffusible electrolyte, measured by the rate of elution of radio-chloride from a 0.1 M potassium chloride solution, was found to be particle diffusion controlled. This is as expected because the distribution coefficient is much less than unity, for Donnan effects act to exclude the diffusible electrolyte from the resin phase. Substantially the same rate of elution was found when the resin was freed of the adhering solution by suction for two seconds, by simply allowing the excess solution to drain from the particles, or by centrifugation. Results of four runs gave P values of 27.4 ± 0.7 sec.$^{-1}$, with $D^r_{Cl} = 8.1 \times 10^{-6}$ cm.^{2}/sec., where D^r_{Cl} is the diffusion coefficient of the diffusible electrolyte.

When the resin is blotted dry to the free-flowing state, a process which removes about 10% of the solution,[5] the rate of elution is reduced about 50% to a P value of about 15 (as compared to $P = 27$ previously). This effect undoubtedly results from the time lag required to rehydrate the resin, and the net flow of solvent into the resin. Also, P is not very constant, but varies continually from 17.4 at $Q/Q_0 = 0.16$ to 15.3 at $Q/Q_0 = 0.28$ down to 13.2 at $Q/Q_0 = 0.47$.

When the resin (equilibrated as before with a 0.1 M potassium chloride solution) is eluted with distilled water rather than with 0.1 M potassium chloride solution, the observed rate of elution is approximately doubled, with a P value of 46.6 ± 2.6 × 10^{-3}. The P parameter did not show random variations here as for elution against 0.1 M potassium chloride, but increased continually, from $P = 41.4$ at $Q/Q_0 = 0.26$ to $P = 50.2$ at $Q/Q_0 = 0.65$. When similar experiments, namely, elution against pure water, are performed with 0.2 M equilibrated resins, P is lowered ($P = 23.5 \times 10^{-3}$), while with 2 M equilibrated resins P is still lower ($P = 18.8 \times 10^{-3}$).

Two factors appear to be operative here. First, the experimental value of D^r_{Cl} appears to be concentration dependent, increasing at lower solution phase concentrations, other things being equal. This effect is observed when 0.1 M equilibrated resin is eluted with pure water. When the resin is equilibrated with more concentrated solutions where a marked de-swelling takes place, and is subsequently eluted against pure water, the flow of solvent into the resin makes for a lower rate of chloride elution. Experiments are now in progress to elucidate these effects further.

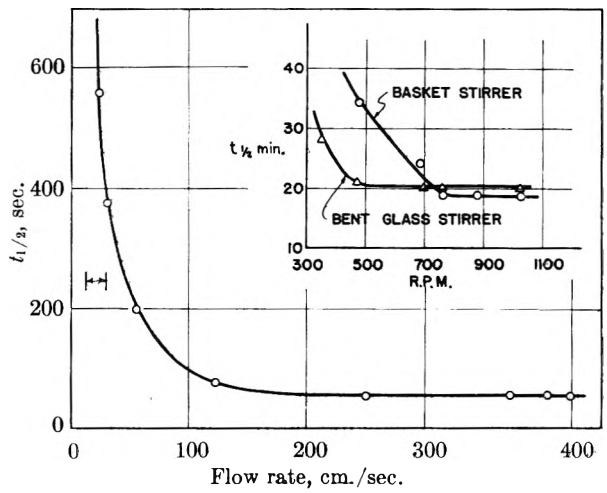

Fig. 4.—Half-time of self-diffusion process for potassium (0.1 M solution) in a shallow bed system as a function of rate of flow. Range of flow rates utilized by Boyd[4] shown (↔). Insert figure for Kressman and Kitchener[6] for half-time of ammonium–tetraethylammonium exchange process as a function of rate of stirring using limited bath method.

Self-diffusion of Solvent.—The rate of elution of deuterated water was measured at high rates of flow in the shallow bed system as described previously. The rate was particle diffusion controlled, with $P = 72.5 \pm 6.8 \times 10^{-3}$ sec.$^{-1}$ in 0.1 M potassium chloride solution, and $P = 65.9 \pm 6.0 \times 10^{-3}$ sec.$^{-1}$ in 0.001 M potassium chloride. The error in each value of P was about ±10%, and due in large part to the extreme experimental difficulties encountered because the process was very rapid, the half-times being less than 5 sec. Also, the error in the determination of deuterium is substantial.

The calculated values of the diffusion coefficients D^r_{HDO} are 21.4 × 10^{-6} cm.^{2} sec.$^{-1}$ in 0.1 M potassium chloride, and 19.4 × 10^{-6} cm.^{2} sec.$^{-1}$ in 0.001 M potassium chloride. The film contribution to these processes is negligible. These values of D^r can be compared with values obtained for the free diffusion of water in water, as obtained by Wang,[11] who obtained values of $D = 23.4 \times 10^{-6}$ cm.^{2} sec.$^{-1}$ for HDO and $D = 26.6 \times 10^{-6}$ cm.^{2} sec.$^{-1}$ for H_2O^{18}.

Discussion

For purposes of convenience, some of the important values obtained in this work with resin A are summarized. For potassium self-diffusion with 0.1 M solutions, $(D^r_K)_{0.1\ M} = 4.7 \times 10^{-6}$ cm.^{2} sec.$^{-1}$,

(11) J. H. Wang, *J. Am. Chem. Soc.*, **73**, 710 (1951); **75**, 466 (1953).

while the value obtained in a 4 M solution phase is $(D_{KCl})_{4\ M} = 22 \times 10^{-6}$. For the diffusible electrolyte, $(K^r_{Cl})_{0.1\ M} = 8.1 \times 10^{-6}$. For deuterated water, with the solution phase 0.001–0.1 M, $D^r_{HDO} = 20 \times 10^{-6}$, while for the value in solution, $D_{HDO} = 23.4 \times 10^{-6}$.

Consider first the effect of concentration of the solution phase upon the rate of the process when the resin is in a shallow bed system, at a rate of flow sufficiently high so that δ is well defined. It is seen that in dilute systems ($\leqslant 0.001$ M) where δ is measured directly, the calculated film thickness is indeed constant over at least a ten-fold concentration range.

The calculation of D^r_K is not as unequivocal as that of δ, but requires some insight into the resin system and the mechanism of transport in it. D^r_K was calculated using 0.1 M data, and while an excellent fit to 0.01 M data was obtained, the fit to 0.2 M data was not nearly as close, and the experimentally determined rate in 1.0 M solutions was considerably faster than that predicted. For example, $(D^r_K)_{0.1\ M} = 4.7 \times 10^{-6}$, while $(D^r_K)_{1\ M} = 6.5 \times 10^{-6}$; the calculated diffusion coefficient in 1 M solutions is therefore about 40% higher than that for 0.1 M solutions.

Before discussing the reasons for choosing 0.1 M data for a valid calculation of D^r_K, it is essential to review the salient physical properties of these systems. First, the micro-structure of the resin is essentially homogeneous, being that of a three-dimensional high polymer network where the average distance between fixed exchange groups is about 8 Å. Pores do not exist in the sense of enclosed passageways, but the open network allows ready movement in all directions. The fact that the diffusion coefficient of the solvent approaches the value it has in true solution ($D^r_{HDO} = 20 \times 10^{-6}$; $D_{HDO} = 23 \times 10^{-6}$) is evidence of the open network.

Boyd and Soldano[12] measured the self-diffusion of solvent using H_2O^{18}, using a limited bath technique, and found that $D^r_{H_2O} = 5.4 \times 10^{-6}$ with a DVB 8 hydrogen form resin and with pure water in the solution phase; the value of D_{H_2O} in free solution is 27×10^{-6}. With DVB 4 resin $D^r_{H_2O} = 9.1 \times 10^{-6}$; with DVB 16 resin $D^r_{H_2O} = 2.2 \times 10^{-6}$. While these diffusion coefficients were found to be relatively higher (compared to values in free solution) than values for sodium self-diffusion, the absolute values found are lower than were found in this investigation. The answer may lie in differences in technique. In this investigation, high rates of flow were used, ensuring a minimum thickness of the unstirred film which eliminated any appreciable F contribution. Also, for very rapid processes such as solvent diffusion where half-times of only about 5 sec. are encountered, the use of the shallow bed system makes for precise control and measurement of experimental conditions. In the limited bath method, where the unstirred film has a thickness of about an order of magnitude greater than that attainable with a shallow bed system, it may be necessary to correct for film diffusion, which was not done. Figure 4 serves to point up the film contribution even at higher concentrations. Also, some solvent may be carried by exchanging cations as water of hydration,[12] and this factor may increase our value of D^r_{HDO}; this effect was absent in the work of Boyd and Soldano,[12] who measured diffusion into pure water.

Where higher degrees of cross-linking exist, or similarly, where the diffusing species has a diameter which is as large or larger than the smaller network openings, or where adsorption of the molecule to the resin matrix exists, the rate of diffusion will be lower than in free solution. The decrease in $D^r_{H_2O}$ with cross-linking observed by Boyd and Soldano[12] is a case in point. Gregor, Collins and Pope[13] measured rates of diffusion of neutral molecules in sulfonic acid resins, and found that for urea $D^r = 1.2 \times 10^{-6}$, while in free solution the corresponding value is 13.6×10^{-6}. Urea is a larger molecule than water, and is highly polarizable. Large molecules such as isobutyl acetate diffused but 0.2% as rapidly in the resin as in solution. Any direct comparison of values of D^r for an exchange cation with those of a neutral molecule must take into account the fact that the diffusive mechanisms may be fundamentally different.

Another factor to consider is the actual ionic composition of the resin phase. The amount of diffusible or non-exchange electrolyte in the resin phase increases sharply with the solution phase concentration in certain concentration ranges, as shown by Gregor, Gutoff and Bregman[2] and Gregor and Gottlieb.[14] For a resin almost identical with that used in this investigation, at concentrations of potassium chloride in the solution phase of 0.01, 0.1 and 1.0 molal, the respective molalities of non-exchange electrolyte (m^r_{Cl-}) and potassium (m^r_{K+}) were: 0.01 m, 0.0069 and 7.85; 0.1 m, 0.0158 and 7.90; 1.0 m, 0.286 and 8.78.[14] It is seen that in 0.01 m solutions $(m_{Cl-}/m_{K+})^r$, the ratio of chloride to potassium, is 0.0009, in 0.1 m it is 0.002, while in 1 m solutions it is 0.033. This means that the amount of diffusible chloride present is negligible and the concentration of potassium is almost constant at solution phase concentrations up to 0.1 M, but that at 1.0 M concentrations the non-exchange electrolyte content is appreciable, and that the potassium which is present to compensate electrically for the chloride is 3.3% of the total. Also, in 0.1 M solutions the concentration of potassium in the resin is 3.35 M, with an average distance of separation of 8.0 Å., while in 1.0 M solutions it is 3.7 M with a spacing of 7.6 Å.

The third factor to consider is that the chloride ion diffuses 70% faster (8.1 compared to 4.7) than the *average* potassium ion, when measured in 0.1 M solutions. The somewhat greater mean activity coefficient of the diffusible electrolyte in 1.0 M solutions compared to 0.1 M solutions[14] suggests that in more concentrated solutions the diffusion coefficient would be greater also. Boyd and Soldano[12] have measured the self-diffusion co-

(12) G. E. Boyd and B. A. Soldano, *J. Am. Chem. Soc.*, **75**, 6105 (1953).

(13) H. P. Gregor, F. C. Collins and M. Pope, *J. Colloid Sci.*, **6**, 304 (1951).

(14) H. P. Gregor and M. Gottlieb, *J. Am. Chem. Soc.*, **75**, 3539 (1953).

efficient with potassium bromide and a DVB 8 resin, and find that $(D^r_{Br})_{1\ M\ NH_4Br}$ is 1.1×10^{-6}, which is considerably lower than our value (8.1×10^{-6} in 0.1 M), but about three times as large as the diffusion coefficient of a sodium ion, measured under similar conditions.[15] Here, as before,[12] a limited bath technique was used, without corrections for the film contribution.

The choice of 0.1 M data as the basis for calculating D^r is therefore based on the following considerations. First, the resin phase composition is essentially constant at concentrations up to 0.1 M. The 0.01 M system data could have been used to calculate D^r_K with the same result, but the minor film diffusion contribution makes the 0.1 M data easier to utilize.

Under these conditions, namely, dilute solutions, the diffusion of potassium ions must essentially involve migration from exchange site to exchange site. Since the sites are fixed in space, movement of an ion from one site to another would require first that an ion jump into an occupied site or into an area adjacent to an occupied site, making for the "activated complex." Then the filling of the "hole" by either any adjacent cation or the one originally present in the occupied site constitutes the diffusive process. The activation energy for the diffusive process in the resin[4,12,15] is significantly higher than for diffusion in a system containing only diffusible anions and cations (free solution). It is this different type of diffusive mechanism which makes for a value of D^r_K which is significantly smaller, in this case, about 20% of the value in free solution.

When the solution phase concentration is raised to 1 M, the diffusivity of the potassium ions is increased in two ways: first, the number of potassium ions in the "activated complex" is increased by the number of added chloride ions; second, the chloride ions allow the more rapid diffusion of potassium ions which are present to compensate for them electrically. Both of these effects act to give larger values for the diffusion coefficient of potassium at higher concentrations.

The authors wish to thank Dr. V. J. Linenbom of the Naval Research Laboratory for his encouragement and interest in this work. They wish to thank Dr. H. P. Broida for his advice and assistance on the heavy water analyses. Finally, they wish to thank Dr. R. A. Marcus for his stimulating comments and criticism. That part of this work performed at the Polytechnic Institute of Brooklyn was supported by a grant from the Office of Naval Research.

(15) G. E. Boyd and B. A. Soldano, *J. Am. Chem. Soc.*, **75**, 6091 (1953).

VISCOMETRIC AND TURBIDIMETRIC MEASUREMENTS ON DILUTE AQUEOUS SOLUTIONS OF A NON-IONIC DETERGENT

BY LAWRENCE M. KUSHNER AND WILLARD D. HUBBARD

Surface Chemistry Section, National Bureau of Standards, Washington 25, D. C.

Received July 16, 1954

The viscosities and turbidities of a number of dilute solutions of a non-ionic detergent, Triton X-100 (a polyoxyethylene condensate of an octylphenol), in water, in 0.04 and in 0.12 M sodium chloride have been determined. The intrinsic viscosity and molecular weight of the micelles are 0.055 dl./g. and 90,000, respectively, independent of added salts. The results are best interpreted in terms of a highly hydrated, spherical micelle of radius equal to the length of a nearly completely extended detergent molecule.

I. Introduction

Since their emergence, less than a decade ago, as commercially important materials, non-ionic detergents have been the subject of a number of investigations. Only a few[1-5] of these, however, have been designed to provide fundamental information regarding the nature of the colloidal aggregates of non-ionic detergent in solution. In the dilute region (less than 1–2%) in aqueous solvents, only the data of Gonick and McBain[2] are relevant.

In general the assumption has been made that non-ionic detergents, in aqueous solutions, behave in a similar manner to the ionic detergents, which have been studied extensively.[6] A more detailed study of the dilute aqueous solutions of a non-ionic detergent was justified, however, for three reasons: (1) non-ionic detergents have negative solubility coefficients in aqueous solvents indicating that their mode of interaction with the solvent is different from that of ionic detergents; (2) whereas in the ionic detergents the hydrophobic portion of the molecule is much larger than the hydrophilic group, in the non-ionics the hydrophilic portion of the molecule is generally at least as large as the hydrophobic part; (3) the absence of an electric charge on the micelles formed by non-ionic detergents eliminates a complicating factor which is always present in the interpretation of data obtained for ionic micellar systems.

Accordingly, viscosity and turbidity measurements have been made on dilute solutions of the non-ionic detergent, Triton X-100, in water, in 0.04 and in 0.12 M sodium chloride solutions.

(1) E. Gonick, *J. Colloid Sci.*, **1**, 393 (1946).

(2) E. Gonick and J. W. McBain, *J. Am. Chem. Soc.*, **69**, 334 (1947).

(3) J. W. McBain and S. S. Marsden, Jr., *J. Chem. Phys.*, **15**, 211 (1947).

(4) S. S. Marsden, Jr., and J. W. McBain, THIS JOURNAL, **52**, 110 (1948).

(5) J. H. Schulman, R. Matalon and M. Cohen, *Discs. Faraday Soc.*, No. 11, 117 (1951).

(6) H. B. Klevens, *J. Am. Oil Chemists Soc.*, **30**, 74 (1953).

II. Experimental

Materials.—The Triton X-100 was supplied by the Rohm and Haas Company, Philadelphia, Pa. It is a condensate

of ethylene oxide with an octylphenol and can be represented by the formula

$$(CH_3)_3CCH_2C(CH_3)_2C_6H_4O(CH_2CH_2O)_nH$$

According to its manufacturer the mean value of n for this material is 10, thus making its mean molecular weight 646. A crude measurement of the freezing point depression of a benzene solution of the substance has given us a value of close to 650 for the molecular weight.

In order to reduce the possibility of contamination by unreacted ethylene oxide or alkyl phenol, the sample was subjected to pumping out for a period of a few days at room temperature.

Viscosity.—The experimental details and necessary corrections to be applied to the measured efflux times have been described previously.[7] The only change in procedure has been the use of smaller pycnometers for the density determinations.[8]

Light Scattering.—All turbidity measurements were made at 436 mμ with a light scattering photometer which has been described in an earlier publication.[9] A semi-octagonal cell was used for the measurements since not only was it large enough to permit a concentration technique for preparing solutions (see following paragraphs), but it also made possible measurement of the dissymmetry of scattering as a check on the cleanliness of the solutions. The dissymmetry of scattering was characterized by the ratio of scattered flux at 45° to the scattered flux at 135°.

Refractive index increments at 436 mμ were determined in the usual manner with a Phoenix differential refractometer.[10] For the three systems considered, Triton X-100 in water, in 0.04 and in 0.12 M sodium chloride, the values of $(\Delta n/\Delta c)$ were identical, 0.155 ml./g.

It was found that the best procedure for obtaining satisfactory turbidity data as a function of concentration was as follows. For each solvent, a master solution containing 2.500 g. of Triton X-100 in 100.0 ml. of solution was prepared. It was then repeatedly forced through a Selas 04 micro-porous porcelain filter until no further reduction of its dissymmetry could be obtained by additional filtration. Using another filter of the same porosity, pure solvent was filtered into a clean scattering cell. The cell was rinsed with these filtered portions of solvent until one sample of about 45 ml. showed no dissymmetry. Its turbidity was determined and it was then used as solvent for that run. In a stepwise manner portions of master solution were then pressure filtered directly into the cell containing solvent. After each addition of master solution, the contents of the cell were carefully mixed and a turbidity measurement made. Knowing the weight of pure solvent in the cell initially and determining the weight of master solution added in each step, the concentration of each solution was easily calculable. In a separate experiment it was determined that repeated filtration did not significantly change the concentration of these solutions.

It was found as a result of the experimental investigation that all of the detergent solutions showed a measurable dissymmetry. Usually the least concentrated solution of a run had a dissymmetry of about 1.05 to 1.08 which then decreased so that above a concentration of 0.3 g./dl. the dissymmetry remained constant at close to 1.03. The origin of this effect has not been established. From the measured micelle weights it is not possible to postulate any reasonable micelle structure in which internal interference effects could give rise to any dissymmetry. The low concentration and absence of micellar charge eliminates the possibility of external interference. The inference is then that some foreign matter was not completely removed from the detergent solutions by our filtration procedure. It must be mentioned however that the same filter with which the dissymmetry of a detergent solution could not be reduced below 1.03, did reduce the dissymmetry of water to 1.01 or less. The foreign matter is then associated with the detergent. This is not unreasonable. The only efforts made to purify the Triton X-100 were designed to remove unreacted phenols or ethylene oxide. Any very large structures formed in the polymerization reaction used for the production of the detergent would still be present. Indeed, any high boiling impurities, regardless of the means of introduction into the sample, would not have been removed by the procedure used. The nature of dependence of the dissymmetry on concentration of detergent merely indicates that the physical form of the dissymmetry-causing units is affected by the presence of micelles, perhaps by solubilization.

(7) L. M. Kushner, B. C. Duncan and J. I. Hoffman, *J. Research Natl. Bur. Standards*, **49**, 85 (1952), RP2346.

(8) H. M. Smith and coöperators, *Anal. Chem.*, **22**, 1452 (1950).

(9) L. M. Kushner, *J. Opt. Soc. Am.*, **44**, 155 (1954).

(10) Manufactured by Phoenix Precision Instrument Co., Philadelphia, Pa., and described in B. A. Brice and M. Halwer, *ibid.*, **41**, 1033 (1951).

Results and Discussion

Fundamental interpretations of viscosity[11] and turbidity[12] data for dilute colloidal solutions are based on the relationships

$$\frac{(\eta_{rel} - 1)}{c} = [\eta] + Dc \qquad (1)$$

and

$$H\frac{c}{\tau} = \frac{1}{M} + 2Bc \qquad (2)$$

In equation 1, $\eta_{rel} = \eta/\eta_0$ where η is the viscosity of the solution of concentration c (in g./dl.) and η_0 is the viscosity of the solvent. The quantity $[\eta]$ is termed the intrinsic viscosity and is $0.025/\rho$ dl./g. for impenetrable spherical particles of density ρ. (It is assumed in the following discussion that ρ is close to unity for our system.) Deviations of $[\eta]$ from this value are interpretable, for the system under consideration, in terms of either non-sphericity of the colloidal particles or solvation. The constant D depends on those interactions in the system which give rise to disturbing hydrodynamic effects. The left-hand side of equation 1 is generally referred to as the reduced specific viscosity.

In equation 2, τ (cm.$^{-1}$) is that part of the turbidity of the solution of concentration c (g./ml.) that is due to the colloidal particles (*i.e.*, $\tau = \tau_{soln} - \tau_0$, where τ_{soln} is the observed turbidity of the solution and τ_0 that of the solvent). M is the weight average molecular weight of the colloidal particles. The constant B is a measure of particle–solvent interaction. H is a constant for a particular particle–solvent system depending on the refractive index of the solvent, the square of the refractive index increment of the solutions, and the fourth power of the wave length of the light used.

It is to be noticed that in both cases the application of the equations to detergent micellar systems requires that a definition of the solvent of the system be made. This problem has been previously discussed with regard to viscosity measurements.[7] The same considerations apply to the analysis of light scattering data.

Figures 1 and 2 show the dependence of viscosity and turbidity, respectively, on the concentration of Triton X-100 in the three solvents investigated. Because of the lack of charge on the micelles, the presence of electrolyte appears to have little effect either on the kinetic properties of the micellar solutions or on the size or number of the colloidal aggregates. In the case of the viscosity data, the separation of the curves is due to the slight difference in the viscosities of the solvents. For the turbidity data, the three sets of points lie

(11) A. E. Alexander and P. Johnson, "Colloid Science," Vol. I, Oxford at The Clarendon Press, New York, N. Y., 1949, p. 358.

(12) P. Doty and J. T. Edsall in "Advances in Protein Chemistry," Vol. VI, Academic Press, Inc., New York, N. Y., 1951.

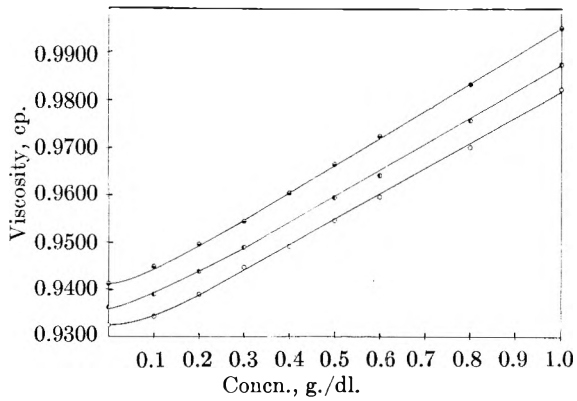

Fig. 1.—The concentration dependence of the viscosity of solutions of Triton X-100 in three aqueous solvents. The units of viscosity are centipoise. Concentrations are expressed as grams of detergent in 100 ml. of solution: bottom curve (○), in distilled H_2O; middle curve (◐), in 0.04 *M* NaCl; top curve (◒), in 0.12 *M* NaCl.

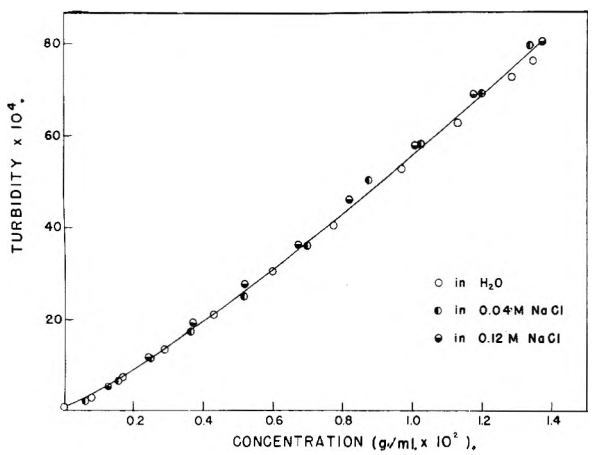

Fig. 2.—The concentration dependence of the turbidity of solutions of Triton X-100 in three aqueous solvents. Turbidities are in cm.$^{-1}$. Concentrations are expressed as grams of detergent in 1 ml. of solution.

very nearly upon one another since, on this scale, the turbidities of the three solvents are practically identical.

Gonick and McBain[2] have reported, on the basis of freezing point depression experiments, a critical micelle concentration of 0.0009 *M* (0.058 g./dl.) for a sample of Triton X-100. Neither in the runs shown in Fig. 2, nor in other data obtained in the region up to 0.1 g./dl., however, was any such effect shown. This is surprising since it has been demonstrated by Debye[13] that light scattering measurements are a sensitive means for determining the sudden onset of micelle formation. A possible explanation of the lack of appearance of a critical micelle concentration would be that the sample of Triton X-100 used for these measurements had a broad distribution of molecular weights. If this were the case the low molecular weight molecules would begin forming micelles at very low concentrations. The higher molecular weight species would undergo micelle formation at somewhat higher concentrations. If the distribution of molecular weights were continuous, then no sharp critical micelle concentration would be observed.

(13) P. Debye, *Ann. N. Y. Acad. Sci.*, **51**, Art. 4, 575 (1949).

On the basis that the level of turbidity clearly indicates the presence of colloidal aggregates in these solutions, yet no critical micelle concentration was evident, it was decided to apply equations 1 and 2 to these data making the assumption that all of the detergent present, even at the lowest concentrations, is micellar (*i.e.*, assume that the solvents for the micelles are water, 0.04 and 0.12 *M* sodium chloride). The results are shown in Figs. 3 and 4.

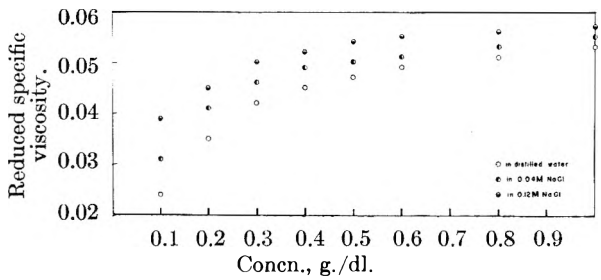

Fig. 3.—The reduced specific viscosity as a function of concentration of detergent assuming that at each concentration all of the detergent dissolved is micellar.

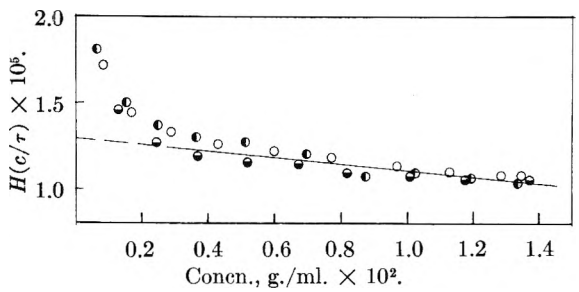

Fig. 4.—$H(c/\tau)$ as a function of concentration of detergent assuming that at each concentration all of the detergent dissolved is micellar; ○, in H_2O; ◐, in 0.04 *M* NaCl; ◒, in 0.12 *M* NaCl.

Clearly the intrinsic viscosity cannot be obtained by an extrapolation of the data in Fig. 3, nor can $[H(c/\tau)]_{c=0} = 1/M$ be evaluated from the experimental points shown in Fig. 4. The departure from linearity in both sets of data however suggests that below a concentration of about 0.3 g./dl., not all of the Triton X-100 dissolved is becoming micellar; that is, the monomer saturation concentration[7] (that concentration of detergent above which essentially all detergent added to the solution becomes micellar) is 0.3 g./dl.

Recalculation of the data, assuming that the appropriate solvent for the micelles for use in equation 1 and 2 is a solution containing 0.3 g./dl. of detergent, results in the linear plots shown in Figs. 5 and 6. From the light scattering data a micelle molecular weight of close to 90,000 is obtained. This corresponds to approximately 140 detergent molecules to a micelle. From Fig. 6 one obtains a value of 0.055 dl./g. for the intrinsic viscosity of the micelles. The significance of this figure is to be discussed.

In view of the lack of micelle charge in non-ionic detergent systems, deviations of the intrinsic viscosity from the theoretical value of 0.025 dl./g. for impenetrable spheres can be interpreted either in terms of micelle non-sphericity or solvent entrapment. We first consider the possibility of non-

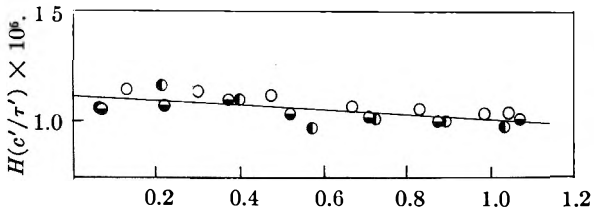

Fig. 5.—Replot of turbidity data assuming a monomer saturation concentration of 0.3 g./dl.: c' = concentration of micelles = total concentration of detergent minus the monomer saturation concentration; τ' is the turbidity of the solution minus the turbidity of a solution containing 0.3 g./dl. of detergent; ○, in H_2O; ◐, in 0.04 *M* NaCl; ◒, in 0.12 *M* NaCl.

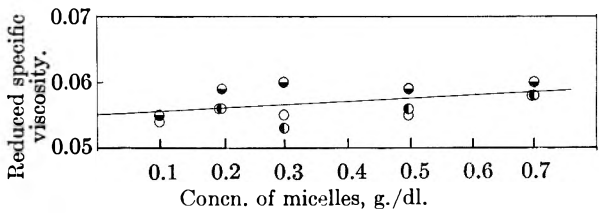

Fig. 6.—Reduced specific viscosity as a function of concentration of micelles assuming a monomer saturation concentration of 0.3 g./dl.: ○, in distilled water; ◐, in 0.04 *M* NaCl; ◒, in 0.12 *M* NaCl.

sphericity. The two most commonly considered non-spherical micelle shapes are the disc and the rod. The disc, discussed by Harkins,[14] has a thickness of twice the length of a detergent molecule. Assuming an extended configuration for a molecule of Triton X-100, one can calculate from the bond lengths and bond angles a length of close to 45.5 Å. for the fully extended molecule. Approximately three fourths of this length is associated with the hydrophilic, oxyethylene chain and one would expect it to be fully extended in an aqueous solvent. The remainder, being hydrophobic, would tend to be curled up. However this portion of the molecule, a highly branched alkyl phenyl group, cannot, because of steric effects, reduce its length by very much. We are then justified in assuming an over-all length of between 40 and 45.5 Å. for the molecules. For purposes of calculation 43 Å. will be used. This means that the Harkins disc has a thickness of 86 Å. From the macroscopic density of Triton X-100 (1.06 g./ml. at room temperature) one calculates that each molecule occupies a volume of about 1000 Å.^{3} The micelle then must have a volume of about 140,000 Å.^{3} A disc of thickness 86 Å. must have a radius of 23 Å. in order to have the required volume. This "disc" approximates a prolate spheroid of revolution of axial ratio 1.9. This should give rise to an intrinsic viscosity of 0.029 dl./g.[15]

For the rod-like model of Debye,[16] the diameter of the rod must be 86 Å. A calculation similar to that used for the disc shows that the length of the rod must be 24 Å. This "rod" is approximated by an oblate spheroid of revolution of axial ratio 3.6. Particles of such shape should have an intrinsic viscosity of about 0.038 dl./g.[15] Neither model suffices to explain the intrinsic viscosity of 0.055 dl./g. found experimentally. Further, in order to satisfy both the hydrophilic and hydrophobic tendencies of the detergent molecules, both of these structures would tend to be distorted toward sphericity. The calculated axial ratios and intrinsic viscosities are therefore maximal values.

If the difference between an intrinsic viscosity of 0.055 and 0.025 dl./g. is to be ascribed to hydration, one calculates that about 43 molecules of water are kinetically bound to each detergent molecule in a micelle. Although this figure may seem high, it is reasonable on the basis of two considerations. (1) The solubility of this detergent in water is due to hydration (thus its negative solubility coefficient). The only places in each detergent molecule at which hydration can occur are the oxygen atoms in the oxyethylene chain. Since there are, on the average, ten such atoms per molecule, it is reasonable that twenty or more water molecules could be bound to each detergent molecule. (2) Approximately three fourths of the length of each detergent molecule must be considered hydrophilic. Most likely the hydrophilic part of the molecules can be thought of as tentacles protruding from the hydrocarbon interiors of the micelles into the aqueous phase. The remaining water molecules that are associated with a micelle are then those that would be trapped by these tentacles and should be considered kinetically as part of the micelle.

If one assumes that the micelle is spherical and has a radius of 43 Å., then its volume would be 333,000 Å.^{3} Of this, 140,000 Å.^{3} are occupied by the 140 detergent molecules and the remainder, 193,000 Å.^{3}, should accommodate the nearly 6000 bound water molecules. From the macroscopic density of water one calculates that 6000 water molecules occupy close to 198,000 Å.^{3}, in close agreement with the volume just calculated as available for the bound water in the spherical micelle. It is seen then that the assumption of a spherical micelle of radius about 43 Å. is consistent with both the number of detergent molecules per micelle as deduced from light scattering measurements and the extent of hydration as calculated from viscosity data.

Summary.—Viscosities and turbidities of dilute solutions of the non-ionic detergent Triton X-100 in water, in 0.04 and in 0.12 *M* sodium chloride, have been determined. Formation of micelles appears to begin at the lowest concentrations, although the monomer saturation concentration does not occur until about 0.3 g./dl. Considering this concentration of detergent as the solvent system for the micelles, one obtains linear dependence of the reduced specific viscosity and $H(c/\tau)$ on concentration of micelles, leading to a value of 90,000 for the micelle molecular weight and 0.055 dl./g. for the intrinsic viscosity of the micelles. The presence of neutral electrolyte has no effect on the properties of the micelles. These data are best interpreted on the basis of a highly hydrated spherical micelle consisting of about 140

(14) W. D. Harkins, *J. Chem. Phys.*, **16**, 156 (1948); R. W. Mattoon, R. S. Stearns and W. D. Harkins, *ibid.*, **16**, 644 (1948).

(15) J. Mehl, J. Oncley and R. Simha, *Science*, **92**, 132 (1940).

(16) P. Debye and E. W. Anacker, THIS JOURNAL, **55**, 644 (1951).

detergent molecules, oriented radially, and entrapping some 6000 molecules of water. The radius of the sphere is that of a nearly completely extended detergent molecule.

NOTES

POTENTIOMETRIC STUDIES ON SODIUM ACETATE–SODIUM PERCHLORATE SYSTEMS IN ACETIC ACID[1]

By Takeru Higuchi, Maria L. Danguilan and Aaron D. Cooper

School of Pharmacy, University of Wisconsin, Madison, Wisconsin

Received June 14, 1954

The present communication is concerned with the influence of sodium perchlorate on the relative basicity of sodium acetate in acetic acid. Although the acetate salt is presumed to be nearly completely ionized (in the sense that electron transfer from the cation to the anion is essentially complete), such compounds have been found to exist mainly in the form of neutral "ion-pairs" in solvents of low dielectric constants.[2,3] No previous attempts seem to have been made, however, to study the possible influence of other salts having a common cation on the dissociation behavior of a base such as sodium acetate in acetic acid.

By means of a glass–calomel electrode assembly, it was possible to obtain results which are in accordance with those obtained by Hall and Werner,[4] the latter workers having employed a chloranil–calomel electrode system as a basis for their potentiometric measurements. In our laboratory it has been found that the glass electrode responds to the hydrogen ion activity of acetic acid systems (or equivalently, to the acetate ion activity). Figure 1 shows, for example, the effect of variation in the relative basicity of acetic acid containing varying amounts of sodium acetate as a function of the concentration of base present as obtained by the present potentiometric method. In accordance with the work of the previous authors,[4] the slope of the dilution curve is close to 0.5, *i.e.*, 0.059/2 volts, per tenfold change in concentration, the solid line representing the theoretical slope and the points the experimental values.

In the presence of a constant sodium perchlorate concentration, as shown in Fig. 2, this slope becomes unity, *i.e.*, 0.059 volt per tenfold change in the sodium acetate concentration, while in the alternative situation, where the sodium acetate concentration

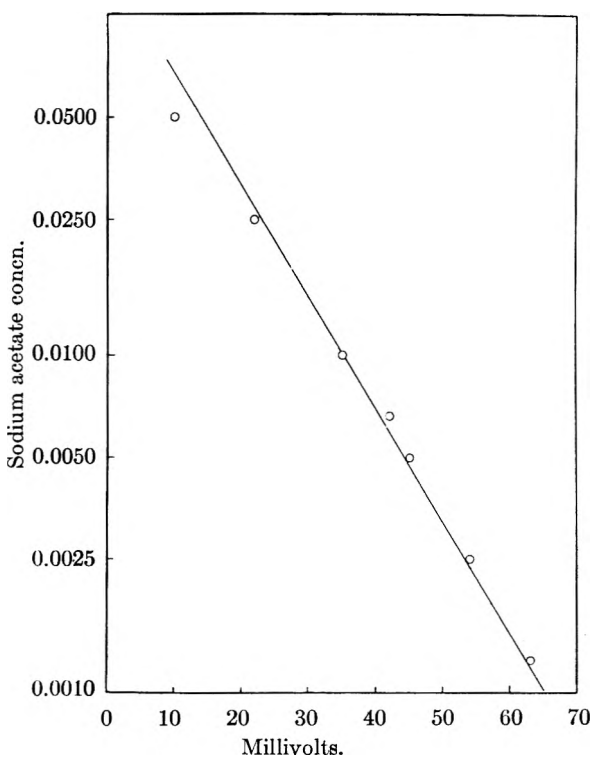

Fig. 1.—Potentiometric study of the behavior of sodium acetate in glacial acetic acid.

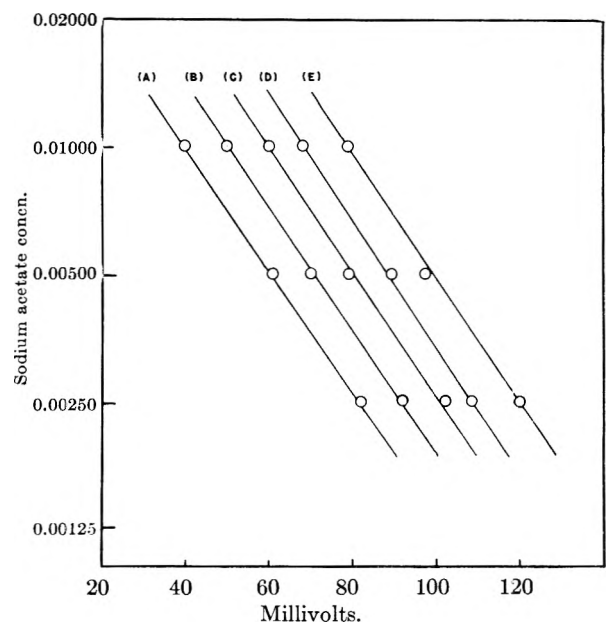

Fig. 2.—Potentiometric determination on sodium perchlorate–sodium acetate system; concn. of sodium perchlorate in *M*: A, 0.00125; B, 0.00250; C, 0.00500; D, 0.01000; E, 0.02000.

(1) Supported in part by a grant from the Research Committee from funds supplied by the Wisconsin Alumni Research Foundation.

(2) I. M. Kolthoff and A. Willman, *J. Am. Chem. Soc.*, **56**, 1014 (1934).

(3) E. Griswold, M. M. Jones and R. K. Birdwhistell, *ibid.*, **75**, 5701 (1953).

(4) N. F. Hall and T. Werner, *ibid.*, **50**, 2367 (1928).

is fixed and that of the perchlorate varied (Fig. 3), a slope of 0.5 for a tenfold change in concentration is observed. In both cases, a linear relationship is present as the concentration of one of the moieties is varied while the other is maintained constant. These results may be rationalized by assuming that sodium perchlorate undergoes greater dissociation than sodium acetate (a greater degree of "ion-pair" separation), hence the sodium ion concentration of the solution may be attributed mainly to the sodium perchlorate. By expressing the dissociation constants for the two salts as

$$K_{NaClO_4} = (Na^+)(ClO_4^-)/(NaClO_4) \quad (1)$$

$$K'_{NaAc} = (Na^+)(Ac^-)/(NaAc) \quad (2)$$

and employing the simplifying assumption[5] above that the concentration of sodium ion is determined essentially through the dissociation of sodium perchlorate, we obtain the relationship

$$(Na^+) \cong \{K(NaClO_4)\}^{1/2} \quad (3)$$

$$(2 + 3) \quad (Ac^-) \cong K'(NaAc)/K^{1/2}(NaClO_4)^{1/2} \quad (4)$$

Equation 4 shows a first-order dependency on the sodium acetate concentration and an inverse square root dependency on the sodium perchlorate concentration. Since experimental data are in close agreement with those predicted by equation 4, it may be concluded that sodium perchlorate is a "stronger electrolyte" than sodium acetate in acetic acid, hence repressing the dissociation of sodium acetate, resulting in a decrease in the relative basicity of the solution.

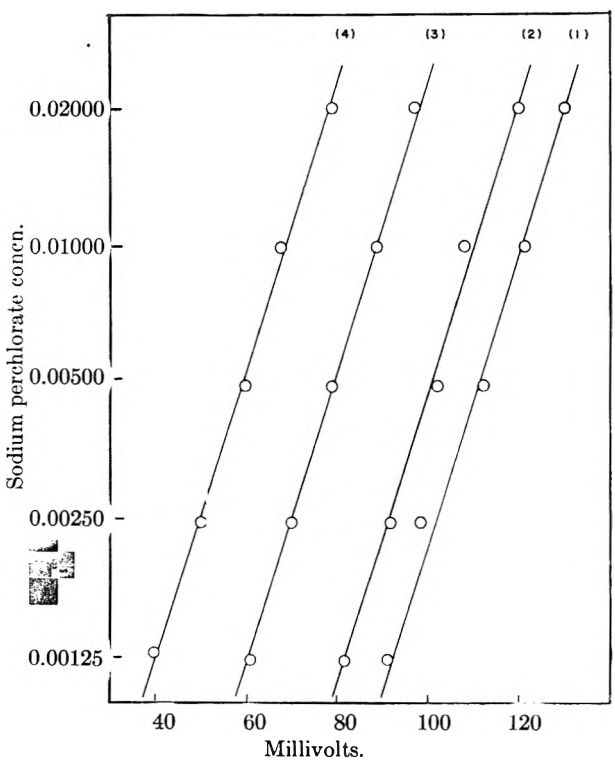

Fig. 3.—Potentiometric determination on sodium acetate–sodium perchlorate system; concn. of sodium acetate in *M*: (1), 0.00125; (2), 0 00250; (3) 0.00500; (4), 0.01000.

(5) This assumption may be shown valid by employing the alternative case, that the sodium ion concentration from the acetate is greater than that from the perchlorate, whereby experimentally determined data do not conform to the derived equation.

It is evident from these behaviors that the common practice of estimating pK values of acids and bases in water by determining the pH of half neutralized solutions cannot be used in certain nonaqueous systems. The apparent basicity of a base, as in the present instance, is dependent in part on the strength of the acid employed in its neutralization. Stronger the acid, weaker the base would appear since the resulting salt formed would be more highly dissociated, leading to a greater suppression of the dissociation of the parent base.

Experimental

Analytical grade reagents were used throughout. Sodium acetate solution, 0.05 molar, was standardized against perchloric acid with quinaldine red as indicator. Sodium perchlorate, 0.025 molar, was prepared *in situ* by mixing equal volumes of 0.05 molar acetic acid solutions of perchloric acid (previously rendered anhydrous with acetic anhydride) and sodium acetate. All other solutions were prepared from these stock solutions.

The potentiometric measurements were carried out using a Beckman Model G pH meter, equipped with a glass electrode and an external calomel electrode joined with the solution by means of an agar–gel bridge (4% agar and 5% potassium chloride). All potentiometric readings were determined relative to that of a 0.100 molar solution of sodium salicylate in acetic acid taken just prior to the determination of the unknown solution. Duplicate determinations on independently prepared solutions agreed, in most part, within one or two millivolts.

DENSITIES OF MOLTEN SODIUM AND RUBIDIUM HYDROXIDES

By Donald Bogart
NACA Lewis Flight Propulsion Lab., Cleveland, Ohio
Received July 26, 1954

The densities of molten sodium and rubidium hydroxides have been determined up to temperatures of 920° using a method based on Archimedes' principle of buoyancy.

The present data for sodium hydroxide in the temperature range 690 to 920° are shown in Fig. 1.

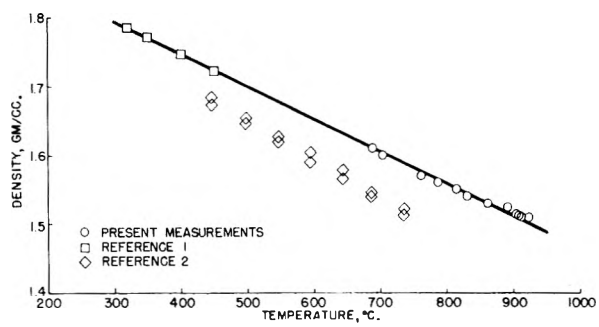

Fig. 1.—Density of molten NaOH.

The previous data[1,2] also indicated, confirm the trend with temperature. The density, ρ(g./cc.), may be expressed as a linear function of temperature, T(°C.), as

$$\rho = 1.94 - 0.00047T$$

The data for rubidium hydroxide (measurements taken on two successive days) are shown in Fig. 2.

(1) K. Arndt and G. Ploetz, Oak Ridge Nat. Lab. Index No. Y-F35-5, Mar. 21, 1952 (translated from *Z. physik. Chem.*, **121**, 439 (1926)).

(2) M. Nishibayashi, Wright Air Development Center Technical Report 53-308, Nov. 1953.

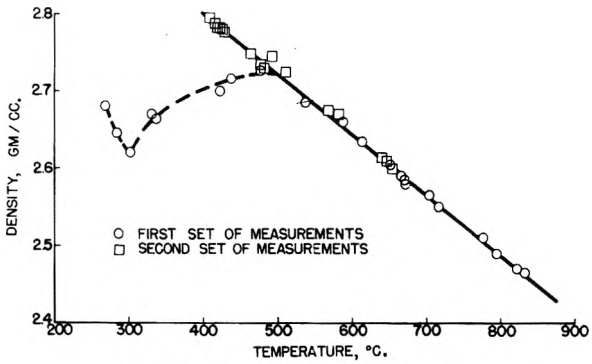

Fig. 2.—Density of molten RbOH.

On the first day, the rubidium hydroxide was found to melt gradually over the temperature range 200 to 250°. Density measurements from 250 to 500° exhibited the reversal shown which may be attributed to the change in density encountered by driving off water from the partly hydrated hydroxide. For higher temperatures the density variation was essentially linear.

During the second set of measurements, rubidium hydroxide melted above 350°. Density measurements in the range 400 to 650° being in agreement with the linear portion of the curve obtained from the first data, indicates no further changes in composition. The density–temperature relationship may be expressed as

$$\rho = 3.11 - 0.00078T$$

The melting point of the dehydrated RbOH was more accurately determined by the cooling curve shown in Fig. 3. The transition occurred at 383°; this value disagrees with a melting point of 300° in the literature.[3] Since in the present investigation a lower melting point was obtained with undried material, it may have been possible that the hydroxide used in the earlier experiments[3] was not completely dehydrated.

Experimental

Both hydroxides were obtained from commercial sources. Analysis indicated the following compositions, given in per cent. by weight:

NaOH	96.2%	RbOH	90.4%
Na_2CO_3	1.0%	Rb_2CO_3	2.1%
H_2O	2.8%	H_2O	7.5%

Each hydroxide was contained in a cylindrical nickel crucible and was gradually heated in a tube furnace controlled through a rheostat. The hydroxides were exposed to air during the tests. Cylindrical nickel plummets were suspended in the molten hydroxides by nickel wire. The loss of weight of the plummets due to the buoyancy of the hydroxides was measured with a precision analytical balance. The volume of the plummets (approximately 5 cc.) was corrected for thermal expansion; this correction is about 5% at 1000°.

Temperatures were measured by means of two chromel–alumel thermocouples spot-welded to the outer wall of the crucible and connected to a direct-reading potentiometer. Temperatures were also measured by immersing a thermocouple directly into the hydroxide; all temperatures agreed within 10°.

Discussion

NaOH.—White vapors were observed above the crucible during the tests. When the nickel crucible was washed out, a considerable quantity of black crystalline material remained which had been formed during the cooling period of about 10 hours; this would not have interfered with the density measurements which were completed during a heating time of about two hours. Loss of weight due to corrosion of the nickel plummet was negligible.

(3) G. Von Hevesy, Oak Ridge Nat. Lab. Index No. Y-F35-6, Apr. 1, 1952 (translated from *Z. physik. Chem.*, **73**, 667 (1910)).

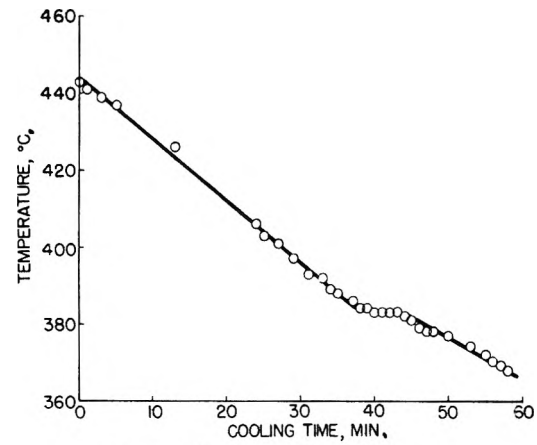

Fig. 3.—Cooling curve for RbOH.

RbOH.—White vapors were again observed leaving the crucible at temperatures above 500°. The nickel wire supporting the plummet failed at a temperature of about 900°. The melt was further heated to about 1000° at which temperature the thermocouples failed. No evidence of boiling was observed and the melt was light yellow and similar in appearance to NaOH at these temperatures. Small black crystals similar to those mentioned above were found when the crucible was washed out. Qualitative analysis of these crystals indicated the presence of some nickel carbonate.

THE CATALYTIC ACTIVITY OF BISULFATE ION IN THE HYDROLYSIS OF ETHYL ACETATE[1]

BY DENNIS W. BARNUM AND GEORGE GORIN

Contributed from the Department of Chemistry, University of Oregon, Eugene, Oregon

Received August 9, 1954

A very large amount of research has been done upon the acid-catalyzed hydrolysis of esters, but there still exists a difference of opinion on whether the reaction is susceptible to acidic species generally, or only to hydrogen ion.[2,3] The very existence of such uncertainty suggests that the catalytic activity of acidic species other than hydrogen ion, if appreciable, cannot be large.

It is therefore surprising to find that the catalytic constant of bisulfate ion has been estimated as 1.5×10^{-3} mole^{-1} min.$^{-1}$, about one-fourth as

(1) Presented at the Northwest Regional Meeting, American Chemical Society, Moscow, Idaho, June 13, 1953.

(2) It is understood that the hydrogen ions are solvated; in this paper, the term "hydrogen ion" refers to the species H_3O^+, and to more or less hydrated forms.

(3) R. P. Bell, "Acid-Base Catalysis," Oxford University Press, London, 1941, p. 48–81, especially p. 80–81; K. J. Laidler, "Chemical Kinetics," McGraw-Hill Book Co., Inc., New York, N. Y., 1950, p. 282–300.

large as that of hydrogen ion.[4] It might be that bisulfate ion is exceptionally active as a catalyst; but it is the purpose of this paper to indicate that such an explanation is unnecessary, as the catalytic constant of bisulfate ion must be considerably smaller than the value quoted.

Table I lists the reaction rate constants for the hydrolysis of ethyl acetate in mixtures of sodium bisulfate and sodium sulfate[4]; Dawson, *et al.*, interpreted the decrease in the values of k and the levelling-off at sodium sulfate concentrations above 1.2 M as due to the gradual and finally complete repression of the ionization of bisulfate by the added sulfate, so that the limiting reaction rate constant would measure the catalysis by undissociated bisulfate ion. The catalytic constant, 1.5×10^{-3}, was calculated on this basis.

TABLE I

HYDROLYSIS OF ETHYL ACETATE IN 0.04 M $NaHSO_4$ + xM Na_2SO_4

x	$10^4 k$, min.$^{-1}$	pH	x	$10^4 k$, min.$^{-1}$	pH
0	1.50	1.69	0.6	0.635	2.26
0.05	1.12		0.8	.615	2.28
.1	0.93		1.0	.61	2.29
.2	.80	2.10	1.2	.61	2.31
.3	.725		1.4	.61	2.31
.4	.68	2.21	1.6	.615	2.31

Although this assumption seemed reasonable, direct measurement of the pH values of the solutions, which are also shown in Table I, do not sustain it; it can be seen that the hydrogen ion activity is far from negligible in all the solutions under consideration. Since the pH values level off at the same sodium sulfate concentrations as the rate constants, this fact, formerly thought so meaningful, is of equivocal significance. Taking reasonable values for the activity coefficient of hydrogen ion and its catalytic constant, 0.7[5] and 9×10^{-3} mole^{-1} min.$^{-1}$,[6] respectively, the reaction rate constant due to hydrogen ion is estimated to be 6×10^{-5} min.$^{-1}$. The closeness of the agreement with the experimental value must be considered fortuitous, because of the unavoidably arbitrary character of some of the values chosen; but it is significant that the right order of magnitude is obtained on the assumption, diametrically opposite to that of Dawson, *et al.*, that hydrogen ion accounts for all the catalysis.

Since a more nearly quantitative treatment of this case is not possible, it is of interest to turn attention to more dilute solutions, in which an estimate of activity coefficients can be made from theory, and primary salt effects are relatively small. Table II lists the reaction rate constants in dilute solutions of sulfuric acid, and Table III those in dilute solutions of sodium bisulfate.[4]

TABLE II

HYDROLYSIS OF ETHYL ACETATE IN xM H_2SO_4

x	$10^4 k$, min.$^{-1}$	$10^4 k$, calcd., D.P.S.	K_{HSO_4}	$10^4 k$, calcd.[8]
0.005	0.545	0.545	1.57	0.54
.01	1.01	1.01	1.76	0.99
.02	1.87	1.88	2.00	1.83
.04	3.49	3.55	2.30	3.37
.05	4.34	4.37	2.43	4.15
.08	6.56	6.81	2.72	6.33
.10	8.24	8.42	2.87	7.73
.12	9.80	10.0	3.01	9.17

TABLE III

HYDROLYSIS OF ETHYL ACETATE IN xM $NaHSO_4$

x	$10^4 k$, min.$^{-1}$	$10^4 k$, calcd., D.P.S.	K_{HSO_4}	$10^4 k$, calcd.[8]
0.008	0.39	0.39	1.73	0.39
.02	0.84	0.84	2.09	0.83
.04	1.50	1.48	2.45	1.42
.06	2.06	2.06	2.72	1.95
.08	2.62	2.62	2.91	2.43
.10	3.13	3.15	3.11	2.90
.15	4.43	4.43	3.45	3.97
.20	5.69	5.64	3.71	4.97
.24	6.67	6.67	3.91	5.73

In order to account for the data, Dawson, *et al.*, assumed that, in the case of sulfuric acid, the ionization constant of bisulfate ion, K_{HSO_4}, was constant and equal to 1.1×10^{-2}, while in the case of sodium bisulfate it varied from 1.17×10^{-2} in the most dilute solution to 1.96×10^{-2} in the most concentrated. On this basis, excellent agreement was obtained with experiment, as can be seen by inspection of the "calculated D.P.S." values, listed in column three of each table. However, it is now clear that the calculations are based on two essentially arbitrary parameters, which should make possible a close fit to almost any set of data of this kind.

Neither assumption in regard to K_{HSO_4} is in accord with the theory of Debye and Hückel, which predicts a larger and more rapid change in the value of the constant. Since independent measurements have shown that the theory applies to dilute bisulfate solutions, in the form

$$\log K'_{HSO_4} = \log K^\circ_{HSO_4} + \frac{4A\sqrt{\mu}}{1 + aB\sqrt{\mu}} = \log 0.0103 + \frac{2.03\sqrt{\mu}}{1 + 1.9\sqrt{\mu}}$$

the values of K'_{HSO_4} were calculated on this basis for the cases under consideration, and are listed in column four of each table. The hydrogen ion

(4) H. M. Dawson E. R. Pycock and E. Spivey, *J. Chem. Soc.*, 291 (1933).

(5) This is the value for the mean activity coefficient of hydrochloric acid in 1.5 M barium chloride. Since, in solutions of this concentration, the activity coefficients are not sensitive to either the concentration of salt or even the charge type of the electrolyte (H. S. Harned and B. B. Owen, "The Physical Chemistry of Electrolytic Solutions," Reinhold Publ. Corp., New York, N. Y., 1950, p. 575–576), the value can be applied as an approximation to the case at hand.

(6) This is the value found for hydrochloric acid in 1.5 M barium chloride (*vide supra*) (F. A. Robinson, *Trans. Faraday Soc.*, **26**, 217 (1930)).

(7) I. M. Klotz found this expression, with $K^\circ = 0.0101$, by colorimetric measurements on potassium bisulfate solutions ("A Precise Spectrophotometric Method for the Determination of Ionization Constants," University of Chicago, Ph.D. Thesis, 1940. Davies, Jones, and Monk (*Trans. Faraday Soc.*, **48**, 921 (1952)) recalculated the e.m.f. data of Hamer (*J. Am. Chem. Soc.*, **56**, 866 (1934)), as necessary to correct for the existence of $NaSO_4^-$ ions, and found $K^\circ = 0.0103$; they also obtained a similar value from independent e.m.f. measurements.

concentrations were computed[8] and the products of the concentration and the catalytic constant, 6.50×10^{-3}, are listed in column five. It can be seen that the calculated values up to $\mu \sim 0.1$ account for >95% of the observed rate. At higher concentrations, the agreement is not so good, but this region is, unfortunately, beyond the reach of the theory.

It should be clear from the first part of this discussion that the assignment of the catalytic constant 1.5×10^{-3} to bisulfate ion was not made on valid grounds, and it is apparent from the results of the alternative calculations that an unequivocal interpretation of the data is not possible. In the range where the Debye–Hückel theory can be expected to hold fairly well, and where the concentration of bisulfate ion is fairly small, its contribution to the catalytic action is too small to be clearly apparent. It may be that, at higher concentrations, this contribution is appreciable; but this cannot be concluded from the present data.

Experimental

Sodium sulfate decahydrate and sodium bisulfate (Mallinckrodt, A. R.) were used without further purification. Solutions were made up by weight and swept out with a stream of nitrogen. The *p*H was measured at 25.0°, both with a gold/quinhydrone–saturated calomel cell and a Beckman Model G *p*H meter. The gold/quinhydrone cell was checked against 0.05 *M* potassium biphthalate, and gave a *p*H value of 3.97 (accepted value 4.01); the Beckman instrument was set to read 4.01 with this buffer, as customary. The two instruments gave results differing by 0.2 *p*H unit or less; the values obtained with the gold/quinhydrone cell are listed in column three of Table I.

(8) A series of successive approximations was used. For $x M$ sulfuric acid

$$C_H = \frac{x - K_{HSO_4}}{2} + \sqrt{2K_{HSO_4}\, x + (x - K_{HSO_4})^2/4}$$

and two successive approximations generally gave sufficiently constant values of C_H. For $x M$ sodium bisulfate

$$C_H + C_{Na^+} = C_{HSO_4} + C_{NaSO_4} + 2C_{SO_4}$$
$$x = C_{HSO_4} + C_{NaSO_4} + C_{SO_4} = C_{Na} + C_{NaSO_4}$$
$$K^c_{NaSO_4} = \frac{C_{Na}C_{SO_4}}{C_{NaSO_4}} = 0.19 + \frac{2.03\sqrt{\mu}}{1 + 1.9\sqrt{\mu}};$$

three or four successive approximations gave nearly constant values of C_H.

SOLUBILITY OF BORON TRIFLUORIDE IN BENZENE AND TOLUENE

BY CHARLES M. WHEELER JR., AND HUGH P. KEATING
Dept. of Chemistry, University of New Hampshire, Durham, N. H.

Received August 30, 1954

The solubility of boron trifluoride in *n*-pentane by Cade, Dunn and Hepp[1] is the only quantitative solubility study reported for this gas. The present paper reports data for two aromatic hydrocarbons, the first solvents in a series of substituted benzene compounds for which solubility data will be obtained.

Experimental

Materials.—Mallinckrodt Analytical Reagent (thiophene free) benzene was dried over sodium wire and distilled in a Todd column packed with glass helices; refractive index of sample used, $n^{25}D$ 1.4979, lit. value[2] 1.49807. Merck Reagent Grade toluene was dried over sodium wire and fractionally distilled, refractive index of fraction used, $n^{25}D$ 1.4939, lit. value[3] 1.49405. Matheson Chemical Company boron trifluoride was used without further purification.

Apparatus.—The apparatus described by Lannung[4] was used for solubility determinations. Modifications were incorporated in the design of the apparatus to allow for the introduction of the gas directly from the gas cylinder and for degassing the solvent by refluxing. Mercury was used to prevent either the gas or solvent from coming into contact with stopcock grease. The solvent volume was about 20 ml. in all experiments and the initial gas volume from between 30 and 35 ml. The gas buret could be read accurately to within 0.05 ml.

The entire gas absorption apparatus was thermostated by circulating water through water jackets, with temperature control of ±0.05°.

Results and Discussion.—The results are expressed in two forms. First, the Ostwald coefficient of solubility, L, with the volume of the solvent measured at the temperature of the experiment and at a total pressure of 760 mm.

The solubilities are also expressed as the mole fraction of boron trifluoride dissolved at a partial gas pressure of one atmosphere. Henry's law was used to convert experimental data to partial pressure of one atmosphere. Table I lists values for L and x_2, mole fraction of boron trifluoride dissolved.

TABLE I

SOLUBILITY OF BORON TRIFLUORIDE IN BENZENE

T, °K.	295	300	305	310	315	320
$L \times 10^{+1}$	6.70	6.62	6.58	6.50	6.45	6.36
$x_2 \times 10^{+3}$	2.47	2.42	2.39	2.36	2.29	2.26

SOLUBILITY OF BORON TRIFLUORIDE IN TOLUENE

T, °K.	300	304	310	312	316	322
$L \times 10^{+1}$	6.30	6.25	6.18	6.15	6.11	6.03
$x_2 \times 10^{+3}$	2.79	2.74	2.68	2.66	2.61	2.54

Calculation of the Enthalpy and Entropy of Solution.—O'Brien[5] has expressed the solubility of a gas in terms of its mole fraction and temperature of solution by the equation

$$-\log x_2 = A/T + B \qquad (1)$$

x_2 is the mole fraction of the dissolved gas, the slope, A, of a plot of $-\log x_2$ *vs.* $1/T$ is identified as $\Delta H/2.303R$, the intercept, B, of the same plot, is identified as $\Delta S/2.303R$. ΔH and ΔS are the changes in enthalpy and entropy of solution.

From a plot of the data shown in Table I, the heat of solution was found to be −792 cal./mole for boron trifluoride in toluene and −691 cal./mole for boron trifluoride in benzene. The slopes of the two plots of $-\log x_2$ converge to give the same intercept and thus the same value of ΔS, −14.96 cal./mole, for boron trifluoride in benzene and toluene.

Surface Tension of Solvents and Solubility.—Uhlig[6] has developed an equation relating the solubility of a gas and the surface tension of a series of solvents. From this relationship it is possible to determine the solute–solvent interaction energy as well as the effective radius of the gas molecule in solution. From the expression

$$\ln L = \frac{-4\pi r^2\sigma + E}{kT} \qquad (2)$$

(1) G. N. Cade, R. E. Dunn and H. J. Hepp, *J. Am. Chem. Soc.*, **68**, 2454 (1946).

(2) M. J. Wojciechowski, *J. Research Natl. Bur. Standards*, **19**, 347 (1937).

(3) A. F. Forziati, A. R. Glasgow, C. B. Willingham and F. D. Rossini, *ibid.*, **36**, 129 (1946).

(4) A. Lannung, *J. Am. Chem. Soc.*, **52**, 68 (1930).

(5) S. J. O'Brien, *ibid.*, **63**, 2709 (1941).

(6) H. M. Uhlig, THIS JOURNAL, **41**, 1215 (1937).

the radius, r, of the gas molecule in solution and the interaction energy, E, can be determined.

We assumed that the radius of the boron trifluoride molecule was constant in benzene and toluene and that the interaction energy between the gas and solvent molecules in the two systems was not appreciably different. With these two assumptions and using experimental solubilities extrapolated to 20°, two simultaneous equations were solved for the radius, r, of the boron trifluoride molecule. The value of the radius of boron trifluoride molecule was found to be 2.03 Å., in good agreement with the calculated value, 2.09 Å., reported by Ruff, Erbert and Menzel.[7] The value for E, the interaction energy was found to be 1890 cal./mole.

Solubility Parameter of Boron Trifluoride.—Hildebrand[8] has shown that the equation

$$-\log x_2 = \log p^0_2 + v_2 (\delta_1 - \delta_2)^2/4.58\ T \qquad (3)$$

allows for the calculation of the solubility parameter, δ_2, of a gas from solubility data, if the parameter, δ_1, for the solvent is known. The solubility parameter for boron trifluoride in benzene and toluene at 25° was calculated using the data obtained in the present research. A plot of log p of boron trifluoride *vs.* $1/T$ from the data of Faraday[9] and Booth and Carter,[10] was extrapolated through the critical temperature to 25°, where p^0_2 was calculated from the density data of LeBoucher.[11] Solubility parameter values for benzene and toluene were obtained from a compilation by Hildebrand.[12] The calculated solubility parameter of boron trifluoride from benzene solubility data was 6.62, from toluene solubility data 6.53.

(7) O. Ruff, F. Erbert and W. Menzel, *Z. anorg. allgem. Chem.*, **207**, 46 (1932).

(8) J. H. Hildebrand, "The Solubility of Non-Electrolytes," 3rd Ed., Reinhold Publ. Corp., New York, N. Y., 1950, p. 244.

(9) M. Faraday, *Phil. Trans.*, **135**, 155 (1945).

(10) H. S. Booth and J. M. Carter, THIS JOURNAL, **36**, 1359 (1932)

(11) L. LeBoucher, W. Fischer and W. Biltz, *Z. anorg. allgem. Chem.*, **207**, 46 (1932).

(12) Ref. 8, Appendix 1.

ADDITIONS AND CORRECTIONS

1953, Vol. 57

R. J. Orr and H. Leverne Williams, Kinetics of the Reactions between Iron(II) and Some Hydroperoxides Based upon Cumene and Cyclohexane.

Page 925. The authors are indebted to Dr. R. L. Wentworth, Industrial Liaison Officer, M.I.T., for calling their attention to a needed correction. In determining the dependence of $\log_{10} A$ on activation energy, it was reported that $\log_{10} A = 1.1E - 3.6$ and a generalized Arrhenius equation for this type of reaction was calculated as

$$k = 2.5 \times 10^{-4} e^{(E(2.56\ RT - 1)/RT)}$$

from the above relation (where E is in kcal/mole). The arithmetic involved was incorrect and the relation is

$$\log_{10} A = 0.53E + 3.86$$

On this basis the equation for the rate constant is

$$k = 7.3 \times 10^{3} e^{E(1.22RT - 1)/RT}$$

Since no conclusions were drawn from the numerical values of the above constants, there is no error introduced from this source into the discussion.—H. LEVERNE WILLIAMS.

1954, Vol. 58

S. C. Lind. α-Particle Ionization and Excitation in Gas Mixtures.

Page 800. In column 1, text line 3 from the end, for "1.71 ± 0.034" read "1.73 ± 0.033."—S. C. LIND.

Author Index to Volume LVIII, 1954

Subject Index to Volume LVIII, 1954

FIRE RETARDANT PAINTS

Number nine of the ADVANCES IN CHEMISTRY SERIES

Edited by the staff of
Industrial and Engineering Chemistry

A collection of papers comprising the Symposium on Fire Retardant Paints, presented before the Division of Paint, Plastics, and Printing Ink Chemistry at the 123rd meeting of the American Chemical Society, Los Angeles, Calif., March 1953

CONTENTS

94 pages

paper bound

$2.50 per copy

Published June 1954, by American Chemical Society 1155 Sixteenth St., N. W. Washington, D. C.

CHEMICAL NOMENCLATURE

Number eight of the
Advances in Chemistry Series
Edited by the staff of *Industrial and Engineering Chemistry*

A collection of papers comprising the Symposium on Chemical Nomenclature, presented before the Division of Chemical Literature at the 120th meeting—Diamond Jubilee—of the American Chemical Society, New York, N. Y., September 1951

INTRODUCTION

This symposium was a unique event. There have been conferences on chemical nomenclature, of which the outstanding one was the Congress of Geneva on organic nomenclature, held in 1892. But as far as my knowledge goes this series of papers presented in New York in 1951 constitutes the first symposium on chemical nomenclature held anywhere. The fortunate circumstance that the Diamond Jubilee of the AMERICAN CHEMICAL SOCIETY occurred immediately before the Sixteenth Conference of the International Union of Pure and Applied Chemistry made it possible to give the symposium a truly international character. Six different countries, Denmark, France, Germany, Great Britain, the Netherlands, and the United States, were represented among the eleven speakers. The three nomenclature commissions of the IUPAC were also represented, two by their presidents and one by its secretary. The letter of greeting from A. F. Holleman, former president of the Commission on the Nomenclature of Organic Chemistry, was written in his ninetieth year. W. P. Jorissen, former president of the Commission on the Nomenclature of Inorganic Chemistry, accepted an invitation to prepare a paper but was forced to withdraw for reasons of health. All the papers were read by their authors.

The symposium covered, in broad range and authoritative manner, the developments and problems of present-day chemical nomenclature. It is indeed gratifying that the papers can be published together as a number of the ADVANCES IN CHEMISTRY SERIES.

AUSTIN M. PATTERSON

112 pages

paper cover

$2.50

CONTENTS

Published August 15, 1953, by
AMERICAN CHEMICAL SOCIETY
1155 Sixteenth Street, N.W.
Washington, D. C.